REPORT DOCUMENTATION P

AFOSR-TR-95 0606

ed
04-0188

1. AGENCY USE ONLY (Leave blank)	2. REPORT DATE	3. REPORT TYPE AND
	August 31, 1995	Final Technical 2/15/93 - 5/14/95

4. TITLE AND SUBTITLE

Multi-Gb/s Computer Interconnect Using Optical Solitons

5. FUNDING NUMBERS

F49620-93-1-0167

63218C
1601/10

6. AUTHOR(S)

Jon Sauer, Mark Ablowitz, Brian Jenkins,
Sarbarish Chakravarty

7. PERFORMING ORGANIZATION NAME(S) AND ADDRESS(ES)

The Regents of the University of Colorado
Campus Box 19
Boulder, CO 80309-0019

8. PERFORMING ORGANIZATION REPORT NUMBER

9. SPONSORING / MONITORING AGENCY NAME(S) AND ADDRESS(ES)

AFOSR/PKX NE
110 Duncan Ave, Suite B115
Bolling AFB, DC 20332-0001

10. SPONSORING / MONITORING AGENCY REPORT NUMBER

F49620-93-1-0167

11. SUPPLEMENTARY NOTES

12a. DISTRIBUTION / AVAILABILITY STATEMENT

APPROVED FOR PUBLIC RELEASE: DISTRIBUTION UNLIMITED

12b. DISTRIBUTION CODE

13. ABSTRACT *(Maximum 200 words)*

Abstract: The following document presents the results of a two year study into the feasibility of using wavelength-division-multiplexed solitons for data communications. Timing jitter caused by nonlinear interactions between multi-wavelength solitons was found to be a fundamental effect limiting the use of wavelength multiplexed solitons for data transmission. Such interactions can be described mathematically by a simple summation of all frequency shifts which occur during pairwise soliton collisions, and the resulting variance in pulse arrival times depends not only on perturbations to the fiber but also on the encoding of information. In a fiber with loss and amplification, it was shown that extensive wavelength multiplexing with solitons is feasible, and possibly preferable to other alternatives for achieving high aggregate throughput in computer communication systems.

UBJECT TERMS	15. NUMBER OF PAGES
DTIC QUALITY INSPECTED 5	16. PRICE CODE

SECURITY CLASSIFICATION OF REPORT	18. SECURITY CLASSIFICATION OF THIS PAGE	19. SECURITY CLASSIFICATION OF ABSTRACT	20. LIMITATION OF ABSTRACT

Multi-Gb/s Computer Interconnect using Optical Solitons

AFOSR Grant F49620-93-1-0167

Final Technical Report

Principal Investigators

Jon R. Sauer

Optoelectronic Computing Systems Center

Mark J. Ablowitz

Program in Applied Mathematics

University of Colorado at Boulder

Boulder, CO 80309

Abstract: The following document presents the results of a two year study into the feasibility of using wavelength-division-multiplexed solitons for data communications. Timing jitter caused by nonlinear interactions between multi-wavelength solitons was found to be a fundamental effect limiting the use of wavelength multiplexed solitons for data transmission. Such interactions can be described mathematically by a simple summation of all frequency shifts which occur during pairwise soliton collisions, and the resulting variance in pulse arrival times depends not only on perturbations to the fiber but also on the encoding of information. In a fiber with loss and amplification, it was shown that extensive wavelength multiplexing with solitons is feasible, and possibly preferable to other alternatives for achieving high aggregate throughput in computer communication systems.

EXECUTIVE SUMMARY

Here we briefly summarize the results of a two year investigation which studied the use of wavelength-division-multiplexed (WDM) solitons in optical fiber for communications and computing. The personnel directly involved in this research were Jon R. Sauer and R. Brian Jenkins, from the Optoelectronic Computing Systems Center, and Mark J. Ablowitz and Sarbarish Chakravarty, from the Program in Applied Mathematics. Others that were involved indirectly during some portion of the research include Christian Radehaus, Alan F. Benner, and Gregory Beylkin. Detailed results of this research can be found in several publications[1, 2, 3, 4]. The doctoral thesis by Brian Jenkins[1] is included as an Appendix.

1. General discussion

With the development of erbium-doped fiber amplifiers, the limits on long-distance communication due to fiber loss have been greatly reduced. Hence, chromatic dispersion and fiber nonlinearities have become the prevalent effects preventing high-performance communication at multi-Gb/s data rates across distances greater than 10^2 km. Since anomalous dispersion is precisely balanced by nonlinear self-phase modulation in the soliton pulse, narrow solitons do not disperse even after propagating long distances. For this reason, the use of solitons for data transmission in fiber has become very attractive. However, solitons on a single wavelength channel still cannot efficiently use the immense bandwidth of the fiber. Practical technological limits on the electrical receiver bandwidth and on the modulation rates of semiconductor or fiber lasers prevent the transmission of data at very high rates, so the use of WDM for soliton communications may be necessary in high-performance systems.

Data transmission over multiple wavelength channels is more complicated in a soliton system than in more traditional communication systems. Pulses on different wavelengths inevitably collide in a dispersive fiber as faster pulses in one wavelength channel overtake slower pulses in a different wavelength channel. In the typical linear transmission system, the effects of such collisions on communications are negligible. In a soliton system, though, pulse interactions are inherently nonlinear, and frequency shifts and timing displacements take place during collisions, possibly distorting data.

In a lossless fiber, the effects of nonlinear soliton interactions would not typically degrade data. Any frequency shifts are only temporary[2, 5] — the soliton eigenvalue is conserved during the collision — and any timing displacements are nearly identical for adjacent pulses[6, 7], having minimal impact on data detection and the bit-error-rate (BER) at the fiber output. However, in a real fiber with loss and with amplifiers spaced periodically throughout the system, WDM soliton collisions may disrupt communications. When solitons collide in the presence of loss and amplification, the interaction is asymmetric, meaning that the attractive "forces" between the solitons are not balanced throughout the collision. Hence, the soliton eigenvalue and the soliton velocity after the collision may be different from their values before the collision[5]. Such permanent frequency (velocity) shifts could potentially result in large timing displacements at the fiber output, thus degrading the BER.

While it might seem that nonlinear interactions would prevent any use of WDM solitons for communication, it was demonstrated by Mollenauer, et. al.[5], that the effects of loss and amplification are path-averaged — the permanent frequency shifts reduce to zero — whenever the wavelengths or

velocities of two soliton channels are close enough to insure that collisions occur over large distances relative to the amplifier spacing. Quantitatively, no permanent frequency shifts result if the collision length, defined as

$$L_c = \frac{2\tau}{D\Lambda}, \tag{1}$$

is twice the amplifier spacing L_a. τ is the full width of the pulse at half the maximum intensity (FWHM) in units of ps, D is the dispersion coefficient in units of ps/nm-km, and Λ is the wavelength spacing between two channels in units of nm.

However, requiring that

$$L_c \geq 2\,L_a \tag{2}$$

limits a WDM soliton system to only a few wavelengths in a narrow spectral bandwidth. Using Eqs. (1) and (2), a maximum wavelength spacing of

$$\Lambda_{\mathbf{max}} = \frac{\tau}{DL_a} \tag{3}$$

may be derived, which defines the bandwidth over which soliton wavelength channels may be multiplexed according to Eq. (2). For values of $\tau \leq 50$ ps, $D = 1$ ps/nm-km, and $L_a = 25$ km, all wavelengths must fit in a bandwidth of $\Lambda_{\mathbf{max}} \leq 2$ nm. This is rather restrictive for WDM, considering that the useful gain-bandwidth of an erbium-doped amplifier is at least 20 nm.

Nearly all previous WDM soliton research has assumed that Eq. (2) is a necessary condition for data transmission to be feasible if WDM solitons are used. In analyzing the interactions between WDM solitons, we recognized that Eq. (2) is more restrictive than necessary for many systems environments. One example would be a long-distance computer interconnect where the distances may be shorter than 10^4 km, as is typically required in transoceanic

communication links. In effect, Eq. (2) prevents the occurrence of worst-case frequency shifts, and much more extensive use of WDM — with many wavelength channels and a high degree of flexibility in choosing channel frequencies — may still be possible for soliton communication if the system is designed simply to achieve optimum performance at a predetermined BER.

2. Research results

The most important results of the research are as follows:

- We have analytically determined (and numerically verified) the frequency shifts which take place during collisions between solitons on an arbitrary number of wavelength channels.
- We have statistically predicted the WDM soliton collision-induced timing jitter that results in a practical fiber communication system assuming that amplifiers are necessary to compensate fiber loss.
- We have shown that solitons can be used for WDM communications to a greater degree than previously thought. This is especially true in communication systems that are shorter than transoceanic telecommunication links. Most WDM soliton systems of practical lengths could achieve BERs less than 10^{-9} even under conditions which violate Eq. (2).

2.1. Analytic derivation of N-soliton interactions To analyze the performance of a WDM soliton system, it is necessary to understand how multiple solitons interact during collisions. Most WDM soliton research has dealt only with the interaction that occurs when two solitons on different wavelengths collide. While it has always been assumed that the interactions in the spectral domain are additive in a pairwise fashion — in analogy to

the pairwise timing displacements originally demonstrated by Zakharov and Shabat[8] — when greater than two solitons collide, this has never been proven analytically. Through an asymptotic analysis of the exact N-soliton solution of the nonlinear Schrödinger equation, we have demonstrated that interactions are additive in the spectral domain only to first order in terms of the inverse frequency spacing $1/\Delta f$ between channels[2].

Practically, this means that during an N-soliton collision the interaction can be treated mathematically as a group of independent two-soliton interactions if the wavelength channels are not multiplexed too densely in wavelength. From a quantitative viewpoint, if the normalized WDM frequency separation Ω is much greater than one, where $\Omega = 2\pi\Delta f\tau/1.763$ and Δf is the physical channel spacing in hertz, the shift in the frequency Ω_p of the pth soliton channel is approximately

$$\delta\Omega_p \approx \frac{8}{\pi^2\Omega} \sum_{\substack{q=1 \\ q\neq p}}^{N} \frac{S_{pq}}{(p-q)\sinh(S_{pq})}, \quad \text{for } p = 1, \ldots, N. \tag{4}$$

The quantity,

$$\begin{aligned} S_{pq} &= S_p - S_q \\ &= (\Omega_p - \Omega_q)z - (t_{op} - t_{oq}) \\ &= (p-q)\Omega z - (t_{op} - t_{oq}), \end{aligned} \tag{5}$$

defines the temporal separation between two solitons, one on the pth channel and one on the qth channel, such that when $S_{pq} = 0$, the center of the collision is located at position z in the fiber. The parameters t_{op}, for $p = 1, \ldots, N$, define the initial timing of the solitons on the N wavelength channels, so that by varying the values of t_{op}, the amount of overlap between the N solitons

during the collision is generalized for arbitrary initial conditions at the fiber input.

As frequency spacings become small, i. e., as the wavelength channels are more densely multiplexed, the total interaction during a collision is not described by the straightforward summation over the N channels, as in (4). Higher-order terms proportional to $1/\Omega^2, 1/\Omega^3, \ldots$ must then be included to fully describe the spectral interactions. However, for values of Ω as small as 5.61, the error in using Eq. (4) is still only 5%. This value of Ω corresponds to a channel spacing of five soliton spectral widths, or $\Delta f = 5(0.3148)/\tau$, as is necessary to insure that frequency shifts during collisions at the fiber output will not be too large[9]. Translated into physical quantities using $\Lambda = \lambda^2 \, \Delta f/c$, where λ is the wavelength and c is the speed of light, (4) is still approximately correct for channel spacings of $\Lambda = 0.25$ nm with $\tau = 50$ ps channels and $\Lambda = 0.625$ nm for $\tau = 20$ ps channels, where the center wavelength is $\lambda = 1.55$ μm.

2.2. Timing jitter in WDM soliton systems An original goal of this research was to statistically predict the the final values of the soliton wavelengths at the fiber output after many collisions had taken place. Upon further analysis, it was seen that the variance in the soliton arrival times at the fiber output is much larger relative to the bit period than is the variance in the wavelength with respect to the channel spacing; system performance depends more on the variance in pulse arrival times, or timing jitter, than on frequency (or wavelength) jitter. Hence, we have determined the timing jitter that results in WDM soliton systems that have an arbitrary number of wavelength channels[1, 3].

Suppose we define the arrival time of a soliton in the jth bit slot of a

given wavelength channel as t_j. If the arrival time of another soliton ρ bit slots later on the same wavelength is $t_{j+\rho}$, then the absolute difference in the arrival times would ideally be given by ρT, where T is the bit period. In reality, though, collisions with solitons on other wavelengths cause jitter in the arrival times, such that

$$t_{j+\rho} - t_j = \rho T + \Delta t, \tag{6}$$

where Δt is used to define the jitter in the relative arrival times of the two solitons. If Δt is negative, the two solitons have moved closer together at the fiber output, whereas if Δt is positive, they have moved farther apart. In either case, if $|\Delta t|$ is too large, data may be distorted.

From a statistical viewpoint, we have shown that the jitter in a WDM system with $N = 2$ is normally distributed with variance

$$\langle \Delta t^2 \rangle = n^3 \left(\frac{T}{\Lambda}\right)^2 \frac{\langle \Delta\lambda^2 \rangle}{6}. \tag{7}$$

The quantity $n = LD\Lambda/T$ is the number of collisions which occur across the full length L of the fiber and $\langle \Delta\lambda^2 \rangle$ is the variance in the permanent wavelength shifts which result from WDM soliton collisions. Since $\langle \Delta\lambda^2 \rangle$ may take on different values depending on perturbations to the fiber, Eq. (7) is a general result which holds for somewhat arbitrary perturbations. As an example, $\langle \Delta\lambda^2 \rangle$ could be defined in a fiber where the only perturbations are loss and amplification, or other perturbations, such as dispersion variations in fibers making up a link, could be included well[5]. Eq. (7) agrees well with recent results[7] which numerically predicted WDM soliton timing jitter.

Of greater importance is the variance $\langle \Delta t^2 \rangle$ in each channel of a WDM system having as many as N channels. Eq. (4) demonstrates independence in the frequency shifts experienced by each channel if the channel spacings

are wide enough. Hence, it is easy to modify Eq. (7) if there are multiple wavelength channels. The total variance in the relative arrival times of adjacent solitons in the pth of N channels is simply a sum of the variances resulting from interactions with the other $N-1$ channels, as in

$$\langle \Delta t^2 \rangle_p = \sum_{\substack{q=1 \\ q \neq p}}^{N} (n_{pq})^3 \left(\frac{T}{\Lambda_{pq}} \right)^2 \frac{\langle \Delta \lambda^2 \rangle_{pq}}{6}, \quad \text{for } p = 1, \ldots, N. \tag{8}$$

The number of collisions, the channel spacing, and the variance in the wavelength shifts between the pth and qth channels are represented by n_{pq}, $\Lambda_{pq} = (p-q)\Lambda$, and $\langle \Delta \lambda^2 \rangle_{pq}$, respectively.

To estimate the bit-error-rate(BER) resulting from Eq. (8), we make an assumption about how much jitter the receiver can tolerate by defining a parameter r to measure receiver sensitivity. If the bit period $T = 5\tau$ and if the maximum value of $|\Delta t|$ allowed by the receiver is given by $rT = 5r\tau$, the receiver is more sensitive to jitter in the arrival times as r decreases. The actual value of r in a system cannot be defined precisely without knowing more details about the receiver, but as an example, if $r = 2/5$, then $|\Delta t|$ must be less than 2τ for the receiver to detect data accurately. If two solitons were initially separated by one bit period $T = 5\tau$ at the input, they may be spaced no closer than 3τ and no farther than 7τ at the output for the receiver to detect each bit. If $\rho = 3$ between two solitons, the initial spacing is $3T = 15\tau$, so they must be separated by at least 13τ and by at most 17τ at the fiber output for the receiver to properly detect data. Since Δt is Gaussian distributed, the BER in the pth channel can then be computed using

$$\text{BER}_p = \text{erfc}\left(rT / \sqrt{2 \langle \Delta t^2 \rangle_p} \right), \quad \text{for } p = 1, \ldots, N, \tag{9}$$

where the complementary error function is defined according to

$$\mathrm{erfc}\left(x_o/\sqrt{2}\right) = \frac{2}{\sqrt{\pi}} \int_{\frac{x_o}{\sqrt{2}}}^{\infty} \exp(-x^2)\, dx. \tag{10}$$

The BER is 10^{-9} when $x_o = 6.1$ and 10^{-12} when $x_o = 7.1$, where $x_o = rT/\sqrt{\langle \Delta t^2 \rangle_p}$.

2.3. System implications of WDM soliton collisions Most soliton research has attempted to solve the problems of communication in long-distance transoceanic transmission links. While the restriction defined by Eq. (2) may be meaningful in such systems, it is not necessarily a realistic limitation for all communications and computing systems. Eqs. (8) and (9) provide the flexibility that is necessary to predict the feasibility of using WDM solitons in many different systems environments.

Since n_{pq} is proportional to the fiber length L, Eqs. (8) and (9) can be used to define a maximum length that can be achieved for a given number of channels and a predetermined BER. It is also possible to use these equations to determine the maximum value of N at a given length and data rate $R = 1/(5\tau) = 1/T$ to insure a given BER. The results are depicted by the solid curves in Fig. 1, where the maximum value of L is plotted as a function of the FWHM and the data rate R per channel for various values of N, and in Fig. 2, where the aggregate throughput NR is plotted for various L. In these plots, the BER is required to be no greater than 10^{-9}. Other system parameters have been chosen as $D = 1$ ps/nm-km at a wavelength of 1.55 μm, $L_a = 25$ km, and $r = 2/5$. All lengths are reduced by 10% if the required BER is 10^{-12} or by 37% if $r = 1/5$. With five soliton spectral widths between adjacent wavelengths, the channel spacings vary from $\Lambda = 0.625$ nm at $\tau = 20$ ps to $\Lambda = 0.25$ nm when $\tau = 50$ ps. These plots describe the system performance as limited by loss and

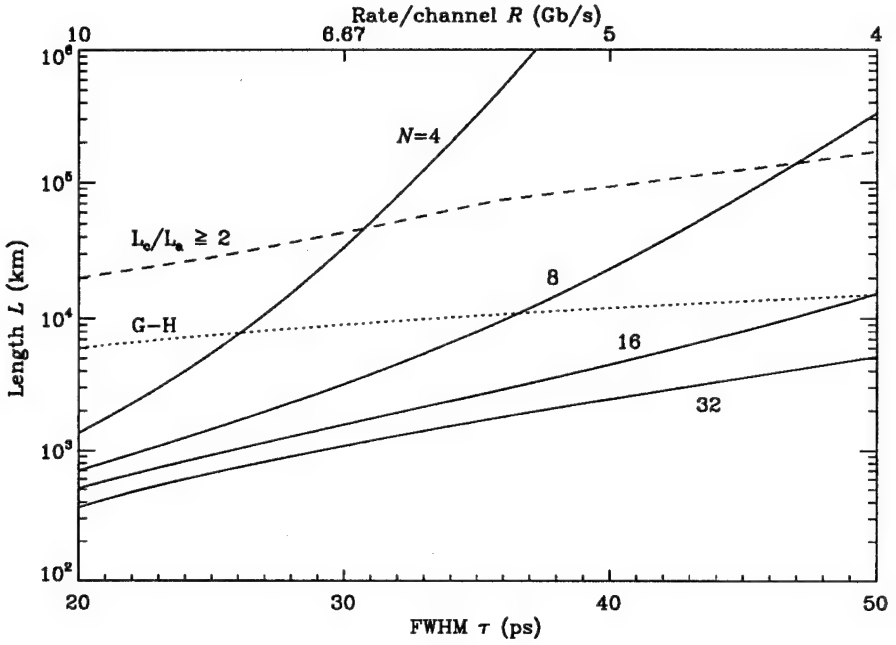

Figure 1. Maximum system length with N channels at a 10^{-9} BER as limited by collision-induced timing displacements. The dashed curve illustrates the maximum length possible if all channels meet the condition that $L_c/L_a \geq 2$ and the dotted curve indicates the maximum system length as limited by Gordon-Haus jitter.

amplification, so if either the channel spacing Λ, the amplifier spacing L_a, or the dispersion D decreases, the ratio L_c/L_a increases, so that wavelength shifts are smaller and aggregate throughput is greater.

When $L_c/L_a \geq 2$, as depicted by the dashed line in each figure, WDM soliton transmission is possible to a distance of 20000 km when $\tau = 20$ ps and to longer distances when τ is greater than 20 ps. However, the number of 20-ps channels is limited to two and the number of 50-ps channels is limited to nine (as seen by dividing the throughput NR on the dashed line in Fig. 2 by the data rate R). If L_c/L_a is less than two, then the system length must be shorter but more channels are allowed, giving greater aggregate throughput.

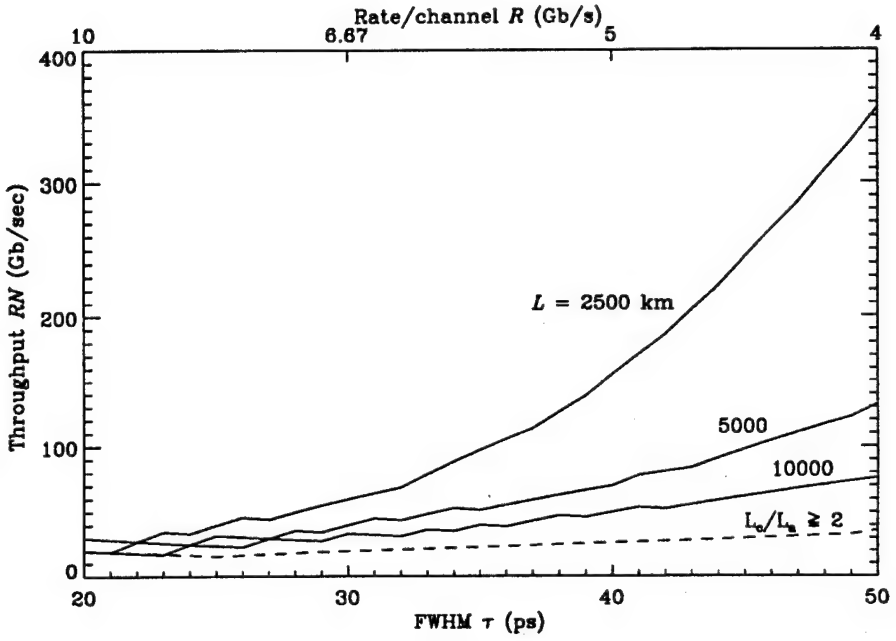

Figure 2. Maximum throughput in a WDM soliton system for various lengths.

For example, in a system 2500 km in length with $\tau = 40$ ps, 32 channels with an aggregate throughput of 160 Gb/s are possible in theory. The bandwidth over which the channels are multiplexed is $31(.315) \approx 10$ nm, less than the gain-bandwidth of an erbium-doped fiber amplifier. The minimum value of $L_c/L_a = 2(40)/1(10)(25) = 0.32$, which occurs between channels 1 and 32, is much smaller than two.

We can also compare the effects of collision-induced jitter to Gordon-Haus jitter[10], as depicted by the dotted line in Fig. 1. With many wavelength channels or high data rates, we see that the length will probably be limited by WDM soliton collision-induced jitter, whereas Gordon-Haus jitter is more likely to limit the length of systems with fewer channels and lower data rates. In a recent WDM soliton experiment[11] using 60-ps solitons, eight 2.5 Gb/s channels were transmitted 10000 km with error rates below 10^{-10}. The channels

were densely multiplexed with $\Lambda = 0.2$ nm in order to reduce collision-induced jitter. Fig. 1 indicates, though, that this system is more likely limited by Gordon-Haus jitter. Although collision-induced jitter increases if Λ is larger (since collision lengths L_c are shorter), estimates of jitter using Eq. (8) indicate that channel spacings much larger than 0.2 nm would be feasible before collision-induced jitter would impact such a system. Hence, our results show that much greater flexibility is possible in choosing channel wavelengths than has previously been assumed in WDM soliton systems.

Finally, from an intuitive standpoint one might expect the throughput in Fig. 2 to increase as the data rate R per channel increases, but our results show the opposite. As R increases, the number of collisions and the magnitude of the wavelength shifts increase substantially for fixed L, so the number of channels N decreases rapidly. In fact, with system parameters defined as in Figs. 1 and 2, jitter prevents the transmission of even two WDM soliton channels at a data rate of 11 Gb/s per channel across a distance of 10000 km (see Fig. 5.14 in the Appendix[1]). Thus, the fundamental limit on throughput due to collision-induced velocity shifts is less restrictive using many slower (and cheaper) channels. While it is unlikely that aggregate throughputs as high as 356 Gb/s, as shown in Fig. 2, can be achieved in the near future — due to practical issues such as four-wave mixing or other amplifier effects, the curves in Fig. 2 suggest that greater use of the spectral domain, using many slower WDM soliton channels, is more likely to increase aggregate system performance than will the simple use of higher data rates. With advances in filtering techniques, WDM soliton transmission is likely to become the preferable means of achieving high-performance data communication in optical fiber.

BIBLIOGRAPHY

[1] R. B. Jenkins, **Wavelength multiplexed solitons in fiber communication systems**. PhD thesis, University of Colorado, Boulder, Colorado, 1995.

[2] S. Chakravarty, M. J. Ablowitz, J. R. Sauer, and R. B. Jenkins, "Multisoliton interactions and wavelength-division multiplexing," **Optics Letters**, vol. 20, no. 2, pp. 136–138, 1995.

[3] R. B. Jenkins, J. R. Sauer, S. Chakravarty, and M. J. Ablowitz, "Data-dependent timing jitter in WDM soliton systems," to be published in **Optics Letters**, vol. 20, no. 19, 1995.

[4] R. B. Jenkins, J. R. Sauer, C. Radehaus, A. F. Benner, M. J. Ablowitz, and G. Beylkin, "Techniques for detecting densely wavelength-multiplexed solitons," in **Multigigabit Fiber Communication Systems,** Leonid G. Kazovsky, Karen Liu, Editors, Proc. SPIE, Vol. 2024, (SPIE, Bellingham, WA), 1993, pp. 258–269.

[5] L. F. Mollenauer, S. G. Evangelides, and J. P. Gordon, "Wavelength division multiplexing with solitons in ultra-long distance transmission using lumped amplifiers," **J. Lightwave Tech.**, vol. 9, no. 3, pp. 362–367, 1991.

[6] H. A. Haus, "Optical fiber solitons, their properties and uses," **Proc. IEEE**, vol. 81, no. 7, pp. 970–983, 1993.

[7] F. Matera, M. Romagnoli, M. Settembre, S. Wabnitz, and Y. Kodama, "Ultimate capacity of WDM soliton transmissions with sliding filters," in **Nonlinear Guided Waves and Their Applications, 1995 Technical Digest Series**, Vol. 6, (Optical Society of America, Washington, DC), 1995, pp. 133–135.

[8] V. E. Zakharov and A. B. Shabat, "Exact theory of two-dimensional self-focusing and one-dimensional self-modulation of waves in nonlinear media," **Soviet Physics JETP**, vol. 34, no. 1, pp. 62–69, 1972.

[9] A. F. Benner, J. R. Sauer, and M. J. Ablowitz, "Interaction effects on wavelength-multiplexed soliton data packets," **J. Opt. Soc. Am. B**,

vol. 10, no. 12, pp. 2331–2340, 1993.

[10] J. P. Gordon and H. A. Haus, "Random walk of coherently amplified solitons in optical fiber transmission," **Optics Letters**, vol. 11, no. 10, pp. 665–667, 1986.

[11] B. M. Nyman, S. G. Evanglides, G. T. Harvey, L. F. Mollenauer, P. V. Mamyshev, M. L. Saylors, S. K. Korotky, U. Koren, V. Mizrahi, T. A. Strasser, J. J. Veselka, J. D. Evankow, A. Lucero, J. Nagel, J. Sulhoff, J. Zyskind, P. C. Corbett, M. A. Mills, and G. A. Ferguson, "Soliton WDM transmission of 8X2.5 Gb/s, error free over 10 Mm," in **Optical Fiber Communication Conference, 1995 Technical Digest Series**, Vol. 8, postdeadline paper PD21, (Optical Society of America, Washington, DC), 1995.

APPENDIX

Included here is the doctoral thesis by Brian Jenkins[1], which discusses the previous results in greater detail. Chapters 1 and 2 from the thesis provide an introduction and describe experimental results. Chapter 3 provides all the analytic theory needed to understand the results presented in Section 2.1. of the Executive Summary. The results from Section 2.2. are examined primarily in Chapters 4 and 5 of the thesis, and the results of Section 2.3. are explained in Chapter 5. Chapter 6 provides a more comprehensive list of conclusions which resulted from the research.

WAVELENGTH MULTIPLEXED SOLITONS IN FIBER COMMUNICATION SYSTEMS

by

R. Brian Jenkins

B. S. Electrical Engineering,

The Ohio State University, 1983

M. S. Electrical Engineering,

The Ohio State University, 1991

A thesis submitted to the

Faculty of the Graduate School of the

University of Colorado in partial fulfillment

of the requirements for the degree of

Doctor of Philosophy

Department of Electrical and Computer Engineering

1995

This thesis for the Doctor of Philosophy degree by

R. Brian Jenkins

has been approved for the

Department of

Electrical and Computer Engineering

by

_____

Jon R. Sauer

_____

Robert Feuerstein

Date _____

Jenkins, R. Brian (Ph.D., Electrical Engineering)

Wavelength Multiplexed Solitons in Fiber Communication Systems

Thesis directed by Professor Jon R. Sauer

Optical fiber is widely used for data communication because of its large bandwidth and low loss between the wavelengths of 1.2 and 1.6 μm. High-performance communication in fiber is often limited by dispersion or nonlinear effects as the bit rate or system length increases. Fortunately, a stable solution of the nonlinear Schrödinger equation, which describes pulse propagation in fiber, is the soliton pulse, which relies on both dispersion and fiber nonlinearity to ensure stable pulse propagation at high bit rates over thousands of kilometers. With the development of erbium amplifiers, soliton propagation is even more appealing, since optical amplifiers passively compensate fiber loss while solitons passively compensate fiber dispersion.

To efficiently utilize fiber bandwidth, it may ultimately be necessary to use wavelength multiplexing. Soliton transmission on multiple frequencies, however, is complicated by nonlinear interactions — frequency (wavelength) shifts and velocity shifts — when solitons collide in the fiber. Consequently, it is thought that extensive wavelength multiplexing will be difficult to achieve with solitons. Through primarily analytical and numerical methods, this thesis examines such issues, predicting timing jitter, bit-error-rates, and performance in wavelength multiplexed soliton systems. It is demonstrated that wavelength multiplexing is likely to be the best alternative for achieving high aggregate throughput in a soliton communication system.

DEDICATION

To my wife and my mother for their support and encouragement through many years of education.

In memory of my father.

ACKNOWLEDGEMENTS

I must first thank my advisor Jon Sauer for his support and useful input during my research. One of his greatest assets is his ability to encourage. Regardless of the difficulty, Jon always takes the optimistic view, demonstrating confidence in my ability to overcome any problem.

I also thank the members of my committee, Bob Feuerstein, Mark Ablowitz, Kelvin Wagner, Harry Jordan, and Alan Mickelson for their useful suggestions. I especially thank two members of my committee. First, I have spent a great deal of time with Bob Feuerstein, both in the laboratory and in fruitful discussions encompassing a wide variety of technical issues. Mark Ablowitz has been a great help with all the mathematics and with his financial support during lapses in funding.

There are several others to whom I am very grateful. First, countless hours of discussion with Sarbarish Chakravarty always proved to be insightful and thought provoking. I also thank John Feehrer for many useful conversations about probability and statistics. John Schlager and Kevin Malone, from the National Institute of Standards and Technology and the Department of Commerce, were extremely helpful and generous in allowing us the use of their fusion splicer. I also thank Alan Craig and the Air Force Office of Scientific Research for their funding of this research.

Finally, I thank my friends and family for their support. I especially thank my wife Amy for her patience and encouragement. It was much more fun and much easier to do this because of her.

CONTENTS

TABLES

TABLE

FIGURES

FIGURE

CHAPTER 1

INTRODUCTION

Modern communication systems often require large amounts of data to be transferred over long distances. Optical fiber is useful for such communications because of its low loss and low dispersion, especially at wavelengths in the near infrared portion of the electromagnetic spectrum. Fiber is becoming common over shorter distances as well because of its large transmission bandwidth and its insensitivity to crosstalk; it is not unusual to hear the term "fiber to the curb". However, for high performance communications, fiber is still limited by several effects; dispersion and loss restrict data transmission over longer distances, and fiber nonlinearities limit data rates as the bit period approaches the period of the optical carrier frequency.

The soliton pulse appears to be the most natural answer to the problems of dispersion and nonlinearity. Solitons are simply pulses in which linear group velocity dispersion is balanced by the nonlinear spectral dispersion known as self-phase modulation. Hence, solitons maintain their shape and velocity over long distances. The development of the erbium-doped fiber amplifier (EDFA) has made soliton communication especially attractive, since an EDFA passively counteracts loss without changing the optical data into an electronic format. Because of their insensitivity to loss and amplification, solitons have been transmitted across distances as long as one million kilometers at data rates of 10 Gb/sec[1]. However, even solitons are unable to efficiently use the

entire fiber bandwidth. Higher order dispersive effects, other nonlinearities, and the simple problem of generating and detecting high speed pulses prevents the transmission of solitons at very high rates.

Wavelength-division-multiplexing (WDM) may be the most effective way of exploiting the immense fiber bandwidth in the low loss region between 1.2 μm and 1.6 μm. WDM uses the spectral domain and the parallelism of optics as a means of overcoming restrictions on communication in the time domain. While using WDM for data transmission is not new, its application to soliton communication has only recently attracted attention as the fundamental problems of communicating in the time domain have been better understood. Encoding data on soliton channels having different wavelengths, though, has its own complexities. A soliton is a nonlinear phenomenon, and the niceties of linear systems, such as superposition, are not inherent in nonlinear systems.

Solitons encoded on different wavelengths propagate with different velocities because of dispersion, inevitably colliding with one another as faster solitons overtake slower solitons. When linear pulses on different wavelengths collide in a fiber, linear superposition holds, oftentimes without any degradation of data. When solitons on different wavelengths collide, nonlinear interactions take place, distorting both the time and frequency domain. While interactions during collisions between solitons on two wavelength channels have been studied for some time, interactions between an arbitrary number of soliton wavelength channels are not well understood. Furthermore, current theoretical restrictions on WDM soliton systems are overly conservative, as they are based on unrealistic assumptions about the fiber communication system. Estimates of performance, including issues such as timing jitter or bit-error-rates,

have never been formulated for WDM soliton communications. The goals of this thesis are to study interactions between WDM solitons, and to develop more realistic predictions of their usefulness for fiber communications, using numerical, analytical, and experimental techniques.

In this chapter, basic issues such as dispersion and self-phase modulation are analyzed, so as to provide the reader with a fundamental physical and mathematical understanding of soliton communication in fiber. In Chapter 2, we examine how solitons are generated and discuss related experimental results. In Chapter 3, we consider how WDM soliton interactions affect propagation in a rigorous mathematical analysis of soliton collisions in an ideal, lossless fiber. The analysis is generalized for an arbitrary number of wavelength channels, whereas previous research dealt with at most two channels. Chapter 4 examines how collisions are perturbed by loss and amplification. Finally, in Chapter 5, we determine how WDM soliton interactions affect the transfer of data in the fiber, deriving expressions for timing jitter and bit-error-rates in a system with an arbitrary number of wavelength channels. Previous WDM soliton systems did not account for the stochastic properties of a digital communication system, so the results enable us to predict how future systems might be practically designed to optimize performance. Conclusions will be drawn and suggestions for future research are discussed in Chapter 6.

1.1 Soliton propagation in fiber

Before discussing soliton propagation, it is useful to understand two effects which degrade fiber communications when occurring by themselves — dispersion and self-phase modulation.

1.1.1 Dispersion A fiber is dispersive in several ways. In multimode fiber, modal dispersion limits data rates and fiber lengths as different modes travel different paths in the fiber, arriving at the fiber output at different times. In birefringent fiber, energy in orthogonal polarizations travel with slightly different velocities, causing polarization mode dispersion. Over very long distances, polarization mode dispersion can be important even in standard fiber. For high performance communications in single mode fiber, the type of dispersion we are most interested in is chromatic dispersion — different wavelengths or frequencies of light travel with different velocities in a fiber. This is the dominant dispersive effect in standard single mode fiber and results because the index of refraction n is a function of the wavelength. For pure silica, the index variation is shown in Fig. 1.1, as derived in a Sellemeier approximation of the index for pure silica[2]. The group velocity of a pulse is related to the group index of refraction,

$$n_g = n - \lambda \frac{dn}{d\lambda}, \tag{1.1}$$

by the relation $v_g = c/n_g$, where c is the speed of light and λ is the wavelength in free space. The group index is also plotted in Fig. 1.1. In reality, one must use the effective group index of the fiber to describe pulse evolution, as it is the index which describes the propagation of the mode in the fiber. The effective index takes on a value between the bulk indices of the fiber core and cladding[2]. Since the group index is around 1.5 and $c = 3 \times 10^8$ m/s, the group velocity v_g is approximately 0.2 mm/ps.

To estimate group velocity dispersion (GVD), a parameter

$$D = \frac{d}{d\lambda}\left(\frac{1}{v_g}\right) \tag{1.2}$$

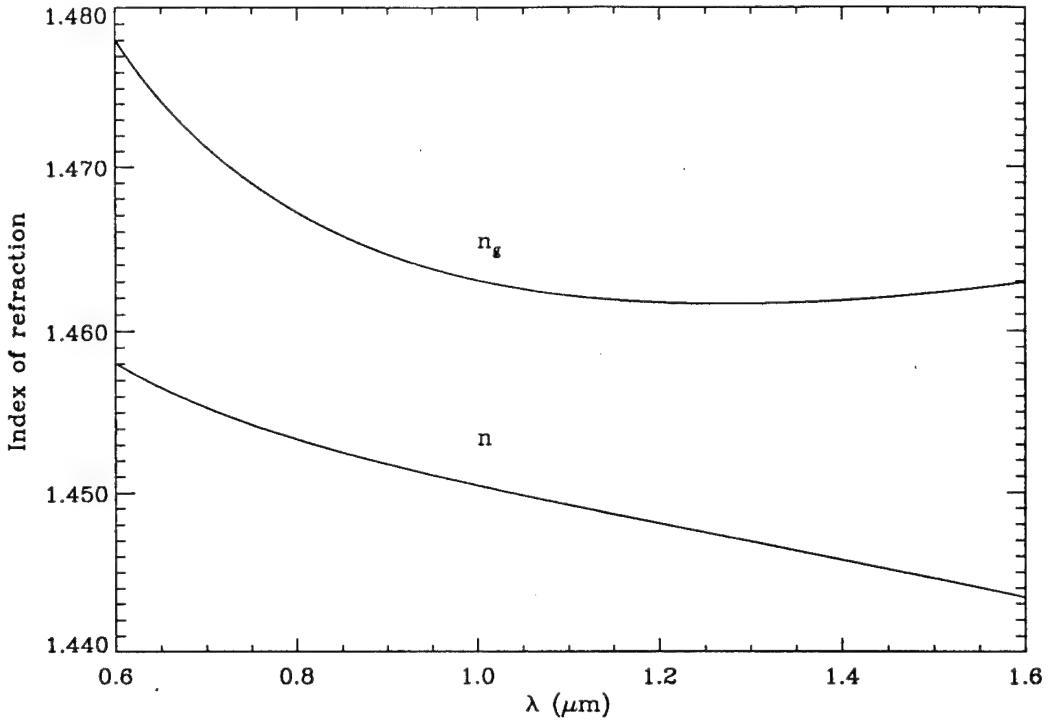

Figure 1.1: Index of refraction and group index of pure silica.

is defined which has dimensions of ps/nm-km. D is called the dispersion coefficient, as it describes how the inverse group velocity varies with respect to wavelength; often it is expressed in terms of its variation with respect to frequency ω, in which case its dimensions are ps^2/km. In terms of n,

$$D = -\frac{\lambda}{c}\frac{d^2n}{d\lambda^2}, \tag{1.3}$$

where D is plotted versus λ in Fig. 1.2. Note that the dispersion coefficient (and the slope of the group index) changes sign around 1.28 μm. For wavelengths greater than 1.28 μm, pulses with higher frequencies travel faster than pulses with lower frequencies, while the opposite occurs at wavelengths shorter than 1.28 μm. Two regimes of dispersion are defined accordingly — dispersion is anomalous when D is positive and dispersion is normal when D is negative.

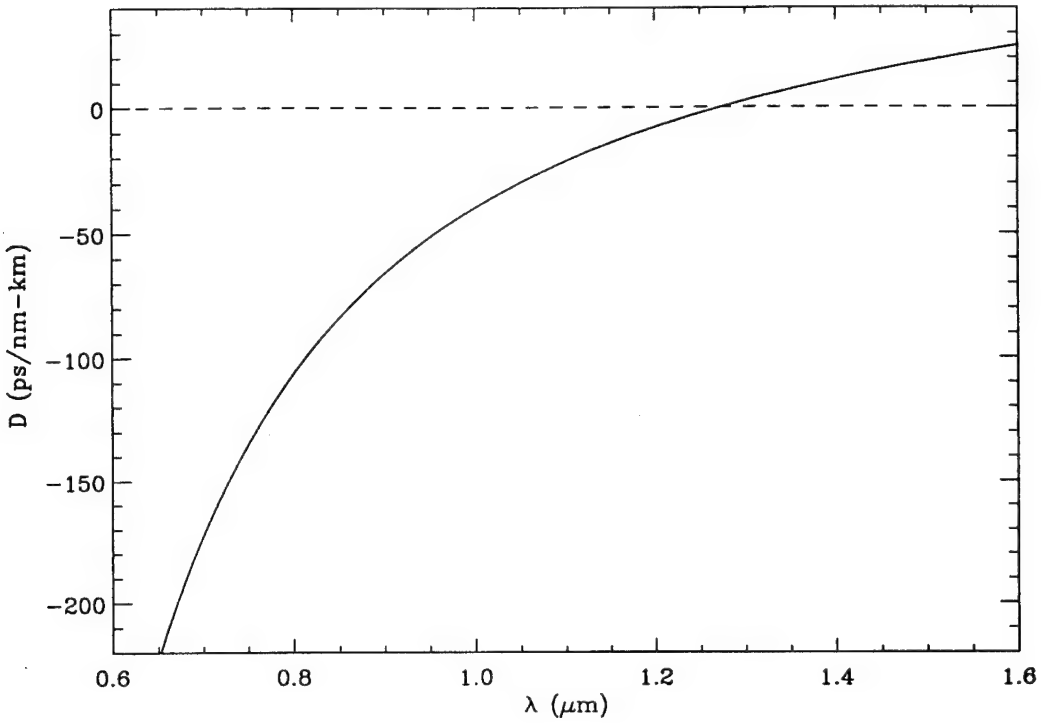

Figure 1.2: Dispersion coefficient in pure silica.

Soliton communication in fiber almost always takes place in the anomalous regime. Note that the variation in the dispersion coefficient is approximately linear in this regime. In fiber, dispersion associated with the waveguide geometry can be used to translate the point of zero dispersion to values around 1.55 μm, the wavelength where loss is minimized in silica fiber. Such a fiber, known as a dispersion shifted fiber, is the type most commonly used for soliton communication for reasons we shall see later.

To understand the effect of GVD on a pulse, solving Maxwell's equations shows that each spectral component in single mode fiber propagates according to[2],

$$\tilde{E}(z,\omega) = \tilde{E}(0,\omega)\exp(i\beta z). \tag{1.4}$$

$\tilde{E}(0,\omega)$ is the initial spectral representation of the wave which propagates down the longitudinal dimension z of the fiber with propagation constant β. We have assumed that the light is linearly polarized and that the field in the transverse dimensions x and y corresponds to the fundamental fiber mode, oftentimes approximated by a Gaussian distribution. The temporal variation of the longitudinal scalar field is given by the inverse Fourier transform of $\tilde{E}(z,\omega)$,

$$E(z,t) = \frac{1}{2\pi}\int_{-\infty}^{\infty} \tilde{E}(z,\omega) exp(-i\omega t) d\omega. \tag{1.5}$$

If the wave is actually a pulse having an envelope which varies slowly with respect to an optical carrier with frequency ω_o and wavelength λ_o, then the field is represented by

$$E(z,t) = F(z,t)\exp[-i(\omega_o t - \beta_o z)], \tag{1.6}$$

where $F(z,t)$ describes the variation of the envelope in time and space and $\beta_o = 2\pi n_o/\lambda_o = n_o k_o$. The group index of refraction at ω_o is n_o. Since the envelope varies slowly in time, the spectral bandwidth is small and the wavenumber β may be written as a Taylor expansion about ω_o,

$$\begin{aligned} \beta - \beta_o &= \left.\frac{\partial\beta}{\partial\omega}\right|_{\omega_o}(\omega-\omega_o) + \frac{1}{2}\left.\frac{\partial^2\beta}{\partial\omega^2}\right|_{\omega_o}(\omega-\omega_o)^2 + \ldots \\ &\approx \beta_1(\omega-\omega_o) + \frac{\beta_2}{2}(\omega-\omega_o)^2. \end{aligned} \tag{1.7}$$

The first and second derivatives of β around the frequency at ω_o are represented as β_1 and β_2. Higher order terms are neglected in a slowly varying envelope approximation when pulse widths are on the order of picoseconds and when the center wavelength λ_o is not too close to the zero dispersion point (1.31 μm in a standard telecommunications fiber). At λ_o, the group velocity is $v_g = 1/\beta_1$

and the dispersion coefficient is related to β_2 by

$$D = -\left(\frac{2\pi c}{\lambda_o^2}\right)\beta_2. \tag{1.8}$$

By solving for $F(z,t)$ in Eq. (1.6) and substituting for $E(z,t)$ from Eq. (1.5) and for $\tilde{E}(z,\omega)$ from Eq. (1.4),

$$F(z,t) = \frac{1}{2\pi}\int_{-\infty}^{\infty} \tilde{E}(0,\omega)\exp[i(\beta-\beta_o)z - i(\omega-\omega_o)t]d\omega. \tag{1.9}$$

It can be seen from Eq. (1.9) that $\beta-\beta_o$ and $\omega-\omega_o$ may be replaced by operators $-i\,(d/dz)$ and $i\,(d/dt)$, respectively, so that Eq. (1.7) may be rewritten (upon multiplication by F) as the propagation equation of the pulse,

$$-i\frac{\partial F}{\partial z} = i\beta_1\frac{\partial F}{\partial t} - \frac{\beta_2}{2}\frac{\partial^2 F}{\partial t^2}. \tag{1.10}$$

If $\beta_2 = 0$, then $F(z,t) = F(0, t-\beta_1 z)$ and the pulse travels without any change in shape.

Typically, Eq. (1.10) is translated into the coordinate frame of the pulse moving at group velocity v_g by a transformation of variables $t-\beta_1 z \rightarrow t$. In the moving reference frame, Eq. (1.10) becomes

$$i\frac{\partial F}{\partial z} = \frac{\beta_2}{2}\frac{\partial^2 F}{\partial t^2}. \tag{1.11}$$

The origin in t is now always at the center of the pulse. When $\beta_2 \neq 0$, the phase in Eq. (1.4) changes differently for individual spectral components as z increases since β is a function of ω. While such changes affect only phase in the spectral domain, the pulse shape is modified in the time domain. In the anomalous dispersion regime ($\lambda_o > 1.28$ μm in Fig. 1.1), the pulse develops a chirp as it propagates, with higher frequencies moving to the front of the pulse and lower frequencies moving to the back. The chirp degrades data communications if

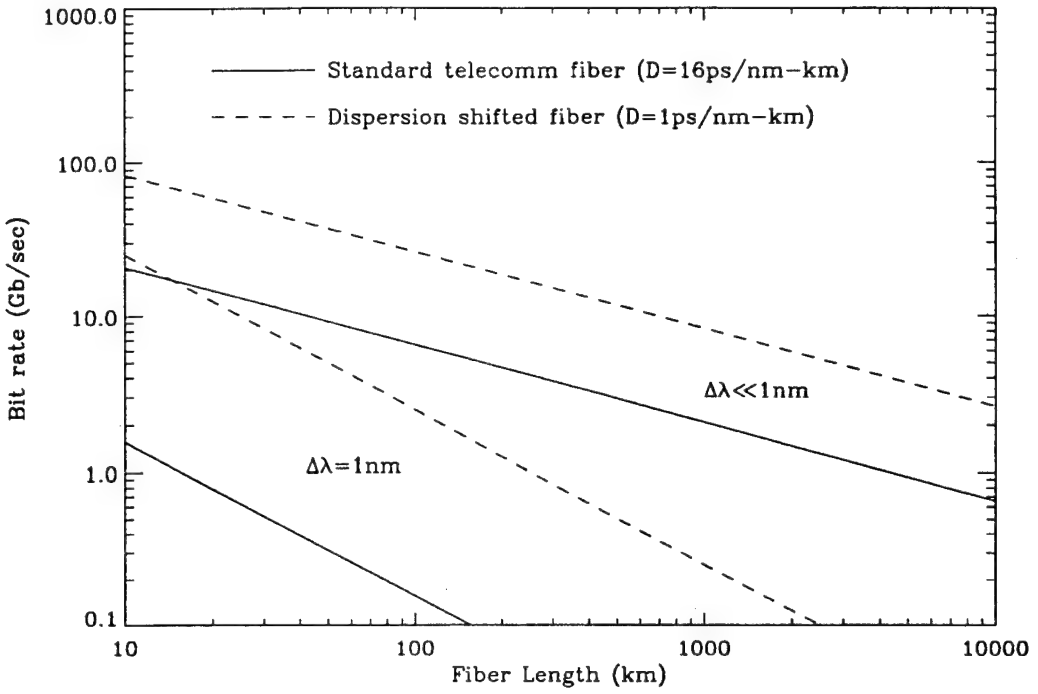

Figure 1.3. Dispersion limited bit rates for given fiber lengths at a wavelength of 1.55 μm.

individual bits disperse into neighboring bits time slots. Figure 1.3 depicts the maximum bit rate for a given fiber length limited by dispersive effects under several conditions. The solid curves depict the allowable bit rates in a standard telecommunications fiber at 1.55 μm with $D = 16$ ps/nm-km when the linewidth $\Delta\lambda$ of the source dominates ($\Delta\lambda = 1$ nm) and when the pulses are transform limited ($\Delta\lambda \ll 1$ nm). The dashed curves describe propagation in a dispersion shifted fiber with $D = 1$ ps/nm-km[2].

1.1.2 Fiber nonlinearity In a nonlinear dispersive medium, the refractive index is dependent on the intensity I and the frequency of the light,

$$\overline{n}(\omega, I) = n(\omega) + n_2 I. \tag{1.12}$$

The index at ω_o approaches n_o as I approaches zero. The nonlinear coefficient n_2 is related to $\chi^{(3)}$, the nonlinear susceptibility tensor which is used to determine the nonlinear component of the polarization vector in Maxwell's equations[3]. Since $\beta = \overline{n}(\omega)\omega/c = \overline{n}(\omega)\, k$, the expansion in Eq. (1.7) must now include an additional term describing the nonlinearity

$$\beta - \beta_o = \beta_1(\omega - \omega_o) + \frac{\beta_2}{2}(\omega - \omega_o)^2 + k_o\, n_2\, I. \tag{1.13}$$

In a derivation analogous to that for Eq. (1.11), the equation describing propagation in a purely nonlinear medium when $\beta_2 = 0$ is

$$i\frac{\partial F}{\partial z} = -\gamma\, |F|^2\, F. \tag{1.14}$$

The factor $\gamma = k_o\, n_2/A_{\text{eff}}$ and $A_{\text{eff}} = \pi r^2$ is the effective area of a propagating mode with radius r. In a dispersion shifted single mode fiber, r is usually around 4 μm, so A_{eff} is typically about 50 μm^2. The nonlinear coefficient in silica fiber is $n_2 = 3.2 \times 10^{-16}$ cm^2/W, so $\gamma = 2.6$ (W-km)$^{-1}$ at 1.55 μm.

The solution of Eq. (1.14) is

$$F(z,t) = F(0,t)\, \exp[i\phi_{\text{nl}}(z,t)], \tag{1.15}$$

where $F(0,t)$ is the initial field and the nonlinear phase factor is

$$\phi_{\text{nl}}(z,t) = \gamma\, |F|^2\, z = k_o\, n_2\, I\, z. \tag{1.16}$$

By substituting Eq. (1.15) into Eq. (1.6), the full phase of the wave is $\phi = \omega_o t - \beta_o z - \phi_{\text{nl}}(z,t)$. Since the instantaneous frequency equals the time derivative of the phase, the instantaneous frequency across the pulse is

$$\omega = \frac{\partial \phi}{\partial t} = \omega_o - k_o\, n_2 \frac{\partial I}{\partial t}\, z, \tag{1.17}$$

and the pulse is chirped as it propagates. For propagation in the positive z direction and with positive n_2, the instanteous frequency is smaller than ω_o on the rising edge of the pulse where $\partial I/\partial t$ is positive, while it is greater than ω_o on the trailing edge where $\partial I/\partial t$ is negative. Hence, as z increases, lower frequencies move to the front of the pulse and higher frequencies move to the back. The intensity of the pulse itself modulates the phase and causes the chirp. Hence, the name given to this nonlinear effect is self-phase modulation(SPM). Note also from Eq. (1.17) that more and more frequencies are added to the spectrum of the pulse as z gets larger. SPM is a nonlinear dispersive effect, but the dispersion takes place in the spectral domain; the temporal pulse envelope in Eq. (1.15) maintains its shape for all z if we assume that $D = 0$ ps/nm-km.

1.1.3 Temporal solitons By themselves, GVD and SPM degrade communications in the fiber. When occurring together, an interesting phenomenon results. Figure 1.4 depicts the behavior of each effect by itself and the result when both occur. The top plot depicts the chirp resulting from SPM in a medium having a positive n_2. Lower frequencies move to the front of the pulse and higher frequencies move to the back. In the second plot, the chirp of a pulse under the effect of anomalous GVD is illustrated; the chirp is opposite that due to SPM. If the intensity of a pulse is chosen properly in a medium exhibiting both GVD and SPM, these effects balance as shown in the third plot. No chirp results and no pulse degradation takes place. Such a pulse is a temporal soliton — a solitary wave bound in time.

The equation describing soliton propagation is the combination of Eqs.(1.11) and (1.14),

$$i\frac{\partial F}{\partial z} = \frac{\beta_2}{2}\frac{\partial^2 F}{\partial t^2} - \gamma |F|^2 F. \tag{1.18}$$

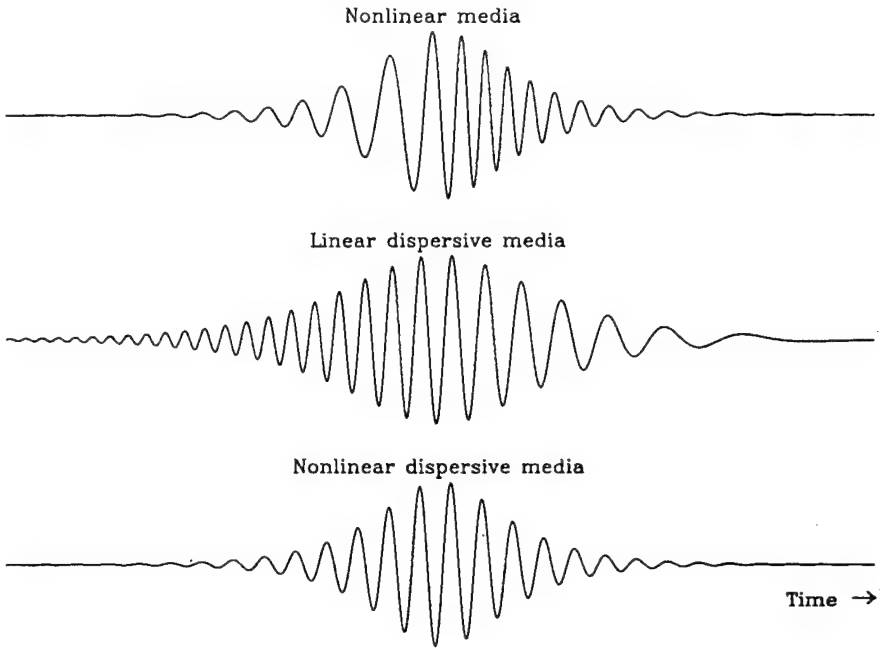

Figure 1.4. Pulse chirp after propagation in a dispersive, nonlinear, and nonlinear dispersive medium.

It is usually more convenient to describe solitons with this equation by normalizing so that the equation is dimensionless. The time, space, and amplitude are scaled in terms of soliton units t_c, z_c, and $\sqrt{P_o}$:

$$\frac{t}{t_c} \rightarrow t \tag{1.19}$$

$$\frac{z}{z_c} \rightarrow z \tag{1.20}$$

$$\frac{F}{\sqrt{P_o}} \rightarrow u. \tag{1.21}$$

The factors z_c and P_o are the soliton characteristic length and peak power, respectively, as defined by

$$z_c = -\frac{t_c^2}{\beta_2} \tag{1.22}$$

$$P_o = -\frac{\beta_2}{\gamma t_c^2}, \tag{1.23}$$

where t_c is the half-width of the soliton at amplitude $\sqrt{P_o}\text{sech}(1)$. Since P_o is the soliton peak power, P_o/A_{eff} is the peak intensity required to exactly balance the effects of GVD and SPM. Different variables could be chosen to represent z and t at this point, but such a convention is confusing. Let it suffice that any mathematical equations involving an amplitude u will immediately indicate that dimensionless quantities are being used in all parameters including time and space. If the meaning of t and z are unclear, their meaning will be explicitly stated. (Recall that the variable t was already renamed in Eq. (1.11) so that the full transformation at this point is $\frac{t-\beta_1 z}{t_c} \rightarrow t$).

The dimensionless propagation equation is known as the nonlinear Schrödinger equation(NLSE) and is written

$$-i\frac{\partial u}{\partial z} = \frac{1}{2}\frac{\partial^2 u}{\partial t^2} + |u|^2 u. \tag{1.24}$$

The general solution to the NLSE[3] is a fundamental soliton,

$$u(z,t) = A\,\text{sech}[A(t - t_o + \Omega z)]\exp[-i\Omega t + i(A^2 - \Omega^2)z/2 - i\phi_o]. \tag{1.25}$$

The parameters A, Ω, t_o, and ϕ_o are variables defining a normalized peak amplitude (inverse pulse width), a normalized frequency (inverse group velocity), an initial time and an initial phase. For convenience, we can assume the initial time and phase are zero and that $A = 1$, so that

$$u(z,t) = \text{sech}[t + \Omega z]\exp[-i\Omega t + i(1 - \Omega^2)z/2]. \tag{1.26}$$

If $A = 1$, the normalized peak amplitude and pulse width are both unity, so the actual peak power of the soliton is P_o and its physical pulse width is t_c, using Eqs. (1.19) and (1.21). A soliton mathematically scaled according to Eqs. (1.19-1.23), but having a pulse width and amplitude different than t_c and

$\sqrt{P_o}$, would require $A \neq 1$. Since the pulse width t_c is the "half-width" of the soliton, the soliton physically takes the form of $\sqrt{P_o}\,\mathrm{sech}(t/t_c)$. The soliton width is more commonly described by the full width at half the maximum intensity(FWHM), given by $\tau = 1.763\,t_c$.

Figure 1.5 illustrates the evolution of the soliton pulse envelope in the normalized reference frame, as in Eq. (1.26) with $\Omega = -10$; the envelope is similar to a Gaussian pulse. Since the spatial dimension of the soliton is scaled by the characteristic length z_c, a soliton that has travelled one spatial unit as in Fig. 1.5 has travelled a physical distance of z_c. This corresponds to the length over which a Gaussian pulse of width t_c would disperse to a width $\sqrt{2}\,t_c$ because of first order dispersion β_2. The soliton period $z_o = (\pi/2)z_c$ is the parameter more commonly chosen to describe soliton propagation. Figure 1.6 depicts the variation of P_o and z_o in a dispersion shifted fiber with $D = 1$ ps/nm-km. The soliton period z_o decreases and the fundamental soliton power P_o increases in a more dispersive fiber as defined by Eqs. (1.22) and (1.23). We will mostly be concerned with solitons having pulse widths greater than 10 ps and periods greater than 100 km, which require peak powers on the order of milliwatts. Propagation of higher order solitons takes place whenever P_o is greater than the fundamental soliton power. The propagation of such pulses is more complicated and their evolution is periodic with respect to z_o as we shall see in Section 1.3.4.

The meaning of Ω in Eq. (1.26) is most easily described by analyzing the spectral domain. When $\Omega = 0$, the frequency of the soliton is identical to the physical frequency ω_o and the corresponding group velocity of the reference frame. Different values of Ω correspond to solitons with frequencies and group

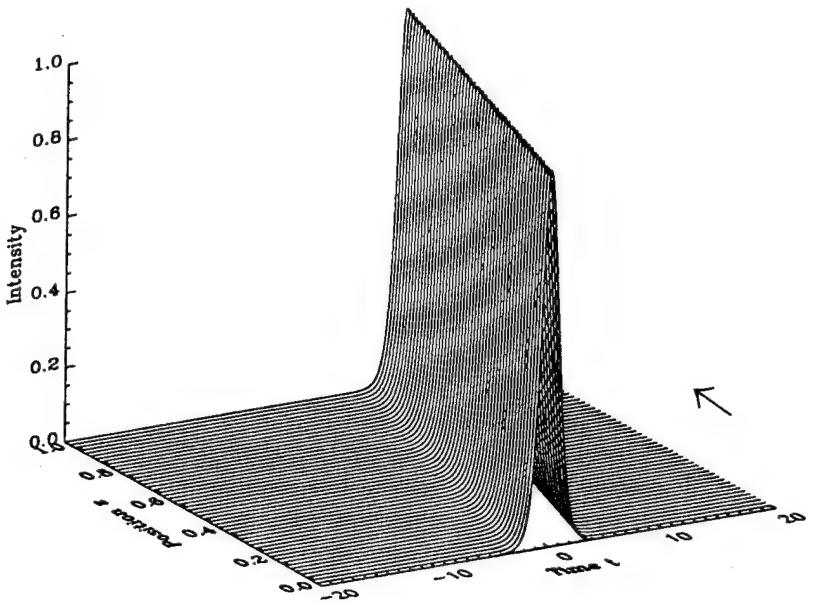

Figure 1.5: Envelope of soliton intensity in time and space.

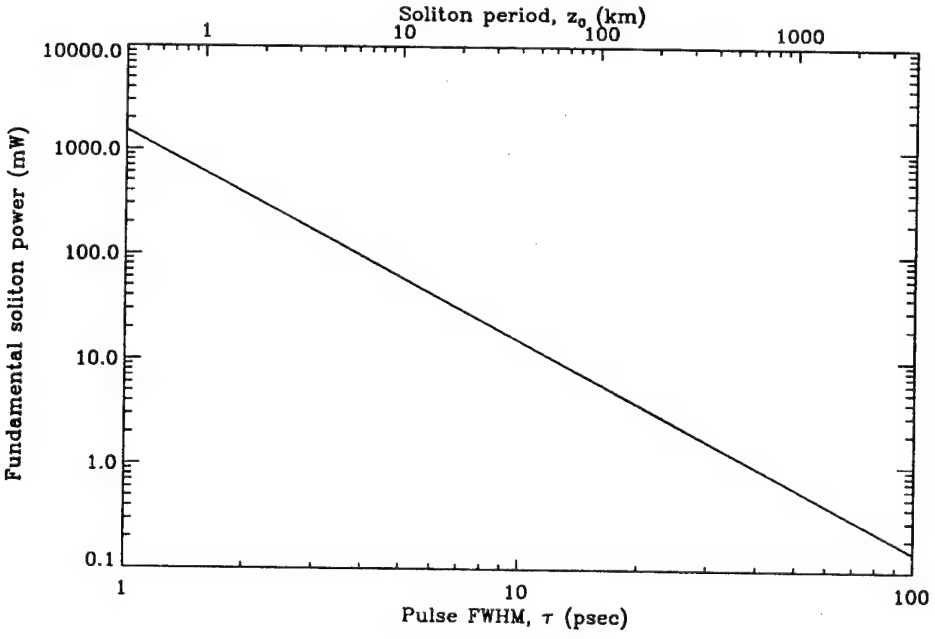

Figure 1.6. Fundamental soliton peak power required at the given soliton pulse width and period when $D = 1$ ps/nm-km.

velocities different than that of the moving reference frame. This is especially useful to understand since the primary thrust of this thesis is to analyze solitons multiplexed by frequency. The Fourier transform of the soliton envelope is

$$\tilde{u}(z,\omega) = \int_{-\infty}^{\infty} u(z,t)\exp(i\omega t)dt, \tag{1.27}$$

where $u(z,t)$ is the normalized solution of the NLSE given in Eq. (1.26), such that ω now refers to radial frequency in a normalized frequency domain. With a change of variables, $s = t + \Omega z$, Eq. (1.27) becomes

$$\tilde{u}(z,\omega) = \exp(i\Phi)\int_{-\infty}^{\infty} \mathrm{sech}(s)\exp[i(\omega-\Omega)s]ds, \tag{1.28}$$

where $\Phi = (1 - 2\Omega\omega + \Omega^2)z/2$. Since

$$\mathrm{sech}(a\,s) \quad \overset{\mathcal{F}}{\leftrightarrow} \quad \tfrac{\pi}{a}\,\mathrm{sech}[\pi\,\omega/(2\,a)], \tag{1.29}$$

then

$$\tilde{u}(z,\omega) = \pi\,\mathrm{sech}[\pi(\omega-\Omega)/2]\exp(i\Phi). \tag{1.30}$$

Thus, the spectrum of $u(z,t)$ consists of a single spectral peak at $\omega = \Omega$.

To scale ω back into a physical frequency, we divide by t_c, so

$$\Omega/t_c = 2\pi\Delta f, \tag{1.31}$$

where the frequency of the normalized peak at Ω is different than the physical reference frequency ω_o by Δf in Hz. The normalized half width of the spectral peak in Eq. (1.30) is $2/\pi$, so the physical half width in rad/s is $2/(\pi t_c)$. Since half widths are changed to the FWHM by the factor 1.763 (recall that $\tau = 1.763\,t_c$), the time-bandwidth product of a soliton is

$$\tau\,\delta\nu = 0.315, \tag{1.32}$$

where $\delta\nu$ is the spectral FWHM of a soliton having a pulse width of τ. Figure 1.7 illustrates the corresponding spectral evolution of the soliton in Fig. 1.5 for $\Omega = -10$. Since Ω also represents an inverse group velocity in Eq. (1.26), the pulse moves 10 time units backwards for each spatial unit; the inverse group velocity of the pulse is physically $v_g^{-1} = \beta_1 + \beta_2(\Omega/t_c)$. The dispersion parameter β_2 is negative in the anomalous dispersion regime, so if $\Omega = -10$, the pulse moves slower than the reference frame, consistent with Fig. 1.5. For example, when $t_c = 28$ ps and $\tau = 50$ ps, the pulse is delayed ten normalized time units or 280 ps with respect to the moving frame in Fig. 1.5. The frequency of the soliton is less than ω_o by $\Delta f = 57$ GHz and its spectral width is $\delta\nu = 6.3$ GHz. If the wavelength corresponding to the reference frame is $\lambda_o = 1.55$ μm, the

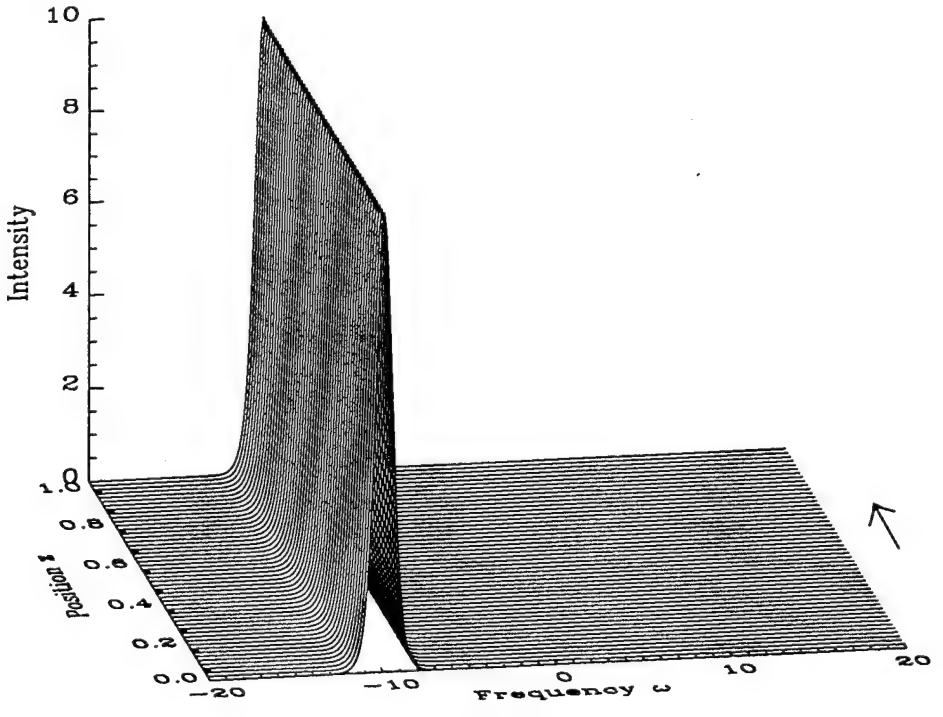

Figure 1.7: Spectral evolution in space of a soliton with $\Omega = -10$.

wavelength of the pulse is larger by 0.46 nm (since $0.46 = 57\,(1550)^2/(3\times10^8)$).

A word should be said here about other conventions oftentimes used to describe soliton propagation. The convention that is probably used most often is in the literature relating to applied mathematics[4, 5]. The form of the NLSE is somewhat different;

$$-i\frac{\partial u}{\partial t} = \frac{\partial^2 u}{\partial z^2} + 2\,|u|^2\,u, \tag{1.33}$$

and its solution is

$$u(z,t) = 2\eta \mathrm{sech}[2\eta(z - 4\xi t - z_o)]\exp[i2\xi z + i4(\eta^2 - \xi^2)t - \phi_o]. \tag{1.34}$$

Time and space are swapped in this solution relative to Eq. (1.25), and time evolves twice as quickly in the normalized frame. This solution also has four parameters, η, ξ, z_o and ϕ_o, related to the soliton amplitude, frequency, initial position, and initial phase. The parameters η and ξ correspond to $A/2$ and $\Omega/2$, respectively. The quantity $\zeta = \xi + i\eta = \Omega/2 + iA/2$ is the eigenvalue associated the Inverse Scattering Transform(IST) algorithm[4]. The IST is a nonlinear transformation of either the time or spectral domain to a scattering domain, in which exact analytical solutions are obtained for a group of physically important nonlinear partial differential equations, one of which is the NLSE. Previous research[6, 7] has shown that data may be encoded onto invariant parameters associated with the soliton eigenvalue. The encoding of data on the imaginary part of the eigenvalue will be discussed briefly in Section 1.3.4. Understanding the system behavior when data is encoded on the real part of the eigenvalue is the primary focus of this thesis.

1.2 Solitons for data communications

A more intuitive understanding of soliton propagation is gained by considering how a fiber guides light. The index of refraction in the center (or the core) of the fiber is higher than that in the outer region (the cladding). Total internal reflection acts to guide the light down the fiber. The fundamental transverse mode of the fiber is dependent on the index gradient in the transverse dimension. In a similar manner, the sech^2 intensity profile of the soliton creates an index gradient through the Kerr effect in Eq. (1.12) for which the pulse itself is the fundamental propagating mode. It is as though the soliton has created its own waveguide to propagate in. A temporal soliton is in effect a "temporal waveguide", as opposed to a typical waveguide that guides energy spatially.

This analogy helps explain restrictions on communicating with solitons. For instance, when two waveguides are brought too close to one another, it is possible for coupling to occur. Similar effects occur when solitons of the same wavelength are too near one another in time; solitons attract or repel one another depending on their relative phases[8, 9, 10]. In Fig. 1.8, two solitons, each with $\Omega = 0$, attract and form a bound pair because they are in phase; in Fig. 1.9, the solitons repel because they are out of phase. If either pulse were isolated, it would propagate at the same velocity as the reference frame. To prevent these interactions, the bit periods used in soliton communications must be somewhat larger than the pulse width τ; bit periods of $T = 5\tau$ are typically suggested[11]. Since soliton data is usually amplitude-shift keyed, it must be encoded in a return-to-zero (RZ) format (see Fig. 1.10) to prevent intersymbol interference. As an example, communications with solitons having 20 ps pulse widths might be limited to a maximum data rate of 10 Gb/s. The

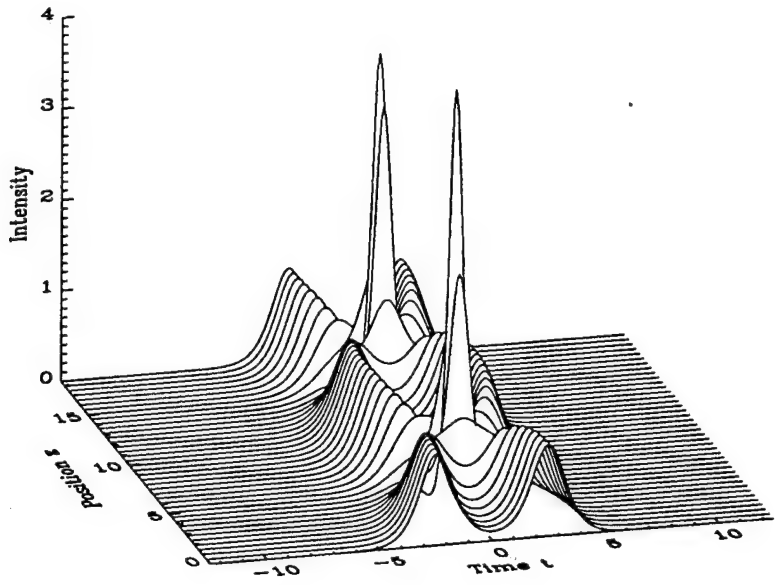

Figure 1.8. Attraction and oscillation of two solitons with initially identical velocities and relative phase of zero.

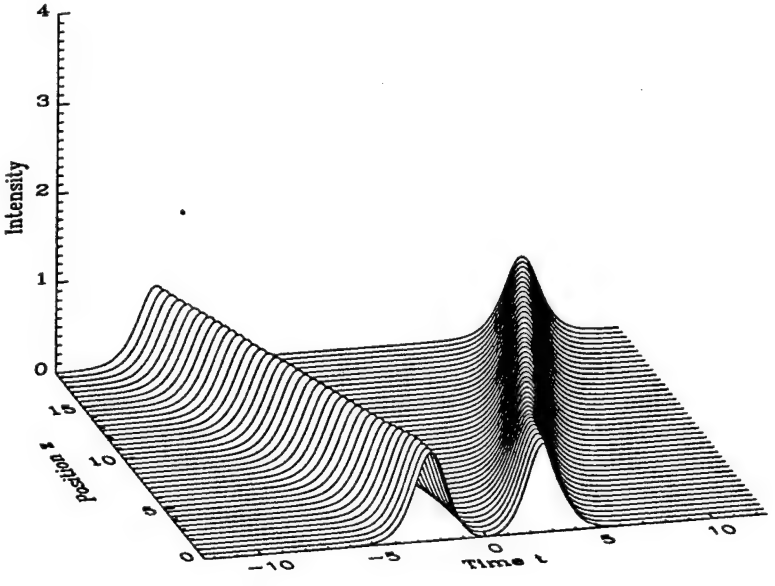

Figure 1.9. Repulsion of two solitons with initially identical velocities and relative phase of π.

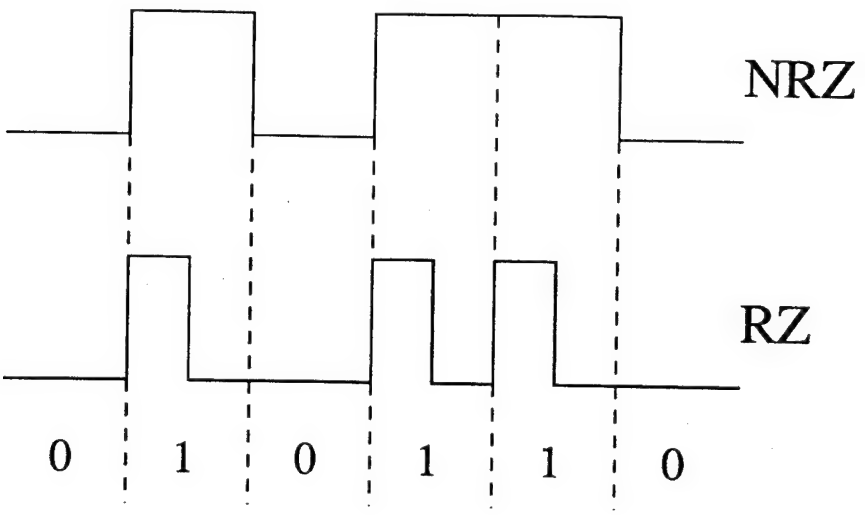

Figure 1.10: NRZ and RZ data encoding formats.

separation between the pulses in Figs. 1.8 and 1.9 is only 2.8τ.

Other phenomena potentially limit soliton communications as well. The soliton self-frequency shift is a process by which the soliton frequency downshifts upon propagation due to the Raman effect[12]. The shift is strongly dependent on the Raman gain bandwidth and is only significant if τ is less than a picosecond and the spectral bandwidth is large. Higher order dispersion was neglected in Eq. (1.7) and also becomes important if pulse widths are small. At very long distances it is possible for acoustic effects[13] or polarization mode dispersion[14] to limit data transmission. Acoustic effects result because each soliton creates a shock wave through electrostriction which resonates in the transverse dimension of the fiber, affecting trailing solitons. Birefringence is small enough in standard fiber to be ignored in the derivation of the NLSE[15] so polarization effects are usually minimal. In fact, solitons may be multiplexed on orthogonal polarizations in weakly birefringent fibers[16]. This allows pulses to be spaced possibly as close as 2.5τ, doubling the data rate.

For pulse widths larger than 1 ps, the most important restrictions on

soliton communication are related to the process of loss and amplification. Generally, soliton propagation is quite robust in the presence of amplifiers[17, 18]. In fact, the amplitude may vary somewhat from its fundamental intensity using lumped amplifiers while maintaining a soliton-like behavior[19, 20, 21]. However, if the soliton period z_o is on the same order of magnitude or smaller than the separation between amplifiers, the soliton energy behaves chaotically because of a resonance between the soliton phase and the amplifier period[18]. Since amplifiers are typically separated by 50 km or less[11], this effect becomes important when the pulse width is less than 10 ps (see Fig. 1.6). A more serious problem results when amplified spontaneous emission(ASE) noise causes fluctuations in the soliton energy[11] and the soliton frequency. The resulting jitter in pulse arrival times is commonly referred to as the Gordon-Haus effect[22] and significantly limits the length of the system, even for pulse widths greater than 10 ps. The effect is decreased by spacing the amplifiers closer together so that the gain of each amplifier is smaller.

Most of these effects are also reduced by propagating in less dispersive fibers. Thus, soliton communications usually takes place in dispersion shifted fibers around 1.55 μm. The dispersion coefficient D in such fibers is usually around 1 ps/nm-km at a wavelength of 1.55 μm. While several other techniques have been suggested to reduce the effects of ASE noise[23, 24, 25], filtering has become the most popular[26, 27]. Bandpass filters are placed along the system at each amplifier, and the center frequency of each filter is chosen to match the frequency of the soliton. The filters act to limit any shifts in the soliton frequency and reduce the jitter in the soliton arrival time at the end of the fiber. They also provide better control over soliton power. The most recent

breakthrough in the application of filter technology is the sliding-frequency guiding filter[28, 29]. By translating the center frequency of each filter slowly (approximately 10 GHz translation over 1000 km), noise is suppressed that could potentially grow under a fixed frequency filter. Solitons are robust enough to adapt their frequency and velocity to the change in the filter frequency. Standard linear pulses are unable to adapt to the sliding effect, and cannot be used in such a system. Sliding filters have been used to transmit solitons at rates of 10 Gb/s in a single channel across 20000 km[30] and at a combined rate of 20 Gb/s across 13000 km in a two channel WDM soliton transmission[31]. They will probably be useful for more extensive WDM[32].

1.3 Other soliton applications

Solitons were first observed physically in 1834. A canal boat stopped, and a Scottish experimentalist, J. Scott Russell, saw "a large solitary elevation, a rounded, smooth and well defined heap of water, which continued its course along the channel, apparently without change of form or diminution of speed"[33]. Russell followed the wave for one or two miles before losing sight of it. The mathematics of his observation were not understood, though, until the turn of the century, when the Korteweg-deVries(KdV) equation was derived[34]. It required another 78 years before the application of solitary waves were found to be supported by the NLSE in optical fiber[35]. This was preceded one year earlier by the first solution of the NLSE using the IST[36].

Solitons were eventually observed experimentally in fiber[37]. This required the development of fibers with low enough loss in the anomalous dispersion regime and a pulsed optical source with enough energy at the appropriate wavelengths. The application of solitons to communications has now

progressed to the point that they have been propagated across distances as long as a million kilometers[1] and at data rates as high as 80 Gb/s[38]. It is possible that the next transoceanic fiber cable will use solitons[39]. However, solitons are being applied in other interesting ways to communications and computing.

1.3.1 Optical switching in fiber Solitons are ideal candidates for use in all-optical switching technologies because their spectrum and phase is conserved after collisions with other solitons. Most switching applications with solitons use polarization maintaining birefringent fiber. Two solitons are encoded on the orthogonal polarizations of the fiber and interact because of cross-phase modulation (CPM), which is mathematically described by a coupled NLSE. CPM occurs because the intensity of a soliton on one polarization (or wavelength) affects the index of refraction seen by a soliton on the orthogonal polarization (or a different wavelength). The interactions cause frequency or timing shifts that may be used for switching. Two examples are soliton dragging and soliton trapping[40].

Soliton trapping takes place when the pulse walk-off due to polarization dispersion is balanced by an attractive force due to CPM. The intensity of each soliton effectively creates a potential well that the other soliton prefers to propagate in. The soliton on the slow axis speeds up and the soliton on the fast axis slows down and the solitons propagate as a single entity. The corresponding wavelengths move towards one another by equal amounts if the intensities of the solitons are identical. A filter centered at the frequency between the two solitons at the output of the fiber passes a signal only if both solitons are present, implementing an AND gate. Such gates demonstrate neither gain nor

are they cascadable, but can achieve contrast ratios as large as 22:1 with 46 pJ switching energy at a switching rate of 0.35 THz[41].

The velocity shift during the interaction between orthogonally polarized solitons also causes a displacement in time. Soliton dragging operates on this principle, but is more general than trapping since the solitons intensities can be different. To implement a NOR gate, signals A and B on identical polarizations are injected into the fiber at different times and interact with a control pulse C on the orthogonal polarization. If either A or B are present, the control pulse C will be shifted out of its timing window if the data is encoded in a time-shift-keyed format. The gate could theoretically implement a NAND gate because the control pulse will shift twice only if both pulses were present, although the pulse synchronization would need to be controlled very precisely. Soliton dragging gates have been used as inverters with switching energies as low as 1 pJ[42]. Dragging gates fulfill all the requirements of a digital optical logic gate. They have gain because a small pulse controls the timing of a larger pulse. They are cascadable and logically complete. The time-shift keyed output of a dragging gate can be converted into an amplitude-shift keyed format by cascading a trapping gate after the dragging gate[40].

One drawback of such gates is their latency. The fiber lengths required for the pulses to interact are relatively long, so the gates would primarily be used in pipelined, feed-forward communications architectures. Such an application was proposed recently in a soliton ring network[43]. The proposed network was a wide area network operating at peak bit rates of 100 Gb/s with several hundred users. Several other switching applications using solitons in fiber are

possible. Switches have been proposed using Sagnac interferometers[44], helically evolving solitons in periodically twisted birefringent fiber[45, 46], twin-core fiber rocking filters[47], and directional couplers[48, 49].

1.3.2 Optical logic gates using spatial solitons By replacing t in Eqs. (1.24) and (1.25) with the spatial variable x, it is possible to describe the propagation of a solitary wave that is spatially bound, instead of temporally bound. Such a laterally confined beam is a spatial soliton. The beam is "self-trapped" because of the balance between linear diffraction and self-focusing. Diffraction is the spatial analog of temporal dispersion and self-focusing is the analog of self-phase modulation. The intensities required to balance these effects are often quite large, and research is being conducted to find materials with large nonlinear coefficients so that the intensities can be reduced. Two such beams propagating at different angles with respect to one another, while experiencing a displacement in space at their collision, maintain their direction of propagation apart from the collision. It was predicted[50] that such an interaction may be used for switching. Further experimental results[51] demonstrate that parallel channels separated by two beam widths can also interact depending on their relative phase, similar to the behavior in a fiber depicted in Figs. 1.8 and 1.9. The beams attract when in phase, forming a bound pair that oscillate about one another periodically, and repel when π out of phase. Spatial soliton interactions are especially important because they typically occur over short distances, with low latency. An example of a tri-state device based on repulsive effects between spatial solitons has been proposed that requires interaction lengths less than a millimeter[52].

Another interesting application is related to the fact that an interference pattern forms at the center of a collision between two spatial solitons[53]. The interference pattern generates an index grating that splits the energy of a weak probe beam that propagates within one of the two solitons. The efficiency of the diffractive effect is dependent on the angle between the two spatial solitons and their relative phase. With a properly chosen angle and phase relationship, the diffraction is highly efficient, with most of the probe beam energy being switched to the opposite spatial soliton channel. It is also possible to control the diffraction by changing the wavelength of the probe beam.

Phase dependent switching, though, has negative implications in computing or communications since phase can be difficult to maintain. It might be possible to avoid phase problems by encoding the interacting solitons on orthogonal polarizations. One proposed technique is analogous to temporal soliton dragging. Asymmetric spatial soliton dragging[54] takes place when two orthogonally polarized spatial solitons with unequal intensities overlap at the interface to a nonlinear medium. Although the pulses are travelling in different directions initially, the weaker of the two pulses is able to drag the larger by over a beam width so that it no longer passes through a spatial aperture. In analogy to temporal dragging in fiber, the interaction takes place because of cross-phase modulation between orthogonal polarizations. Such a device has gain, is fully cascadable, and can be implemented as a logically complete NOR gate. An extension of the spatial soliton is the possibility that packets of energy can be bound in all dimensions of space and time[55]. These so called "light bullets" could interact in similar ways to those suggested above but might require less energy due to their spatial confinement. While such entities are

now possible only in theory, spatial solitons are fascinating and require more research to fully assess their usefulness in computing and communications.

1.3.3 Dark solitons The soliton in Eq. (1.25) is often called a bright soliton and propagates because of a balance between anomalous GVD and SPM. In the anomalous regime, the chirp resulting from GVD was negative and the instantaneous frequency across the pulse in Fig. 1.4 decreased. The chirp resulting from SPM using Eq. (1.17) was positive because of the sign of n_2 and the derivative of the intensity profile. The two effects balanced and a bright soliton formed. In the normal dispersion regime, the chirp of the pulse due to GVD is opposite that shown in Fig. 1.4, and the instantaneous frequency across the pulse increases due to both GVD and SPM. No soliton forms because the effects of GVD and SPM cannot balance. However, a different kind of soliton can still propagate in the normal dispersion regime. Such a pulse is called a dark soliton. A dark soliton is simply a dark pulse on a bright continuous wave (CW) background. The pulse propagates without dispersing.

A dark soliton is formed because a positive chirp due to GVD can still be balanced by a negative chirp due to SPM. Both effects must be opposite that in Fig. 1.4. Since n_2 is positive in both dispersion regimes, the nonlinearity only creates a negative chirp in Eq. (1.17) if the intensity in the leading edge of the pulse decreases while increasing in the trailing edge. A dark "hole" in a bright background is the only way this is possible. The amplitude of a dark soliton is described by a hyperbolic tangent and is the solution of the NLSE equation when the sign of β_2 is positive.

Theoretically, a dark soliton requires an infinite amount of energy because a CW (continuous wave) beam is necessary for its formation. Practically,

dark solitons can still propagate stably even if the background is not fully CW. In a recent experiment[56], a dark soliton 5 ps in width was propagated over a kilometer of fiber at a wavelength of 850 nm and required peak powers around 500 mW. Trains of dark solitons in fiber have also been propagated[57] but required peak powers of around 1000 W. Dark spatial solitons have been proposed for implementing devices such as logic gates[58]. Finally, dark solitons have been used to compress bright optical pulses in the normal dispersion regime[59] and can also propagate with a bright soliton in the normal dispersion regime as a pair if the pulses couple through CPM[60, 61].

1.3.4 Higher order soliton propagation If a pulse entered the fiber with width and velocity identical to the soliton in Eq. (1.26), but with a coefficient greater than one, the pulse would evolve as a higher order soliton. For instance, Fig. 1.11 demonstrates the evolution of a higher order

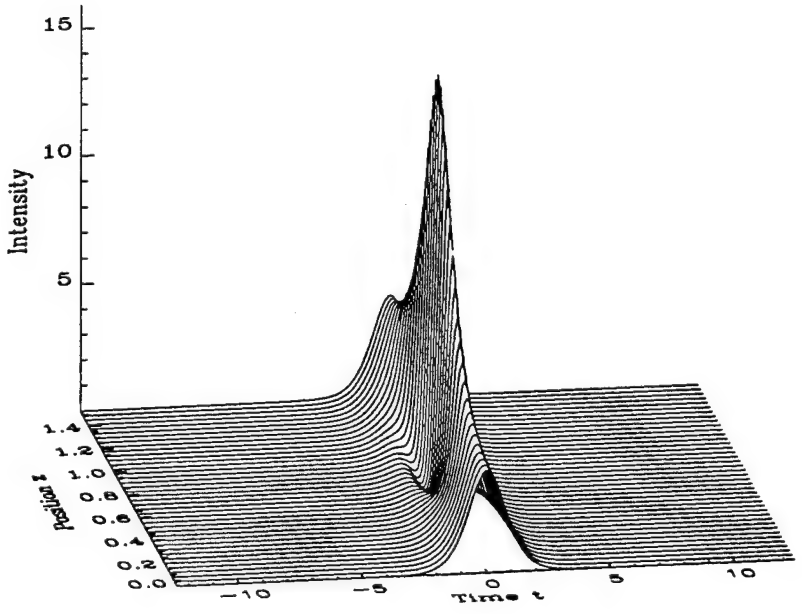

Figure 1.11. Evolution of a higher order soliton with initial condition 2sech(t).

soliton having an initial condition $u(0,t) = 2\,\mathrm{sech}(t)$. The pulse evolution is solved using the IST and it repeats after one soliton period $z_o = (\pi/2)z_c$, or 1.57 spatial units in the normalized frame. While it is possible in theory[7] to encode multivalued data using such pulses, their evolution is unstable. Slight perturbations in the velocity or frequency cause higher order solitons to break up into distinct pulses and dispersive radiation. It is still unknown whether such pulses could be used to transmit data in fiber communication systems.

1.4 Wavelength multiplexed solitons in fiber

The emphasis of prior WDM soliton research has been on the interactions between only two channels. The frequency and velocity shifts that result during a two-soliton collision have been studied analytically[62] and experimentally[63, 64] and will be discussed in great detail in Chapters 3 and 4. Interactions at the fiber input[65, 66] and also in the presence of loss and amplification[62, 67, 68, 69] have been studied as well, and filters[32, 31, 70] have been proposed as a means of reducing interactions. WDM solitons have also been used to make quantum measurements of the photon number[71, 72]; such measurements may be useful in detecting squeezed states in quantum theory[73, 74]. Only recently have researchers begun to study the effects of collisions between arbitrary numbers of WDM soliton channels. The problem of detecting soliton data on N channels in spite of frequency distortion was studied several years ago[6, 75], while the first experiment with greater than two wavelengths was demonstrated this past year[76]. This thesis will further clarify those issues which affect the application of WDM solitons within practical communication systems.

CHAPTER 2

SOLITON SOURCES

The development of soliton sources has been a subject of interest for quite some time[77], since practical soliton sources (and receivers) are necessary before solitons may be used in actual telecommunication systems[78]. In many respects, soliton generation is not difficult, since the soliton pulse is the only stable solution to the NLSE. Even a square wave with sufficient energy at the proper wavelength eventually (after several soliton periods) evolves as a soliton by shedding some of its energy as dispersive radiation. In this chapter we discuss different techniques for generating solitons in optical fiber. The three types of sources we consider are color center lasers(CCL), semiconductor sources, and fiber lasers. We also discuss experimental results using both a CCL and a fiber ring laser.

2.1 Color center lasers

Color center lasers(CCL) are one of the most common sources of high-energy narrow pulses in the infrared region of the electromagnetic spectrum. They receive their name because the active medium of the laser is the color center, a point defect in a crystal lattice[79]. When the color center is illuminated by an optical pump, it absorbs a photon and moves to a higher energy state. However, this state is short-lived, and the center quickly drops to an excited state at a lower energy level, while emitting a phonon into the crystal lattice. When the electron drops back to the ground state, energy is radiated as

a photon with lower energy than the pump. If the crystal is placed in an optical cavity and is pumped with enough energy to create a population inversion, the energy transitions are stimulated by the pump, and the color center lases. The emission process occurs over a relatively large band of energies, so the tuning range of the CCL output wavelength is rather large. Although many different color centers exist, the one used in our laboratory is an $(F_2^+)_H$ point defect in a NaCl:OH crystal.

The path of the beam in a Burleigh FCL-230 color center laser is shown in the diagram in Fig. 2.1. The horizontally polarized pump enters from the left of the diagram, passes through two alignment apertures, and is then reflected into the cylindrical crystal chamber. Since the crystal is hygroscopic, the crystal chamber must remain in a vacuum, and it must also be kept at liquid nitrogen temperatures or the color centers disassociate from the crystal when illuminated by the pump or the room light. After the pump is focused onto the crystal by the concave mirrors, the beam passes through the partially transmissive beam splitter into the rectangular cavity on the right. To insure that the CCL mode-locks at precisely the modulation frequency of the pump, the beam path in the chamber on the right is folded so that the

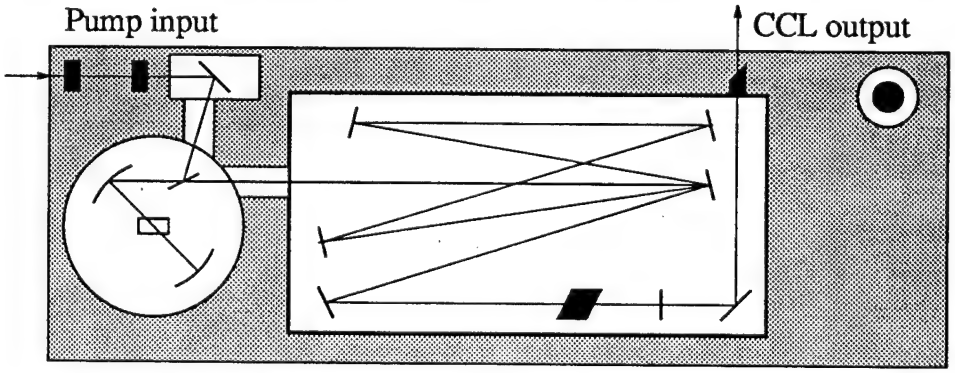

Figure 2.1: Beam path in the Burleigh FCL-230.

CCL cavity length matches that of the pump laser. The wavelength is tuned with the birefringent plate at the bottom of the diagram in the rectangular chamber. The birefringence of the plate changes with orientation and wavelength, so that the desired wavelength passes through the plate with no change in polarization. Undesired wavelengths are rotated towards vertical and are blocked by Brewster windows in the cavity. Thus, the CCL output is horizontally polarized at the wavelength for which the plate birefringence is zero. The cavity end mirror is located just after the birefringent tuner.

The pump for an NaCl:OH CCL requires two horizontally polarized colinear beams. The first beam at 1.06 μm is generated by an Nd^{3+}:YAG laser, mode-locked at 82 MHz, with pulse widths around 60-70 ps and average power of 4 W. The second beam consists of 3 mW of green light, generated by frequency doubling the YAG output. This beam insures that the color centers are correctly oriented with respect to the polarization of the pump. If the green light is absent, the crystal is bleached, since color centers with the correct orientation settle into the orthogonal (and incorrect) orientation with some finite probability during each absorption and emission cycle.

The NaCl:OH CCL may be tuned over a wavelength range from 1.49 μm to 1.7 μm, with pulse widths of 9-12 ps and average power as large as 400 mW. Since the mode-locking frequency is 82 MHz, the peak power of each pulse may be as high as 400 W. Given the results in Fig. 1.6, only about 10 mW peak power is required to generate 10 ps solitons in a dispersion shifted fiber with $D = 1$ ps/nm-km. Since the energy out of the CCL is many times larger than that required for soliton generation, the CCL is a flexible research tool. For an actual communication system, though, the CCL is rather large,

expensive, and impractical, requiring significant attention and maintenance if it is to be used on a regular basis.

2.1.1 Pulse compression and WDM with the CCL The plot in Fig. 1.11 depicts the evolution of a soliton with peak power four times that necessary for soliton propagation. Initially, the pulse compresses, reaching a minimum width after propagation of half a soliton period. Since the peak power of the CCL is many times greater than that required for a 10 ps soliton, we expect to see significant compression. Using approximately 2 km of dispersion shifted fiber with a dispersion zero wavelength near 1.56 μm, pulses as small as 360 fs were observed — a compression factor of at least 25$\times$ — as measured by an autocorrelator. The soliton period of a 10 ps pulse is tens of kilometers (see Fig. 1.6), so even greater compression is theoretically possible, given the length of the fiber used in our experiments.

The spectral width of a pulse out of the CCL is 25 GHz, so the spectral width of the compressed pulse is large enough to separate into wavelength multiplexed solitons with pulse widths on the order of picoseconds, using the configuration in Fig. 2.2. The output of the compression fiber is separated into individual spectral components by the grating demultiplexer. Specific wavelengths are chosen or blocked using the mask, and the initial timing relationship of the pulses is determined by varying the positions of the mirrors after the mask. Such an arrangement was used in recent experiments to study collisions between two densely wavelength multiplexed solitons[64, 80].

2.2 Semiconductor soliton sources

Semiconductor laser diode sources are perhaps the most practical way of generating solitons, since they are compact and are capable of generating

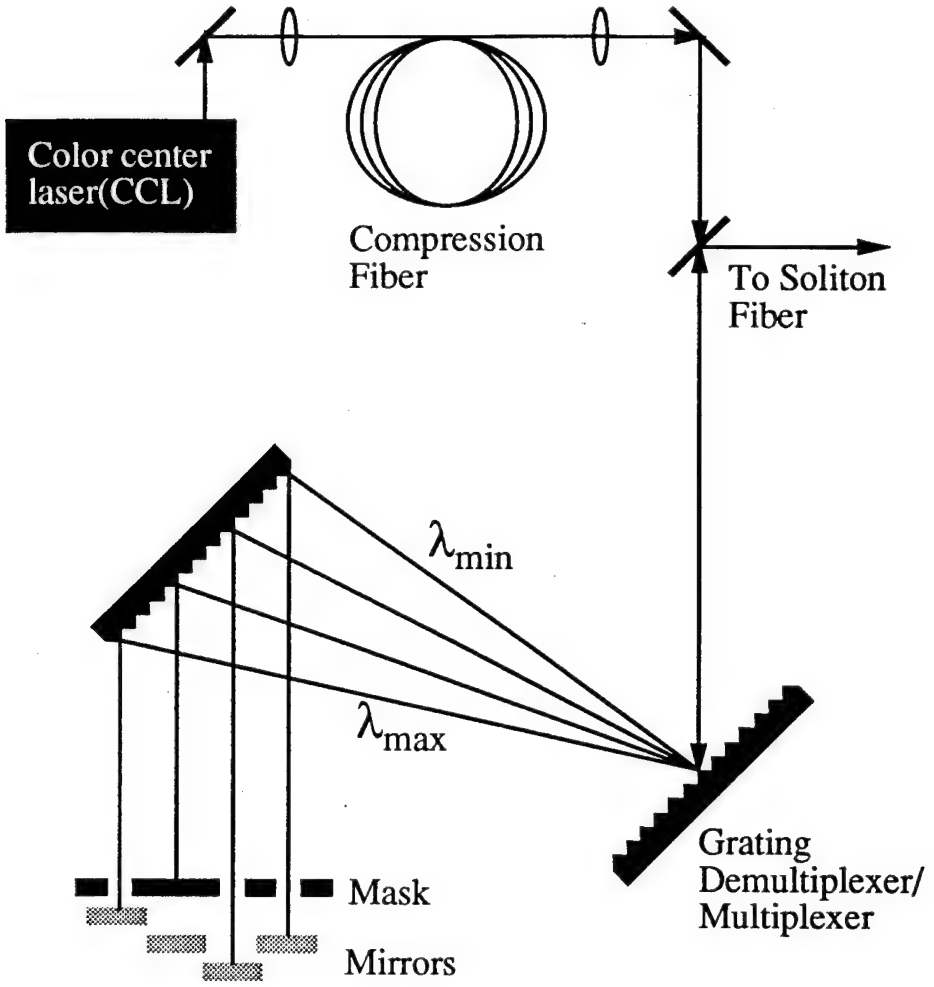

Figure 2.2: Wavelength multiplexing with the CCL.

pulses at gighertz rates with sufficient power (often in combination with an optical amplifier). Mode-locked external cavity lasers have been used in many soliton experiments to date[1, 38, 81]. However, the output of laser diodes are often asymmetric and chirped[3], resulting in dispersive radiation and increased noise as the pulses evolve into solitons[82]. External cavity lasers also require difficult alignment procedures and precise control of the cavity length[83, 84]. Here we briefly discuss two recent examples of semiconductor-based soliton sources which overcome these disadvantages.

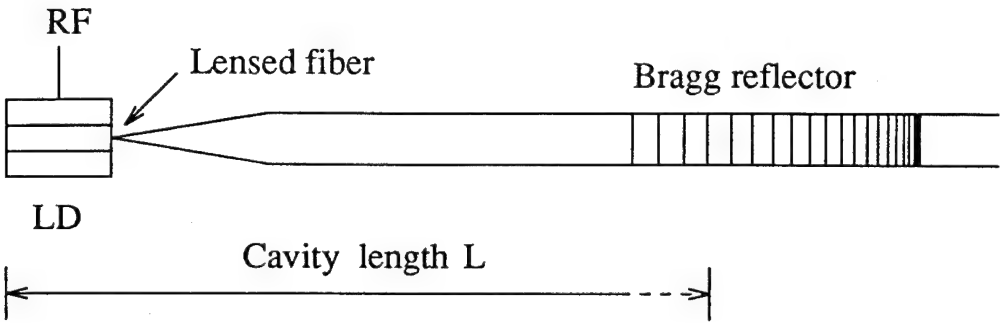

Figure 2.3: Configuration of a hybrid soliton pulse source.

2.2.1 Hybrid soliton pulse source The pulse source depicted in Fig. 2.3 is a robust device which generates nearly transform limited mode-locked pulses without spectral instability or sensitivity to cavity length[83]. The optical source is an RF modulated laser diode, high reflectivity coated on the left facet and anti-reflection coated on the other, so that the light may be coupled into the linearly chirped fiber Bragg reflector. To manufacture the Bragg relector, a photosensitive fiber is exposed to the interference pattern of two ultra-violet waves. The interference pattern modulates the index of refraction, creating an index grating which reflects light when the Bragg matching condition is met. Since the grating is chirped — the modulation frequency of the refractive index increases with distance away from the diode — longer wavelengths reflect from the end of the grating closer to the laser diode, while shorter wavelengths reflect from the opposite end. The transmissivity at the center wavelength λ_c of the Bragg reflector is shown in Fig. 2.4.

The mode-locking frequency of a laser is dependent on the cavity length L according to the relation

$$f_m = \frac{c}{2\,n\,L}. \tag{2.1}$$

For the laser in Fig. 2.3, the cavity length varies with wavelength. Hence, as

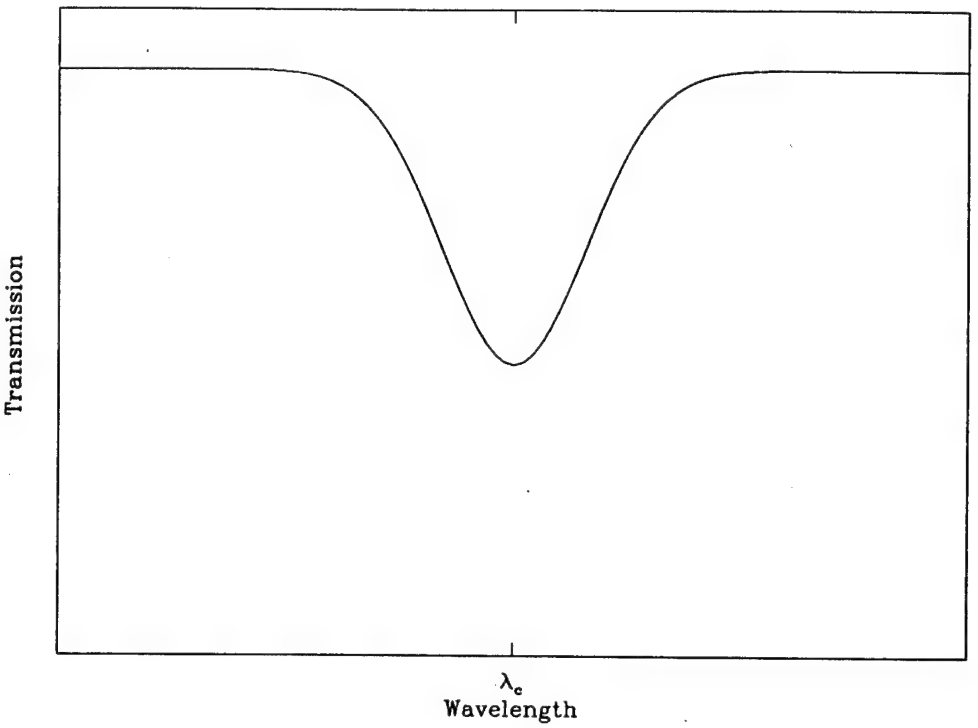

Figure 2.4. Transmissivity versus wavelength of a Bragg reflector with center wavelength λ_c.

f_m changes, the operating wavelength is self-tuned to the wavelength at which Bragg matching occurs, with longer wavelengths mode-locking at higher modulation frequencies and shorter wavelengths mode-locking at lower modulation rates. Independent control of the wavelength may be possible with temperature tuning or by stretching the fiber[83].

In a specific example, if the center of the reflector is placed 41 mm from the laser diode, the mode-locking frequency at the center of the grating is 2.5 GHz. If the spectral chirp in the reflector is about 0.2 nm over 1 cm of fiber, we expect modulation rates to vary between 2.2-2.8 GHz with a 0.2 nm variation in wavelength. In actual experiments with these design constraints[83], good mode-locking is achieved across a frequency range of 700 MHz, from

2.1 GHz to 2.8 GHz, while the wavelength varies across 0.3 nm. With pulse widths around 50 ps, the peak powers of 5-10 mW are sufficient for soliton generation (see Fig. 1.6). The time-bandwidth product is less than 0.4 for many of the modulation frequencies, close to the ideal value for solitons given in Eq. (1.32), so the pulses are almost chirp free. Shorter pulse widths are possible with more precise control of the chirp rate of the Bragg grating reflector.

2.2.2 Dual-wavelength soliton source A second semiconductor laser that has practical merit as a soliton source operates on the following principle[84]. If the phase of a CW laser with carrier frequency f_o is modulated, so that the instantaneous phase is given by

$$\Phi(t) = A \sin(2\pi f_m t) + \Phi_o, \tag{2.2}$$

the frequency of the CW wave will vary by an amount determined by the derivative of $\Phi(t)$. Hence, the deviation from the CW frequency f_o is

$$\begin{aligned} \delta f(t) &= \frac{\delta\omega(t)}{2\pi} = \left(\frac{1}{2\pi}\right)\frac{\partial\Phi}{\partial t} \\ &= A f_m \cos(2\pi f_m t), \end{aligned} \tag{2.3}$$

where $\Phi(t)$ and $\delta f(t)$ are plotted in Fig. 2.5. If the resulting waveform is passed through a low-pass filter (such as a step low-pass fiber grating filter[84]) with cutoff frequency just above $f_o - Af_m$, as depicted by the lower of the two dashed lines in the second plot of Fig. 2.5, a train of pulses emerges with optical frequency $f_o - Af_m$, as seen in the third plot of Fig. 2.5. Conversely, if a high-pass filter with cutoff just below $f_o + Af_m$ is placed after the phase modulator, the pulse train in the bottom plot results. The pulses emitted by such a laser have shapes between those of sech^2 and Gaussian pulses[84].

The two pulse trains at $f_o - Af_m$ and $f_o + Af_m$ are referred to as

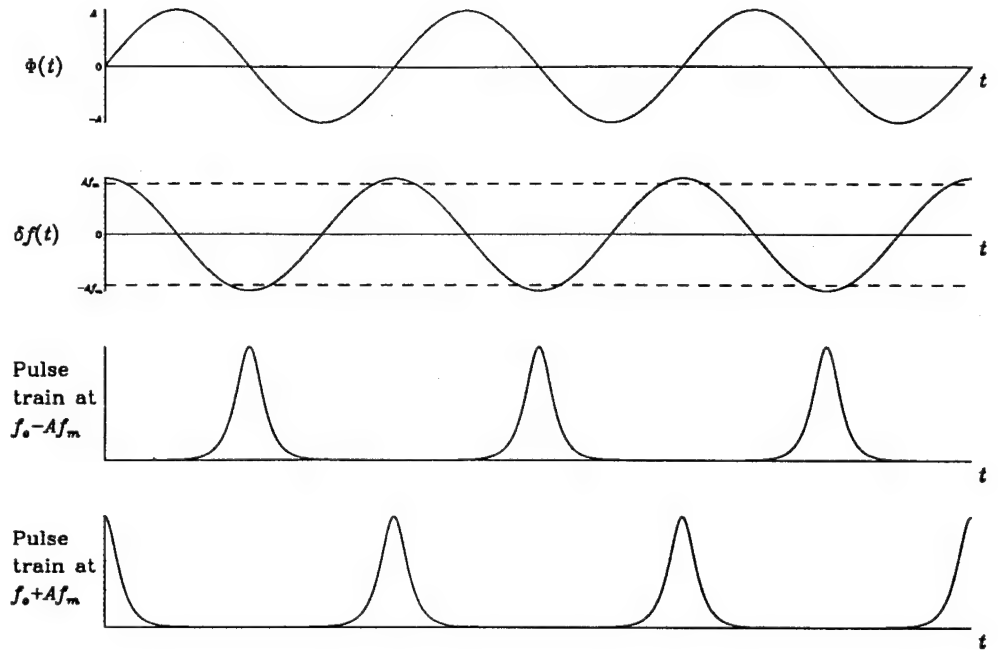

Figure 2.5. Phase modulation of a CW signal, the carrier frequency deviation, and the pulse trains that result after low- or high-pass filtering of the waveform.

Stokes and anti-Stokes pulse trains, respectively, where the repetition rate of each train is f_m and the bit period is $T = 1/f_m$. Since the derivative of $\delta f(t)$ is nearly zero at its maximum and minimum, the pulses are nearly chirp-free and transform-limited. Furthermore, the frequency of each train is independent of the bias Φ_o in Eq. (2.2), so the device is insensitive to drift in the modulator bias.

The duty cycle τ/T of the pulse train generated by the laser is inversely proportional to the amplitude A of the phase modulation. Hence, the ratio of the energy in the pulse train to the input energy drops as A increases. In an experimental example[84], the phase of a 1 mW output CW semiconductor laser at 1.56 μm is sinusoidally modulated by a lithium niobate phase modulator at modulation rates between 2.5 and 15 GHz. With approximately

32 dBm of RF power, the amplitude of phase modulation is $A = 1.5\pi$. At 10 GHz modulation, pulse widths of 21 ps are obtained and approximately 25-30% of the CW input energy is transmitted to the pulse train. The source is highly stable in long distance transmission of soliton pulses. If an appropriately wide ($2Af_m = 94$ GHz) optical notch filter is used in such a system, the device becomes a source for two-channel WDM soliton transmission, although some practical technique is required to independently modulate each pulse train.

2.3 Fiber lasers

The third type of source we consider are fiber ring lasers. Like semiconductor sources, fiber lasers are compact, but the pulses generated by fiber lasers are chirp-free and symmetric[85]. Pulses at Gb/s rates are achieved either through active or passive mode-locking; we only discuss actively-mode locked fiber lasers since picosecond pulses are easily generated in this manner[85, 86, 87]. Sub-picosecond pulses are generated with passive mode-locking[88, 89].

An actively mode-locked fiber ring laser is illustrated in Fig. 2.6, where an EDFA (or a semiconductor optical amplifier[90]) provides gain. The modulator is usually an integrated electro-optic device, such as a $LiNbO_3$ Mach-Zehnder amplitude modulator, driven by an RF signal at gigahertz rates. Consequently, the laser is loss-modulated, such that the gain of the EDFA only compensates the cavity loss when the modulator is "on". The polarization controller guarantees that the polarization is maintained in the cavity, although a polarization maintaining fiber would be more robust. The isolator prevents back-reflections, insuring unidirectional operation of the laser. The tunable filter, while not required, stabilizes laser operation and allows for wavelength tunability.

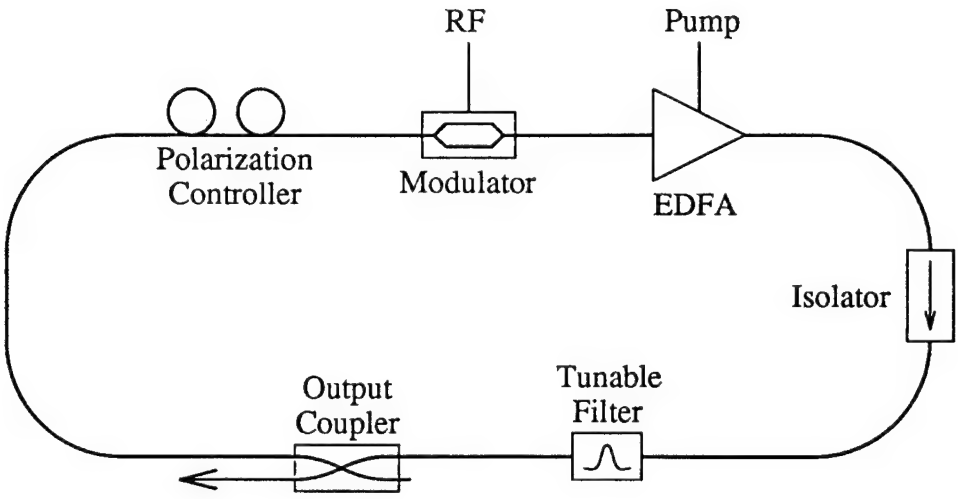

Figure 2.6: Typical confiuration of an actively mode-locked fiber laser.

Since the cavity length in a fiber ring laser is on the order of meters (the EDFA typically requires such lengths to provide sufficient gain), the laser must be harmonically mode-locked to generate Gb/s pulses. The RF signal frequency must be matched to the fiber cavity length L by the relation

$$f_m = \frac{m\,c}{n\,L}, \tag{2.4}$$

where m must be an integer. As an example, in a cavity 10 m in length with $n = 1.5$, m must be at least 50 to achieve a pulse rate of 1 Gb/s. Hence, there are 50 pulses traversing the fiber ring at any given time.

The FWHM of a pulse generated by an actively mode-locked laser results from the interplay between the laser gain-bandwidth and the modulator transfer function[91, 92]. The gain acts to narrow the pulse spectrally, while the modulator narrows the pulse temporally. The spectral gain is often assumed to be Gaussian with width Δf, and the amplitude modulation is defined according to

$$M(t) = \exp[-\Delta_m(1 - \cos\omega_m t)], \tag{2.5}$$

where $\omega_m = 2\pi f_m$ and Δ_m is the modulation depth. $M(t)$ is plotted for two values of Δ_m in Fig. 2.7. The pulse preferentially experiences gain near the peak of the modulation, at which point $M(t)$ may be approximated by the Gaussian function

$$M(t) \approx \exp\left(-\Delta_m \omega_m^2 t^2/2\right), \qquad |t| \ll T, \tag{2.6}$$

where $T = 1/f_m$.

Thus, the pulse is temporally narrowed and spectrally broadened by the Gaussian transmission function of the modulator, while it is temporally broadened and spectrally narrowed by the Gaussian gain-bandwidth of the

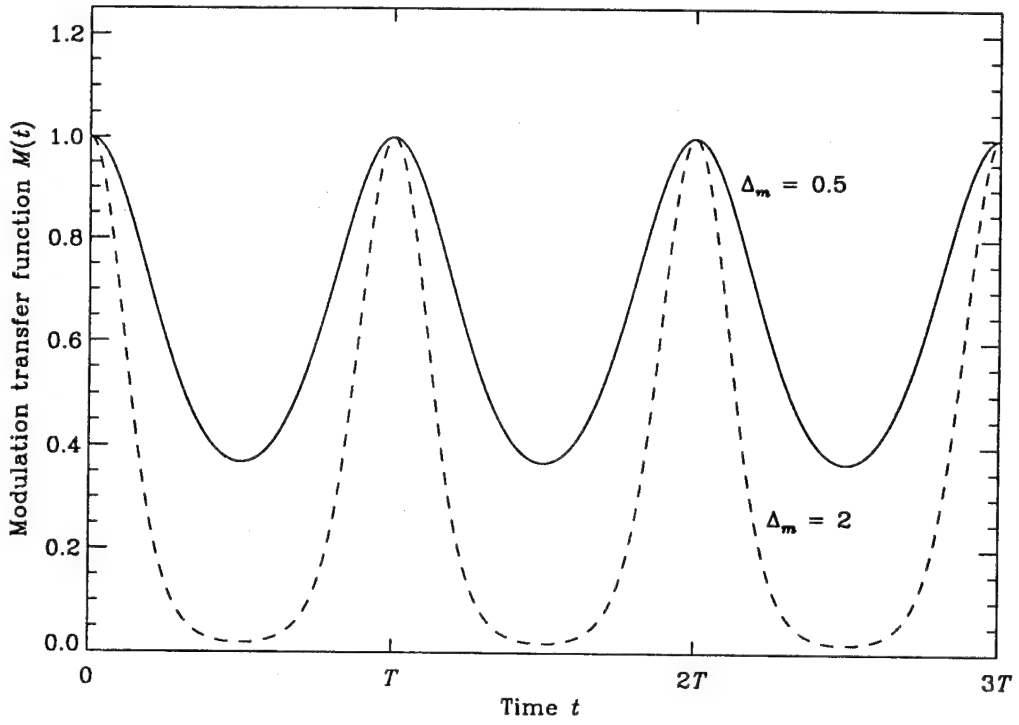

Figure 2.7: Amplitude modulation for different modulation depths.

laser. The pulse width that results is given by[85]

$$\tau = \frac{0.45}{(f_m \, \Delta f \, \sqrt{\Delta_m})^{1/2}}. \tag{2.7}$$

If the cavity includes a tunable filter, Δf is equal to the bandwidth of the filter; if no tunable filter is used, Δf is determined by the dominant gain limiting effect of the cavity. Shorter pulses are obtained without the filter[85, 86], since the erbium gain bandwidth is rather large, but laser operation is less stable and precise control over the laser wavelength is difficult.

In a recent demonstration using fiber lasers[85], transform-limited Gaussian pulses were obtained, at pulse widths which varied from 5 ps to 100 ps by carefully controlling the bandwidth of the tunable filter or the modulation depth, in agreement with Eq. (2.7). Since the pulse envelopes do not match the sech^2 envelope of a soliton, some dispersive radiation results upon propagation, although it is small since the pulse shapes are similar. A main drawback of fiber lasers is their susceptibility to slight changes in the fiber length as the temperature of the fiber increases during operation. If the cavity length changes by even a slight amount, the mode-locking condition in Eq. (2.4) is violated. Such effects are dynamically avoided by piezoelectrically tuning the cavity length to the proper fiber mode[85, 93]. Fiber lasers are also sensitive to drift in modulator bias. The dual-wavelength soliton source in Section 2.2.2 is less sensitive to such problems.

2.4 Experimental results

In this section we present the results of experiments demonstrating the operation of an EDFA and a mode-locked fiber laser. All measurements were made using a Tektronix DSA 602 digitizing signal analyzer with 1 GHz

bandwidth, a Hewlett-Packard 71450A optical spectrum analyzer, and optical power meters.

2.4.1 Erbium-doped fiber amplifier Erbium amplifiers are becoming essential components in fiber communication systems. They are likely to be used in the next trans-Pacific fiber scheduled for 1996[2]. Although erbium is only one in a class of rare-earth ions that are used to implement fiber amplifiers, an EDFA is especially important because it amplifies at 1.55 μm, the low loss wavelength of standard optical fibers. Rayleigh scattering is the dominant loss mechanism below this wavelength, while infrared absorption dominates at longer wavelengths[94]. An EDFA amplifies a signal through the process of stimulated emission, so the principle of operation is no different than that of a typical laser. The most efficient pumping wavelengths are 0.98 μm and 1.48 μm, at which a small-signal gain as high as 40 dB can be achieved with a pump power of tens of milliwatts.

Figure 2.8 demonstrates the configuration of an EDFA. The pump is an Oki 1.48 μm Fabry-Perot laser diode with a maximum specified CW output power of 50 mW at a forward current of 500 mA; we typically operate with power less than 40 mW, requiring current less than 400 mA. The temperature of the pump laser is controlled by a thermoelectric cooler, and the current is driven by the circuit[95] illustrated in Fig. 2.9. The current delivered by this circuit is

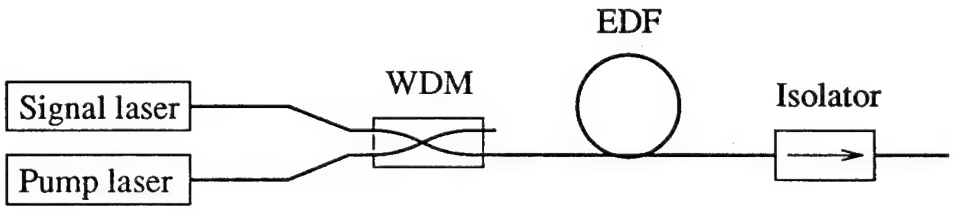

Figure 2.8: EDFA configuration.

limited to 100 mA, so the circuit is modified to supply the current requirements of the pump laser. If the 10 kΩ resistor to ground from the negative pin of the OP-5 op-amp is replaced with a 5 kΩ or smaller resistor, more current is pulled from the LM317 voltage regulator. The 25 Ω resistor between the two OP-27 op-amps must also be replaced with a 2 Ω resistor. Other modifications to the circuit in Fig. 2.9 are suggested in [95]. The remaining components used in the amplifier in Fig. 2.8 include an Amphenol 1485/1545 nm WDM, 25 m of erbium-doped fiber(EDF) donated by AT&T, and an E-Tek isolator at 1550 nm. The 3.0 μm diameter of the EDF core is smaller than that of standard fiber, so the EDF is fusion spliced to standard fiber to minimize

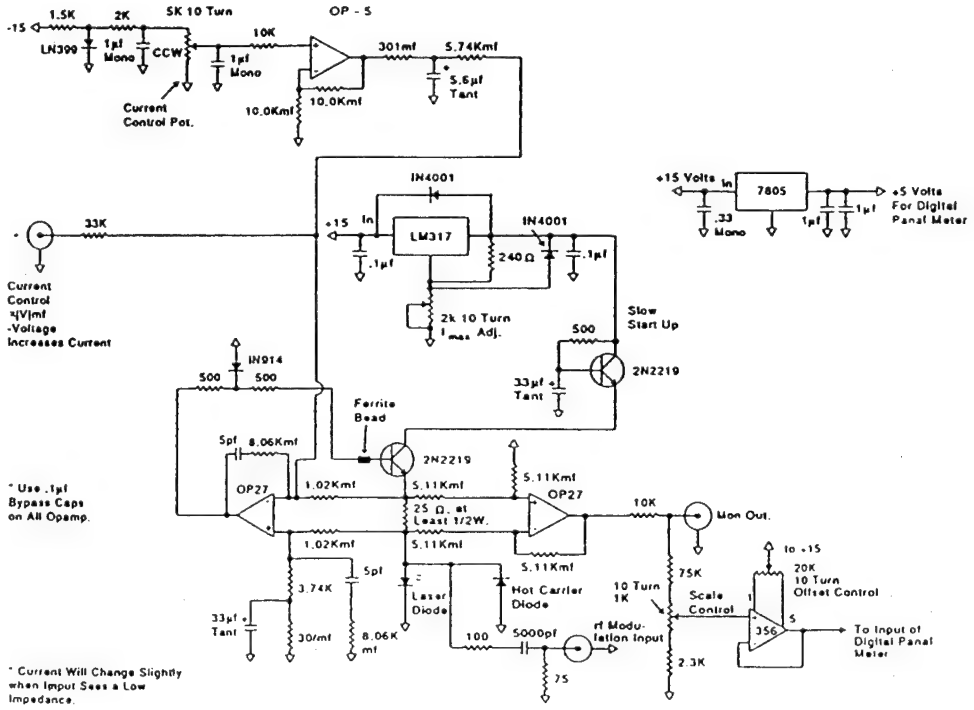

Figure 2.9: Laser diode current driver.

coupling losses. The signal used to test the EDFA is generated by a 1.54 μm distributed feedback(DFB) laser diode.

The spontaneous emission spectrum of the EDFA without any signal present is shown in Fig. 2.10. The pump energy at 1.48 μm is seen toward the left of the plot, while the spontaneous emission spectrum of the EDFA is seen around 1.56 μm. The spontaneous emission spectrum shown here differs somewhat from that usually associated with erbium. Problems with the pump laser and with connector losses consistently disrupted measurements. Index matching fluid may be used to improve coupling between fibers. The more accurate two-hump erbium emission spectrum is observed if more pump power

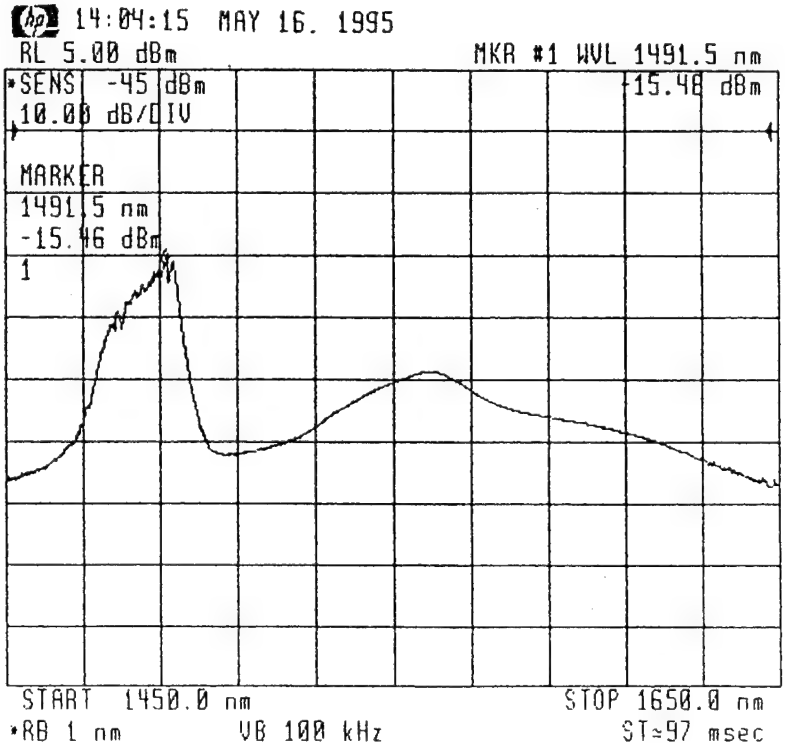

Figure 2.10: Pump and spontaneous emission spectrum of an EDFA.

is coupled into the EDF. When a signal is present, we can achieve small-signal gain as high as 40 dB at a signal level of -40 dBm, while the gain saturates at higher signal levels. A plot of the gain and the output power versus the input signal level is shown in Fig. 2.11. The behavior of the EDFA without an isolator is somewhat erratic. Sharp peaks are observed at times in the emission spectrum; we attribute this to lasing that results from back-reflections at the fiber interfaces. The behavior also changes significantly if the isolator is moved to different positions in the system. Performance is optimized by positioning the isolator as shown in Fig. 2.8.

2.4.2 Mode-locked fiber laser By configuring the EDFA from the previous section in a ring, as in Fig. 2.6, mode-locked lasing is observed.

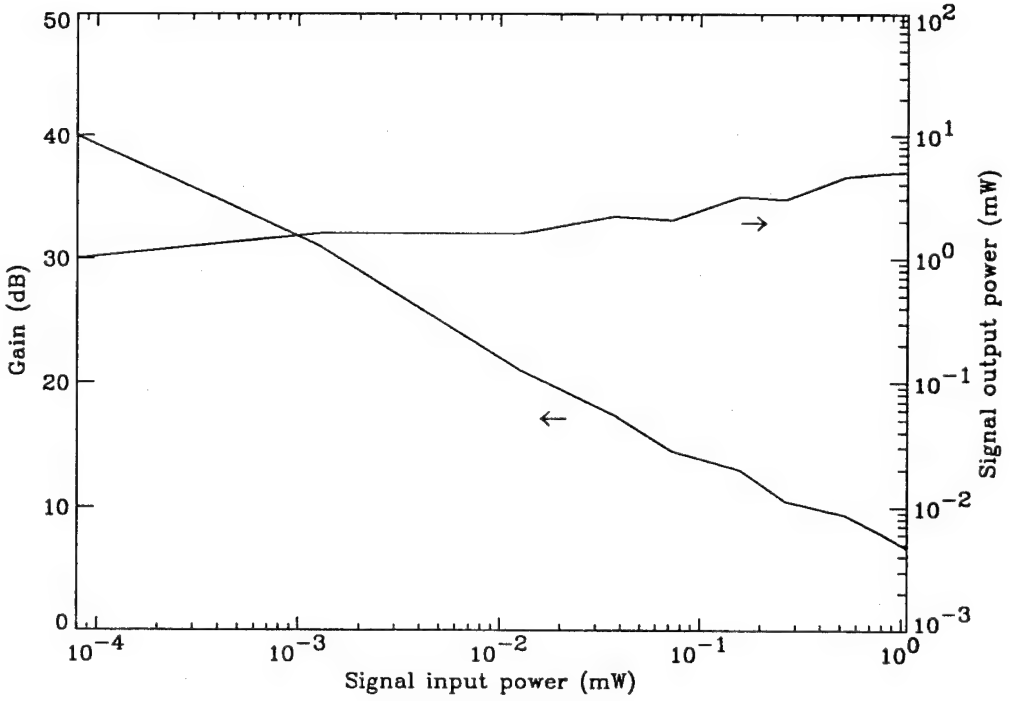

Figure 2.11. Gain and signal power output by an EDFA versus input signal power.

Rather than using a modulator, as depicted, a 2×2 $LiNbO_3$ switch with a 3 dB bandwidth of 175 MHz is used. Although the switch is designed for operation at 1.3 μm, by carefully adjusting the bias settings, extinction ratios of at least 16 dB (and as high as 20 dB) are obtained for 1.55 μm light at one output port of the switch; hence, the switch is sufficient to use as a modulator at 1.55 μm. The second output port is conveniently used in place of the output coupler in Fig. 2.6. The switch is polarization sensitive, so a polarization controller was placed just before it.

Mode-locked lasing is rather easy to achieve. Although the cavity length is not known precisely, by assuming a length of 30 m (the EDF is 25 m in length), the fundamental harmonic corresponding to one round-trip about the cavity is estimated to be 6.7 MHz using Eq. (2.4). With careful tuning of the modulation frequency, mode-locked pulses are seen at a frequency of 6.1 MHz, so the cavity length is actually around 33 m. The mode-locked pulses at the fundamental harmonic, illustrated in the top plot of Fig. 2.12, have a pulse width of 10 ns. Although the laser wavelength is typically around 1.56 μm, a precise measurement of the wavelength is difficult to determine, as there is a significant amount of mode-hopping indicated by the spectrum analyzer.

By increasing the mode-locking frequency to integer multiples of the fundamental, pulse trains at higher data rates and with shorter pulse widths are obtained, as shown in the lower two plots of Fig. 2.12. The pulse widths at frequencies 40 and 80 times the fundamental are 780 ps and 680 ps, respectively. The pulse widths are actually shorter than this; the measurement is limited by the 1 GHz bandwidth of the signal analyzer, so pulse widths much less than

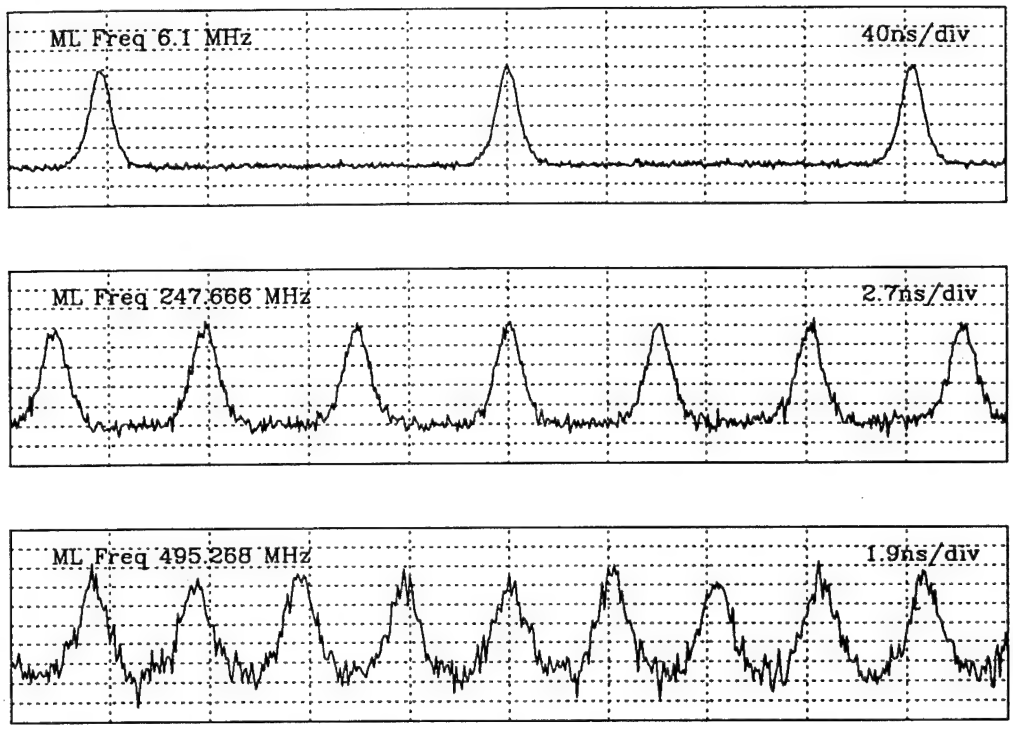

Figure 2.12. Mode-locked fiber laser pulse trains with mode-locking frequencies equal to the fundamental, 40× the fundamental, and 80× the fundamental. Corresponding pulse widths are 10 ns, 780 ps, and 680 ps, respectively.

1 ns are difficult to measure with accuracy. Strict adherence to Eq. (2.7) is also difficult to verify, since neither the gain bandwidth nor the modulation depth is known. Performance is improved, though, by using a Hewlett-Packard 8082A pulse generator instead of sinusoidal modulation to vary the switch state, since the modulation depth is larger with the pulse generator. Since the modulation depth decreases and the cavity loss increases beyond the cutoff frequency of the switch, the laser operation becomes very unstable beyond a mode-locking frequency of 125 MHz. The instability is easy to observe given the noise on the pulse train at 495 MHz in Fig. 2.12. The mode-hopping on the spectrum analyzer is also much worse at the higher frequencies.

Several things would stabilize the laser. First, connector losses would be reduced and back-reflections minimized by fusion splicing all fiber joints. The laser operation is also sensitive to vibrations; taping the fibers to the table helped to some extent. Furthermore, one should use an EDF specifically designed for laser applications. Such fibers are shorter and have higher erbium concentrations, providing higher gain than standard amplifier fiber over shorter (on the order of one meter) distances. While we attempted to use this type of fiber, mode-locking was found to be difficult, probably because of improper fiber length and insufficient gain. The length must be chosen more accurately in such a fiber (due to its shorter length) to achieve the proper amount of gain. Generally speaking, the fundamental harmonic in such a fiber would be larger, so mode-locking at higher frequencies would be easier. Ultimately, a high-speed modulator and a tunable filter are required to stabilize the laser output and shorten the pulses. The inclusion of these devices is necessary before actual solitons can be observed. The tunable filter also provides an easy mechanism for observing interactions between WDM solitons under different conditions. We discuss the theory of such interactions in the following chapters.

CHAPTER 3

WDM SOLITON INTERACTIONS IN AN IDEAL FIBER

To understand interactions between WDM solitons in fiber communication systems, it is useful to first analyze collisions between solitons in an ideal fiber. Initially, we discuss interactions between two WDM solitons, and then proceed to the more arbitrary case with N WDM soliton channels. While several factors are ignored by assuming the fiber is ideal, loss is probably the most important, since energy dissipation and amplification can significantly affect interactions between solitons. Such effects will be discussed in the next chapter. In addition, we assume that all wavelength channels have the same linear polarization; it is unlikely that this would be true in actual systems. We also ignore birefringence[15], although it can be important if fibers have very low dispersion[11] or if propagation distances are long[14]. Finally, since the pulse widths of interest are longer than 10 ps, higher order dispersion is ignored, as are other fiber nonlinearities. We will see in Chapter 4 (and briefly in Section 3.3.2) that fiber nonlinearities can be important when using WDM extensively for fiber communications.

3.1 General discussion

Distortion at a collision between two solitons is illustrated by Fig. 3.1, where each curve is a plot of the exact solution of the NLSE. (The exact solution of the NLSE will be discussed in greater detail in Section 3.3.) The amplitude of each pulse is plotted as a function of fiber position z and time t.

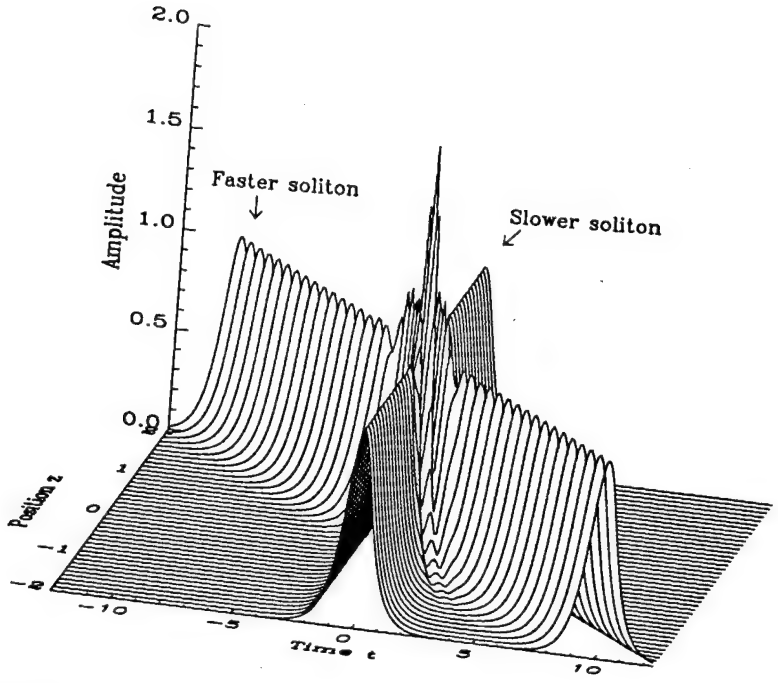

Figure 3.1: Two soliton collision at time $t = 0$ and position $z = 0$.

Two solitons on different wavelengths are initially separated but collide because they travel with different group velocities. The collision occurs at normalized time $t = 0$ and at normalized position $z = 0$. The slower soliton travels at the group velocity of the reference frame, and the faster soliton passes through the slower soliton and moves ahead of it as z increases. If the collision occurs at the end of the fiber, the distortion may prevent accurate detection of data. Although linear pulses also distort when they collide, if each pulse is a soliton, an additional nonlinear effect takes place during the collision. Figure 3.2 shows that each soliton is shifted slightly in time after the collision. The dashed curves depict the timing of each soliton if no collision had occurred. No such displacements result if the collision occurs between standard linear pulses.

The temporal evolution of each soliton is better understood by analyzing the frequency spectrum in Fig. 3.3, where the spectral amplitude is

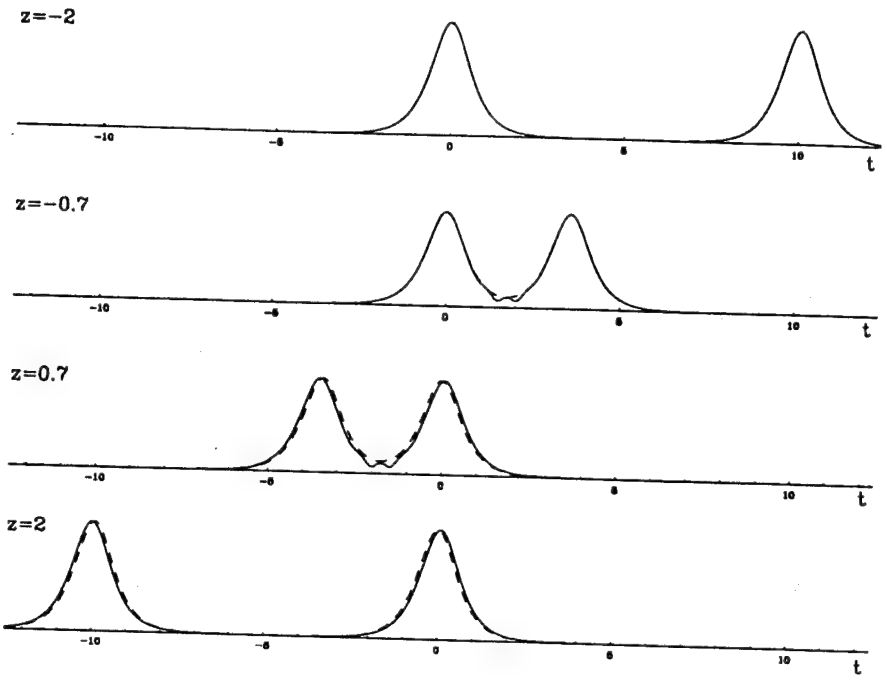

Figure 3.2. Timing of each pulse in Fig. 3.1 at successive values of z. The dashed curves depict the timing of each soliton if no collision had taken place.

plotted as a function of fiber position z and frequency ω. The spectrum is derived by discretizing the waveform in Fig. 3.1 and computing its fast-Fourier transform[96] at each position z. (Here, the 25 unit wide temporal waveform is discretized into 256 data points. Hence, after periodic continuation, the amplitude of each spectral component in Fig. 3.3 is scaled by a factor $256/25 = 10.24$ times larger than the usual soliton spectral amplitude of π in Eq. (1.30).) In the anomalous dispersion regime, higher frequencies travel with greater velocity, and since the spectral intensity of a soliton is represented by a sech^2 envelope as in Eq. (1.30), the positive spectral component in Fig. 3.3 corresponds to the faster soliton in Figs. 3.1 and 3.2. The spectrum at $z = 0$, the center of the collision, corresponds to the solid curve in Fig. 3.4. The dashed curve depicts the frequency component of each soliton when no collision is taking place. At

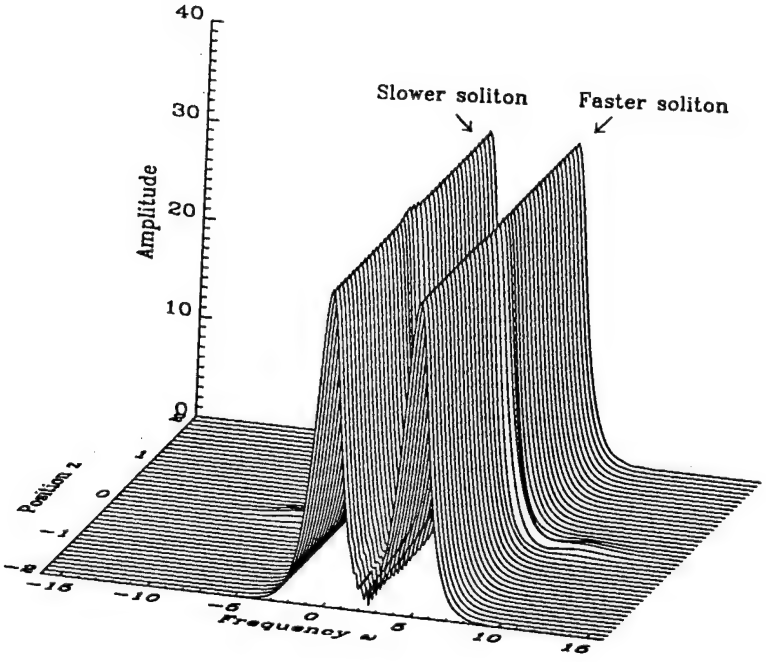

Figure 3.3: Fourier representation of the two soliton collision.

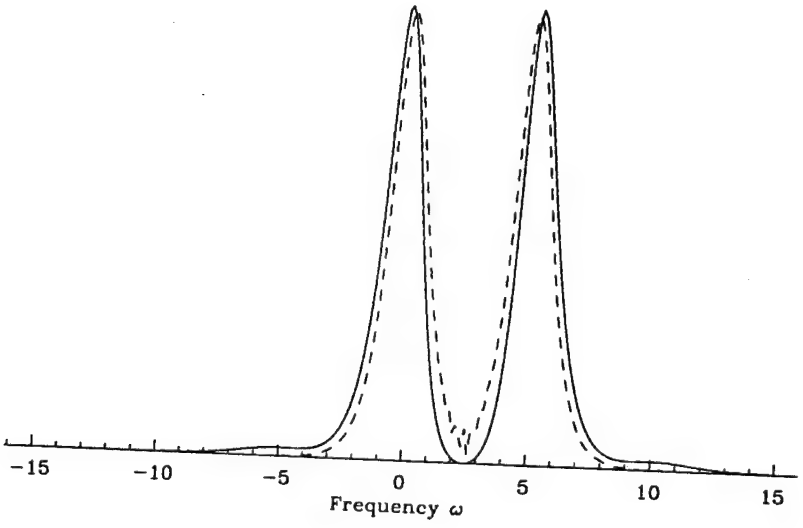

Figure 3.4. Frequency distortion at a two soliton collision. Dashed curve represents each spectral component when no collision is taking place.

the center of the collision, the frequency of the faster soliton has increased, and the frequency of the slower soliton has decreased. Since higher frequency pulses travel with greater velocity, the velocity of the faster soliton has increased momentarily, while the velocity of the slower soliton has decreased. Thus, the faster soliton moves forward slightly in time because of the collision, whereas the slower soliton is delayed, consistent with the behavior in Fig. 3.2. Note in Fig. 3.3 that each soliton returns to its original frequency after the collision, so the velocity changes only during the collision. The displacements in time in Fig. 3.2 are small because the interaction in the frequency domain in Fig. 3.3 is small. In fact, the soliton frequencies are relatively undistorted in comparison to the distortion in time at the collision. Thus, separating each soliton by wavelength with a grating demultiplexer will insure accurate detection of data if the timing displacement in Fig. 3.2 is not too large.

Since solitons require more energy than standard pulses, the solitons on different wavelengths interact because the potential wells under each pulse merge during a collision, creating a deeper well. Energetically, each soliton prefers to remain in the potential well, so the solitons attract — the faster soliton speeding up and the slower soliton slowing down. The collision is time-reversible, so the interaction is symmetric, and the velocity of each soliton returns to its original value after the collision is completed. In analogy to the interaction between solitons on orthogonal polarizations in Section 1.3.1, the interaction results from cross-phase modulation(CPM), as each soliton sees a gradient in the index of refraction created by the intensity of the other soliton through the Kerr effect in Eq. (1.12).

Intuitively, the behavior of two solitons during a collision is explained

by the simple example of two sprinters in a race. As a faster runner approaches a slower runner, no interaction takes place between them (unless, of course, one runner violates the rules), and the faster sprinter simply passes the slower. However, if the surface of the track were flexible, like a trampoline, faster runners would have an advantage over slower runners. As a faster runner approached a slower runner, the depression in the surface of the track under each runner would merge. The velocity of the faster sprinter would increase and the velocity of the slower sprinter would decrease because the combined weight of both runners would form a deeper well in the surface of the track. After the faster sprinter passed the slower sprinter, though, the velocity of the faster runner would decrease and the velocity of the slower would increase, and both runners would eventually return to their original speeds. However, the faster runner would have advanced in position relative to the slower runner. This is analogous to the behavior of the solitons in Figs. 3.1 and 3.3. GVD is similar to the different velocity of each sprinter, and the fiber nonlinearity corresponds to the flexibile surface of the track.

3.2 Quantitative analysis of two-soliton interactions

The interaction between two solitons is described quantitatively by analyzing the coupled NLSE resulting from CPM. Suppose that the frequency of the faster soliton is $\Omega_u = \Omega$, and that the frequency of the slower soliton is $\Omega_v = 0$. If Ω is arbitrary and much greater than one (a value for Ω of at least five, as in Figs. 3.1 and 3.3, is usually sufficient), the evolution of the faster soliton is described by

$$u(z,t) = \mathrm{sech}(t + \Omega z)\exp[-i\Omega t + i(1-\Omega^2)z/2], \tag{3.1}$$

as in Eq. (1.26), and the slower soliton corresponds to

$$v(z,t) = \mathrm{sech}(t)\exp(iz/2). \tag{3.2}$$

Actual frequency and wavelength spacings between two soliton channels with a normalized frequency separation of Ω are shown in Fig. 3.5 for $\tau = 20$ ps and $\tau = 50$ ps. Using Eq. (1.32) and recalling that $\Omega = 2\pi\Delta f\tau/1.763$ from Eq. (1.31), a typical channel spacing of five soliton spectral widths, or

$$\Delta f = 5\delta\nu = \frac{1.575}{\tau}, \tag{3.3}$$

corresponds to $\Omega = 5.61$, as depicted by the dashed line. We will always assume that the pulse width τ is the same in both channels. The pulse evolution

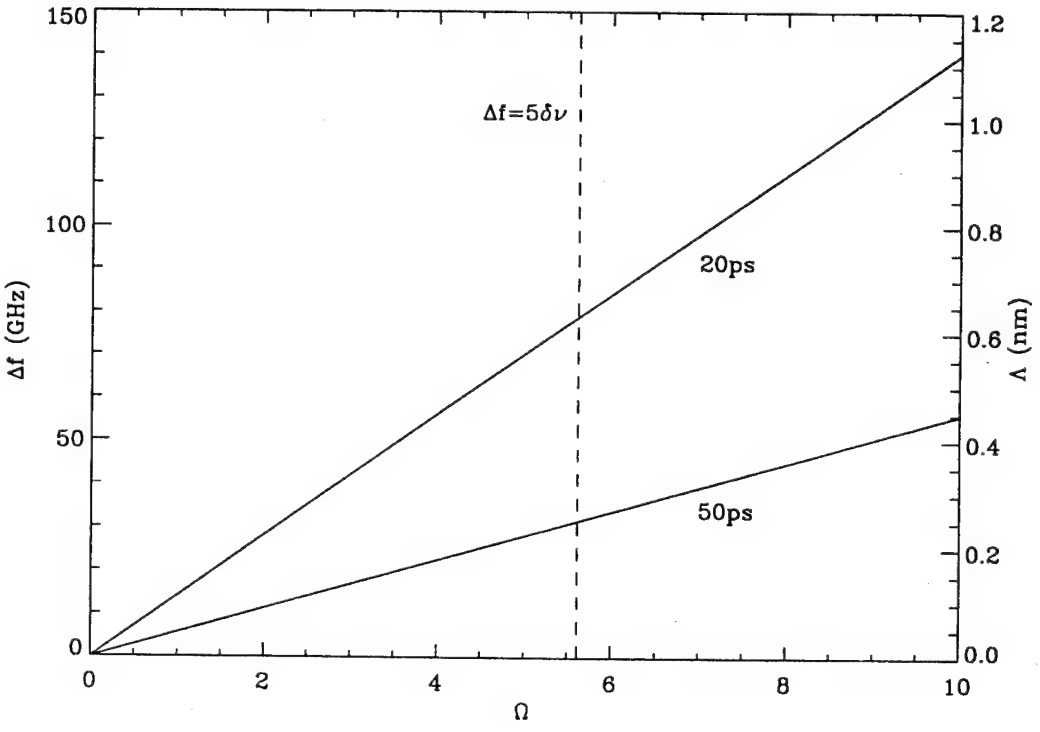

Figure 3.5. Frequency and wavelength separation versus Ω for $\tau = 20$ ps and $\tau = 50$ ps.

described by u and v is less accurate if the frequency spacing is small, since larger timing and frequency shifts occur for smaller values of Ω.

In an analysis parallel that given in [62], we replace u in the NLSE in Eq. (1.24) with $u + v$, since both u and v are solutions to the NLSE. The resulting coupled equations in u and v are

$$-i\frac{\partial u}{\partial z} = \frac{1}{2}\frac{\partial^2 u}{\partial t^2} + (|u|^2 + 2|v|^2)u \tag{3.4}$$

$$-i\frac{\partial v}{\partial z} = \frac{1}{2}\frac{\partial^2 v}{\partial t^2} + (|v|^2 + 2|u|^2)v. \tag{3.5}$$

Equations (3.4) and (3.5) describe the propagation of two pulses with unique frequencies under the effects of CPM. In deriving each equation, four-wave mixing terms were ignored — an invalid assumption if the frequencies are not well separated or when there are many wavelength channels[97].

The mean frequency of any pulse u may be derived using

$$\langle \omega_u \rangle = \frac{\mathrm{Im} \int \left(\frac{\partial u^*}{\partial t}\right) u \, dt}{\int |u|^2 \, dt} = \frac{1}{\mathcal{E}} \mathrm{Im} \int \left(\frac{\partial u^*}{\partial t}\right) u \, dt, \tag{3.6}$$

where Im denotes the imaginary part, u^* is the complex conjugate of u, and $\mathcal{E}$ is the pulse energy. Any variation in $\langle \omega_u \rangle$ is predicted by taking the derivative of $\langle \omega_u \rangle$ with respect to z and substituting for $\partial u/\partial z$ and $\partial u^*/\partial z$ using Eq. (3.4). The result,

$$\frac{d\langle \omega_u \rangle}{dz} = \frac{2}{\mathcal{E}} \int \frac{\partial |u|^2}{\partial t} |v|^2 \, dt, \tag{3.7}$$

is derived in the appendix in Section A.1. With u and v defined by Eqs. (3.1) and (3.2), the normalized soliton energy $\mathcal{E} = 2$ and the mean frequencies of the faster and slower soliton are Ω_u and Ω_v, respectively. Since $\partial |u|^2/\partial t = (1/\Omega)\partial |u|^2/\partial z$ for u defined by Eq. (3.1),

$$\frac{d\Omega_u}{dz} = \frac{1}{\Omega}\frac{d}{dz} \int dt \, \mathrm{sech}^2(t + \Omega z)\mathrm{sech}^2(t), \tag{3.8}$$

so that a small shift in Ω_u at a collision is given by

$$\delta\Omega_u = \frac{1}{\Omega}\int dt\,\mathrm{sech}^2(t+\Omega z)\mathrm{sech}^2(t). \tag{3.9}$$

The solution to Eq. (3.9) is

$$\delta\Omega_u = \frac{4}{\Omega}\frac{\Omega z\cosh(\Omega z)-\sinh(\Omega z)}{\sinh^3(\Omega z)}, \tag{3.10}$$

and the shift in the slower soliton at the collision is $\delta\Omega_v = -\delta\Omega_u$, as shown in Eq. (A.7). The maximum value of $\delta\Omega_u$ occurs at the center of the collision and is equal to $4/(3\Omega)$, as seen in the plot of $\Omega\,\delta\Omega_u$ in Fig. 3.6. (Although a frequency spacing of Ω is used here, much of the soliton literature[62] uses 2Ω, so the maximum frequency shift is oftentimes represented by $2/(3\Omega)$.) Thus, at $z = 0$ the mean frequency of the faster soliton is $\Omega + 4/(3\Omega)$ and

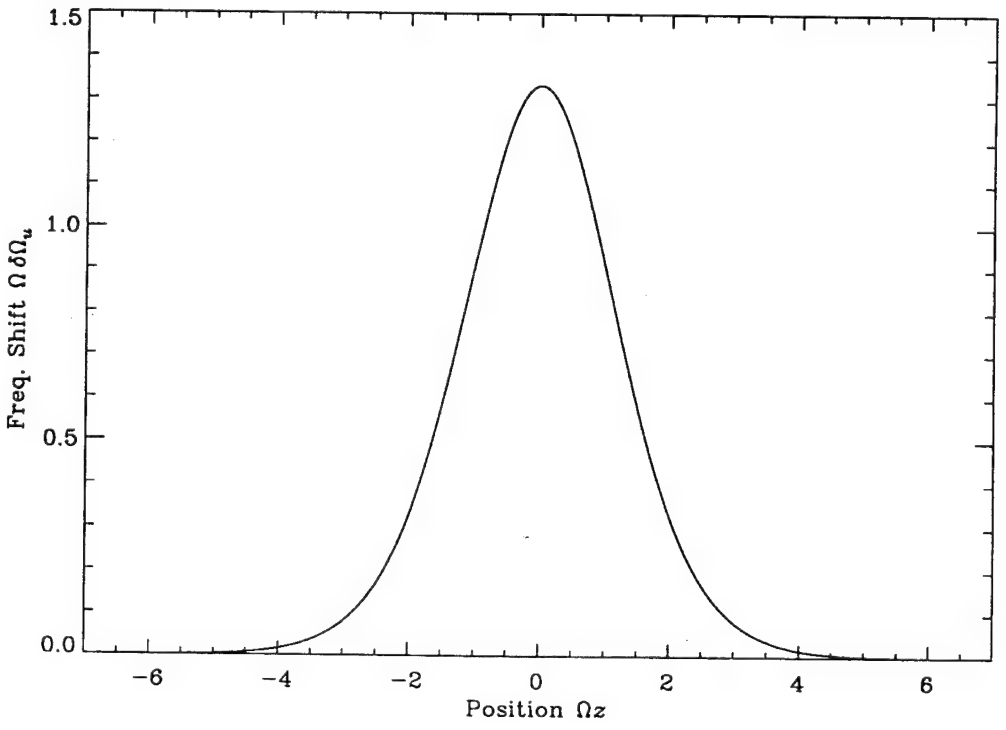

Figure 3.6: Shift in the average frequency of the faster soliton at a collision.

the mean frequency of the slower soliton is $-4/(3\Omega)$. (Recall from Eqs. (1.26) and (1.30) that a soliton with $\Omega = 0$ moves at the group velocity v_g of the moving reference frame, so that a soliton with negative normalized frequency moves slower than the reference frame.) With $\Omega = 5$ as in Figs. 3.3 and 3.4, the mean frequencies of the faster and slower solitons at $z = 0$ are 5.27 and -0.27, respectively. Figure 3.7 illustrates the variation in Ω_u and Ω_v during the collision when $\Omega = 5$. Also plotted for comparison with dashed curves are the shifts if $\Omega = 2.5$; the maximum shifts are twice as large and the collision occurs over a distance twice as long if the frequency separation is half as large. Note that while the solitons attract in time, they repel in frequency.

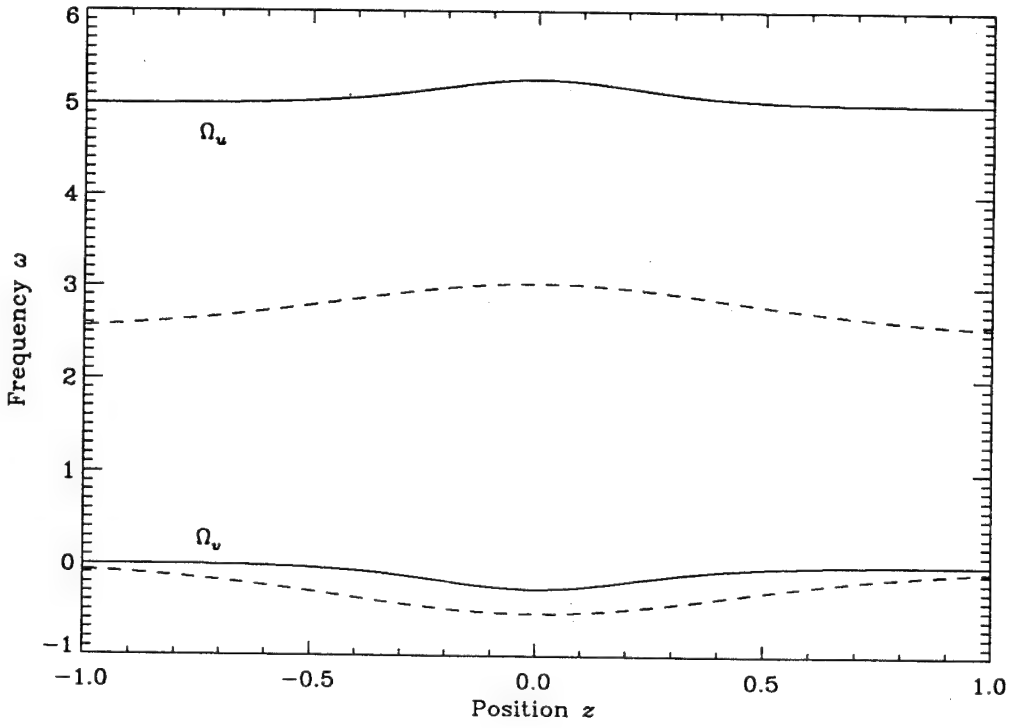

Figure 3.7. The average frequencies Ω_u and Ω_v during a collision at $z = 0$ with $\Omega = 5$ on the solid curves and $\Omega = 2.5$ on the dashed curves.

By translating the normalized values of frequency into physical dimensions, the frequency spacing of $\Omega+\delta\Omega = \Omega+8/(3\Omega)$ at the center of the collision is related to a physical spacing of $\Delta f+\delta f$, where $\delta f = 4(1.763)/(3\pi\Omega\tau)$, given $\Omega = 2\pi\Delta f\tau/1.763$ and $\delta\Omega = 8/(3\Omega)$. The maximum shift in the frequency of the faster soliton is

$$\delta f_u = \frac{2(1.763)}{3\pi\Omega\tau}, \tag{3.11}$$

and the shift in the slower soliton is $\delta f_v = -\delta f_u$. Corresponding wavelength shifts are $\delta\lambda_u = -(\lambda^2/c)\delta f_u = -\delta\lambda_v$. Also, since $(-\Omega)$ represents the inverse group velocity of the faster soliton $u(z,t)$ in Eq. (3.1), the integral of (3.10) over z yields the magnitude of the timing displacement depicted in Fig. 3.2. The displacement, as given by Eq. (A.12), is

$$\delta t_u = -\int_{-\infty}^{\infty} \delta\Omega_u(z)\, dz = -\frac{4}{\Omega^2}, \tag{3.12}$$

and $\delta t_v = -\delta t_u$. The faster soliton u moves forward in time by $4/\Omega^2$ while the slower soliton v is delayed by an equal amount. When $\Omega \gg 1$, $|\delta t_u|$ approximates the exact value of $\ln(1+4\Omega^{-2})$ predicted by IST theory in [36]. The physical magnitude of the displacement caused by a collision is

$$\delta t_{\text{coll}} = \pm\frac{4}{\Omega^2}\, t_c = \pm\frac{0.1768}{(\Delta f)^2\tau}, \tag{3.13}$$

where the plus and minus signs refer to the shifts in the slower and faster solitons, respectively. The maximum shift in the wavelength and the timing displacement of the slower soliton are plotted in Fig. 3.8 as a function of the initial wavelength spacing Λ for pulse widths of $\tau = 20$ ps and $\tau = 50$ ps. The dashed lines correspond to the wavelength spacing when the channels are spaced by five spectral widths. The shifts are consistent with experimental

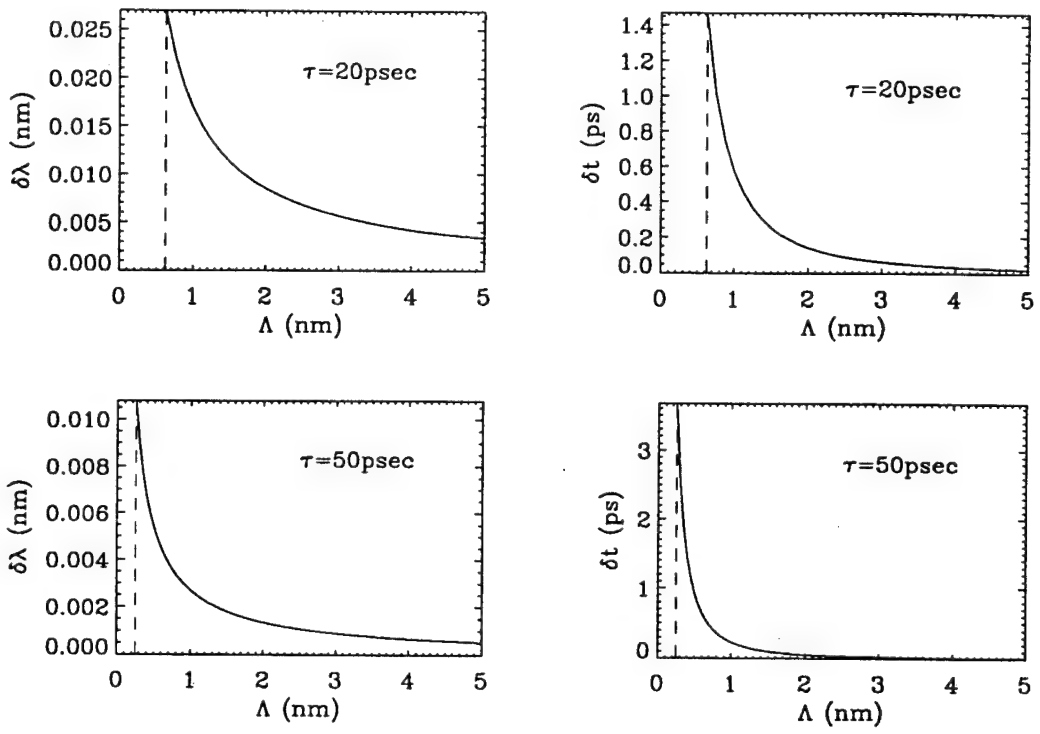

Figure 3.8. The maximum shift in the mean wavelength of the slower soliton at a collision and the timing displacement caused by the collision. $\Omega = 5.61$ on the dashed lines.

values at collisions between two WDM solitons[63]. The implications of these shifts in a communication system are discussed in detail in Chapter 5.

3.2.1 Phase independent interactions Neither the frequency shift in Eq. (3.10) nor the timing shift in Eq. (3.12) depend on the relative phase between the two solitons. Such phase independence is valid for large Ω[40, 75], in contrast to the behavior for $\Omega = 0$ in Figs. 1.8 and 1.9 where the frequencies of each soliton are identical. Mathematically, the phase independence of WDM soliton interactions is easily explained using Eq. (3.7), since the frequency shift is dependent only on the modulus of u and v. Physically, this result is most easily understood by analyzing the effect of the waveform intensity on the index

of refraction during the collision.

Suppose the waveform is approximated by a superposition of a pulse U with frequency $\Omega/2$ and a second pulse V with frequency $-\Omega/2$, as in

$$\begin{aligned} q &= U + V \\ &= \operatorname{sech}[t - t_o + \Omega z/2] \exp[-i\Omega t/2 + (1 - \Omega^2/4)z/2 + \phi] \\ &\quad + \operatorname{sech}[t - \Omega z/2] \exp[i\Omega t/2 + (1 - \Omega^2/4)z/2]. \end{aligned} \tag{3.14}$$

The intensity is given by

$$I = |q|^2 = |U|^2 + |V|^2 + 2|U|\,|V| \cos(\Omega t + \phi). \tag{3.15}$$

With $\Omega = 0$, the intensity is plotted in Fig. 3.9(a) for $\phi = 0$ and in Fig. 3.9(b) for $\phi = \pi$, where t_o is chosen so that the solitons are separated by just a few pulse widths. The index of refraction is proportional to the intensity, so the index is higher between the pulses in Fig. 3.9(a) and lower between the pulses in Fig. 3.9(b). According to Fermat's principle of least time[98] (or Maupertuis' principle of least action[99, 100]), light attempts to propagate in the medium with the higher index of refraction, so the pulses in Fig. 3.9(a) attract (as in Fig. 1.8), and the pulses in Fig. 3.9(b) repel (as in Fig. 1.9). With WDM solitons, the value of Ω is no longer zero, so the intensity beats according to Eq. (3.15) at a frequency of Ω, as depicted in Fig. 3.9(c) and (d). The index of refraction between the solitons increases on average for all values of ϕ, and the pulses attract regardless of the phase difference.

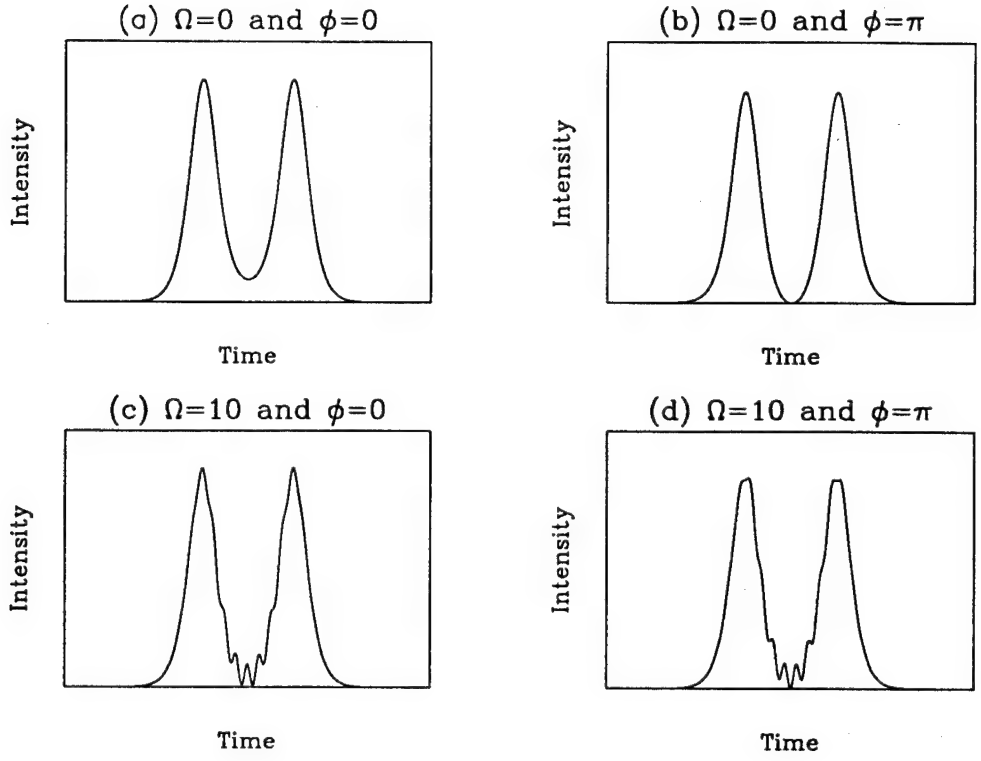

Figure 3.9. Effect of the relative phase ϕ between two solitons on waveform intensity.

3.3 Quantitative analysis of N-soliton interactions

To predict the effects of interactions between an arbitrary number of wavelength channels, we analyze the exact N-soliton solution of the NLSE[6, 8],

$$u(z,t) = \sum_{j=1}^{N} q_j(z,t), \tag{3.16}$$

where $u(z,t)$ is now a generalized waveform describing the propagation of as many as N solitons and the $q_j(z,t)$ are solutions of the linear matrix equations

$$\sum_{k=1}^{N} A_{jk}\, q_k = 1. \tag{3.17}$$

A is an $N \times N$ matrix with components

$$A_{jk} = \frac{\exp(-i\chi_j - S_j) + \exp(-i\chi_k + S_k)}{2 - i(\Omega_j - \Omega_k)}, \tag{3.18}$$

and with parameters,

$$S_j = t - t_{oj} + \Omega_j z \tag{3.19}$$

$$\chi_j = -\Omega_j t + (1 - \Omega_j^2) z/2, \tag{3.20}$$

where each soliton has unit amplitude. An initial offset t_{oj} is necessary here if we assume that the timing relationship between the solitons is arbitrary. A single soliton as in Eq. (1.25) is equivalent to the inverse of a single diagonal component of A, as given by

$$\frac{1}{A_{jj}} = \mathrm{sech}(S_j) \exp(i\chi_j). \tag{3.21}$$

In contrast, the N soliton solution in Eqs. (3.16) and (3.17) is a sum of all the components in the inverse matrix A^{-1},

$$u(z,t) = \sum_{j=1}^{N} q_j(z,t) = \sum_{j,k=1}^{N} (A^{-1})_{jk}, \tag{3.22}$$

where the notation $\sum_{j,k}$ indicates a double summation over j and k.

3.3.1 Asymptotic expansion of the exact N-soliton waveform In general, A^{-1} is rather complicated and Eq. (3.22) is difficult to solve, even for N as small as two. One way to analyze an N-soliton waveform is to carry out an asymptotic expansion of A^{-1}[101]. First, we note that A may be defined as $A = D + M$, where the components in D and M are the diagonal and off-diagonal components of A, respectively. Assuming the frequency separation $\Omega_j - \Omega_k$ between any two channels in the denominator of A_{jk} is large, we define a small parameter

$$\epsilon \equiv \frac{1}{\Omega} = \max_{j,k} \left(\frac{1}{|\Omega_j - \Omega_k|} \right), \tag{3.23}$$

where Ω is the frequency separation between adjacent channels. Expanding A^{-1}, we have

$$\begin{aligned} A^{-1} = (D+M)^{-1} &= [D(I+P)]^{-1} \\ &= (I+P)^{-1}D^{-1} \\ &= (I-P+P^2-P^3+\ldots)D^{-1}, \end{aligned} \tag{3.24}$$

where $P = D^{-1}M$. Since the components of the off-diagonal matrix M correspond to the components A_{jk} for $j \neq k$, the terms $P^n D^{-1}$ in the asymptotic expansion are $O(\epsilon^n)$. So to leading order, Eq. (3.22) becomes

$$\begin{aligned} u(z,t) &= \sum_{j,k=1}^{N} (A^{-1})_{jk} \\ &= \sum_{j,k=1}^{N} \left[(D^{-1})_{jj} - (D^{-1}MD^{-1})_{jk}\right] + O(\epsilon^2) \\ &= \sum_{j=1}^{N} \left[q_j^{(0)}(z,t) + q_j^{(1)}(z,t)\right] + O(\epsilon^2). \end{aligned} \tag{3.25}$$

The terms $q_j^{(0)}(z,t)$ and $q_j^{(1)}(z,t)$ describe the zeroth and first order effects of $q_j(z,t)$ in Eq. (3.22).

Since $(D^{-1})_{jj} = 1/A_{jj}$ as in Eq. (3.21), the asymptotic approximation of the exact N-soliton solution consists of a sum of N fundamental solitons minus a correction factor $\sum (D^{-1}MD^{-1})_{jk}$ which describes interactions between the solitons to first order. As $\epsilon = (1/\Omega) \to 0$, interactions are negligible and the waveform is a superposition of N distinct solitons,

$$\begin{aligned} u(z,t) &\approx \sum_{j=1}^{N} q_j^{(0)}(z,t) + O(\epsilon) \\ &\approx \sum_{j=1}^{N} \operatorname{sech}(S_j)\exp(i\chi_j) + O(\epsilon). \end{aligned} \tag{3.26}$$

No interactions are observed during collisions between these solitons since the frequency separation Ω is very large. This is consistent with Eqs. (3.10) and

(3.12), where the timing displacements and frequency shifts at a two-soliton collision go to zero as $\Omega \to \infty$. In this regime, each spectral peak at Ω_j is described according to Eq. (1.30), so

$$\begin{aligned} \tilde{u}(z,\omega) &\approx \sum_{j=1}^{N} \tilde{q}_j^{(0)}(z,\omega) + \mathrm{O}(\epsilon) \\ &\approx \pi \sum_{j=1}^{N} \mathrm{sech}[\pi(\omega - \Omega_j)/2] \exp[i\Phi_j(z)] + \mathrm{O}(\epsilon), \end{aligned} \tag{3.27}$$

where the $\Phi_j(z)$ are

$$\Phi_j(z) = (1 - 2\Omega_j\omega + \Omega_j^2)z/2 + (\omega - \Omega_j)t_{oj}. \tag{3.28}$$

To estimate the first order effects on the soliton evolution, the second term of the summation in (3.25) must be included. These effects (as derived in the appendix in Section A.2) are described by

$$\begin{aligned} \sum_{j=1}^{N} q_j^{(1)}(z,t) &= -\sum_{j,k=1}^{N} (D^{-1}MD^{-1})_{jk} \\ &\approx -2i\epsilon \sum_{j=1}^{N} \left[\mathrm{sech}(S_j) \exp(i\chi_j) \left(\sum_{\substack{k=1 \\ k\neq j}}^{N} \frac{\tanh(S_k)}{j-k} \right) \right], \end{aligned} \tag{3.29}$$

where the frequency separation $\Omega_j - \Omega_k = (j-k)\Omega = (j-k)/\epsilon$. Equation 3.29 is the first order correction to $q_j^{(0)}(z,t)$. Including this term in Eq. (3.25), the N-soliton waveform is described to leading order by

$$\begin{aligned} u(z,t) &= \sum_{j=1}^{N} \left[\mathrm{sech}(S_j) \exp(i\chi_j) \left(1 - 2i\epsilon \sum_{\substack{k=1 \\ k\neq j}}^{N} \frac{\tanh(S_k)}{j-k} \right) \right] + \mathrm{O}(\epsilon^2) \\ &= \sum_{j=1}^{N} \left[q_j^{(0)}(z,t) \left(1 - 2i\epsilon \sum_{\substack{k=1 \\ k\neq j}}^{N} \frac{\tanh(S_k)}{j-k} \right) \right] + \mathrm{O}(\epsilon^2). \end{aligned} \tag{3.30}$$

As $\epsilon \to 0$, $u(z,t)$ approaches $q^{(0)}(z,t)$ as given in Eq. (3.26). Note also that the $\mathrm{O}(\epsilon)$ term is imaginary, changing the phase of $q_j^{(0)}(z,t)$. The only effect this has

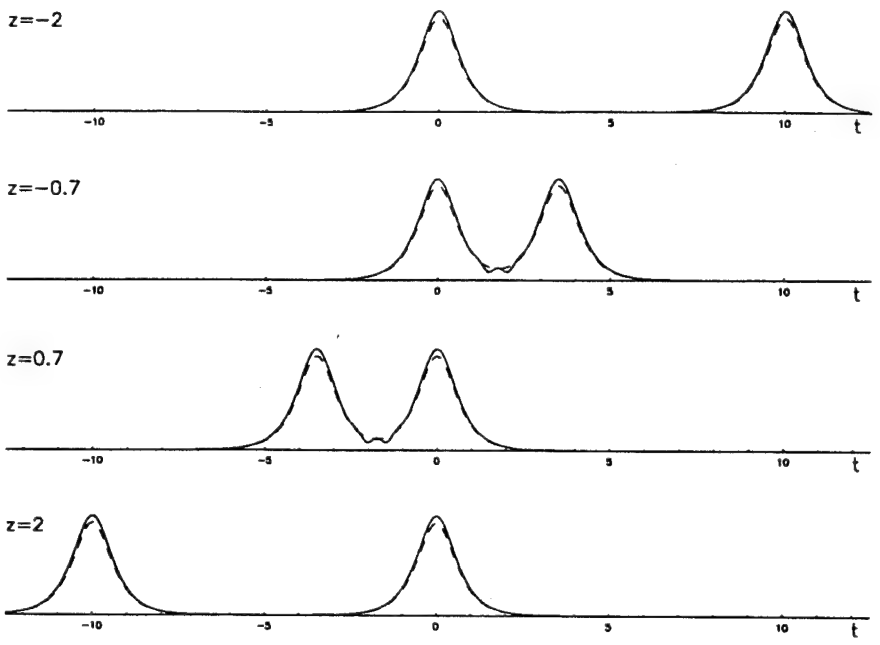

Figure 3.10: Pulse behavior in space under leading order asymptotic effects.

on the envelope of the N-soliton waveform is a slight increase in the amplitude of each soliton, as demonstrated at various z in Fig. 3.10 for $N = 2$ with $\Omega_1 = 0$ and $\Omega_2 = 5$. The solid curves depict $u(z,t)$ in Eq. (3.30) and the dashed curves depict $q_j^{(0)}(z,t)$. In comparison to Fig. 3.2, no timing displacements result since timing shifts are $O(\epsilon^2)$. (Recall from Eq. (3.12) that the timing shift is proportional to $\Omega^{-2} = \epsilon^2$.) Timing displacements would be observed if the next term $q_j^{(2)}(z,t)$ were included in the expansion of (3.25).

To describe the spectral evolution of an N-soliton waveform, the Fourier transform of $u(z,t)$ is required. It is relatively straightforward to derive the Fourier transform of $q_j^{(0)}(z,t) = \mathrm{sech}(S_j)\exp(i\chi_j)$; this was done in Eqs. (1.27)—(1.30) and the result is given by $\tilde{q}_j^{(0)}(z,\omega) = \pi\mathrm{sech}(\pi\alpha_j/2)\exp(i\Phi_j)$ in

Eq. (3.27), where we define $\alpha_j = \omega - \Omega_j$. The Fourier transform of

$$q_j^{(1)}(z,t) = -2i\epsilon\, q_j^{(0)}(z,t) \left(\sum_{\substack{k=1 \\ k\neq j}}^{N} \frac{\tanh(S_k)}{j-k} \right) \tag{3.31}$$

is derived in Section A.2 and is given by

$$\tilde{q}_j^{(1)}(z,\omega) = 2\epsilon\, \tilde{q}_j^{(0)}(z,\omega) \left(\sum_{\substack{k=1 \\ k\neq j}}^{N} \frac{\sin(\alpha_j S_{jk})}{(j-k)\sinh(S_{jk})} \right), \tag{3.32}$$

where $S_{jk} = S_j - S_k = (j-k)\Omega z - (t_{oj} - t_{ok})$. This is the first order correction to $q_j^{(0)}(z,\omega)$, so the overall spectral waveform is

$$\begin{aligned} \tilde{u}(z,\omega) &= \sum_{j=1}^{N} \tilde{q}_j(z,\omega) \qquad (3.33) \\ &= \sum_{j=1}^{N} \tilde{q}_j^{(0)}(z,\omega) \left(1 + \sum_{\substack{k=1 \\ k\neq j}}^{N} \frac{2\epsilon \sin(\alpha_j S_{jk})}{(j-k)\sinh(S_{jk})} \right) + \mathrm{O}(\epsilon^2) \\ &= \sum_{j=1}^{N} \pi \mathrm{sech}(\pi\alpha_j/2) \exp(i\Phi_j) \left(1 + \sum_{\substack{k=1 \\ k\neq j}}^{N} \frac{2\epsilon \sin(\alpha_j S_{jk})}{(j-k)\sinh(S_{jk})} \right) + \mathrm{O}(\epsilon^2). \end{aligned}$$

The spectrum at a collision between two solitons, with $\Omega_1 = 0$ and $\Omega_2 = 5$, is shown in Fig. 3.11. The dashed curve is a plot of $\tilde{q}_j^{(0)}(z,\omega)$, and the solid curve is a plot of $\tilde{q}_j^{(0)}(z,\omega) + \tilde{q}_j^{(1)}(z,\omega)$ at the midpoint of a collision. Note that the frequency space during the collision is nearly the same as that depicted by the solid curve in Fig. 3.4.

Frequency shifts at interactions between N WDM solitons are described by analyzing a single spectral peak of $\tilde{u}(z,\omega)$ in Eq. (3.33). The value of α_j when the derivative $d|\tilde{q}_j(z,\omega)|/d\alpha_j$ equals zero defines the shift in the spectral peak of the jth soliton at any position z in the fiber. Here we solve for the peak of the soliton spectrum, since it is uniquely defined from a mathematical standpoint. This is in contrast to the shift in the mean frequency, as

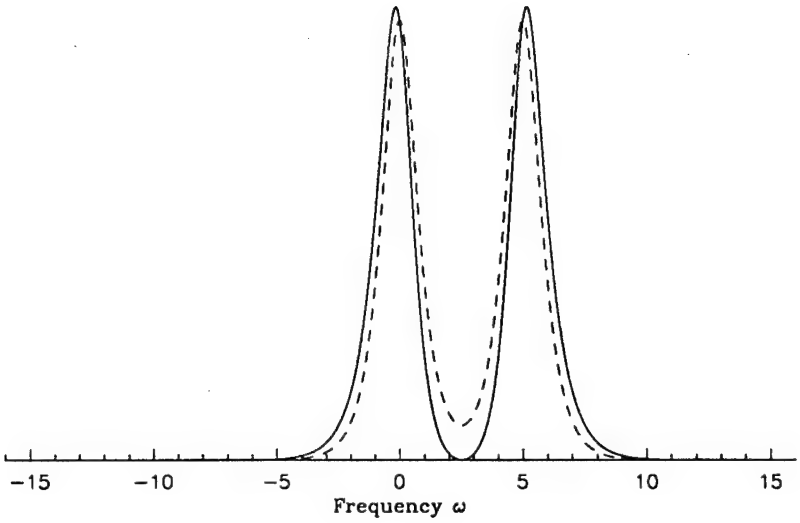

Figure 3.11. The frequency spectrum at a collision with (solid curve) and without (dashed curve) first order effects.

solved for in Section 3.2 during a two soliton collision. If the shift in the peak is small, then it is described by the transcendental equation,

$$\alpha_j \approx \frac{4}{\pi^2}\left(\frac{2\epsilon\sum_{k\neq j}\frac{S_{jk}}{(j-k)\sinh(S_{jk})}}{1+2\epsilon\alpha_j\sum_{k\neq j}\frac{S_{jk}}{(j-k)\sinh(S_{jk})}}\right). \tag{3.34}$$

However, if α_j is $O(\epsilon)$, as was true for the shift in the mean frequency in Eq. (3.10), then the value of the second term in the denominator is $O(\epsilon^2)$, and the shift in the peak frequency is approximated by

$$\delta\Omega_j = \alpha_j \approx \frac{8}{\pi^2\Omega}\sum_{\substack{k=1\\k\neq j}}^{N}\frac{S_{jk}}{(j-k)\sinh(S_{jk})}. \tag{3.35}$$

This result is important because it demonstrates that the frequency shift in the jth peak is simply a sum of the shifts caused by any of the other $N-1$ solitons. It is well known that timing displacements at collisions between N solitons are

additive, since the solitons collide in a pairwise fashion[36]. Equation (3.35) confirms that spectral shifts are also additive to leading order.

It is interesting to compare the shift in the frequency peak of a single soliton to the shift in its mean frequency at a collision with a second soliton. The shift in the mean frequency is different than the shift in the peak since the envelope of a single frequency component is not symmetric during the collision (see Figs. 3.4 and 3.11). Taking $N = 2$, with $S_1 = t$ and $S_2 = t + \Omega z$, $S_{21} = \Omega z$, so the shift in the peak frequency of the soliton originally at $\Omega_2 = \Omega$ is

$$\delta\Omega_2 = \frac{8}{\pi^2 \Omega} \frac{\Omega z}{\sinh(\Omega z)}. \tag{3.36}$$

The peak frequency of the soliton initially at $\Omega_1 = 0$ shifts by $\delta\Omega_1 = -\delta\Omega_2$. In contrast, the mean frequencies shift according to Eq. (3.10). Plots of each shift are depicted in Fig. 3.12, where the solid curve corresponds to the shift in the peak frequency given by Eq. (3.36), and the dashed curve corresponds to the shift in the mean as described by Eq. (3.10). The maximum shift in the peak frequency is $8/(\pi^2\Omega)$, an amount that is 40% less than the maximum shift of $4/(3\Omega)$ in the mean frequency. However, the peak frequency begins to shift earlier during the collision. In fact, by taking the integral of the shift in the inverse group velocity $-\delta\Omega_2$, the timing displacement (equal to the area under each curve) is identically equal to $-4/\Omega^2$ for both curves. With respect to Fig. 3.8, the shift in the peak wavelength is 40% less than the shift in the mean, while the timing shifts are as shown.

3.3.2 Numerical verification of N-soliton interactions To verify the shift predicted by Eq. (3.35), we numerically compute the exact solution of the NLSE using Eq. (3.16) and its Fourier transform for $N = 2$ and $N = 3$. The results are inductive, ensuring the accuracy of Eq. (3.35) for

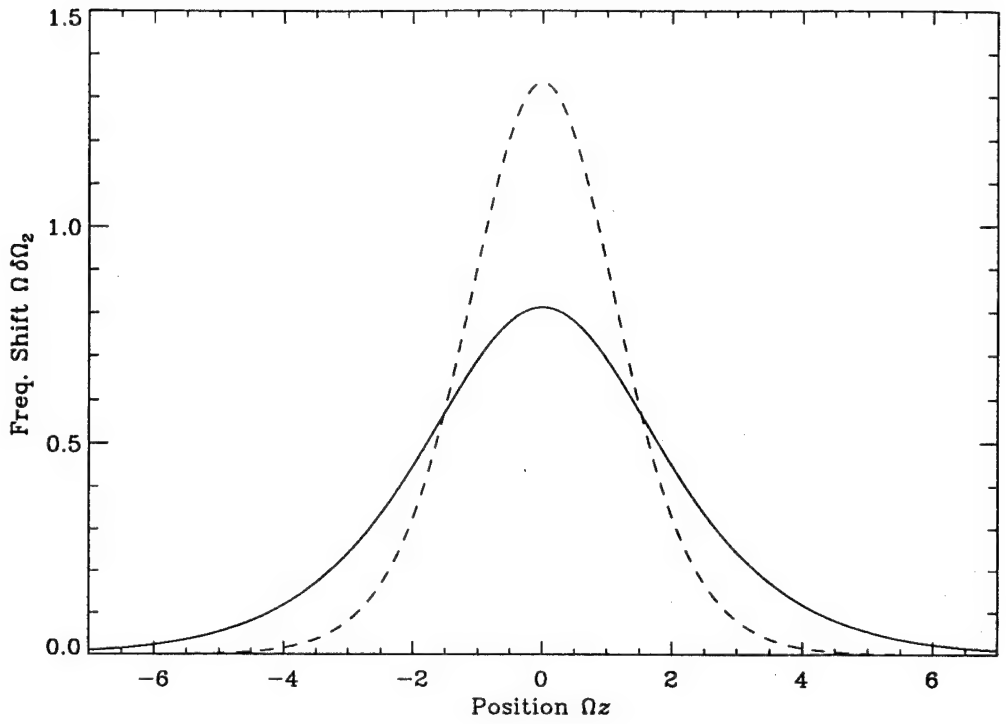

Figure 3.12. Shift in the peak (solid curve) and the mean (dashed curve) frequency of the faster soliton at a collision with a slower soliton.

arbitrary values of N. Discretized values of the exact temporal waveform are computed in C at each position along the fiber, and the spectrum is determined by taking a fast-Fourier transform of the discrete points in time. The spectral evolution in Fig. 3.3 was computed in this manner for each position z in Fig. 3.1. The algorithm is generalized for $N = 2$ or $N = 3$, so that the exact solution for $N = 2$ is computed by setting the amplitude of the third soliton equal to zero. (The analytic form of the exact solution for $N = 3$ is rather complicated, as listed in the program in Appendix B.) Since the spectrum is discretized, the actual value of the peak of each soliton frequency component is not well defined. To estimate the actual position of a peak, the five points around the peak are interpolated with a Lagrange polynomial[75], and the location of

the maximum is predicted by taking the derivative of the polynomial. (The Mathematica program used to calculate the location of each frequency peak is also included in Appendix B.)

First, we take $N = 2$ and determine the accuracy of Eq. (3.36). As expected, the results are most accurate when Ω is large, since $O(\epsilon^2)$ and higher effects were neglected during the expansion of Eq. (3.25). The dotted curves in Fig. 3.13 depict the shift in Ω_2 during a two soliton collision, as derived from a numerical computation of the exact two-soliton solution of the NLSE with initial frequencies $\Omega_1 = 0$ and $\Omega_2 = \Omega$. The solid curves depict the shift as given by Eq. (3.36). For values of Ω greater than ten, the error between

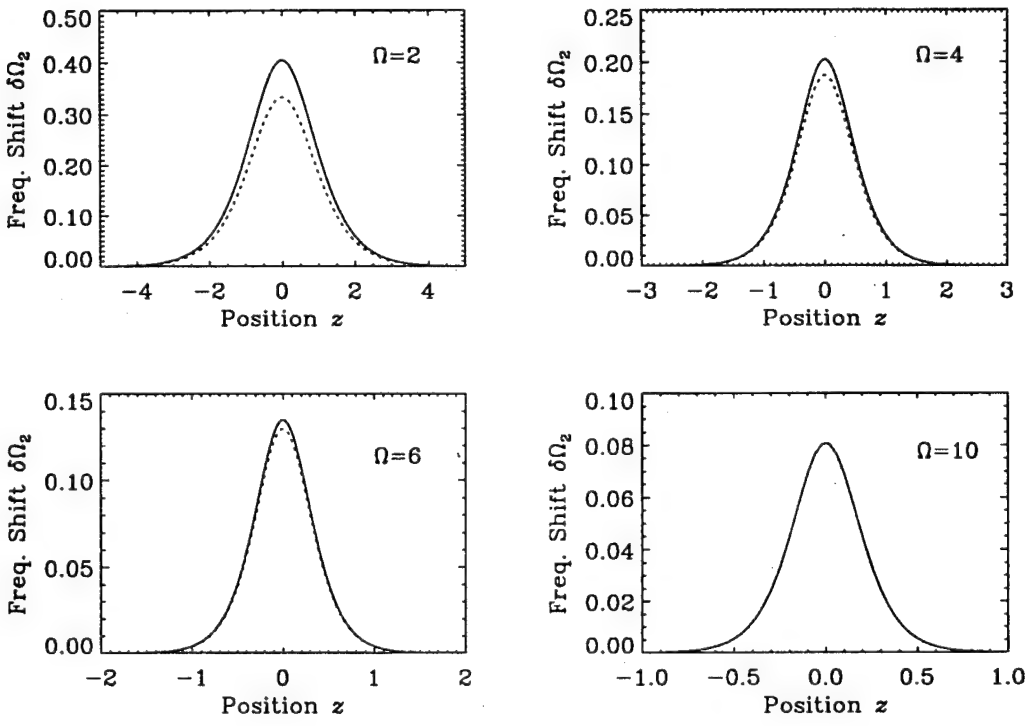

Figure 3.13. Numerically (dotted curves) and asymptotically (solid curves) estimated frequency shift at a two-soliton collision.

the asymptotic value and the exact value is less than 1.5%, so the difference between the curves is hardly noticeable. When $\Omega = 5$, the shift estimated by Eq. (3.36) is 5% too large, so the shifts in each peak of Fig. 3.11 are 5% greater than the shifts in each peak of Fig. 3.4. The discrepancy between Eq. (3.36) and the numerical results becomes larger when Ω is smaller, as seen in Fig. 3.14, where the maximum shift of $8/(\pi^2\Omega)$ from Eq. (3.36) is plotted on the solid curve and numerical estimates of the maximum shift are plotted on the dotted curve. By fitting a polynomial to the dotted curve, the maximum value of the numerical shift is predicted to second order, as in

$$\delta\Omega_{\max} = \frac{8}{\pi^2\Omega} - \frac{0.277}{\Omega^2}. \tag{3.37}$$

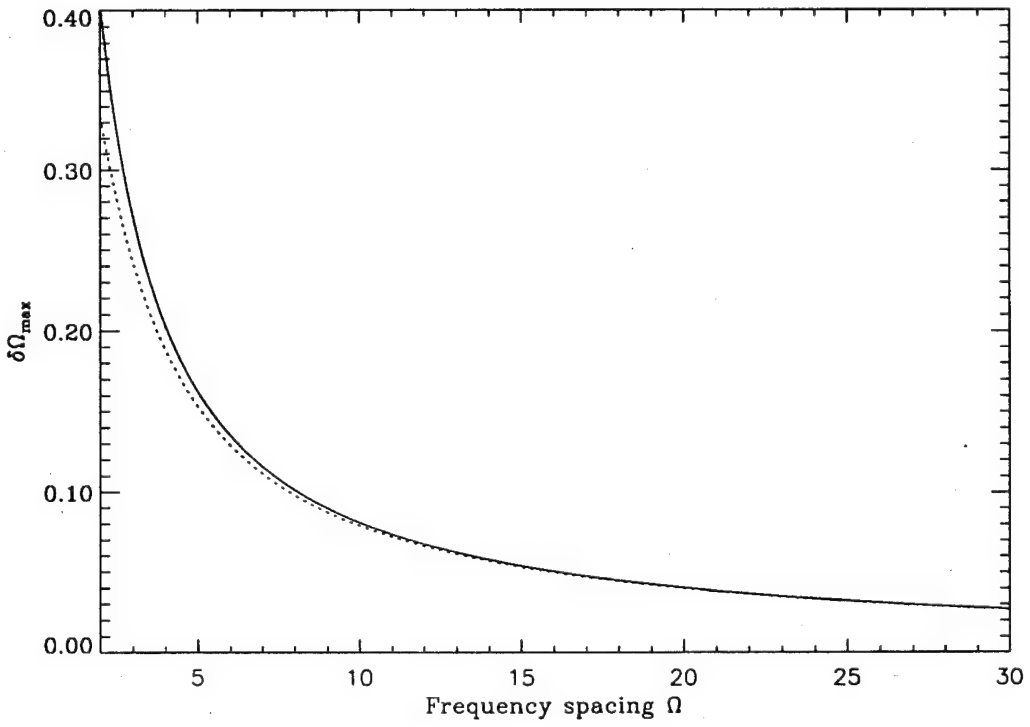

Figure 3.14. Numerically computed maximum shift (dotted curve) and the analytically estimated shift (solid curve).

Since the value of Ω must typically be greater than five to prevent large frequency and timing shifts, a first order estimate of the shift is usually sufficient, so Eq. (3.36) is adequate in most cases.

To verify the accuracy of Eq. (3.35) for arbitrary N, we first compute the waveform at a simultaneous collision between three solitons, as depicted in Fig. 3.15. The value of t_{oj} for each soliton is equal to zero, so the collision occurs at $t = 0$ and $z = 0$. The waveform is made up of three soliton components $q_1(z,t)$, $q_2(z,t)$, and $q_3(z,t)$ with initial frequencies $\Omega_1 = -10$, $\Omega_2 = 0$, and $\Omega_3 = 10$, respectively, as illustrated by the spectrum in Fig. 3.16.

As seen in the spectrum, distortion primarily affects frequencies Ω_1 and Ω_3. A small amount of distortion is seen in the frequency component at Ω_2, although it is most likely just a shift in amplitude, given the results in Fig. 3.17. Each curve in Fig. 3.17 represents the contour of one of the three frequency peaks, easily found by viewing Fig. 3.16 from above. Each dotted curve corresponds to the numerically computed results using the data from Fig. 3.16, and the solid curves correspond to Eq. (3.35). No difference is seen between the numerically computed location of each frequency peak and the asymptotic estimates. Given the results in Fig. 3.14, it is likely the discrepancy between the curves would be greater if Ω was less than ten. There is no frequency shift in the peak of the component at Ω_2 because the combined effects of the first and third soliton on the second soliton cancel, as predicted by Eq. (3.35). The maximum shift in Ω_3 is given by the sum of its interactions with the first and second soliton, so its value at the center of the collision is $\Omega_3 = 10 + 8/(10\pi^2) + 8/(20\pi^2) = 10.12$. Consistent with the behavior at a two-soliton collision, the soliton frequency components repel as the pulses attract

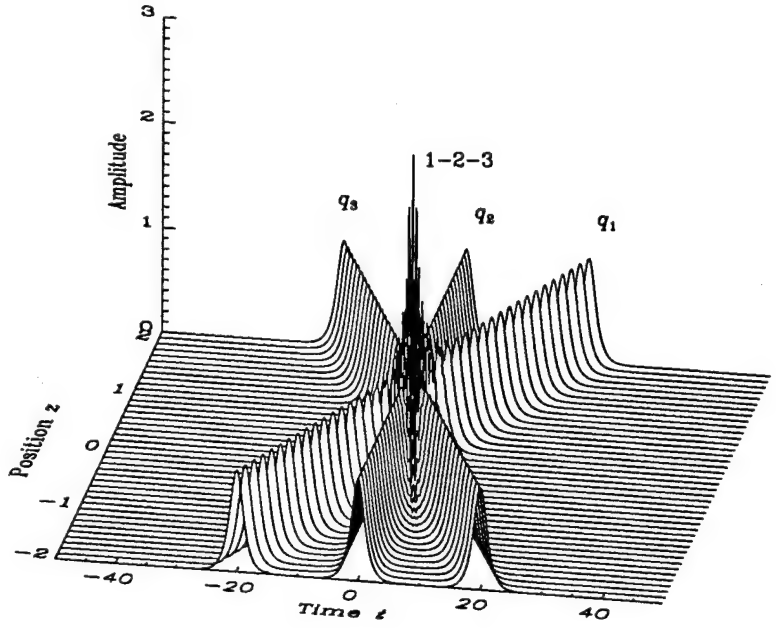

Figure 3.15: Simultaneous collision of three solitons.

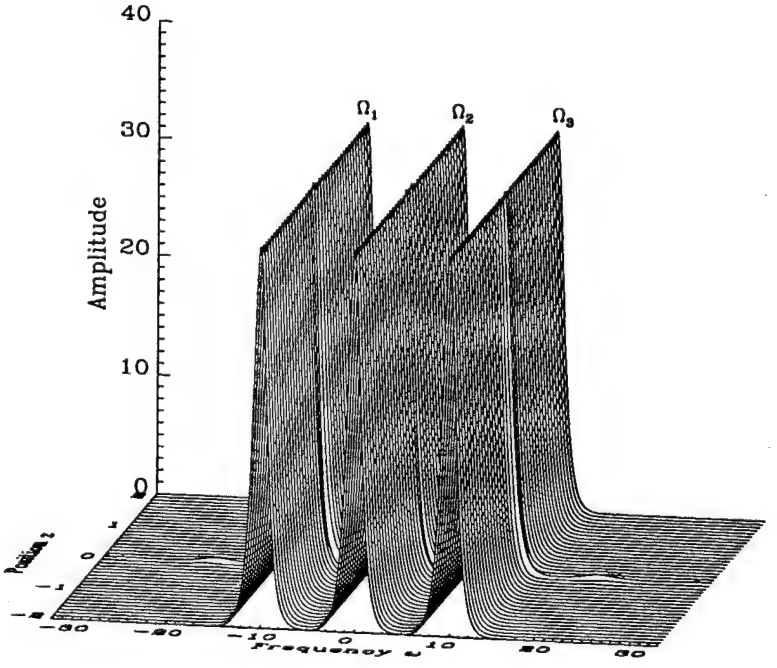

Figure 3.16: Frequency spectrum at simultaneous collision of three solitons.

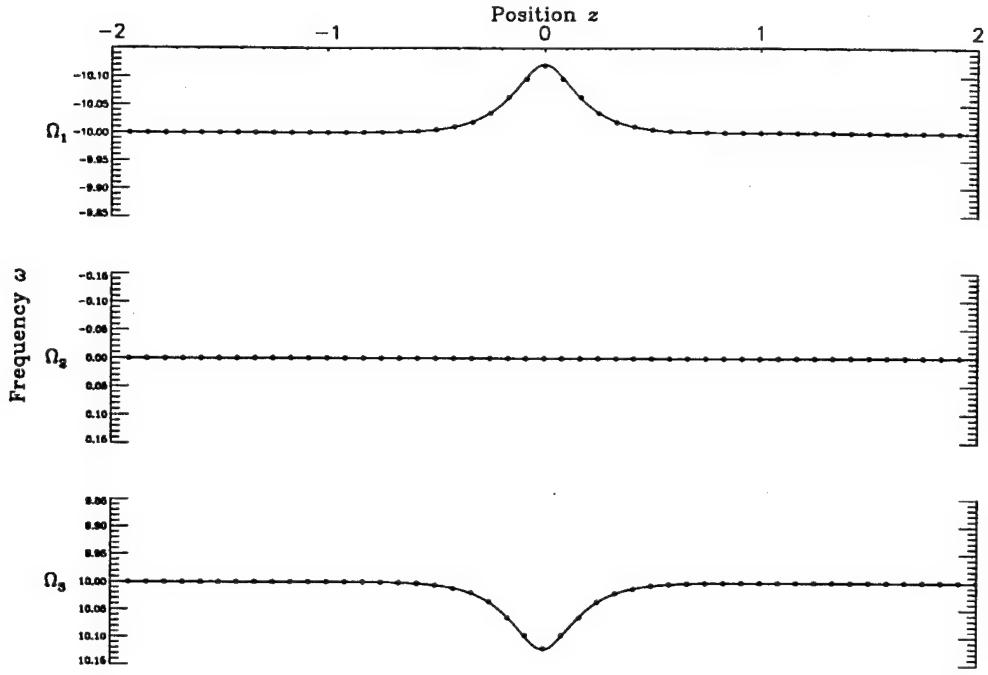

Figure 3.17. Numerically (dotted curves) and asymptotically (solid curves) predicted contours of the spectral peaks during a simultaneous collision with $N = 3$.

in the time domain, so the frequency of the slower soliton decreases to a value of $\Omega_1 = -10.12$.

The most interesting numerical results are observed when determining the accuracy of Eq. (3.35) if the collisions between the three solitons are not simultaneous, as depicted in Fig. 3.18. Although the frequency of each soliton is the same as before, as seen in Fig. 3.19, the timing is different, with $t_{o1} = 5$, $t_{o2} = -5$, and $t_{o3} = 10$. Each t_{oj} represents the timing of each pulse at the position $z = 0$. Given these parameters, solitons one and two collide at $z = -1$, solitons one and three collide at $z = 0.25$, and solitons two and three collide at $z = 1.5$. Distortion is seen in the corresponding frequency components in Fig. 3.19 at the position of each collision. The position of a collision is predicted by solving for z when the value of $S_{jk} = -S_{kj} = S_j - S_k = 0$. As an example,

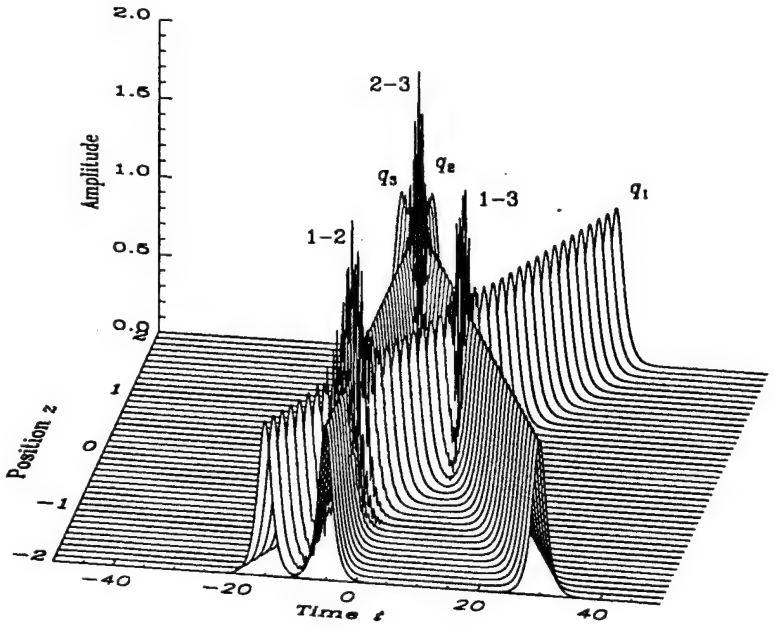

Figure 3.18: Random collisions between solitons with $N = 3$.

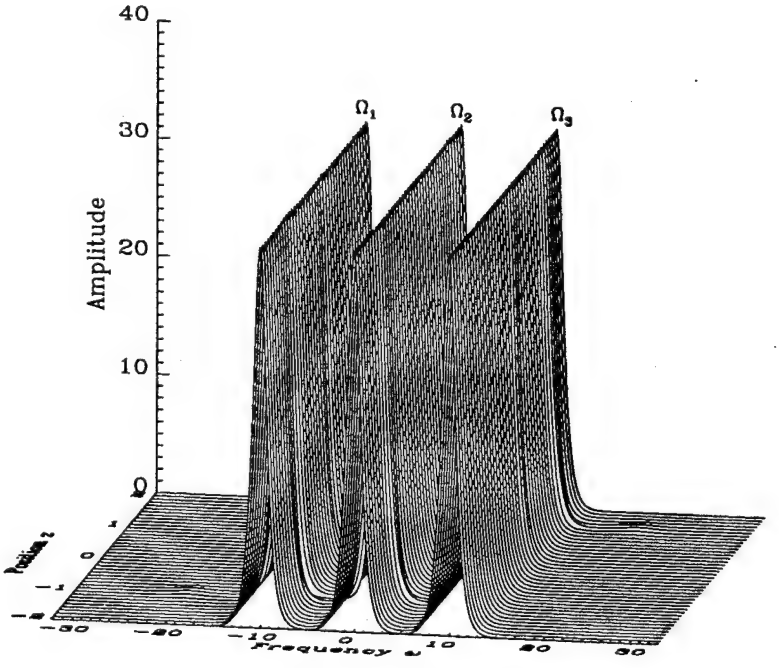

Figure 3.19. Frequency spectrum during random collisions between solitons with $N = 3$.

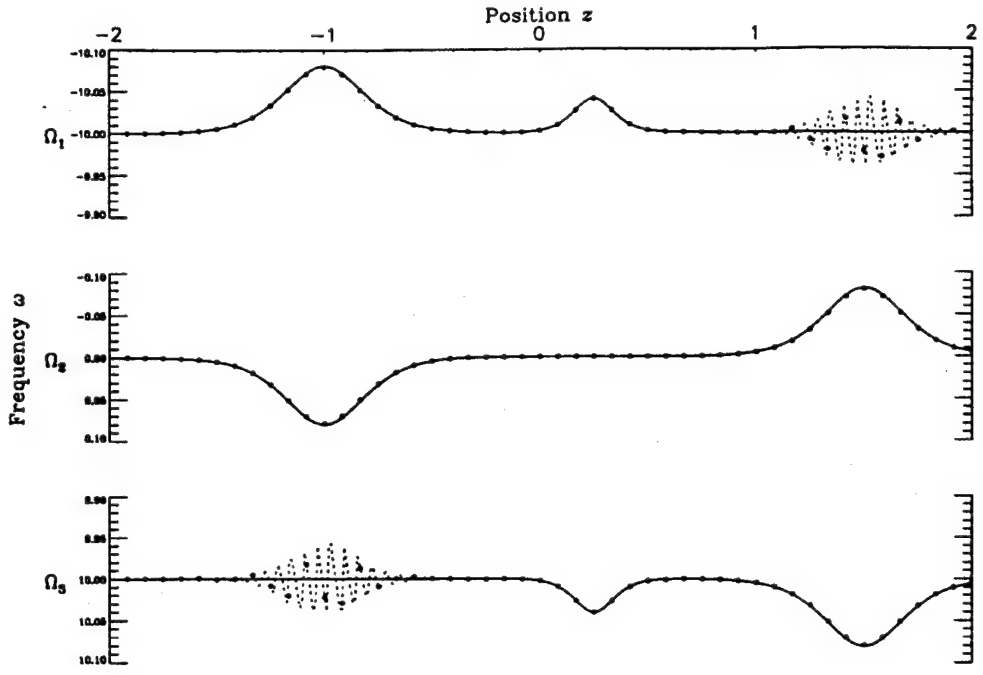

Figure 3.20. Numerically (dotted curves) and asymptotically (solid curves) predicted contours of three spectral peaks during random soliton collisions.

the collision between soliton one and soliton two occurs at the position defined by the equation

$$\begin{aligned} S_{12} = S_1 - S_2 &= (\Omega_1 - \Omega_2)z - (t_{o1} - t_{o2}) \\ &= -10z - 10 = 0. \end{aligned} \tag{3.38}$$

The positions of the other two collisions are predicted in a similar manner.

The frequency shifts at each collision are analyzed as before by using contour plots of each frequency peak, as illustrated in Fig. 3.20. If the collisions are not simultaneous, the estimated shifts using Eq. (3.35) agree for the most part with the numerics. For instance, the magnitude of the shifts between solitons one and two at $z = -1$ and solitons two and three at $z = 1.5$ equal $8/(\pi^2 10) = 0.08$ since the frequency separation at each of these collisions is $\Omega = 10$. The maximum shift during the collision between solitons one and

three at $z = 0.25$ is half as large because the frequency spacing is twice as large.

Of greater interest, though, is the discrepancy between the asymptotics and the numerics in soliton three at $z = -1$ and soliton one at $z = 1.5$. While the first order asymptotic analysis predicts no distortion in either frequency peak at these positions, the numerical results indicate that the peak of the component at Ω_3 oscillates during the collision between solitons one and two, and that the peak at Ω_1 oscillates during the collision between solitons two and three. The oscillations cannot be seen in Fig. 3.19 because the magnitude of the shift is small relative to the channel spacing, but the numerical computation of the frequency peak using the Lagrange polynomial is able to detect the effect (the details of the oscillation were observed by using a very fine discretization of positions z).

The source of the oscillation appears to be a type of four-wave mixing(FWM) between colliding solitons[3]. Note that in Fig. 3.19, during the collision between solitons one and two at position $z = -1$, there is a small frequency component located at a frequency of $\omega = -20$. This is a FWM mixing component corresponding to the frequency difference $2\Omega_1 - \Omega_2 = -20$. A second FWM component results during the collision and has a frequency of $\omega = 2\Omega_2 - \Omega_1 = 10$, identical to the spectral component of soliton three. A more detailed analysis of Fig. 3.19 shows that the oscillation in the spectral peak of the third soliton at position $z = -1$ is a direct result of beating between the phases of the FWM component and the spectral component at Ω_3.

It is useful to note that there is no oscillation in the peak at Ω_2 in Fig. 3.20 during the collision between solitons one and three at $z = 0.25$. This

is reasonable since there is no FWM component at $\omega = \Omega_2$ during this collision. The FWM frequencies are $\omega = 2\Omega_1 - \Omega_3 = -30$ and $\omega = 2\Omega_3 - \Omega_1 = 30$ during a collision between solitons one and three; these FWM components are barely noticeable in Fig. 3.19 at $z = 0.25$. FWM terms are dropped in the derivation of the coupled NLSE for two solitons in Eqs. (3.4) and (3.5), although actual FWM components are easy to see at $\omega = 10$ and $\omega = -5$ in the spectrum of the two-soliton collision in Fig. 3.3.

The full implications of FWM on fiber communications is beyond the scope of this thesis, but it should be mentioned here that oscillations as depicted by Fig. 3.20 do not actually degrade data in a soliton channel that corresponds to a FWM frequency. For example, consider the collision between solitons one and two and the corresponding oscillation in the soliton spectral component at Ω_3. In reality, the oscillation only occurs in the spectral domain — the FWM energy at $\omega = \Omega_3$ exists in the fiber specifically at the location of the collision between solitons one and two, and not at the location of soliton three. In other words, the frequency and velocity of a given pulse may not be affected by FWM interactions that occur somewhere else in the fiber. The oscillation only exists in the Fourier domain as a result of a Fourier integration across infinite time. However, this does not mean that FWM may be ignored; FWM at Ω_3 still might act as a noise source at the receiver for the third channel, especially if the collision between solitons one and two happened to occur at an amplfier. Such FWM effects have been studied by several researchers[97, 102, 103], with implications that will be discussed briefly in the next chapter.

CHAPTER 4

PERTURBATIONS AND WDM SOLITONS

In this chapter, we discuss how perturbations influence the soliton interactions described in Chapter 3. Our emphasis is primarily on the effects of loss and amplification, since these non-Hamiltonian perturbations are possibly the most important factors limiting the application of solitons to WDM communications. Exceptions to this may include interactions between WDM solitons during collisions at the fiber input or other nonlinearities such as stimulated Raman scattering, stimulated Brillouin scattering, or four-wave mixing, as will be discussed in the latter half of the chapter.

4.1 Loss and amplification

Intuitively, one might expect variations in pulse energy to significantly impair soliton propagation, since the soliton energy must be chosen properly to balance chromatic dispersion. However, as mentioned in Section 1.2, soliton propagation in a lossy fiber is still quite robust if amplifiers are not spaced too far apart. We denote this amplifier spacing as L_a in Fig. 4.1, where the average energy, as shown by the dashed line, must equal the fundamental soliton energy required for SPM to balance GVD[19]. The gain G of each EDFA in Fig. 4.1 is chosen to compensate the attenuation that occurs when propagating a distance L_a. If the attenuation coefficient $\alpha = 0.21$ dB/km, then in dB $G = 0.21L_a$, where L_a must typically be less than 50 km. Limiting the amplifier spacing also helps decrease jitter and energy fluctuations due to ASE noise, and we shall

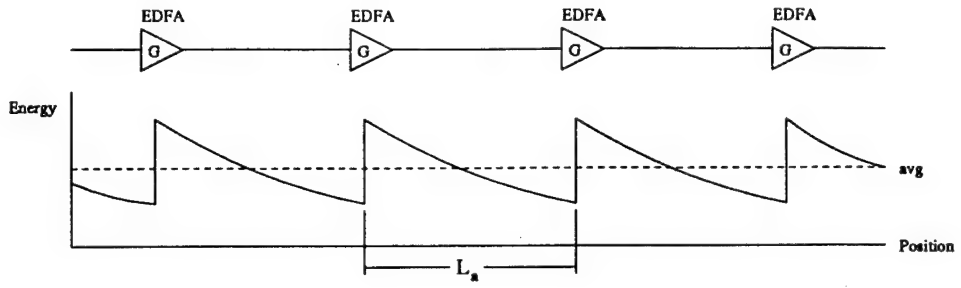

Figure 4.1: Lumped amplifiers and the corresponding energy profile.

see that it also reduces the magnitude of interactions between WDM solitons.

4.1.1 Loss and amplification during WDM soliton collisions

If two WDM solitons collide in a lossless fiber, the interaction is balanced — velocity shifts are symmetric about the center of the collision (see Fig. 3.6). This is reasonable since the nonlinear attraction between the solitons is just as strong during the last half of the collision as during the first half. When there is loss, though, the nonlinear attraction in the first half of the collision differs from the attraction in the last half of the collision. The imbalance in the attractive force may cause a permanent shift in the velocity of each soliton.

To describe the interaction quantitatively, the NLSE in Eq. (1.24) may be rewritten to account for energy dissipation and amplification[62], as in

$$-i\frac{\partial u}{\partial z} = \frac{1}{2}\frac{\partial^2 u}{\partial t^2} + g|u|^2 u, \tag{4.1}$$

where the energy gain/loss profile of the fiber is described by $g = \mathcal{E}(z)/\mathcal{E}_o$. The average pulse energy in the fiber is $\mathcal{E}_o$, as was depicted by the dashed line in Fig. 4.1, and the variation in the energy over z is given by $\mathcal{E}(z)$. With a lumped amplifier, such as an EDFA, g is an exponentially decreasing function between the amplifiers, with a sharp increase at the location of each amplifier. Since g is the normalized pulse energy, it is dimensionless and its value must average to one to exactly cancel fiber loss.

In a derivation parallel that of Eqs.(3.4)—(3.8), the average frequency of a pulse u under the effects of loss during CPM with a second pulse v is

$$\frac{d\langle\omega_u\rangle}{dz} = \frac{2g}{\mathcal{E}_o}\int \frac{\partial|u|^2}{\partial t}\,|v|^2\,dt. \tag{4.2}$$

The integration is taken over $\{-\infty,\infty\}$ unless explicitly stated otherwise. If u and v describe the evolution of the faster and slower solitons, respectively, as defined by Eqs. (3.1) and (3.2), Eq. (4.2) may be written as

$$\frac{d\Omega_u}{dz} = g\left(\frac{1}{\Omega}\frac{d}{dz}\int dt\,\mathrm{sech}^2(t+\Omega z)\mathrm{sech}^2(t)\right), \tag{4.3}$$

where we recall from Chapter 3 that Ω is the frequency difference between Ω_u and Ω_v and that $d\Omega_v/dz = -d\Omega_u/dz$.

The quantity in the parentheses on the right side of (4.3) is $d\Omega_u/dz$ in an ideal fiber, as given by Eq. (3.8). Consequently,

$$\left.\frac{d\Omega_u}{dz}\right|_{\text{loss}} = g\left.\frac{d\Omega_u}{dz}\right|_{\text{lossless}} \tag{4.4}$$

where each side must be integrated to determine the frequency variation in a fiber with loss and amplification. The derivative on the right side of (4.4) is most easily found by differentiating $\delta\Omega_u$ in Eq. (3.10) (or by taking the derivative of the curve in Fig. 3.6). The result is depicted by the dashed curve in Fig. 4.2, for which the attenuation constant $\alpha = 0$. The solid curve corresponds to $d\Omega_u/dz$ on the left side of (4.4), as found by multiplying the dashed curve by $g = \mathcal{E}(z)/\mathcal{E}_o$. Here $\mathcal{E}(z)$ is given by the dotted curve, so the collision at $z = 0$ takes place on an amplifier. Hence, the dashed curve is weighted more strongly during the latter half of the collision, when the energy in each pulse is greater. The position z in Fig. 4.2 is scaled by the collision length L_c. The collision length is the distance over which the collision

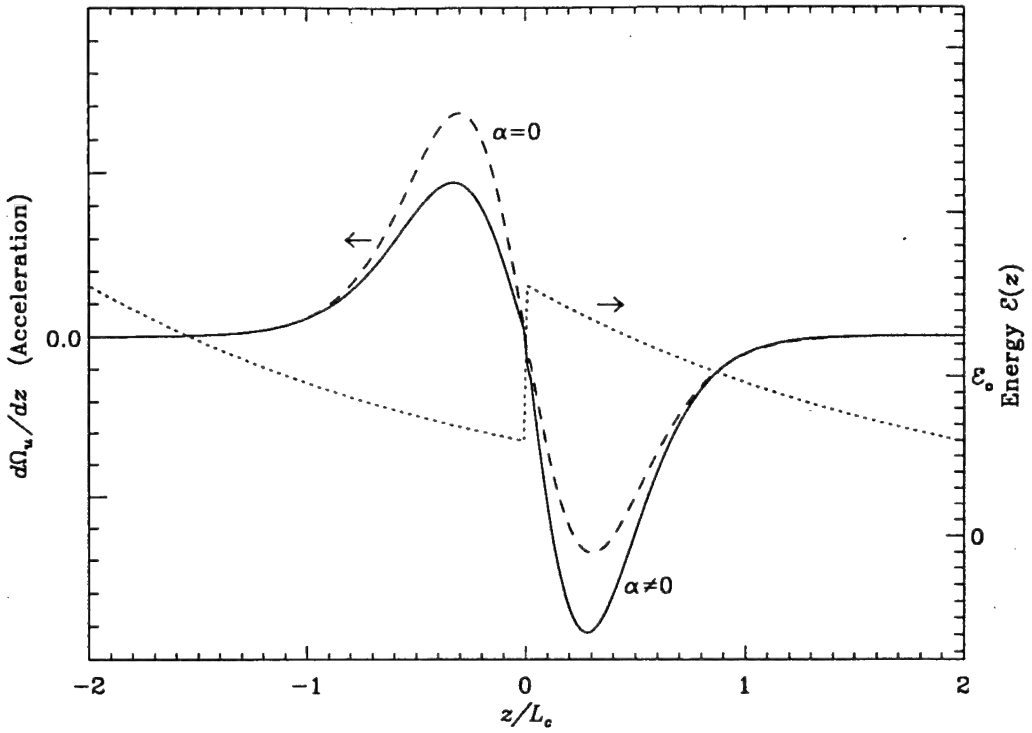

Figure 4.2. The variation in $d\Omega_u/dz$ during a collision: without loss ($\alpha = 0$); and at an amplifier ($\alpha \neq 0$) for the energy profile shown in the dotted curve.

occurs, starting when the half-power points of the solitons overlap. With a frequency spacing of Ω between the solitons, the dimensionless collision length (normalized to the soliton characteristic length in Eq. (1.22)) is equal to

$$L_c = \frac{3.526}{\Omega}, \tag{4.5}$$

where 3.526 is twice the FWHM in normalized time (recall that $\tau/t_c = 1.763$) and Ω is the difference between the normalized inverse group velocities of the faster and slower solitons.

Since frequency is directly proportional to velocity in the anomalous dispersion regime, positive $d\Omega_u/dz$ in Fig. 4.2 represents an acceleration of the faster soliton and negative $d\Omega_u/dz$ represents a deceleration. Since the

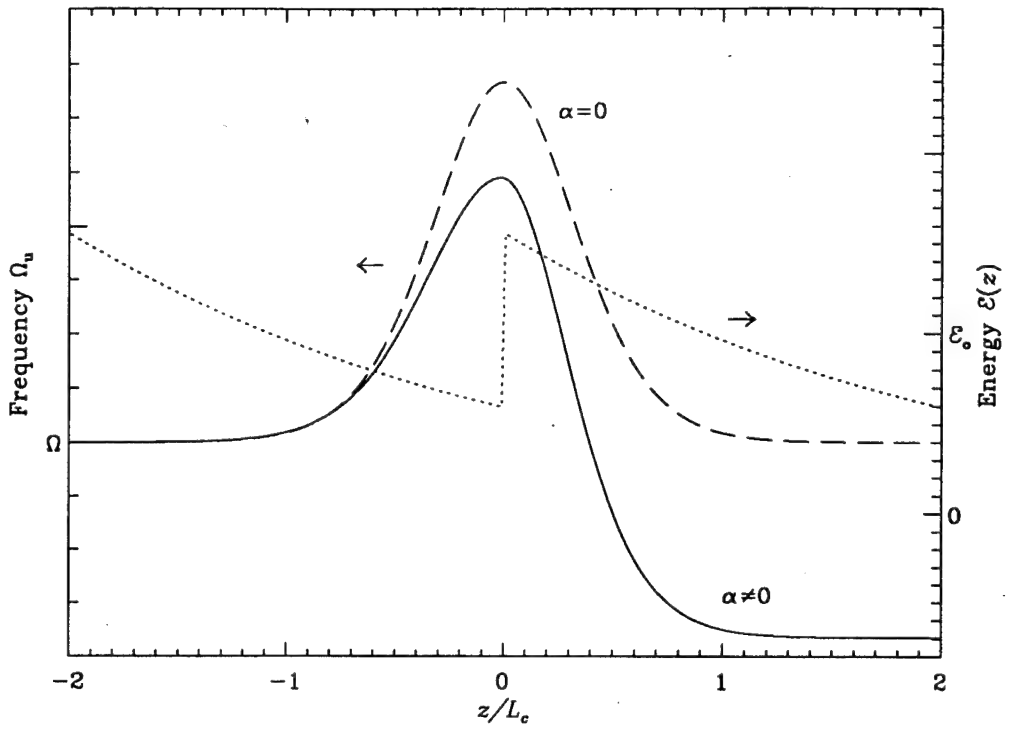

Figure 4.3. Negative frequency shift after collision on an amplifier. Energy is plotted on dotted curve.

acceleration during the first half of the collision in Fig. 4.2 is not balanced by the deceleration in the trailing half, a net negative velocity (frequency) shift remains after the collision, as depicted by the solid curve in Fig. 4.3. For comparison, the frequency variation in a lossless fiber (as in Eq. (3.10)) is illustrated by the dashed curve. The solid and dashed curves in Fig. 4.3 are found by integrating over the corresponding curves in Fig. 4.2. Note that loss and amplification simply perturb the interaction that would have taken place in an ideal fiber. In Fig. 4.3, the frequency decreases and the faster soliton slows down (which means the slower soliton speeds up) because the two solitons attract most strongly during the second half of the collision, when the intensity of each pulse is larger. In contrast, Fig. 4.4 depicts the frequency

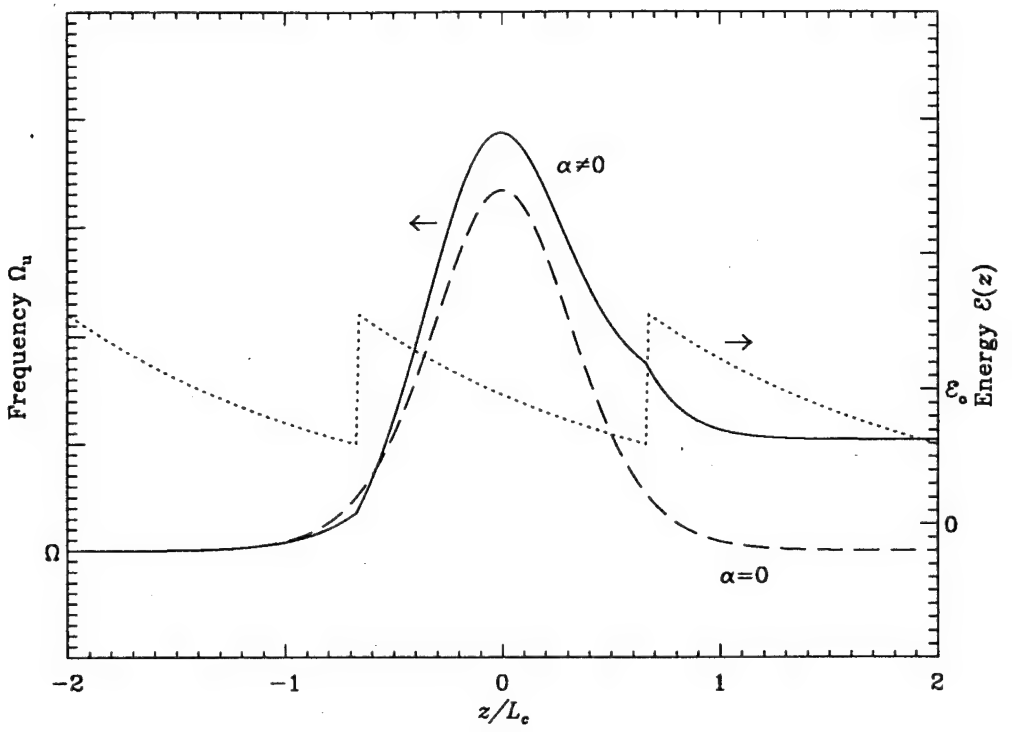

Figure 4.4. Positive frequency shift after collision between amplifiers. Energy is plotted on dotted curve.

shift when the collision occurs between amplifiers; the faster soliton speeds up (and the slower soliton slows down) since the attraction is stronger during the first half of the collision.

To analytically solve for the permanent shift in Ω_u caused by the perturbation, we integrate Eq. (4.3), so that

$$\begin{aligned} \Delta\Omega_u &= \int dz \, \frac{g}{\Omega} \frac{d}{dz} \left(\int dt \, \mathrm{sech}^2(t + \Omega z) \mathrm{sech}^2(t) \right) \\ &= \Omega_u|_{\infty} - \Omega_u|_{-\infty} , \end{aligned} \tag{4.6}$$

where $\Omega_u|_{-\infty}$ is the initial value of Ω_u and $\Omega_u|_{\infty}$ is the value of Ω_u after the collision. For clarification, note that $\delta\Omega_u$ in Chapter 3 signified temporary

frequency shifts in an ideal fiber, whereas $\Delta\Omega_u$ signifies the permanent frequency shift that remains after a collision. If we define variables $U = g/\Omega$ and $V = \int dt\,\mathrm{sech}^2(t+\Omega z)\mathrm{sech}^2(t)$, we can integrate by parts in Eq. (4.6). The value of V as given by Eq. (3.10) is zero far away from the collision, so $UV \to 0$ for $|z| \to \infty$ and the residual shift is determined by the term $-\int V dU$, as in

$$\Delta\Omega_u = -\frac{1}{\Omega}\int dz \frac{dg}{dz}\left(\int dt\,\mathrm{sech}^2(t+\Omega z)\mathrm{sech}^2(t)\right). \tag{4.7}$$

If the normalized gain g is an arbitrary function of z, we may represent it in terms of its Fourier variable $\tilde{g}(k)$ using

$$g(z) = \int dk\,\tilde{g}(k)\exp(ikz), \tag{4.8}$$

such that $dg/dz = i\int dk\,k\tilde{g}(k)\exp(ikz)$. Upon a change of variables, the integral over t in (4.7) may be written as a convolution of $\mathrm{sech}^2(\Omega z)$ with itself, such that

$$\Delta\Omega_u = \frac{-i}{\Omega}\int dk\,k\,\tilde{g}(k)\left(\int dz\,\exp(ikz)\left[\mathrm{sech}^2(\Omega z) * \mathrm{sech}^2(\Omega z)\right]\right). \tag{4.9}$$

The Fourier transform of a convolution is given by the product of the individual transforms. Since the transform of $\mathrm{sech}^2(\Omega z)$ is given by $2x/(\Omega\sinh x)$, with $x = \pi k/(2\Omega)$ (see reference [104]),

$$\Delta\Omega_u = \frac{32}{\pi^2}\int_0^\infty \frac{dk}{k}\frac{x^4}{\sinh^2 x}\,\mathrm{Im}\,\tilde{g}(k), \tag{4.10}$$

where we have used the identity $\tilde{g}(-k) = \tilde{g}^*(k)$ by assuming that $g(z)$ is real.

Thus far, we have treated g as an arbitrary function of z. Of course, g is probably a periodic function of z, as in Fig. 4.1, with amplifiers periodically placed along the fiber with spacing L_a. Thus, the integral over k is more appropriately written as a Fourier series over a fundamental harmonic given

by $k = 2\pi/L_a$ (with L_a normalized to the characteristic length), such that

$$\Delta\Omega_u = \frac{16L_a}{\pi^3} \sum_{m=1}^{\infty} \frac{m^3 x^4}{\sinh^2(mx)} \operatorname{Im} \tilde{g}_m, \tag{4.11}$$

where $x = \pi k/(2\Omega) = \pi^2/(\Omega L_a) = 2.8 L_c/L_a$. The dimensionless quantity L_c/L_a is the ratio of the collision length to the amplifier spacing, which will be a very useful parameter in the following discussion. The Fourier coefficients in (4.11) are defined by

$$\tilde{g}_m = \frac{1}{L_a} \int_{-z_c}^{L_a - z_c} dz\, g(z) \exp(-imkz), \tag{4.12}$$

where the amplifier is located an arbitrary distance z_c before the collision at $z = 0$. (This is to be distinguished from the soliton characteristic length z_c in Chapter 1.) We will typically refer to z_c as the position of the center of a collision relative to an amplifier position. Insuring that g averages to one, the gain profile between amplifiers is

$$g(z) = \frac{\alpha L_a \exp[-\alpha(z + z_c)]}{1 - \exp(-\alpha L_a)}. \tag{4.13}$$

By solving for $\tilde{g}_m$ in (4.12) and taking the imaginary part,

$$\begin{aligned} \operatorname{Im} \tilde{g}_m \;=\; & \frac{\alpha L_a}{[(\alpha L_a)^2 + (2\pi m)^2]^{1/2}} \times \\ & \sin\left[(2\pi m z_c/L_a) - \tan^{-1}(2\pi m/\alpha L_a)\right], \end{aligned} \tag{4.14}$$

so that $\Delta\Omega_u$ in (4.11) may be solved accordingly. As usual, the shift in the slower soliton is $\Delta\Omega_v = -\Delta\Omega_u$.

Rather than continuing to use normalized variables at this point, more insight is gained by translating into physical dimensions. The actual wavelength shift after a collision is given by $\Delta\lambda = -1.763(\lambda^2/c)\Delta\Omega_u/(2\pi\tau)$. After substituting for $\Delta\Omega_u$ using Eqs. (4.11) and (4.14),

$$\Delta\lambda(z_c) = \sum_{m=1}^{\infty} c_m \sin\left(2\pi m z_c/L_a - \phi_m\right), \tag{4.15}$$

where $\phi_m = \tan^{-1}[2\pi m/(\alpha L_a)]$, and all variables now carry physical dimensions. The coefficients are defined by

$$c_m = -\frac{(0.2274)\,\lambda^2\, L_a\, m^3\, x^4 \mathrm{csch}^2(mx)}{c\, z_o\, \tau[1+(2\pi m/\alpha L_a)^2]^{1/2}}, \tag{4.16}$$

where z_o is the soliton period, as in Fig. 1.6, and $x = 2.8L_c/L_a$. While the magnitude of the wavelength shift increases with greater loss αL_a, it is inversely proportional to τ^3 (z_o is proportional to τ^2), so shifts decrease as the pulse width (or the soliton period) increases.

In physical dimensions, the collision length L_c in the parameter x is found by multiplying $3.526/\Omega$ from Eq. (4.5) by the characteristic length using Eqs. (1.22) and (1.8). By substituting for Ω from Eq. (1.31),

$$\begin{aligned} L_c &= \frac{2\tau}{\int_\Lambda D(\lambda)\, d\lambda} \\ &= \frac{2\tau}{\overline{D}\Lambda}, \end{aligned} \tag{4.17}$$

where τ is the intensity FWHM and $\overline{D}$ is the average value of the dispersion coefficient D between two channels separated in wavelength by Λ. Given two wavelengths λ_1 and λ_2 and a dispersion slope of S_0 at a zero dispersion wavelength of λ_0, the average value of the dispersion coefficient is

$$\overline{D} = S_0 \left(\frac{\lambda_1 + \lambda_2}{2} - \lambda_0 \right). \tag{4.18}$$

The length L_c in Eq. (4.17) is the distance over which two pulses move 2τ with respect to one another given the relative group velocity $(\overline{D}\Lambda)^{-1}$ between the pulses. L_c is plotted versus the channel spacing Λ in Fig. 4.5 for $\tau = 20$ and 50 ps, where we assume $\overline{D} = 1$ ps/nm-km.

Figure 4.6 illustrates the wavelength shift from Eq. (4.15) for three values of L_c/L_a when $\tau = 20$ ps. We have chosen $L_a = 25$ km, so collisions

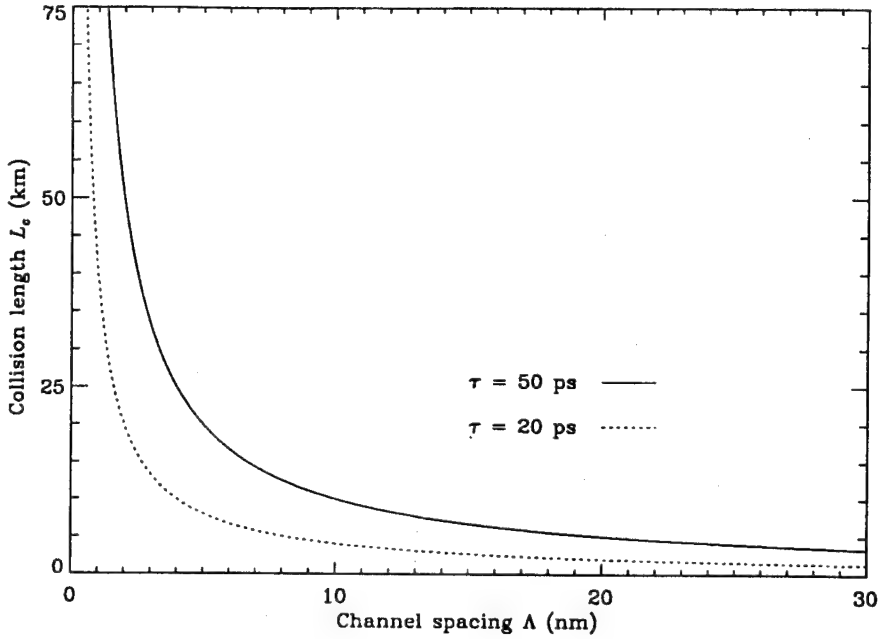

Figure 4.5. Collision length L_c as a function of the channel spacing Λ with amplifier spacing $L_a = 25$ km and average dispersion $\overline{D} = 1$ ps/nm-km.

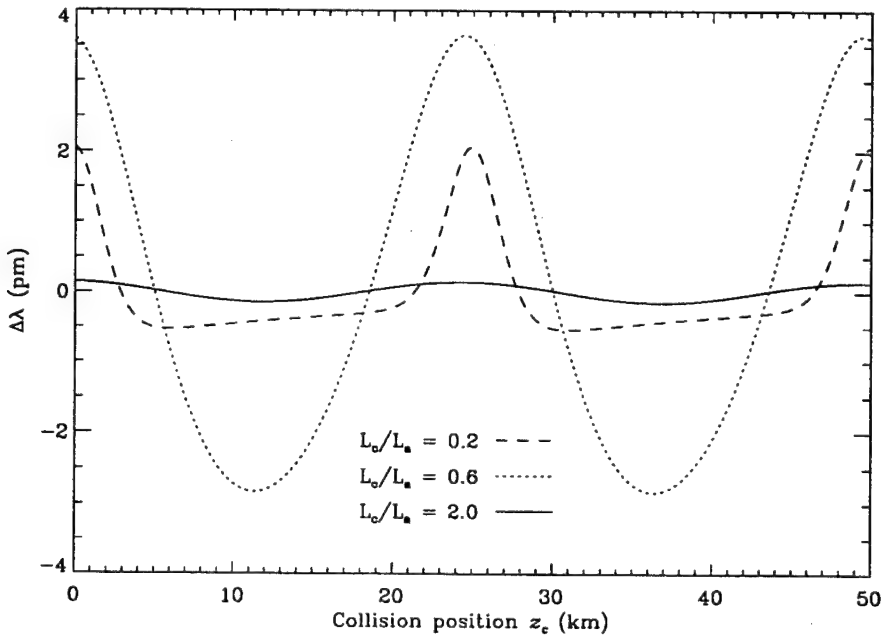

Figure 4.6. The residual wavelength shift in the faster soliton after a collision at z_c for $\tau = 20$ ps, $L_a = 25$ km, and $\overline{D} = 1$ ps/nm-km.

occur at amplifiers when $z_c = 0$, 25, and 50 km. We have assumed typical system parameters of $D = 1$ ps/nm-km and $\alpha = 0.048$ km^{-1} (0.21 dB/km loss) at a center wavelength of $\lambda = 1.55$ μm, with a dispersion slope of $S_0 = 0.067$ ps/nm^2-km at a zero dispersion wavelength $\lambda_0 = 1.535$ μm. For $L_c/L_a = 0.2$, 0.6, and 2.0, the channels are centered about 1.55 μm with spacing $\Lambda = 8.0$, 2.67, and 0.8 nm, respectively. So, for example, the initial wavelength of the faster channel is 1.546 μm and the initial wavelength of the slower channel is 1.554 μm when $L_c/L_a = 0.2$, such that $\overline{D} = 1$ ps/nm-km. In an example with $L_c/L_a = 0.6$, if the collision occurs on the amplifier at $z_c = 25$ km, the wavelength of the faster soliton is about 3.5 pm larger after the collision. Since a shift in wavelength is inversely proportional to a shift in frequency, the positive wavelength shift at each amplifier in Fig. 4.6 is consistent with the negative residual frequency shift in Fig. 4.3, whereas the negative wavelength shift between amplifiers is consistent with the positive frequncy shift in Fig. 4.4.

We may also describe the wavelength shift by its root-mean-square value $\Delta\lambda_{\rm rms}$, which will prove useful in the statistical analyses of Chapter 5. If the shift in wavelength is represented by the Fourier series in (4.15), then

$$\Delta\lambda_{\rm rms} = \left(\sum_{m=1}^{\infty} c_m^2 \right)^{1/2}, \tag{4.19}$$

where the c_m are defined by (4.16). Plots of $\Delta\lambda_{\rm rms}$ versus L_c/L_a are depicted in Fig. 4.7 for several different pulse widths. The rms shifts when $\tau = 20$ ps and $L_c/L_a = 0.2$, 0.6, and 2.0, as in Fig. 4.6, are $\Delta\lambda_{\rm rms} = 0.75$, 2.3, and 0.1 pm, respectively. Since the shift is inversely dependent on τ^3, the rms values for $\tau = 50$ ps are $2.5^3 = 15.625$ times smaller than for $\tau = 20$ ps. Also, since the shift in the wavelength of the slower soliton is identical in magnitude to the shift in the faster soliton, the rms value is the same in either channel.

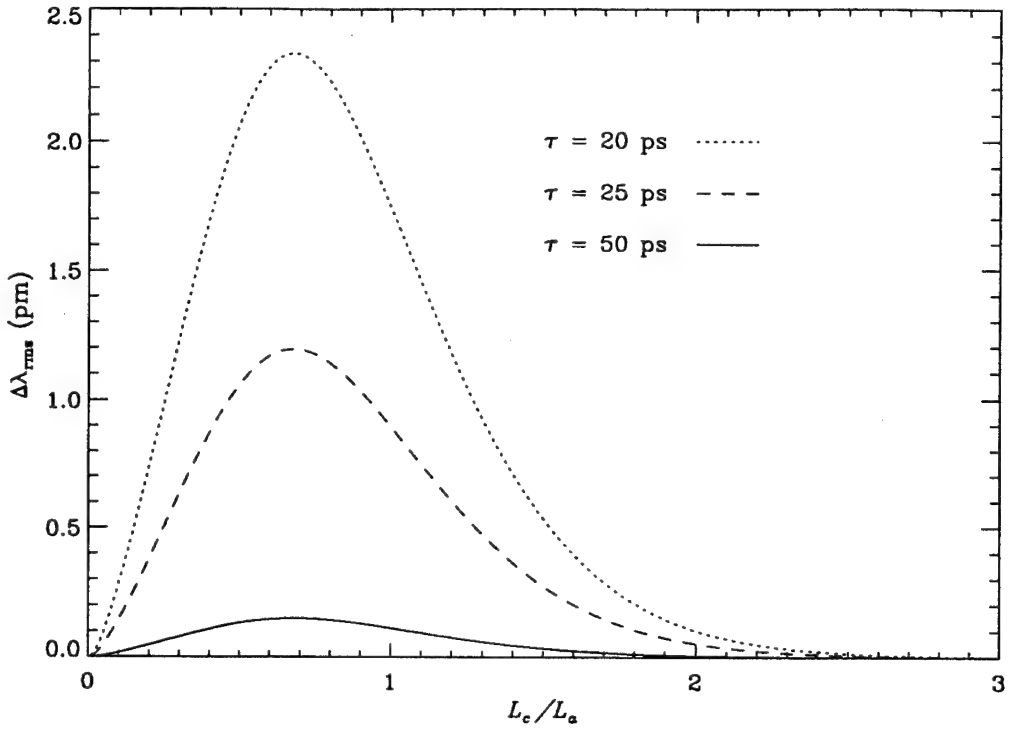

Figure 4.7. The rms shift in wavelength resulting from collisions of length L_c across an amplifier spacing of $L_a = 25$ km if $\overline{D} = 1$ ps/nm-km.

The quantity $x^4 \operatorname{csch}^2(m\,x)$ in Eq. (4.16) reaches a peak near $x = 1.9$ and becomes small beyond $x \approx 6$. Since $x = 2.8L_c/L_a$, values of $\Delta\lambda_{\rm rms}$ peak around $L_c/L_a = 0.7$ and become negligible beyond $L_c/L_a \approx 2$, as illustrated in Fig. 4.7. Intuitively, this is reasonable since the average effects of loss and amplification are small if collisions occur over multiple amplifiers. As an example, the frequency variation when $L_c/L_a = 3$, as depicted in the solid curve Fig. 4.8, differs negligibly from the variation in a lossless fiber, again depicted by the dashed curve. This is in contrast to Figs. 4.3 and 4.4, where $L_c/L_a = 0.5$ and $L_c/L_a = 0.75$, respectively. Given the relationship between L_c and the channel spacing Λ in Eq. (4.17), we plot L_c/L_a versus Λ in Fig. 4.9 for the specified values of L_a and D; corresponding values of $\Delta\lambda_{\rm rms}$ are shown in Fig. 4.10.

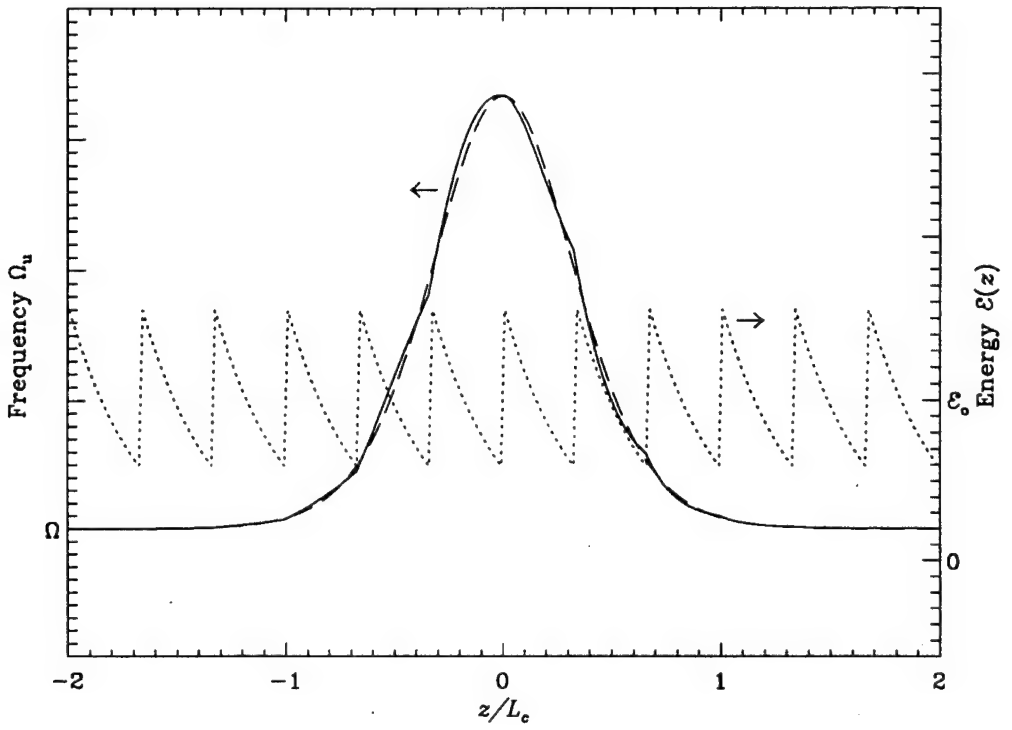

Figure 4.8: Frequency variation with $L_c/L_a = 3$.

For values of $L_c/L_a > 2$, as indicated by the region above the dashed line in Fig. 4.9, the values of Λ cannot be too large, since collisions occur over longer distances only if the group velocities of two channels are relatively close.

The permanent wavelength (velocity) shifts caused by perturbations can significantly alter the arrival time of a soliton at the end of the fiber. If the fiber is lossless, the timing displacement in the faster soliton after a collision is given by Eq. (3.13),

$$\delta t_{\text{coll}} = -\frac{0.1768}{(\Delta f)^2 \tau}, \tag{4.20}$$

where the minus sign indicates that the faster soliton moves forward in time. The effect of a perturbation may be included by adding a second term to δt_{coll}

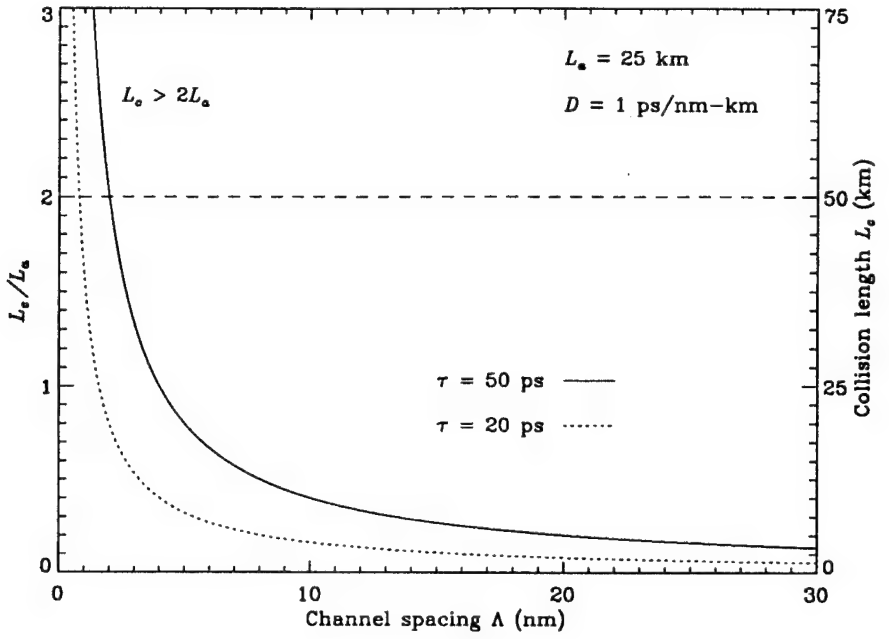

Figure 4.9: The ratio L_c/L_a as a function of the channel spacing Λ.

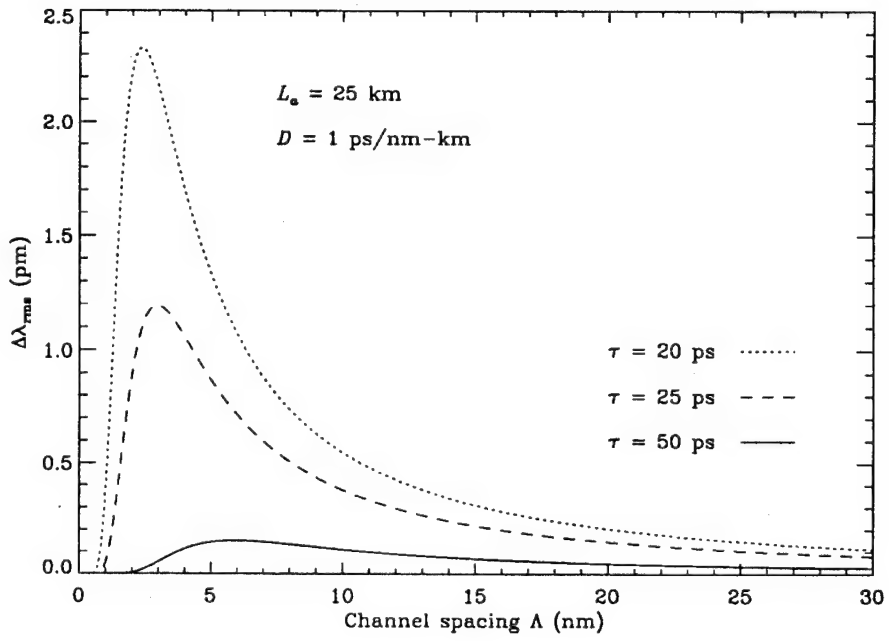

Figure 4.10: Rms shift as a function of the channel spacing.

to account for any residual wavelength shift, as in

$$\delta t = \delta t_{\text{coll}} + \delta t_{\text{res}}. \tag{4.21}$$

For the wavelength shift depicted by Fig. 4.11, δt_{coll} is related to the area under the dashed curve. If the perturbative effect at position z is estimated by taking the difference $\partial\lambda(z)$ between the dashed and solid curves, then

$$\delta t_{\text{res}} = \overline{D} \int_{-\infty}^{L} \partial\lambda(z)\, dz \approx \overline{D}\, \Delta\lambda(z_c)\, (L - z_c), \tag{4.22}$$

where L is the length of the fiber and $\Delta\lambda(z_c)$ is the asymptotic value of $\partial\lambda(z)$ after a collision at z_c. Thus, the displacement in the arrival time of the faster soliton at the fiber output after a single collision is

$$\delta t = \overline{D}\, \Delta\lambda(z_c)\, (L - z_c) - \frac{0.1768}{(\Delta f)^2 \tau}. \tag{4.23}$$

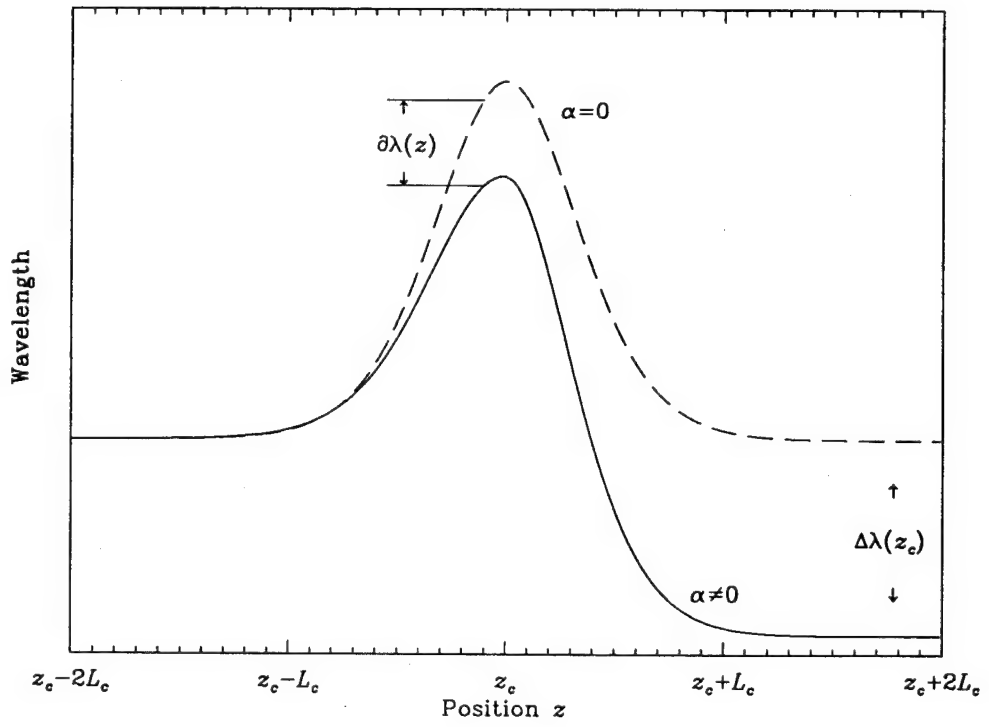

Figure 4.11: Wavelength shift during a collision centered at position z_c.

In a fiber with loss and amplification, $\Delta\lambda(z_c)$ is given by Eq. (4.15). A positive shift in wavelength in (4.23) delays the soliton and a negative shift advances the soliton, consistent with pulse behavior in the anomalous dispersion regime. The displacement in the slower soliton is equal in magnitude to δt but opposite in sign.

Loss and amplification have been the only perturbations we have analyzed thus far. The analysis would be similar for any other perturbation for which the NLSE is written according to Eq. (4.1). An example is a system in which the dispersion coefficient differs in each fiber making up the transmission link, as analyzed in [62]. Unless fibers are selected carefully, the dispersion will inevitably vary between individual fibers. Equation (4.1) holds for such a perturbation because dispersion variations directly alter the peak power required for stable soliton propagation. To apply our analysis to a perturbation of this kind, the Fourier variable $\tilde{g}(k)$ in Eq. (4.10) must be replaced with the proper function describing the perturbative effect on the pulse intensity. If the perturbation is periodic in fiber position, the Fourier coefficients $\tilde{g}_m$ in Eq. (4.11) must be changed appropriately. Furthermore, the quantity L_a could be replaced with the more general term L_p to describe the period of the perturbation, such that $\Delta\lambda_{\text{rms}}$ becomes negligible for values of $L_c/L_p > 2$.

While dispersion variations between fibers potentially degrade WDM soliton communication, they may also be used to negate the perturbative effects of loss and amplification discussed thus far. Taking the soliton peak power P_o from Eq. (1.23), we define the soliton order N as[3]

$$N^2 = \frac{P_o \gamma t_c^2}{|\beta_2|}, \tag{4.24}$$

where $N = 1$ for a fundamental soliton. It is apparent that the soliton order and

pulse width t_c remain constant when P_o varies as long as the dispersion β_2 varies accordingly. If the energy varies exponentially, as in Fig. 4.1, the dispersion must vary exponentially as well. Hence, dispersion decreasing fibers have been proposed as a means of reducing or perhaps eliminating many of the negative effects of loss and amplification[62, 105], even for soliton communications in a single wavelength channel.

4.1.2 ***N*-soliton interactions in a perturbed fiber** Equation (3.35) demonstrates that a multiple soliton collision in an ideal fiber is effectively a sum of independent two-soliton interactions; in other words, the total interaction may be accurately estimated by linearly summing over each pairwise soliton interaction. For the ideal fiber in Section 3.3, this was shown to be true by asymptotically expanding the exact N-soliton waveform, but it can also be demonstrated using the perturbed NLSE from Eq. (4.1). In an analysis parallel that used to describe CPM between two pulses, we replace u in Eq. (4.1) with $u+v+w$. The coupled NLSE is now given by three equations,

$$\begin{aligned} -i\frac{\partial u}{\partial z} &= \frac{1}{2}\frac{\partial^2 u}{\partial t^2} + g\left[|u|^2 + 2(|v|^2+|w|^2)\right]u \\ -i\frac{\partial v}{\partial z} &= \frac{1}{2}\frac{\partial^2 v}{\partial t^2} + g\left[|v|^2 + 2(|u|^2+|w|^2)\right]v \\ -i\frac{\partial w}{\partial z} &= \frac{1}{2}\frac{\partial^2 w}{\partial t^2} + g\left[|w|^2 + 2(|u|^2+|v|^2)\right]w, \end{aligned} \tag{4.25}$$

where FWM components are neglected as before. In the equation for u, CPM with v and w results from the summation over the intensities $|v|^2$ and $|w|^2$. Thus, the mean frequency of u, as in Eq. (4.2), is described by

$$\frac{d\langle\omega_u\rangle}{dz} = \frac{2g}{\mathcal{E}_o}\int \frac{\partial|u|^2}{\partial t}\left(|v|^2+|w|^2\right)dt. \tag{4.26}$$

Since the variation in ω_u at a three-soliton interaction is given by the sum of the individual effects with solitons v and w, by induction we see that N-soliton

interactions are additive for any perturbation described by Eq. (4.1). This will prove useful in Chapter 5, where we will treat interactions between different soliton wavelength channels as independent stochastic processes.

4.2 Soliton interactions at the transmitter and receiver

We continue our analysis of perturbations by describing WDM interactions during collisions at the fiber input or output. It is not surprising that data can be degraded by soliton collisions at the fiber output. Optical receivers often require a frequency filter to limit noise and a photodetector to measure the optical power. If the frequency of a soliton at the output shifts significantly from its expected value because of a collision, the receiver might not detect the data. However, when the initial frequency separation between the soliton channels is large, the frequency shift in each soliton is small enough to prevent degradation of the data. Larger channel spacings are also helpful because interactions at the fiber input become phase dependent, even for WDM solitons, if the the channel spacing is too small[64]. The effects of collisions at the fiber output were discussed in [6, 75], where it was predicted that a channel spacing of five soliton spectral widths is sufficient to prevent large frequency shifts during collisions between an arbitrary number of channels. The dashed line in Fig. 3.5 indicates that the minimum channel spacings for pulse widths of $\tau = 20$ and 50 ps are 0.625 and 0.25 nm, respectively.

Collisions at the fiber input may also be important, since velocity shifts at the input are permanent[65]; a timing displacement that results can cause intersymbol interference with a neighboring soliton if it does not also experience a collision at the input. When solitons interact at the fiber input, only that fraction of the collision that occurs inside the fiber is affected by

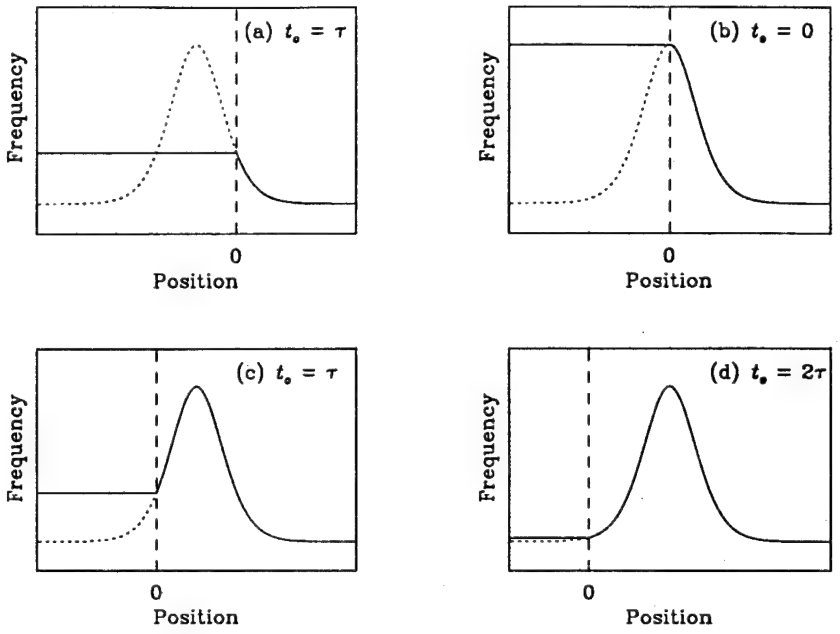

Figure 4.12. Frequency shifts resulting at fiber input for different initial pulse separations.

the Kerr nonlinearity. For the faster of the two solitons, several examples are shown in Fig. 4.12, where the fiber input is at position zero in each plot. The dashed curves correspond to Fig. 3.6, and the solid curves demonstrate that solitons interact only during that part of the collision that takes place in the fiber. (Here we assume the fiber is lossless. Loss and amplification are included in the analysis in [66].)

In Fig. 4.12(a), the solitons are separated by one pulse width at the fiber input, as denoted by $t_o = \tau$, and only the trailing part of the collision occurs in the fiber, so the frequency of the faster soliton decreases somewhat. In (b), the center of the collision occurs at the fiber input since the initial separation is zero. The frequency shift is largest during such a collision, since the first half of the collision takes place in the absence of any nonlinearity while

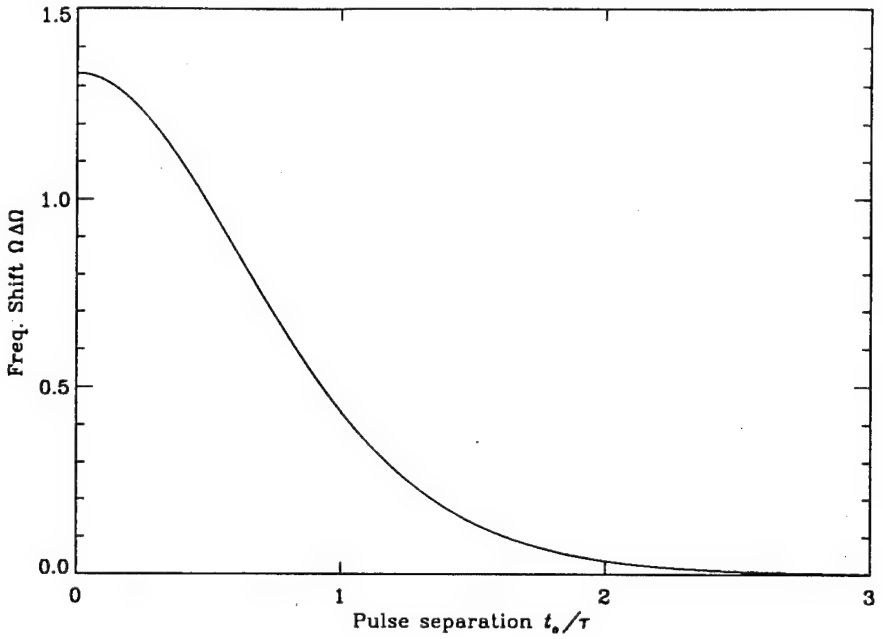

Figure 4.13. Permanent frequency shift at fiber input as a function of initial separation.

the second half occurs in the fiber. In (c), the bulk of the collision occurs in the fiber, but since the pulses are only one pulse width apart at the input, the magnitude of the residual shift is identical to the shift in (a). Finally, almost the entire collision takes place in the fiber in (d) — the nonlinearity affects most of the collision, so only a very small shift remains after the collison.

The shift in the frequency of the faster soliton after a collision at the fiber input is always negative, as seen in Fig. 4.12, while the shift in the frequency of the slower soliton is always positive. The normalized magnitude of any shift as a function of the initial separation t_o is depicted by Fig. 4.13. As an example during a collision between two 20 ps solitons with $t_o = 0$, the wavelength shift in the faster of the two solitons is at most 0.027 nm if there are five soliton spectral widths between the channels, such that $\Lambda = 0.625$ nm

(see Fig. 3.8). The shift is smaller if there are greater than five spectral widths between channels. The corresponding shift in the arrival time at the end of the fiber depends on the length and dispersion of the fiber. Such shifts can be reduced by using frequency filters[32], by synchronizing the sources of each soliton channel at the fiber input[62], or by increasing the channel spacing Ω.

4.3 Fiber nonlinearities

We conclude this chapter by briefly considering how fiber nonlinearities other than SPM affect WDM soliton propagation. The nonlinearities we are interested in include four-wave mixing, stimulated Raman scattering and stimulated Brillouin scattering. While these processes have not yet been analyzed in detail for WDM soliton systems, their influence on WDM communications is the subject of much research[97, 102, 103]. Here we simply predict their impact on WDM soliton transmission.

4.3.1 Stimulated Raman scattering Stimulated Raman scattering(SRS) in fiber[97, 3] arises from an interaction between optical photons and the molecules of fused silica. An incident photon is scattered to a lower frequency while the molecule undergoes a transition to a different vibrational state. The optical wave generated at the lower frequency is referred to as the Stokes wave, while the incident wave is referred to as the pump. If the pump is conincident with a second wave having frequency identical to the Stokes wave, the second wave experiences gain at the expense of the pump. In reality, a continuum of vibrational frequencies exist in an amorphous material such as fused silica, so the gain bandwidth over which SRS occurs may be quite large. In optical fiber at a wavelength of 1.55 μm, the bandwidth is around 15 THz, with a peak gain coefficient of $g_R = 7 \times 10^{-12}$ cm/W at a Stokes shift of 13 THz.

If only a single optical wave is transmitted into the fiber - as would be true for communications in a single wavelength channel - Raman scattering may spontaneously generate weak signals across the Raman gain spectrum. If the pump power exceeds a certain threshold, the frequency component downshifted 13 THz from the pump builds exponentially. The critical pump power at which this occurs in conventional fiber is

$$P_c = \frac{32\, A_{\text{eff}}}{g_R\, L_{\text{eff}}}, \tag{4.27}$$

where A_{eff} is the effective area of the fiber cross-section and L_{eff} is the effective length of a dissipative fiber. For typical values of $A_{\text{eff}} = 50\ \mu\text{m}^{\,2}$ and $L_{\text{eff}} \approx 1/\alpha = 1/0.048 = 21$ km, the critical peak power required for spontaneous Raman scattering is slightly greater than 1 W. Given fundamental peak powers as in Fig. 1.6, it is clear that spontaneous Raman scattering is not of significance until the soliton pulse widths are around 1 ps or less. The soliton self-frequency shift mentioned briefly in Section 1.2 is an example.

Because of its large gain bandwidth, SRS can play a significant role in the degradation of WDM systems. If the aggregate power in multiple wavelength channels is large enough, the wavelength channels at higher frequencies can act as pumps for the channels at lower frequencies. Given a bandwidth of 15 THz, crosstalk induced by SRS may result even for channels separated by 100 nm. If there are N channels with frequency spacing Δf, the critical power-per-channel at which signal degradation occurs, as derived in [97], is equal to

$$P_c = \frac{500}{N(N-1)\Delta f}, \tag{4.28}$$

where Δf must be specified in GHz and P_c is in watts. In WDM systems with high bit rates and non-zero group velocity dispersion (as would be true in a

soliton system), the critical power increases by a factor of two. Taking this into account, Fig. 4.14 depicts the critical power required in each channel for SRS to degrade the system. The solid curve depicts P_c for $\tau = 50$ ps, where a frequency spacing of five soltion spectral widths is given by $\Delta f = 1.575/\tau = 31.5$ GHz, and the dashed curve depicts P_c for $\tau = 20$ ps and $\Delta f = 78.8$ GHz. For 20 ps solitons with peak power around 4 mW (see Fig. 1.6), greater than 30 channels are possible before SRS degrades the system; for $\tau = 50$ ps and a peak power less than 1 mW, greater than 100 channels may be possible.

4.3.2 Stimulated Brillouin scattering The process of stimulated Brillouin scattering(SBS) is similar to SRS in that energy from an incoming photon acts as a pump for a Stokes wave at a lower frequency[97, 3].

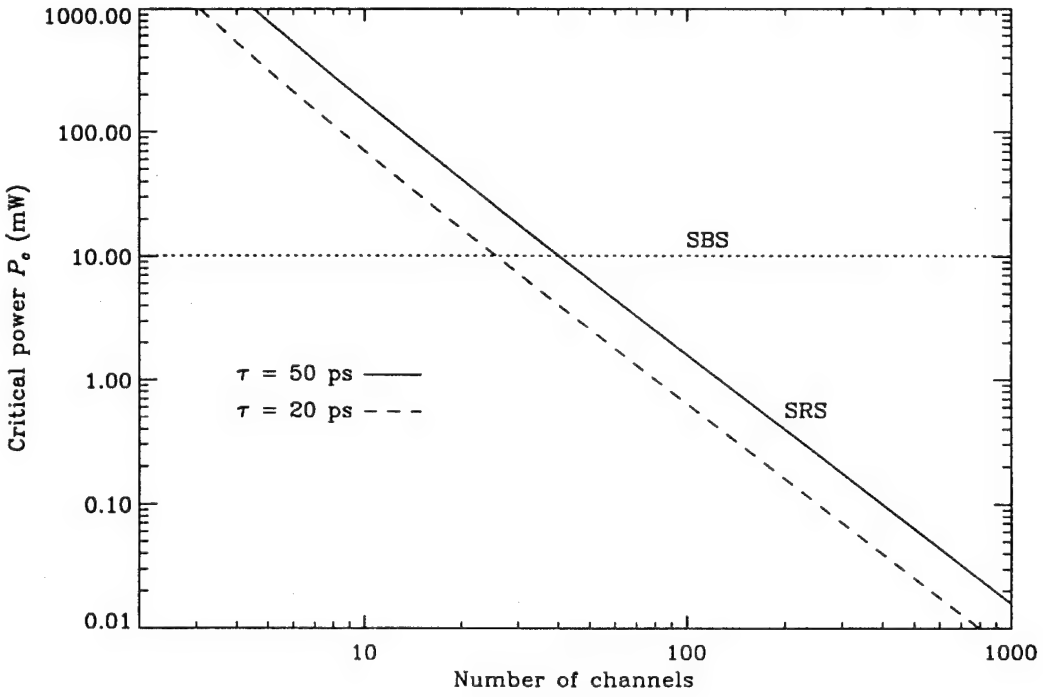

Figure 4.14. The critical power required in each channel for which SRS and SBS degrade data.

However, for SBS the energy conversion generates an acoustic phonon instead of an optical phonon. SBS is an electrostrictive process in which an incoming optical wave modulates the index of refraction by creating an acoustic pressure wave. Subsequent incoming light is scattered by the index grating, experiencing a Doppler shift to a lower Stokes frequency. Since energy and momentum are conserved, the actual frequency shift may be derived in momentum space, where the Bragg matching condition is met only across a narrow bandwidth and if the Stokes wave propagates backwards relative to the pump. The typical SBS gain bandwidth of 20 MHz is much smaller than for SRS and occurs at a Stokes shift of $f_B = 2nv_a/\lambda = 11.1$ GHz, where $n = 1.445$ is the index of refraction at $\lambda = 1.55$ μm and $v_a = 5.96$ km/s is the velocity of the acoustic wave. The peak value of SBS gain at this frequency shift is $g_B = 4 \times 10^{-9}$ cm/W, which is over two orders of magnitude greater than the SRS gain g_R[97].

Since the bandwidth for SBS is small, crosstalk occurs between two WDM channels only if the frequency spacing is precisely 11.1 GHz. For a typical WDM soliton spectral spacing, this translates into a pulse width greater than 100 ps, so it is unlikely that crosstalk will be the dominant SBS effect in soliton transmission. However, the critical power level at which spontaneous Brillouin scattering can degrade a system is much lower than that for spontaneous Raman scattering. In conventional fiber, the critical power,

$$P_c = \frac{42\, A_{\text{eff}}}{g_B\, L_{\text{eff}}}, \tag{4.29}$$

is only 2.5 mW, where the previous values of effective area and length were used. While this power level is approximately the same as the peak power for 20 ps solitons, it is derived under the assumption that the incident power is CW (continuous wave). If data is modulated at high rates, the gain coefficient

g_B must be scaled to a lower value since the gain only occurs over a narrow spectrum. If data is amplitude-shift keyed in a non-return-to-zero(NRZ) format with 100% modulation depths, the gain is reduced according to

$$g = g_B \left[\frac{1}{2} - \frac{1}{4} \frac{B}{\Delta\nu_B} \left(1 - \exp(-\Delta\nu_B / B)\right) \right], \tag{4.30}$$

where $\Delta\nu_B = 20$ MHz is the gain bandwidth and B is the bit rate. For bit rates greater than 1 Gb/s, we find $g = g_B/4$, so that the critical power at which SBS degrades data is raised to 10 mW, independent of the pulse width. This power level is depicted by the dotted curve in Fig. 4.14, where we see that SBS is the dominant effect when there are fewer than about 30 channels.

4.3.3 Four-wave mixing Four-wave mixing(FWM) is a parametric process that originates from the same nonlinearity that causes SPM and CPM. As seen at the end of Chapter 3, FWM occurs during WDM soliton collisions as a result of mixing between optical waves of different frequencies. For two waves with frequencies f_1 and f_2, FWM components appear at sideband frequencies of $2f_1 - f_2$ and $2f_2 - f_1$. In terms of a coupled NLSE describing the evolution of two pulses in Chapter 3, the FWM components correspond to the terms u^2v^* and v^2u^* which were dropped in the derivation of Eqs. (3.4) and (3.5). The presence of these components is easily seen in the three-dimensional plots of multi-soliton collisions in Section 3.3.2.

The impact that FWM has on a WDM system is rather difficult to assess, as it is dependent on many system parameters, including the channel spacing, fiber dispersion, fiber length and cross-sectional area, as well as the power in each wavelength channel. For FWM to efficiently generate power at different frequencies, though, phase matching must occur, a condition which is

not met if the group velocity mismatch between two channels is large. Consequently, large frequency spacings or large dispersion coefficients discourage the onset of FWM. In a dispersion shifted fiber with $D = 1$ ps/nm-km, the FWM interaction is inefficient for frequency separations greater than around 50 GHz[97], which corresponds to soliton pulse widths less than about 30 ps. For 50 ps solitons, the frequency spacing is around 30 GHz, so FWM apparently affects only neighboring channels. Hence, the critical power level at which FWM degrades a system is independent of the number of wavelength channels, as was also true for SBS.

The degree to which FWM will affect WDM soliton systems is unclear at this point. While it has been suggested that FWM can degrade systems at power levels as low as a few milliwatts[97], under proper conditions it was also shown that FWM only generates spurious energy that disperses away quickly after collisions, even for non-soliton pulses[102]. However, it seems apparent that FWM can still degrade standard NRZ pulses in a wavelength channel (even for single channel communications[106, 107]) that is located too close to the wavelength of zero dispersion. The spurious energy created by FWM does not disperse away in such a channel[102]. Since soliton systems operate with non-zero dispersion, it has been suggested that WDM soliton systems might be the ideal choice for long-distance communications[76].

CHAPTER 5

SYSTEM IMPLICATIONS

Thus far, the nonlinear interactions during collisions between WDM solitons have been analyzed in detail. We have discussed how WDM solitons interact in ideal fibers and described how interactions are perturbed by energy dissipation and amplification. It was also shown that the equations describing interactions between two solitons are easily extended for an arbitrary number of solitons by summing over each individual two-soliton interaction. The emphasis of this chapter is to determine whether WDM soliton collisions preclude accurate transmission of data. First, we review current restrictions on the use of WDM solitons in fiber communication systems. We then analyze more practical implications of WDM soliton communications in a statistical analysis of soliton timing jitter and system performance.

5.1 WDM soliton communication systems

The goal of any communication system is the transfer of information from one place to another. The standard components of a fiber communication system are illustrated in Fig. 5.1. The information is oftentimes encoded as a stream of binary data bits that modulates the output of an optical source. Soliton sources were discussed specifically in Chapter 2. For WDM communications, the optical energy from multiple sources having unique wavelengths must be combined at the input of the fiber and separated at the output of the fiber, usually with a grating multiplexer and demultiplexer, as depicted by

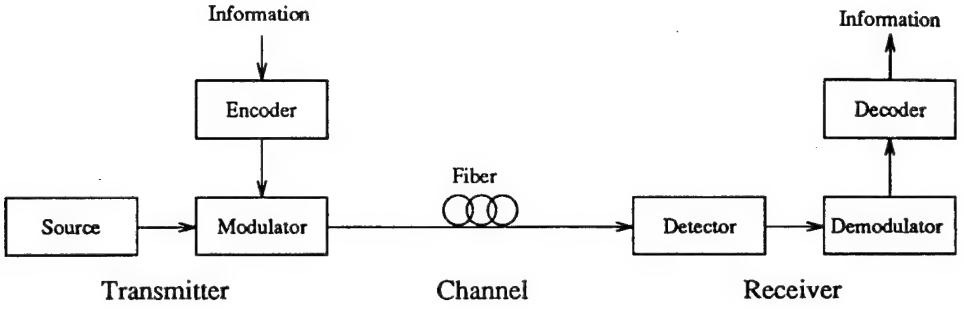

Figure 5.1: A typical fiber communication system.

Fig. 5.2, where $\lambda_1 < \lambda_2 < \lambda_3$. While Fig. 5.2 could be implemented with bulk optical components, an inexpensive device which integrates the transmitters(receivers) with the multiplexers(demultiplexers) would be more compact, more robust, and more practical. This has been a major hindrance to more extensive use of WDM in communications. A substantial amount of research is being conducted to develop such devices[108, 109, 110].

The fiber channel for WDM communications actually consists of multiple data channels, each represented by an individual wavelength or spectral component. For most WDM communications, the wavelength channels are

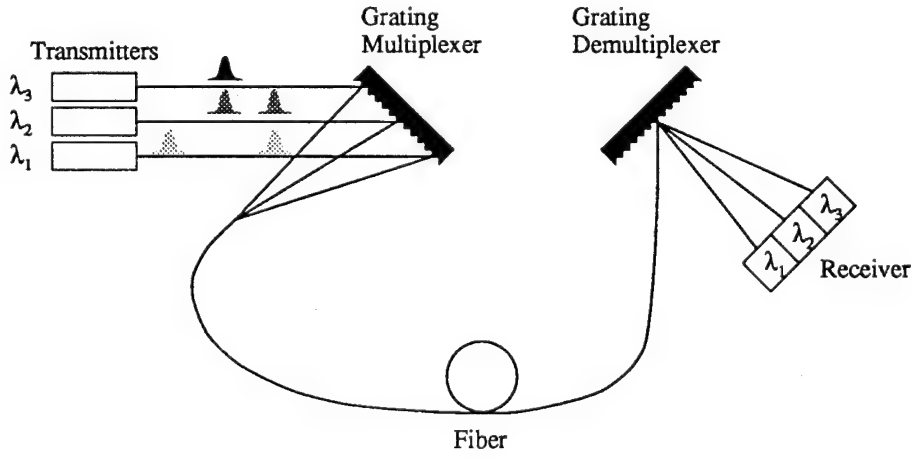

Figure 5.2. Wavelength multiplexing and demultiplexing in a fiber communication system with three wavelength channels.

independent of one another, meaning that communication across multiple information channels occurs simultaneously in a single physical fiber channel. More recent research has explored the possibility of encoding information in the spectral domain, in a so-called bit-per-wavelength(BPW) fashion, rather than in the time domain[111, 112]. In such a system, the wavelength channels are not independent, since each wavelength represents a single bit in the data byte or packet. Data encoded in this manner might use the wide transmission bandwidth of optical fiber most efficiently. We will assume that individual wavelength channels are independent of one another, although the results may be applied to BPW communications with simple modifications.

In WDM soliton systems, the results of Chapters 3 and 4 imply that tradeoffs must be made in regards to the optimal channel spacing and the number of wavelength channels which may be multiplexed. When the channel spacing Λ is small, the maximum value of the wavelength shift during a collision is as large as depicted in Fig. 3.8. Since a minimum channel spacing of five soliton spectral widths may be required to prevent degradation of data at the fiber output because of such a shift[6], the minimum wavelength spacing may be defined as

$$\Lambda_{\min} = \left(\frac{\lambda^2}{c}\right) \frac{1.575}{\tau}, \tag{5.1}$$

where $\Delta f = 1.575/\tau$ is taken from Eq. (3.3). Values of $\Lambda_{\min}$ correspond to the dashed line in Fig. 3.5.

In contrast, as the channel spacing increases, the magnitude of a permanent wavelength shift after a collision increases, as depicted in Fig. 4.10. Although the permanent shifts, as represented by $\Delta\lambda_{\rm rms}$, are only on the order

of picometers, many such shifts over the full length of the fiber may cause significant displacements in pulse arrival times[62]. It is typically suggested that the ratio of the collision length to the amplifier spacing must be greater than two to prevent such jitter[62, 63, 2]. Given the definition of L_c in Eq. (4.17), a maximum channel spacing may be defined to insure that $L_c \geq 2L_a$, as in

$$\Lambda_{\max} = \frac{\tau}{\overline{D} L_a}. \tag{5.2}$$

Values of $\Lambda_{\max}$ correspond to the dashed line in Fig. 4.9. The variation of $\Lambda_{\min}$ and $\Lambda_{\max}$ with τ is shown in Fig. 5.3 for the specified values of the amplifier spacing L_a and dispersion D.

Current limits imposed on a WDM soliton system by Eqs. (5.1) and (5.2) are easy to determine. Since all the channels in the system must meet

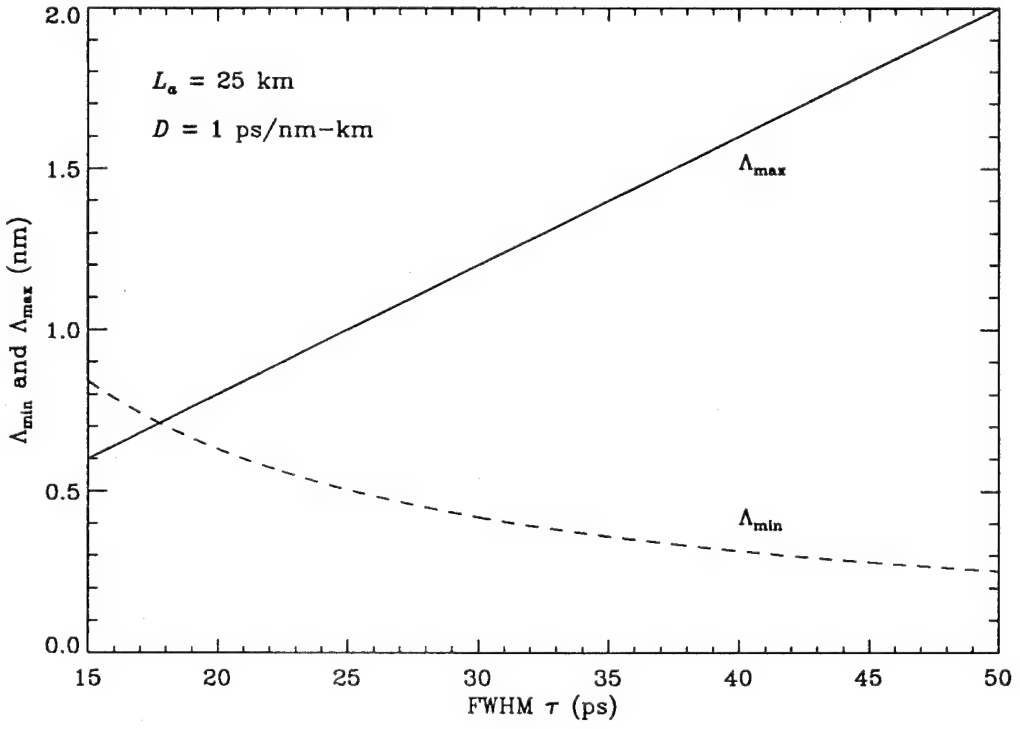

Figure 5.3. Suggested minimum and maximum allowable wavelength spacings.

the condition that $L_c \geq 2L_a$, $\Lambda_{\max}$ defines the maximum bandwidth within which all channels may be multiplexed. Hence, the maximum number of WDM channels that may be multiplexed on the fiber is restricted to

$$N_{\max} = 1 + \frac{\Lambda_{\max}}{\Lambda_{\min}}, \tag{5.3}$$

as plotted by the dotted curve in Fig. 5.4. Since only integral numbers of channels are physically possible, the actual number of channels allowed at each pulse width are shown by the solid lines. Noting that $\Lambda_{\min}$ is larger than $\Lambda_{\max}$ for values of $\tau < 18$ ps, WDM is theoretically possible only for soliton pulse widths greater than 18 ps (N must be at least two). Furthermore, the spectral bandwidth in Fig. 5.3 over which soliton channels may be multiplexed is limited

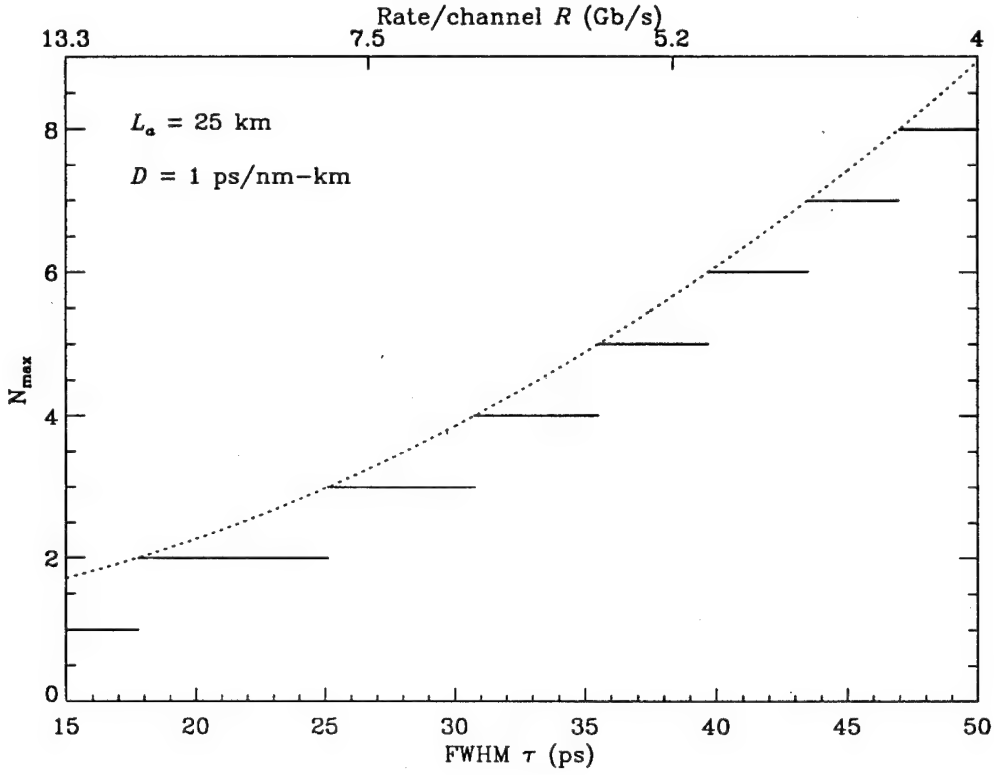

Figure 5.4. Maximum number of WDM channels possible at each pulse width for the listed parameters.

to less than 2 nm for pulse widths of 50 ps or less. Given a typical EDFA bandwidth of approximately 30 nm, a maximum WDM soliton bandwidth of 2 nm is both inefficient and inflexible. This is especially true since it is difficult to multiplex wavelength channels as close together as 0.25 nm — the value of $\Lambda_{\min}$ for $\tau = 50$ ps. Using the channel data rate $R = 1/T = 1(5\tau)$ plotted on the upper axis of Fig. 5.4, the maximum throughput $RN_{\max}$ is computed for each pulse width and plotted in Fig. 5.5. The discontinuities correspond to the discretization in channel number.

Since present WDM technology may limit further reduction of $\Lambda_{\min}$, it is reasonable to treat $\Lambda_{\min}$ as a realistic limitation to the system. Thus, in

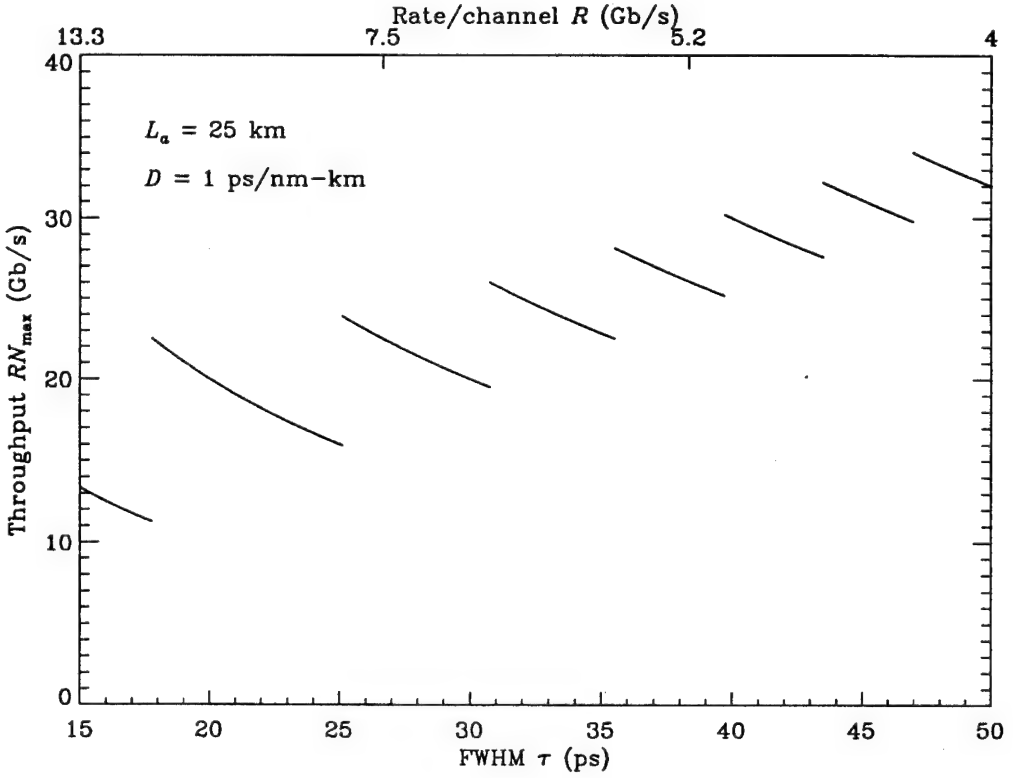

Figure 5.5. Maximum throughput at each pulse width as limited by $\Lambda_{\min}$ and $\Lambda_{\max}$.

the following discussion we always assume that adjacent wavelength channels are spaced by five soliton spectral widths, as given by $\Lambda_{\mathbf{min}}$ in Eq. (5.1) and plotted in Fig. 5.3. However, $\Lambda_{\mathbf{max}}$ was defined according to Eq. (5.2) simply because values of $\Delta\lambda_{\mathbf{rms}}$ become negligibly small when $L_c/L_a > 2$ in Fig. 4.7. In other words, the restriction on $\Lambda_{\mathbf{max}}$ is based on worst-case assumptions about the system. Actual predictions of timing jitter and bit-error-rates that result from WDM soliton interactions have never been formulated, and thus it is uncertain whether $\Lambda_{\mathbf{max}}$ as given by Eq. (5.2) is realistic. By analyzing the statistics of WDM soliton interactions, more reliable limits on communication with WDM solitons may be derived.

Two random processes are significant for our discussion. First, we assume the data is encoded in some psuedo-random fashion. It is impossible for the data to be entirely random, as this would represent noise. However, the analysis is simplified by treating the data as random and uniformly distributed. Thus, we assume that bit values of zero and one each occur with probability 1/2 and that individual bits are statistically independent of one another. In a WDM soliton system, the presence of a soliton indicates a one and the absence indicates a zero. If data is random, soliton collisions occur only if the bit values in both channels are one. A second random variable that influences WDM soliton interactions is the timing or position of any collision. As an example, we note that adjacent 50 ps solitons with a bit period of 250 ps are only about 5 cm apart in the fiber since the group velocity is about 0.02 cm/ps. Thus, in a single wavelength channel there are about 200×10^6 solitons in a fiber 10000 km long, with as many as 500×10^3 solitons between two amplifiers separated by 25 km. Hence with multiple wavelength channels, collisions will

be occuring throughout the fiber at random positions.

Two effects that we ignore are phase and amplifier noise. It was already shown in Section 3.2.1 that soliton interactions are phase independent, so randomness in phase is of no consequence. However, noise will ultimately limit a WDM system, just as it limits communications over a single wavelength channel. Amplifier noise affects both the energy of the soliton[11] and the timing, as described by the Gordon-Haus effect[22]. Such effects have been examined in detail and may be applied to a WDM soliton system in a straightforward manner. We neglect them here, and focus on determining the timing jitter that is intrinsic to soliton interactions in a WDM system.

5.2 Timing jitter in WDM soliton systems

As given by Eq. (4.23), the timing displacement that results from a single collision between two WDM solitons is

$$\begin{aligned} \delta t &= \delta t_{\text{res}} + \delta t_{\text{coll}} \\ &= \overline{D}\,\Delta\lambda(z_c)\,(L - z_c) - \frac{0.1768}{(\Delta f)^2 \tau}. \end{aligned} \tag{5.4}$$

This is the shift in the arrival time of the faster soliton at the end of the fiber. (The slower soliton shifts by the same amount but in the opposite direction.) Collision-induced timing shifts are illustrated in Fig. 5.6, where solitons on wavelength channel λ_1 are shown separately from solitons on a second channel λ_2. The bit value in the jth bit slot of the second channel is defined as b_j. Solitons in bit slots $i-1$ and i in λ_1 are colliding with solitons in bit slots $j-1$ and j, respectively, in λ_2. The position at the center of each collision is z_c, so each soliton shifts by δt. Soliton $i+1$ in channel one does not shift because it is not colliding with any soliton in channel two — the bit value in

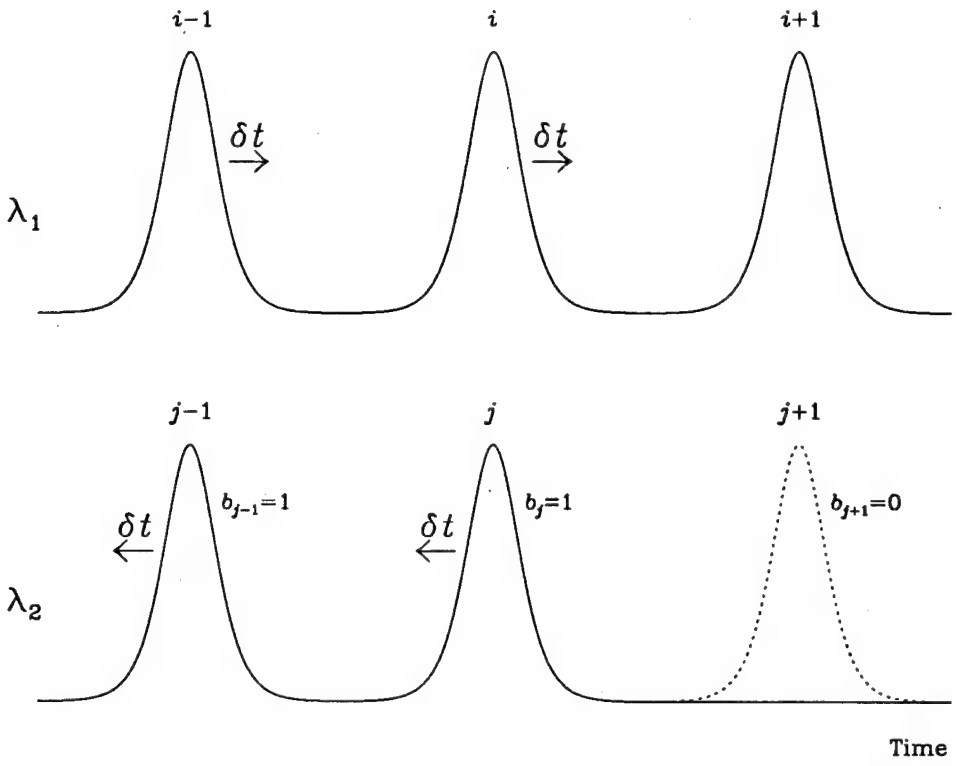

Figure 5.6. Timing shifts δt at two collisions and absence of shift if no collision occurs.

the corresponding bit slot of channel two is $b_{j+1} = 0$.

Since the solitons in bit slots i and $i-1$ of channel one both shift by δt, they cannot interfere at the end of the fiber. However, solitons i and $i+1$ might interfere if δt is large. (Here we assume that solitons exist in both bit slots i and $i+1$. We will consider a more general scenario momentarily.) Hence, it is the relative shift

$$\Delta t_{j,j+1} = (b_j - b_{j+1})\delta t \tag{5.5}$$

that potentially degrades data in bit slots i and $i+1$ of channel one at the output of the fiber. If $\Delta t_{j,j+1}$ is positive, solitons i and $i+1$ may be too close at the end of the fiber, whereas if $\Delta t_{j,j+1}$ is negative, they may be too far apart,

possibly interfering with bit slots $i-1$ or $i+2$. Although there is only one bit period $T = 5\tau$ between solitons in Fig. 5.6, adjacent solitons in channel one may actually be separated by several bit periods ρ since data is encoded on each channel. Thus, the relative shift may be redefined in more general terms as

$$\Delta t_{j,j+\rho} = (b_j - b_{j+\rho})\delta t. \tag{5.6}$$

Since the reception of too many consecutive zeros at the receiver often disrupts clock extraction and degrades receiver sensitivity, ρ is typically no greater than around five.

In reality, numerous collisions occur in the fiber. To clarify the situation, Fig. 5.7 depicts the fiber profile, where an 'X' marks the center of each possible collision. There are at most n collisions, with

$$n = \frac{L}{Z_c}, \tag{5.7}$$

where the fiber length is L and the collision period is

$$Z_c = \frac{T}{D\Lambda}. \tag{5.8}$$

Z_c is the minimum distance that soliton i propagates between each collision. The position of a collision between soliton i in channel one and soliton j in channel two is now defined as z_j, where j takes on at most n values. Whether

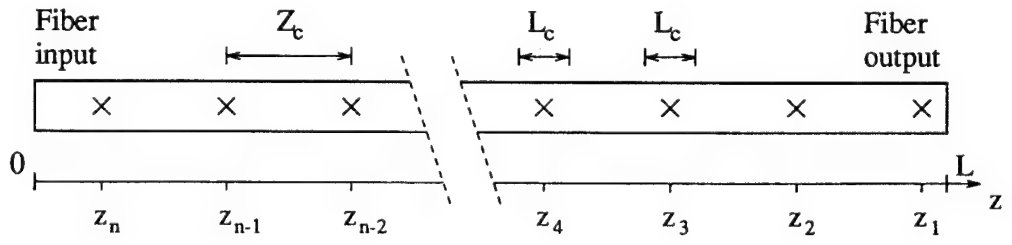

Figure 5.7: Profile of collision positions in the fiber.

a collision actually occurs depends on the value of b_j at each position z_j. With regards to Fig. 5.6, if the solitons on λ_1 are faster than the solitons on λ_2, then soliton i will collide with soliton $j-1$ at position z_{j-1} after propagating a distance Z_c; hence, $z_{j-1} - z_j = Z_c$. As before, L_c is the collision length defined in Eq. (4.17), so if $T = 5\tau$, the collision period is related to the collision length by $Z_c/L_c = 2.5$. Note that if positions z_1 and z_n are either too close or too far from the ends of the fiber, collisions may occur at the fiber input or output, and the results in Section 4.2 apply.

The total relative shift between two solitons in channel one after n possible collisions is

$$\begin{aligned}\sum_{j=1}^{n} \Delta t_{j,j+\rho} &= \sum_{j=1}^{n} (b_j - b_{j+\rho})\, \delta t \\ &= \sum_{j=1}^{n} (b_j - b_{j+\rho})(\delta t_{\text{res}} + \delta t_{\text{coll}}) \\ &= \sum_{j=1}^{n} (b_j - b_{j+\rho}) \left[\overline{D}\, \Delta\lambda(z_j)\, (L - z_j) \right. \\ &\qquad \left. - 0.1768/(\Delta f)^2\, \tau \right]. \end{aligned} \tag{5.9}$$

Carrying out the summation, the total shift becomes

$$\begin{aligned}\sum_{j=1}^{n} \Delta t_{j,j+\rho} &= \sum_{j=1}^{n} (b_j - b_{j+\rho})\, \delta t_{\text{res}} \\ &\qquad + \delta t_{\text{coll}} \sum_{j=1}^{\rho} (b_j - b_{j+n}). \end{aligned} \tag{5.10}$$

We see in this equation that most of the terms related to δt_{coll} cancel if ρ is small. Adjacent solitons in λ_1 collide with nearly identical solitons from λ_2 over the full length of the fiber, and since δt_{coll} is identical for each collision (note that it is independent of j), only a few terms remain. The terms that do not cancel contribute little to the overall variance in arrival times (as we shall

see momentarily), so we approximate the total relative shift by

$$\begin{aligned} \Delta t &= \sum_{j=1}^{n} \Delta b_j \, \delta t_{\text{res}} \\ &= \sum_{j=1}^{n} \Delta b_j \, \overline{D} \, \Delta\lambda_j \, (L - z_j), \end{aligned} \tag{5.11}$$

where $\Delta b_j \equiv b_j - b_{j+\rho}$ and $\Delta\lambda_j \equiv \Delta\lambda(z_j)$. Hence, only residual shifts δt_{res} significantly affect the relative arrival time of two solitons at the end of the fiber. Simply stated, it is primarily perturbations which cause timing jitter at the end of the fiber.

If we arbitrarily choose values for the collision positions as

$$z_j = (n - j) \, Z_c \tag{5.12}$$

and substitute for L and Z_c in Eq. (5.11) by using Eqs. (5.7) and (5.8), the relative shift is simplified, as in

$$\Delta t = T \sum_{j=1}^{n} j \, \Delta b_j \, \frac{\Delta\lambda_j}{\Lambda}. \tag{5.13}$$

The result in Eq. (5.13) agrees with intuition since the value of Δt will be large relative to the bit period T whenever the wavelength shifts $\Delta\lambda_j$ are large relative to the channel spacing Λ. The meaning of Δt is analogous to that of $\Delta t_{j,j+1}$ in Eq. (5.5); adjacent solitons move closer to one another when Δt is positive and they move farther apart when Δt is negative. Whether the absolute value of Δt is too large depends on how much jitter the receiver can withstand.

Since we assume the data is random and uniformly distributed, the quantity Δb_j equals zero with probability 1/2, or ± 1, each with probability 1/4. Furthermore, since the values of z_j are random and unrelated to the positions of the amplifiers (or any other perturbation), the wavelength shifts

$\Delta\lambda_j$ are also random, and Δt is a sum of products of the two random variables, Δb_j and $\Delta\lambda_j$. The probability density function of a product $Z = XY$ of two independent random variables[113] is solved using

$$f_Z(z) = \int \frac{1}{|y|} f_X\left(\frac{z}{y}\right) f_Y(y)\, dy, \tag{5.14}$$

where $f_X(x)$ and $f_Y(y)$ are the probability density functions of X and Y. When applied to the product $\Delta b_j\, \Delta\lambda_j$, the mean is zero and the variance is

$$\langle (\Delta b_j\, \Delta\lambda_j)^2 \rangle = \frac{\langle \Delta\lambda \rangle^2 + \langle \Delta\lambda^2 \rangle}{2}, \tag{5.15}$$

as derived in the appendix in Section A.3. The quantities $\langle \Delta\lambda \rangle$ and $\langle \Delta\lambda^2 \rangle$ are the mean and variance, respectively, of the wavelength shifts $\Delta\lambda_j$.

The variance of a sum of independent random variables is given by the sum of the variances, so for Eq. (5.13) we write

$$\langle \Delta t^2 \rangle = \left(\frac{T}{\Lambda}\right)^2 \sum_{j=1}^{n} j^2 \left(\frac{\langle \Delta\lambda \rangle^2 + \langle \Delta\lambda^2 \rangle}{2}\right). \tag{5.16}$$

Since for large n

$$\sum_{j=1}^{n} j^2 = \frac{n(n+1)(2n+1)}{6} \approx \frac{n^3}{3}, \tag{5.17}$$

the variance in Δt is approximately

$$\langle \Delta t^2 \rangle \approx n^3 \left(\frac{T}{\Lambda}\right)^2 \left(\frac{\langle \Delta\lambda \rangle^2 + \langle \Delta\lambda^2 \rangle}{6}\right). \tag{5.18}$$

This is the variance in the relative displacement of adjacent solitons in either of the two channels at the fiber output. It is the most general result of the analysis with two wavelength channels. By substituting for n from Eq. (5.7), it is easy to see that the variance is proportional to the system length, increasing in relation to L^3. This is analagous to the L^3 dependence of Gordon-Haus timing jitter[22] resulting from ASE noise. Furthermore, individual terms in

the summation of (5.16) are small in relation to the total variance $\langle \Delta t^2 \rangle$ in (5.18), given the limit

$$\lim_{n\to\infty} \frac{j^2}{n^3} = 0 \qquad \text{for all } j = 1, \ldots, n, \tag{5.19}$$

so the Lindeberg condition of the Central Limit Theorem[114] holds and the distribution of Δt approaches the Gaussian distribution for large n. (Values of n are usually greater than ten and will oftentimes be in the hundreds.)

To apply Eq. (5.18) specifically in a fiber with loss and amplification, the average value of the wavelength shift from Eq. (4.15) is $\langle \Delta\lambda \rangle = 0$ (there is no dc term in the Fourier series), so its variance is

$$\langle \Delta\lambda^2 \rangle = \Delta\lambda_{\text{rms}}^2 = \sum_{m=1}^{\infty} (c_m)^2, \tag{5.20}$$

where the coefficients c_m were defined in Eq. (4.16). Thus, the jitter in relative arrival times in a fiber with loss and amplification is given by the variance

$$\langle \Delta t^2 \rangle = n^3 \left(\frac{T}{\Lambda}\right)^2 \frac{\Delta\lambda_{\text{rms}}^2}{6}, \tag{5.21}$$

and the standard deviation

$$\sqrt{\langle \Delta t^2 \rangle} = n^{3/2} \left(\frac{T}{\Lambda}\right) \left(\frac{\Delta\lambda_{\text{rms}}}{\sqrt{6}}\right). \tag{5.22}$$

In a practical application of Eq. (5.22), Figs. 5.8 and 5.9 depict the standard deviation as a function of the system length for values of $L_c/L_a = 2$ and $L_c/L_a = 0.7$, respectively. As an example, we compute the value of $\sqrt{\langle \Delta t^2 \rangle}$ when $\tau = 20$ ps for $L = 10000$ km (the maximum transoceanic distance). With $L_c/L_a = 2$, we find in Fig. 4.7 that $\Delta\lambda_{\text{rms}} = 0.0001$ nm and in Fig. 4.9 that $\Lambda = 0.8$ nm. If $T = 5\tau = 100$ ps and $\overline{D} = 1$ ps/nm-km, the collision period is $Z_c = T/(\overline{D}\Lambda) = 100/(1)(0.8) = 125$ km and the total number of collisions

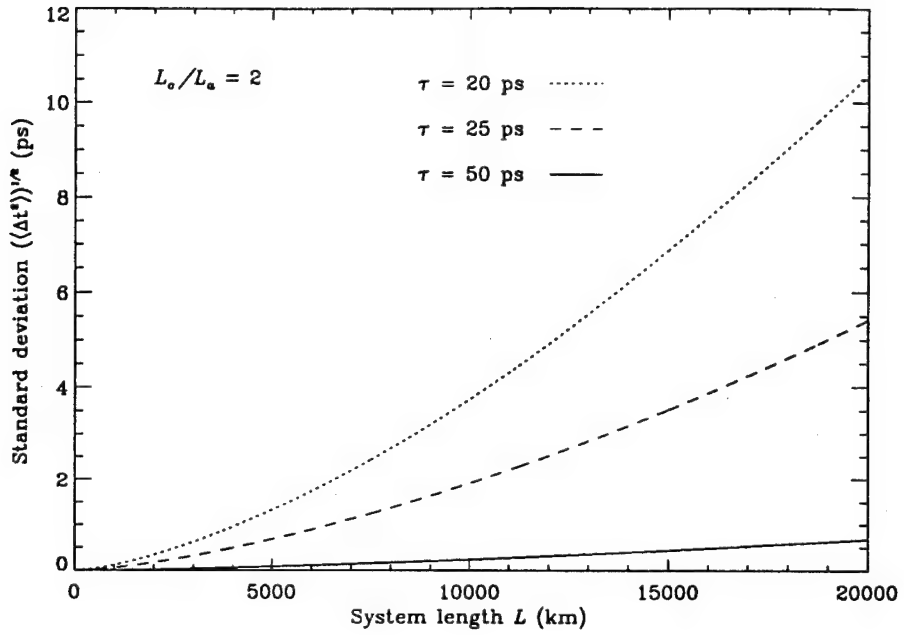

Figure 5.8: Standard deviation in Δt as a function of L when $L_c/L_a = 2$.

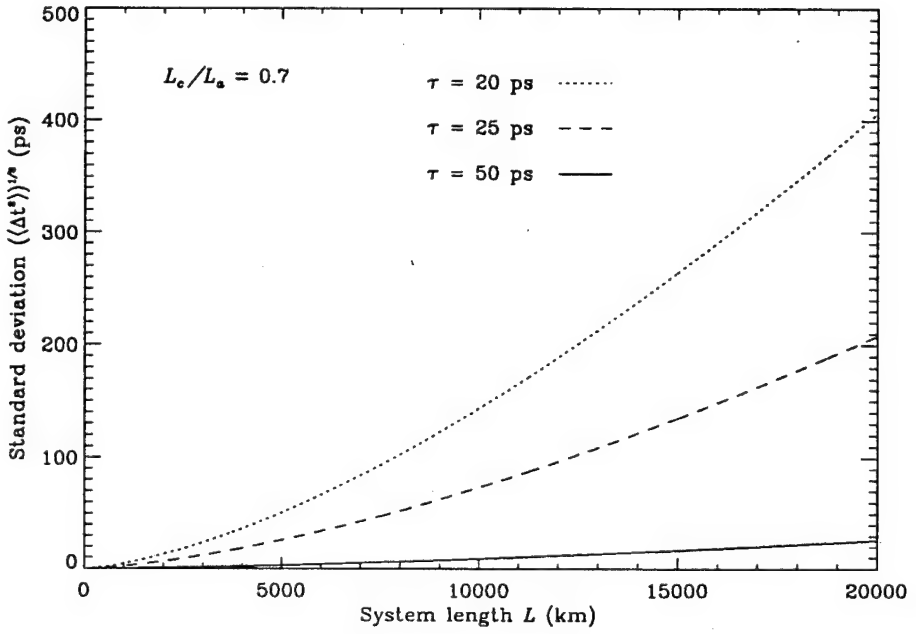

Figure 5.9: Standard deviation in Δt as a function of L when $L_c/L_a = 0.7$.

is $n = L/Z_c = 10000/125 = 80$, so the standard deviation is $\sqrt{\langle \Delta t^2 \rangle} = 3.7$ ps, close to the value shown in Fig. 5.8 at $L = 10000$ km. Estimates of jitter using Eq. (5.22) match recent numerical estimates in [70].

To estimate the bit-error-rate(BER) resulting from Eq. (5.21), we make an assumption about how much jitter the receiver can tolerate by defining a parameter r to measure receiver sensitivity. If the maximum value of $|\Delta t|$ allowed by the receiver is given by $rT = 5r\tau$, the receiver is more sensitive to jitter in the arrival times of adjacent solitons as r decreases. The actual value of r in a system cannot be defined precisely without knowing many details about the receiver, but as an example, if $r = 2/5$, then $|\Delta t|$ must be less than 2τ for the receiver to detect data accurately. If adjacent solitons are initially separated by $T = 5\tau$ at the input, they may be spaced no closer than 3τ and no farther than 7τ at the output for the receiver to detect each bit. If $\rho = 3$ between two solitons, the initial spacing is $3T = 15\tau$, so they must be separated by at least 13τ and by at most 17τ at the fiber output for the receiver to detect data. Since Δt is Gaussian distributed, the bit error rate is computed according to

$$\mathrm{BER} = \sqrt{\frac{2}{\pi}} \int_{x_o}^{\infty} \exp(-x^2/2)\, dx, \tag{5.23}$$

where the lower limit of integration is $x_o = rT/\sqrt{\langle \Delta t^2 \rangle}$. In terms of a complementary error function, we have

$$\begin{aligned} \mathrm{BER} &= \mathrm{erfc}\left(x_o/\sqrt{2}\right) \\ &= \frac{2}{\sqrt{\pi}} \int_{\frac{x_o}{\sqrt{2}}}^{\infty} \exp(-x^2)\, dx. \end{aligned} \tag{5.24}$$

The BER is 10^{-9} when $x_o = 6.1$ and 10^{-12} when $x_o = 7.1$. For the data in Figs. 5.8 and 5.9, error rates are shown in Figs. 5.10 through 5.12. For

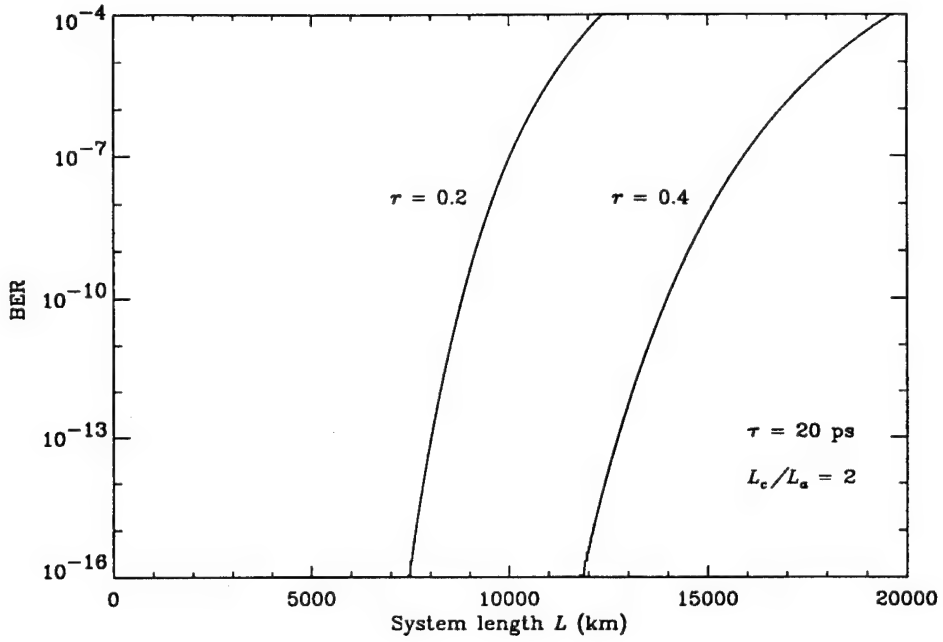

Figure 5.10: BER for $\tau = 20$ ps and $L_c/L_a = 2$ at various system lengths.

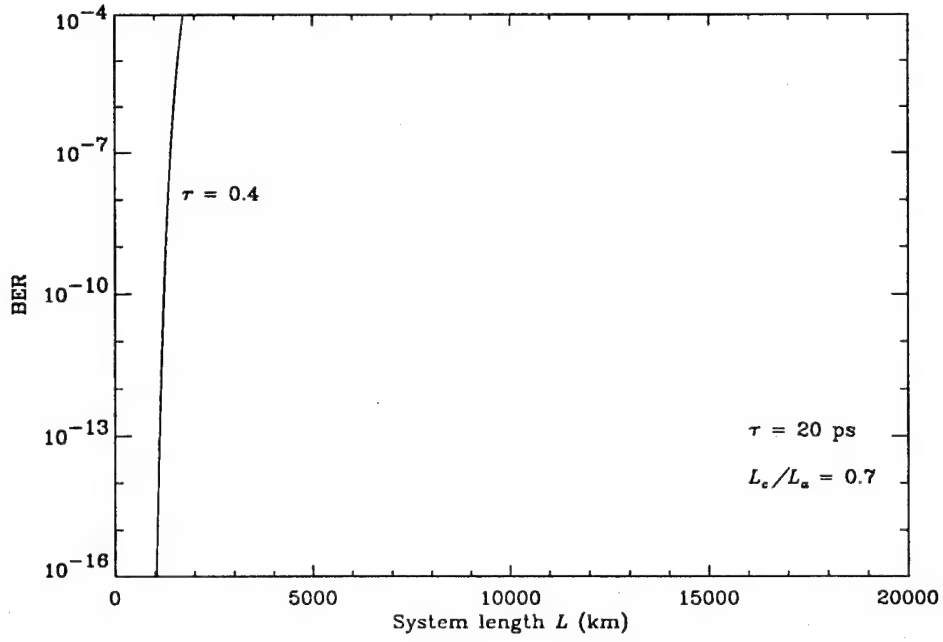

Figure 5.11: BER for $\tau = 20$ ps and $L_c/L_a = 0.7$ at various system lengths.

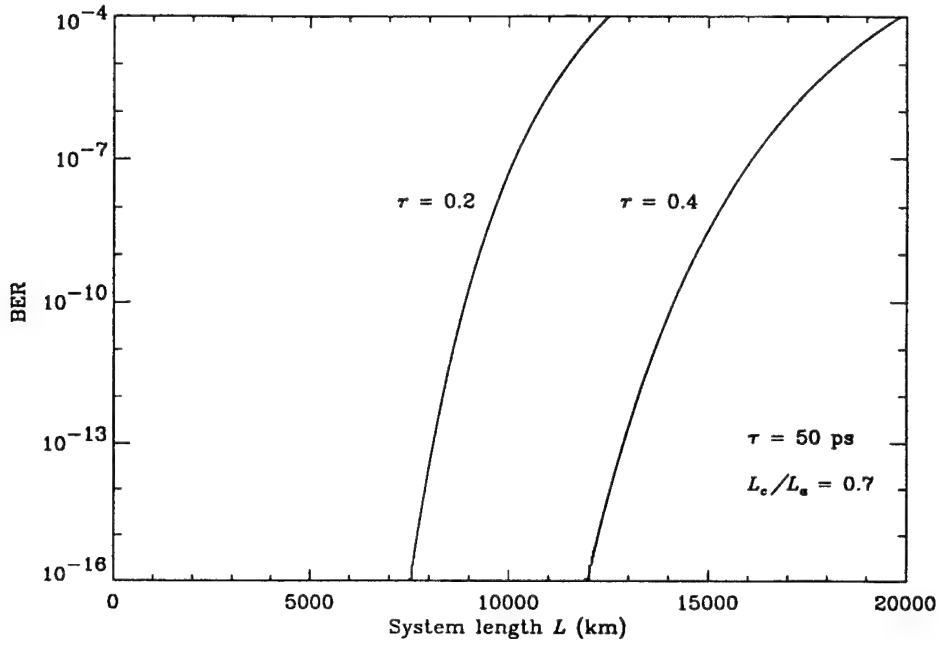

Figure 5.12: BER for $\tau = 50$ ps and $L_c/L_a = 0.7$ at various system lengths.

$\tau = 20$ ps and $L_c/L_a = 2$ in Fig. 5.10, the BER is less than 10^{-12} up to lengths of 13000 km for $r = 0.4$ (the relative shift can be as large as 2τ). The BER is very dependent on receiver sensitivity, as seen by the difference between the curves for $r = 0.2$ and $r = 0.4$. A similar plot for $\tau = 50$ ps and $L_c/L_a = 2$ is not shown because the error rates are well below 10^{-16} for lengths up to 20000 km. If $\tau = 20$ ps and $L_c/L_a = 0.7$, as shown in Fig. 5.11, the BER increases dramatically, as would be expected, so that it is impossible to transmit WDM solitons over any distance greater than about 1000 km. However, for $\tau = 50$ ps and $L_c/L_a = 0.7$ in Fig. 5.12, we see that WDM solitons can still be transmitted over relatively long distances even with $L_c/L_a < 2$. It seems clear from these results that $\Lambda_{\max}$ in Eq. (5.2) may be overly conservative, at least for pulse widths nearing 50 ps.

Before analyzing jitter for an arbitrary number of wavelength channels, we estimate the error made by approximating the total jitter by Eq. (5.11) instead of using the exact value in (5.10). The variance of the quantity $(b_j - b_{j+n})$ in Eq. (5.10) is 1/2, so it is rather straightforward to show that the contribution of the second term in Eq. (5.10) to the variance of Δt is given by

$$\langle \Delta t^2 \rangle_{\text{corr}} = \frac{\rho}{2} (\delta t_{\text{coll}})^2, \tag{5.25}$$

where we label this as the correction factor to $\langle \Delta t^2 \rangle$. With inclusion of this term, the corrected BER is

$$\text{BER}_{\text{corr}} = \text{erfc}\left(rT / \sqrt{2(\langle \Delta t^2 \rangle + \langle \Delta t^2 \rangle_{\text{corr}})} \right). \tag{5.26}$$

The accuracy of Eq. (5.11) is estimated for $\tau = 20$ ps by plotting the two curves from Fig. 5.10 again in Fig. 5.13, where the dashed and dotted curves now illustrate BER_{corr} for the specified values of ρ. We see that the correction factor becomes more significant if adjacent solitons are farther apart (ρ increases), if the receiver is more sensitive (r decreases), or if low error rates are required. In a full analysis, the value of ρ must be treated as a random variable, accounting for psuedo-random properties of any data encoding scheme that is used. For purely random data, we can show that the average value of ρ is no greater than two in a data stream of infinite length. With multiple wavelength channels in the system, the contribution from each additional channel is very small; the correction factor in (5.25) scales according to $1/(\Delta f)^4$ since δt_{coll} in Eq. (5.9) is proportional to $1/(\Delta f)^2$. Consequently, the approximation made in Eq. (5.11) is valid regardless of the number of channels. Timing jitter in a system with an arbitrary number of channels is the subject of the next section.

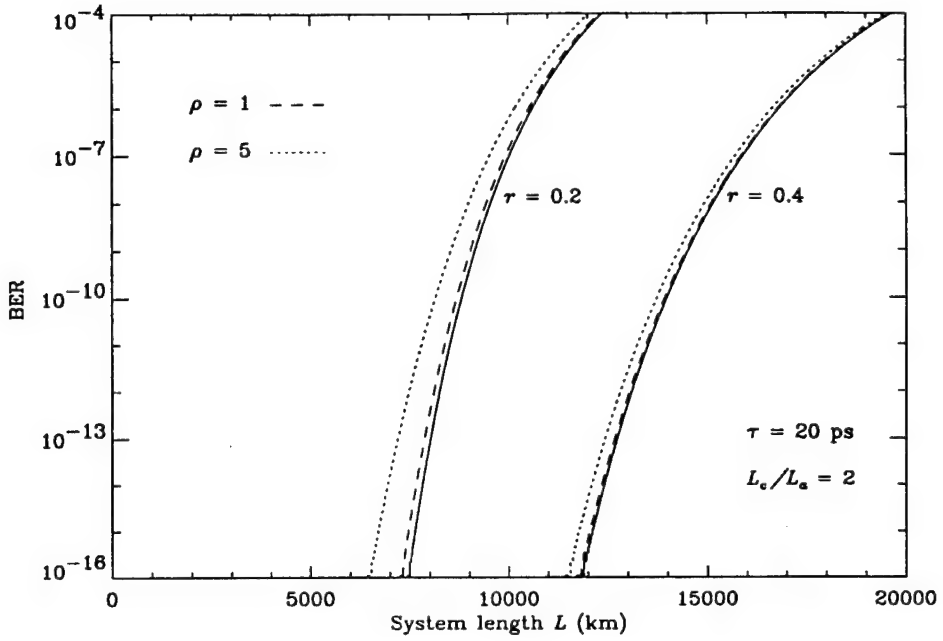

Figure 5.13. BER for $\tau = 20$ ps and $L_c/L_a = 2$. Dashed and dotted curves plot the corrected error rate $\mathrm{BER}_{\mathrm{corr}}$.

5.3 Performance limits in WDM soliton systems

The results in Section 3.3 and in [101] demonstrate that interactions between multiple channels are linearly additive if adjacent channels are asymptotically separated in frequency. Hence, it is easy to modify Eq. (5.21) if there are multiple wavelength channels; the total variance in the relative arrival times of adjacent solitons in the pth of N channels is simply a sum of the variances resulting from interactions with the other $N-1$ channels, as in

$$\begin{aligned} \langle \Delta t^2 \rangle_p &= \sum_{\substack{q=1 \\ q \neq p}}^{N} (n_{pq})^3 \left(\frac{T}{\Lambda_{pq}} \right)^2 \frac{\langle \Delta \lambda^2 \rangle_{pq}}{6} \\ &= \sum_{\substack{q=1 \\ q \neq p}}^{N} \left(\frac{L}{Z_c^{pq}} \right)^3 \left(\frac{T}{\Lambda_{pq}} \right)^2 \frac{\langle \Delta \lambda^2 \rangle_{pq}}{6}. \end{aligned} \tag{5.27}$$

The channel spacing, collision period, and variance in wavelength shifts between the pth and qth channels are given by $\Lambda_{pq} = |\lambda_p - \lambda_q|$, $Z_c^{pq} = T/(\overline{D}_{pq}\Lambda_{pq})$,

and $\langle \Delta\lambda^2 \rangle_{pq}$, respectively. The average dispersion between the channels is $\overline{D}_{pq} = S_0(\lambda_p + \lambda_q - 2\lambda_0)/2$, where S_0 is the slope of the dispersion at the zero dispersion wavelength λ_0. The BER in the pth channel is

$$\mathrm{BER}_p = \mathrm{erfc}\left(rT/\sqrt{2\langle \Delta t^2 \rangle_p}\right), \tag{5.28}$$

where the complementary error function is defined in (5.24).

Equations (5.27) and (5.28) may be applied in a system with loss and amplification just as in previous examples with only two wavelength channels. Unless explicitly stated otherwise, we assume the following parameters:

- amplifier spacing $L_a = 25$ km;
- dispersion coefficient $D = 1$ ps/nm-km at 1.55 μm and dispersion slope $S_0 = 0.067$ ps/nm^2-km at a zero dispersion wavelength $\lambda_0 = 1.535$ μm;
- attenuation $\alpha = 0.048$ km^{-1} or 0.21 dB/km;
- adjacent channel spacing $\Lambda = \Lambda_{\min}$ as defined by Eq. (5.1) and depicted in Fig. 5.3;
- receiver sensitivity $r = 0.4$ requiring $|\Delta t| < 2\tau$;
- bit period $T = 5\tau$ and data rate $R = 1/T$ in each channel.

The C program which computes the jitter for an arbitrary number of channels is listed in Appendix B.

As an example with four 20 ps channels and $L = 10000$ km, Table 5.1 lists the standard deviation in Δt and the BER in each channel for the parameters listed above. Since the jitter in each channel is considerably larger than the pulse width, the BER in each channel is much too high for accurate transmission of data. Jitter is worse when channels are farther apart (since collisions occur over shorter distances if Λ_{pq} is larger), consistent with the plots in Fig. 4.10. Hence, in this example, the jitter is largest in channels one and

four. If either the dispersion coefficient or the amplifier spacing is halved, the ratio $L_c^{pq}/L_a = 2\tau/(\overline{D}_{pq}\,\Lambda_{pq}\,L_a)$ is twice as large, so we expect the results to improve. This is demonstrated in Table 5.2, where the average dispersion is 0.5 ps/nm-km, and in Table 5.3, where the amplifier spacing is 12.5 km. Equation (5.3) predicts a value of $N_{\max} = 3$ for these parameter values; in reality, we see that four channels are possible in each case since the error rate in each channel is no greater than 10^{-23}.

Equations (5.27) and (5.28) also enable us to determine how much

Table 5.1. Jitter and BER in four 20 ps channels at a distance of $L = 10000$ km.

Wavelength λ_p (nm)	Dispersion D (ps/nm-km)	Standard deviation $(\langle \Delta t^2 \rangle_p)^{1/2}$ (ps)	BER_p
$\lambda_1 = 1549.062$	0.94	125	10^{-1}
$\lambda_2 = 1549.688$	0.98	49.7	10^{-1}
$\lambda_3 = 1550.312$	1.02	39.2	10^{-1}
$\lambda_4 = 1550.938$	1.06	129	10^{-1}

Table 5.2. Jitter and BER in four 20 ps channels at a center wavelength of 1.5425 μm with $L = 10000$ km.

Wavelength λ_p (nm)	Dispersion D (ps/nm-km)	Standard deviation $(\langle \Delta t^2 \rangle_p)^{1/2}$ (ps)	BER_p
$\lambda_1 = 1541.562$	0.44	2.77	$< 10^{-30}$
$\lambda_2 = 1542.188$	0.48	0.161	$< 10^{-30}$
$\lambda_3 = 1542.812$	0.52	0.055	$< 10^{-30}$
$\lambda_4 = 1543.338$	0.56	2.78	$< 10^{-30}$

Table 5.3. Jitter and BER in four 20 ps channels with $L = 10000$ km and with amplifier spacings reduced to $L_a = 12.5$ km.

Wavelength λ_p (nm)	Dispersion D (ps/nm-km)	Standard deviation $(\langle \Delta t^2 \rangle_p)^{1/2}$ (ps)	BER_p
$\lambda_1 = 1549.062$	0.94	3.98	10^{-23}
$\lambda_2 = 1549.688$	0.98	0.179	$< 10^{-30}$
$\lambda_3 = 1550.312$	1.02	0.105	$< 10^{-30}$
$\lambda_4 = 1550.938$	1.06	3.98	10^{-23}

flexibility there is in choosing the best channel spacing. Table 5.4 demonstrates the jitter and error rates in eight 50 ps channels, again at a distance of 10000 km, with an adjacent channel spacing of $\Lambda = \Lambda_{\min} = 0.25$ nm. While the BER in each channel is much less than 10^{-30}, the channel spacing of 0.25 nm may be restrictive. By doubling the channel spacing to 0.5 nm, the jitter increases, but error rates are still well below 10^{-30}, as shown by Table 5.5. If the channel spacing is doubled once more, so that $\Lambda = 1.0$ nm, as in Table 5.6, the BER of 10^{-6} in channel eight is too high. However, it is easily reduced by sliding each wavelength two nanometers closer to the dispersion zero wavelength, as shown in Table 5.7. Since the average value of the dispersion coefficient between channels one and eight is $\overline{D}_{18} = 0.871$ ps/nm-km, then $L_c/L_a = 2(50)/(0.871)(7)(25) = 0.656$, which is very near the peak value of $\Delta\lambda_{\text{rms}}$ for channels one and eight (see Fig. 4.7). While the curves in Fig. 5.3 imply that 50 ps soliton channels may occupy a bandwidth no larger than 2 nm, Table 5.7 demonstrates that more flexibility is possible if system parameters are chosen properly.

The restrictions on $\Lambda_{\min}$ and $\Lambda_{\max}$ in Fig. 5.3 only permit wavelength

Table 5.4. Jitter and BER in eight 50 ps channels with channel spacing 0.25 nm and $L = 10000$ km.

Wavelength λ_p (nm)	Dispersion D (ps/nm-km)	Standard deviation $(\langle \Delta t^2 \rangle_p)^{1/2}$ (ps)	BER_p
$\lambda_1 = 1549.125$	0.94	0.085	$< 10^{-30}$
$\lambda_2 = 1549.375$	0.96	0.019	$< 10^{-30}$
$\lambda_3 = 1549.625$	0.97	0.002	$< 10^{-30}$
$\lambda_4 = 1549.875$	0.99	0.000	$< 10^{-30}$
$\lambda_5 = 1550.125$	1.01	0.000	$< 10^{-30}$
$\lambda_6 = 1550.375$	1.03	0.001	$< 10^{-30}$
$\lambda_7 = 1550.625$	1.04	0.015	$< 10^{-30}$
$\lambda_8 = 1550.875$	1.06	0.085	$< 10^{-30}$

Table 5.5. Jitter and BER in eight 50 ps channels with channel spacing Λ = 0.5 nm and L = 10000 km.

Wavelength λ_p (nm)	Dispersion D (ps/nm-km)	Standard deviation $(\langle \Delta t^2 \rangle_p)^{1/2}$ (ps)	BER_p
$\lambda_1 = 1548.25$	0.88	4.86	$< 10^{-30}$
$\lambda_2 = 1548.75$	0.92	2.97	$< 10^{-30}$
$\lambda_3 = 1549.25$	0.95	1.40	$< 10^{-30}$
$\lambda_4 = 1549.75$	0.98	0.405	$< 10^{-30}$
$\lambda_5 = 1550.25$	1.02	0.158	$< 10^{-30}$
$\lambda_6 = 1550.75$	1.05	0.860	$< 10^{-30}$
$\lambda_7 = 1551.25$	1.08	2.52	$< 10^{-30}$
$\lambda_8 = 1551.75$	1.12	5.24	$< 10^{-30}$

Table 5.6. Jitter and BER in eight 50 ps channels with channel spacing Λ = 1.0 nm and L = 10000 km.

Wavelength λ_p (nm)	Dispersion D (ps/nm-km)	Standard deviation $(\langle \Delta t^2 \rangle_p)^{1/2}$ (ps)	BER_p
$\lambda_1 = 1546.5$	0.76	15.2	10^{-11}
$\lambda_2 = 1547.5$	0.83	14.2	10^{-12}
$\lambda_3 = 1548.5$	0.90	12.3	10^{-16}
$\lambda_4 = 1549.5$	0.97	9.29	10^{-26}
$\lambda_5 = 1550.5$	1.03	6.44	$< 10^{-30}$
$\lambda_6 = 1551.5$	1.10	8.79	10^{-29}
$\lambda_7 = 1552.5$	1.17	14.2	10^{-12}
$\lambda_8 = 1553.5$	1.24	20.0	10^{-6}

Table 5.7. Jitter and BER in eight 50 ps channels with channel spacing Λ = 1.0 nm and a center wavelength of 1548 nm.

Wavelength λ_p (nm)	Dispersion D (ps/nm-km)	Standard deviation $(\langle \Delta t^2 \rangle_p)^{1/2}$ (ps)	BER_p
$\lambda_1 = 1544.5$	0.63	9.96	10^{-23}
$\lambda_2 = 1545.5$	0.70	9.14	10^{-27}
$\lambda_3 = 1546.5$	0.77	7.61	$< 10^{-30}$
$\lambda_4 = 1547.5$	0.83	5.30	$< 10^{-30}$
$\lambda_5 = 1548.5$	0.90	2.99	$< 10^{-30}$
$\lambda_6 = 1549.5$	0.97	4.58	$< 10^{-30}$
$\lambda_7 = 1550.5$	1.03	8.62	$< 10^{-30}$
$\lambda_8 = 1551.5$	1.10	13.3	10^{-13}

multiplexing of two soliton channels for pulse widths greater than 18 ps. This appears to be accurate if the fiber dispersion is $D = 1$ ps/nm-km, the length is 10000 km, and the required BER is 10^{-12}, as shown by Fig. 5.14. However, for shorter or less dispersive fibers (or if a higher BER is permitted), the minimum pulse width decreases. As an example, the minimum pulse width allowed in a WDM system 1000 km long with dispersion of 0.5 ps/nm-km is less than 10 ps. Further reductions are also possible if amplifiers are spaced closer together, as illustrated by the dashed curve for $L = 100$ km and $L_a = 25$ km — a fact that is especially useful if wavelength multiplexing were used to transmit very narrow solitons over shorter distances.

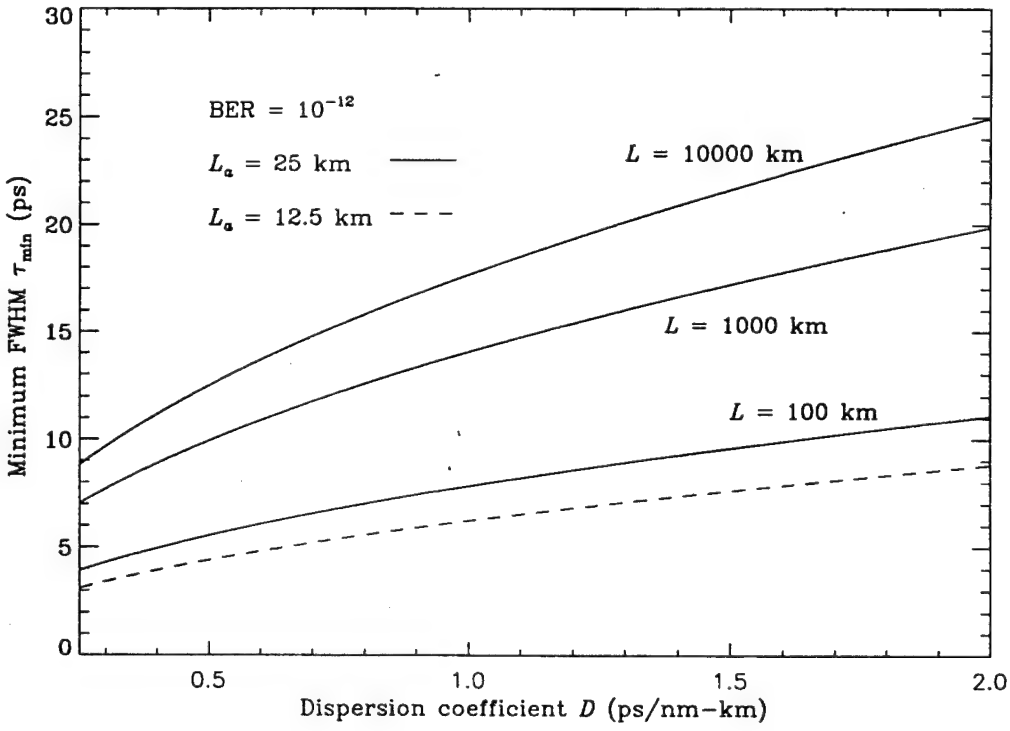

Figure 5.14. Minimum FWHM necessary to transmit WDM solitons across the specified distance. The dashed curve corresponds to $L = 100$ km and $L_a = 12.5$ km.

Finally, using Eq. (5.27), we can determine the maximum length of any system for a given BER. As an example, if the BER must be less than 10^{-9}, we require

$$\begin{aligned}\left(\frac{r\,T}{6.1}\right)^2 &\geq \langle \Delta t^2 \rangle_p \\ &\geq \sum_{\substack{q=1 \\ q\neq p}}^{N} \left(\frac{L}{Z_c^{pq}}\right)^3 \left(\frac{T}{\Lambda_{pq}}\right)^2 \frac{\langle \Delta\lambda^2 \rangle_{pq}}{6} \\ &\geq \sum_{\substack{q=1 \\ q\neq p}}^{N} \left(L\,\overline{D}_{pq}\right)^3 \left(\frac{\Lambda_{pq}}{T}\right) \frac{\langle \Delta\lambda^2 \rangle_{pq}}{6} \end{aligned} \tag{5.29}$$

for all values of p. By replacing T with 5τ and solving for L, the maximum system length is given by

$$L \leq \frac{2.72\,\tau\,r^{2/3}}{\max_p \left(\sum_{q\neq p} (\overline{D}_{pq})^3\,\Lambda_{pq}\,\langle \Delta\lambda^2 \rangle_{pq}\right)^{1/3}}, \tag{5.30}$$

so that L is limited by the channel in which the jitter is largest.

Using the parameter values listed at the beginning of this section, the solid curves in Fig. 5.15 illustrate the maximum length that is possible for various pulse widths and the specified numbers of channels N. If the required BER is 10^{-12} or if the receiver sensitivity requires $r = 0.2$, lengths in Fig. 5.15 are reduced by 10% and 37%, respectively. With adjacent wavelengths separated by $\Lambda_{\min}$, the channel spacings vary from $\Lambda = 0.625$ nm at $\tau = 20$ ps to $\Lambda = 0.25$ nm at $\tau = 50$ ps. If either the channel spacing Λ, the amplifier spacing L_a, or the dispersion D decreases, the ratio L_c/L_a increases, so that wavelength shifts are smaller, allowing system lengths to be longer.

The maximum length which insures both a 10^{-9} BER and $L_c/L_a \geq 2$ in each channel is depicted by the dashed line. Hence, when $L_c/L_a \geq 2$, WDM soliton transmission is error-free up to a distance of 20000 km for $\tau = 20$ ps and to longer distances when τ is greater than 20 ps. However, the number of 20 ps

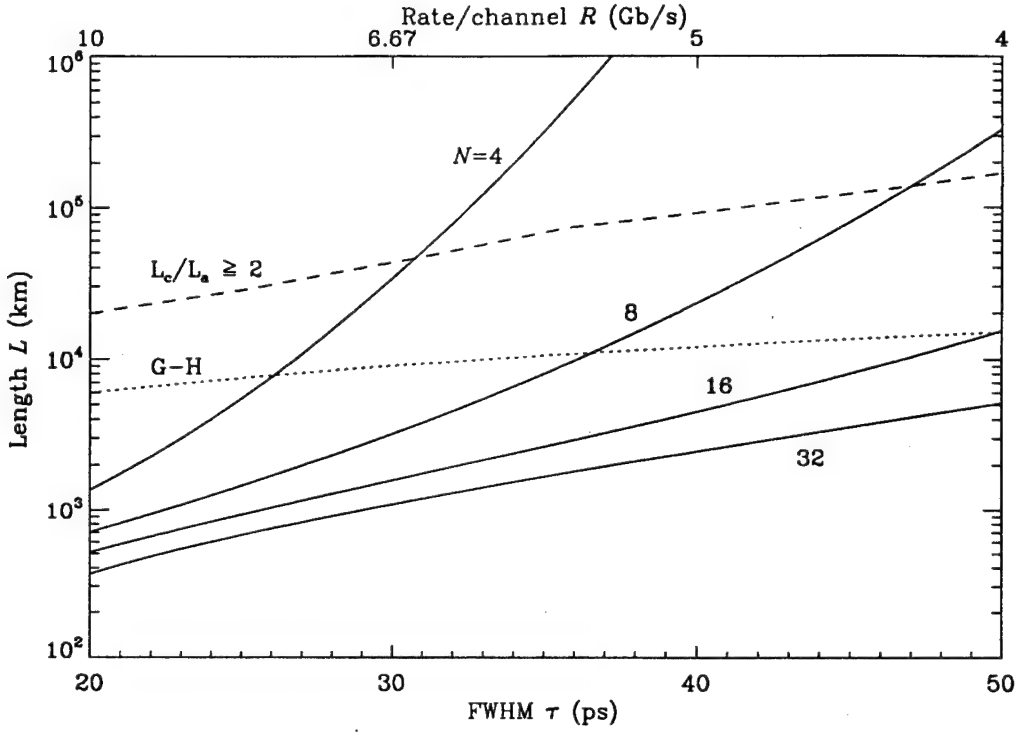

Figure 5.15. Maximum system length with N channels at a 10^{-9} BER as limited by collision-induced timing displacements. The dashed curve illustrates the maximum length possible if all channels meet the condition that $L_c/L_a \geq 2$ and the dotted curve indicates the maximum system length as limited by Gordon-Haus jitter.

channels is limited to two and the number of 50 ps channels is limited to eight, as shown previously in Fig. 5.4. If L_c/L_a is less than two, then the system must be shorter, but more channels are possible. For instance, with 40 ps solitons in a system 2500 km in length, 32 WDM channels — requiring a $31(0.315) = 10$ nm bandwidth — are theoretically possible. Since $L_c/L_a = 2(40)/1(10)(25) = 0.32$ between channels 1 and 32, the minimum value of L_c/L_a achieved in such a system is much less than the current limit of two.

To compare the effects of collision-induced jitter to Gordon-Haus jitter[22], we assume the single channel length limits due to the Gordon-Haus

effect are the same in each WDM channel. Recall from Chapter 1 that Gordon-Haus jitter arises from amplified spontaneous emission noise. Using previous system parameters, a maximum bit-rate–length product RL of 60 GHz-Mm is depicted by the dotted line of Fig. 5.15, as derived from [22] using $(RL)^3 \leq 0.1372\tau r^2 A_{\text{eff}}/(h\alpha n_2 DT)$. The nonlinear coefficient and the effective area of the fiber core are given by $n_2 = 3.2 \times 10^{-16}$ cm^2/W and $A_{\text{eff}} = 50$ μm^2, respectively, and h is Planck's constant. With many wavelength channels or high data rates, we see from Fig. 5.15 that the length will probably be limited by WDM soliton collision-induced jitter. Gordon-Haus jitter is more likely to limit the length of systems with fewer channels and lower data rates. In a recent WDM soliton experiment[76] using 60 ps solitons, eight 2.5 Gb/s channels were transmitted 10 Mm with error rates below 10^{-10}. The channels were densely multiplexed with $\Lambda = 0.2$ nm in order to insure $L_c/L_a \geq 2$, thus reducing collision-induced jitter. Figure 5.15 indicates, though, that this system is more likely limited by Gordon-Haus jitter, since the length as limited by collision-induced jitter is well over 10^6 km (as found by extrapolating the curve with $N = 8$ to $\tau = 60$ ps). Although collision-induced jitter increases if Λ is larger (since collision lengths L_c are shorter), estimates of jitter using Eq. (5.27) indicate that much larger channel spacings would be feasible before collision-induced jitter would impact such a system. Simply put, it was unnecessary in the experiment in [76] to multiplex the channels so densely.

For a given system length, Fig. 5.15 can also be used to predict the number of channels N possible at each pulse width and data rate. The results are shown in Fig. 5.16 for system lengths of $L = 2500$, 5000, and 10000 km. In a fiber 2500 km in length with $\tau = 50$ ps, 89 channels in an $88(0.25) =$

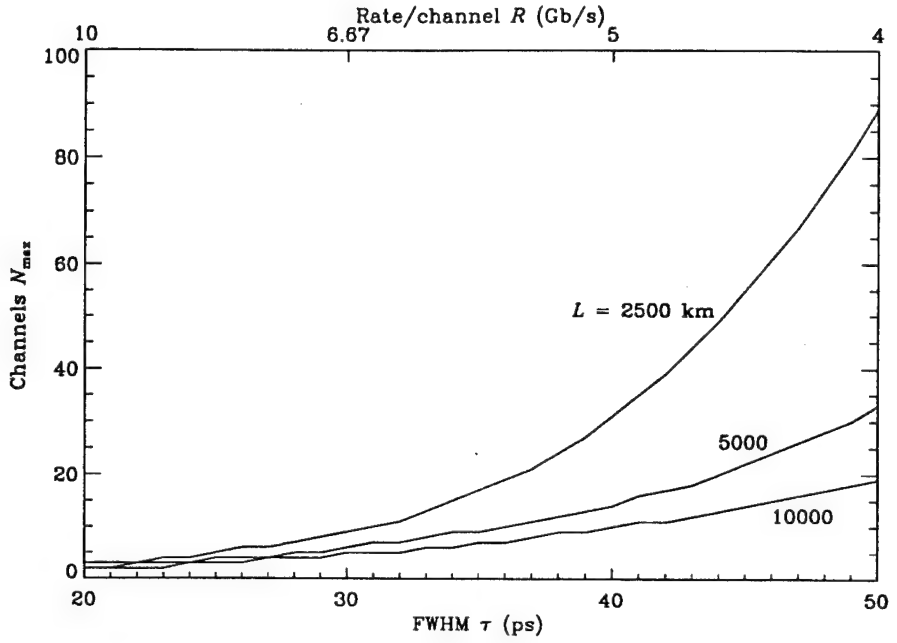

Figure 5.16. Maximum number of channels possible to maintain a BER of 10^{-9} at each length.

22 nm bandwidth are possible before collision-induced timing jitter degrades the system. In contrast, only two channels are possible if the pulse width is 20 ps and the system length is 10000 km. There are discontinuities in each curve since only integral values of N are possible, as was true in Fig. 5.4.

Aggregate throughput, predicted by multiplying the maximum number of channels N by the data rate R, is plotted in Fig. 5.17. The dashed curve corresponds to the plot in Fig. 5.5, insuring that $L_c/L_a \geq 2$. Intuitively, one might expect the throughput in Fig. 5.17 to increase as the data rate per channel increases, but these results show the opposite. As the data rate R increases, the number of collisions and the magnitude of the wavelength shifts increase substantially for fixed L, so the number of channels N decreases rapidly. Thus, the fundamental limit on throughput due to collision-induced

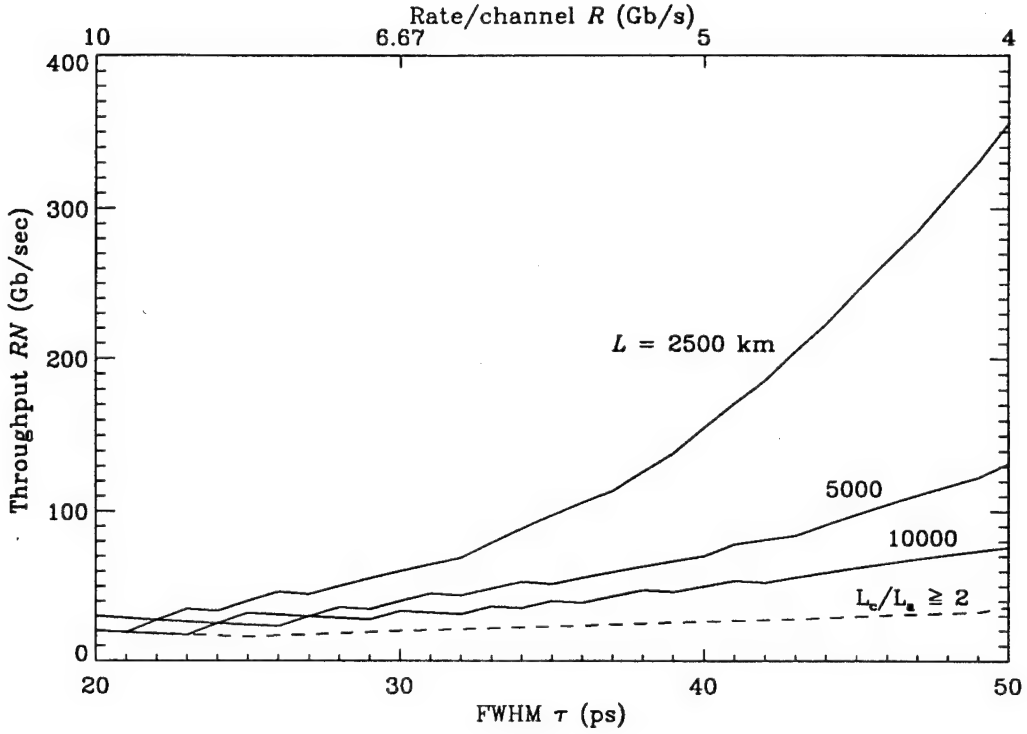

Figure 5.17. Maximum throughput in a WDM soliton system for various lengths.

velocity shifts is less restrictive using many slower (and cheaper) channels. For the previous example with $\tau = 50$ ps and $L = 2500$ km, the data rate in each channel is 4 Gb/s, so the aggregate throughput with 89 WDM channels is $89 \times 4 = 356$ Gb/s.

While these results suggest that more extensive WDM using solitons is preferable to other alternatives for achieving high aggregate throughput, it is unlikely that 356 Gb/s of data can actually be transmitted over a distance of 2500 km. Practical limitations might include fiber nonlinearities, as discussed in Section 4.3, or other amplifier effects. The gain, for instance, is not constant across the full bandwidth of an EDFA; different channels might experience more gain than others[78], violating the requirement in Fig. 4.1 that the average pulse

energy correspond to the fundamental soliton energy. There is also the problem of cross-saturation[2], whereby the gain of one channel saturates because of the aggregate power in other channels. If data is encoded in an amplitude-shift keyed format, the gain may fluctuate from one bit to the next, degrading signal-to-noise ratios.

The effect of filters[28, 32] on the system is also of great interest. Figure 5.17 implies that there is little to gain in a WDM soliton system simply by increasing the data rate of individual channels. However, if filters change the slope of the curves in Fig. 5.17, so that higher aggregate throughput results by using higher data rates, then it is reasonable to use pulse widths as short as possible. If filters only flatten the throughput curves, it is more reasonable to use slower, less expensive channels. These issues are influenced by many factors, such as filter design constraints, or by the soliton spectral width and WDM channel spacings that are required. The ultimate limits on WDM soliton systems will not be determined until such issues are resolved.

CHAPTER 6

SUMMARY AND CONCLUSIONS

The primary goals of this thesis, as stated at the outset, are:

1. To understand how WDM solitons, encoded on an arbitrary number of wavelength channels, interact during collisions in an optical fiber.
2. To determine the impact that collision-induced frequency and timing shifts have on communication in WDM soliton systems.

The first of these objectives was emphasized in Chapters 3 and 4, while the second was discussed in Chapter 5. In this chapter, we make more general observations, summarizing the previous results and speculating how WDM soliton systems will be impacted by effects other than soliton collisions. We conclude by suggesting areas for further research.

6.1 General observations regarding WDM soliton systems

Collisions are inevitable in a WDM soliton system because of chromatic dispersion. The overall interaction during a collision consists of a temporary wavelength shift (which always occurs, whether the fiber is lossless or not) and possibly a permanent wavelength shift if the interaction is perturbed — by loss and amplification, for instance. Interactions between an arbitrary number of wavelength channels are desribed by linearly summing the pairwise effects of each two-soliton interaction. This is already known to be true for temporal displacements at soliton collisions[36]; Chapter 3 demonstrates that it is true in the spectral domain as well (if adjacent channels are widely separated).

Temporary velocity shifts have no significant effect on data communication under certain conditions. First, if adjacent wavelength channels are separated by at least five soliton spectral widths, frequency shifts during collisions at the fiber output will be very small. Furthermore, the number of bit periods between adjacent solitons (as defined by ρ) must not be too large, or jitter caused by the temporary velocity shifts during collisions near either end of the fiber may significantly increase bit-error-rates.

Soliton interactions are more important in systems with loss and amplification or if collisions occur at the input to the fiber, since permanent shifts in the soliton frequencies and velocities can cause unpredictable displacements in pulse arrival times at the fiber output. If the displacements are too large, intersymbol interference may occur between adjacent bit slots. By themselves, though, permanent or residual wavelength shifts do not cause intersymbol interference — the jitter is ultimately data dependent. As an example, if each bit slot is encoded as a one, a continuous train of solitons is transmitted in each channel. Although pulse arrival times are displaced by collisions, all solitons shift by the same amount (since $\Delta b_j = 0$ for all j), so there is no interference at the fiber output. Jitter, or variance in the pulse arrival times, results because data is being transmitted across the fiber; a fraction of the bit slots are empty, so adjacent solitons may shift by different amounts, with some probability of interference at the fiber output.

The magnitude of collision-induced soliton jitter is a function of many system parameters. They are summarized as follows:

- Permanent velocity and wavelength shifts are fundamentally related to the ratio of the collision length to amplifier spacing L_c/L_a. The

shifts become smaller as this ratio becomes larger, since the effects of loss and amplification path-average when collisions occur over multiple amplifiers. Consequently, to reduce timing jitter, it is typical to restrict L_c/L_a to values greater than two. While this limits the use of WDM in soliton systems, the results of Chapter 5 show that such a requirement is more restrictive than necessary, since the jitter varies significantly with other system parameters as well.

- It is clear that jitter is reduced if the amplifier spacing L_a is smaller, since L_c/L_a will be larger. Smaller amplifier spacings generally stabilize soliton systems, reducing both ASE noise (the cause of Gordon-Haus jitter) and chaotic fluctuations in soliton energy that result when pulse widths are narrower and soliton periods are shorter. Of course, the system is more expensive since more amplifiers are required.
- The system length L strongly influences the performance that is possible in a WDM soliton system, since the variance in pulse arrival times is dependent on L^3. The stipulation that L_c/L_a be greater than two ignores the issue of system length; L_c/L_a may be less than two in many systems if L is smaller than 10000 km.
- As the dispersion D is decreased, the collision lengths L_c are larger, so the jitter becomes smaller. Less dispersive fibers are generally helpful in soliton systems, reducing the peak power of the solitons as well as Gordon-Haus jitter. Hence, soliton propagation nearly always occurs in dispersion shifted fibers. However, fibers with low dispersion can be harmful in a WDM system since four-wave mixing is more efficient in less dispersive fibers. The system is also sensitive to the dispersion

variation between different fibers, which may be treated as a perturbation in the same manner as loss and amplification. Although fibers may be selected carefully to minimize dispersion variations, such an option is more expensive. The use of dispersion-decreasing fibers could be an interesting way of reducing the negative effects of amplifiers[62].

- Reducing the channel spacing Λ helps to reduce jitter since the collision length increases if the relative group velocities (and thus the channel spacing) are as close as possible. While temporary effects of collisions increase as Λ decreases, more analysis is required to determine how the variance in soliton frequencies and arrival times are impacted.
- Jitter is less severe if the data rate R decreases (or the bit period $T = 1/R$ increases) while the pulse width τ is held constant, since fewer collisions occur if the solitons in each channel are farther apart. However, the variance of pulse arrival times is only linear in R (see Eq. (5.29)), while it decreases exponentially with increasing pulse width (since $\langle \Delta\lambda^2 \rangle \propto 1/\tau^6$), so the pulse width influences the jitter much more strongly than does the bit period T. In some respects, this implies that it might be best to increase data rates by allowing $T < 5\tau$. This might be possible in shorter systems, since adjacent pulse interactions are less severe if L is smaller.
- The tolerance r of the receiver is an important parameter that ultimately determines the performance of the system. We have attempted to assume reasonable values for r in our predictions of system performance. More must be known about soliton receivers before precise values of r can be determined.

- The parameter that is easiest to change to improve system performance is the pulse width τ. The number of collisions in a given length of fiber decreases at slower data rates, and since wavelength shifts are proportional to $1/\tau^3$, increasing τ reduces jitter significantly. (The system is also less sensitive to Gordon-Haus jitter if τ is larger[11, 22]). Furthermore, collision lengths increase as τ increases, so more flexibility is available in choosing the wavelengths of individual channels. As demonstrated in Chapter 5, the aggregate capacity of WDM soliton systems is optimized by using as many slower channels as possible.

6.2 Other factors affecting WDM soliton communication

As determined in Chapter 5, only two or three WDM channels are possible as pulse widths become narrower and data rates are made higher. Given this fact, collision-induced timing jitter is probably the effect which fundamentally limits such systems. To improve system performance, τ should be increased, so the channel data rates decrease while the number of channels are increased. Since aggregate throughput is higher, there are few drawbacks to using slower data rates in each channel. As data rates decrease, though, other factors besides collision-induced timing jitter, such as amplifier effects or nonlinearities, probably limit the number of channels in the system. Here we simply predict which effects will be dominant in WDM soliton systems.

While collision-induced timing jitter may be the limiting factor in a system with high data rates, ASE noise and Gordon-Haus jitter may be more significant in a system with lower data rates. Collision-induced timing jitter and Gordon-Haus timing jitter have the same L^3 dependence on system length, but the pulse width τ affects each differently. Gordon-Haus jitter decreases

less rapidly as τ increases than does collision-induced jitter (the Gordon-Haus variance in pulse arrival times[11] is dependent on $1/\tau$ while the collision-induced variance is dependent on $1/\tau^6$), so with larger pulse widths, Gordon-Haus may dominate, as in Fig. 5.15 with lower values of N. Other amplifier effects, such as cross-saturation, may act to limit the number of wavelength channels, since the power in the fiber increases as more channels are added.

The effect of nonlinearities (SRS, SBS, FWM) on WDM soliton systems is somewhat difficult to assess at this time without empirical observations in systems using more extensive WDM. Preliminary results seem to imply that in practical systems — ones with pulse widths greater than 20 ps — FWM is probably the dominant nonlinear process. It might easily limit a soliton system having lower data rates, since the channel spacings are smaller in such systems. By carrying out the asymptotic expansion in Chapter 3 to higher orders, it may be possible to quantitatively estimate FWM effects in a system having an arbitrary number of channels. With pulse widths around 20 ps or less, the channel spacings are larger, so the FWM process is less efficient. Since the peak power of such solitons is near the Brillouin threshold, spontaneous Brillouin scattering may be the dominant process, especially for pulse widths between 1 and 20 ps. (SRS is unlikely to affect such systems since only a few channels are possible given the results of Chapter 5.) For pulse widths below 1 ps, Raman gain (the soliton self-frequency shift) and higher order dispersion affect any soliton system, including a WDM system.

6.3 Areas for further research

- Filtering is perhaps the area of research that holds the most promise for reducing the effects of WDM soliton interactions. While filters

have not yet been used in any soliton system with greater than two channels, Fabry-Perot filters are likely to be used in systems with extensive wavelength multiplexing[32]. It may be possible to predict the extent to which jitter is reduced in filtered systems by modifying the derivation in Chapter 5.

- While permanent wavelength shifts have been observed in systems with loss and amplification[63], the magnitudes of the shifts, as predicted by the theory in Chapter 4, have not been verified. If further empirical and theoretical results indicate that the permanent shifts are different than predicted, the derivation of timing jitter in Chapter 5 is still applicable as long as the variance in the wavelength shifts $\langle \Delta\lambda^2 \rangle$ can be determined.
- It would be helpful to experimentally verify the predictions in Chapter 5. This would require a significant amount of equipment, including such things as multi-wavelength soliton sources and BER testers. The results with two channels have already been verified numerically in [70].
- The derivation in Chapter 5 does not include jitter in pulse arrival times caused by collisions at the fiber input, as discussed in Chapter 4. Although such collisions may be avoided in practice, the results in Chapter 5 could be more general with inclusion of these effects.
- The jitter in bit-per-wavelength soliton systems could be predicted by modifying the estimates of jitter in Chapter 5. Preliminary studies indicate such an encoding technique may be difficult since the average shifts in arrival times are substantially different from one wavelength channel to the next.

- More research is necessary in regards to soliton transmitters and receivers. Many related issues, such as data encoding techniques and clock extraction, must also be studied before soliton communications will be practical. Other modulation schemes in a WDM soliton system could be useful. As an example, the use of phase-shift keyed data might significantly reduce effects of collision-induced jitter since solitons are present in every bit slot (Δb_j as defined for an amplitude-shift keyed system would always be zero).
- Higher-order soliton propagation might be a useful way of encoding multi-valued data in the form of a soliton "packet". While such solitons are unstable to slight perturbations, they still present an intriguing option for significantly improving performance.
- The use of solitons for switching applications continues to be an interesting area of research. Progress in the development of practical soliton switches could significantly enhance system performance.
- Finally, dispersion compensation techniques in linear systems using NRZ encoded data continue to improve. A good knowledge of both types of systems is necessary to fully understand all the issues relevant to optical data communication in fiber.

The use of WDM for soliton communication is an exciting area of research. The improvements in performance that might be achieved by combining the parallelism of the spectral domain with the advantages of soliton transmission are significant. The author hopes that this research is a useful starting point for further progress in the use of solitons for optical communications and signal processing.

BIBLIOGRAPHY

[1] M. Nakazawa, E. Yamada, H. Kubota, and K. Suzuki, "10Gbit/s soliton data transmission over one million kilometers," **Electronics Letters**, vol. 27, no. 14, pp. 1270–1272, 1991.

[2] G. P. Agrawal, **Fiber-Optic Communication Systems**. John Wiley and Sons, 1992.

[3] G. P. Agrawal, **Nonlinear Fiber Optics**. Academic Press, 1989.

[4] M. J. Ablowitz and H. Segur, **Solitons and the Inverse Scattering Transform**. SIAM, 1981.

[5] P. G. Drazin and R. S. Johnson, **Solitons: an introduction**. Cambridge University Press, 1989.

[6] A. F. Benner, J. R. Sauer, and M. J. Ablowitz, "Interaction effects on wavelength-multiplexed soliton data packets," **J. Opt. Soc. Am. B**, vol. 10, no. 12, pp. 2331–2340, 1993.

[7] A. Hasegawa and T. Nyu, "Eigenvalue communication," **J. Lightwave Tech.**, vol. 11, no. 3, pp. 395–399, 1993.

[8] J. P. Gordon, "Interaction forces among solitons in optical fibers," **Optics Letters**, vol. 8, no. 11, pp. 596–598, 1983.

[9] F. M. Mitschke and L. F. Mollenauer, "Experimental observation of interaction forces between solitons in optical fibers," **Optics Letters**, vol. 12, no. 5, pp. 355–357, 1987.

[10] Y. Kodama and K. Nozaki, "Soliton interaction in optical fibers," **Optics Letters**, vol. 12, no. 12, pp. 1038–1040, 1987.

[11] J. P. Gordon and L. F. Mollenauer, "Effects of fiber nonlinearities and amplifier spacing on ultra-long distance transmission," **J. Lightwave Tech.**, vol. 9, no. 2, pp. 170–173, 1991.

[12] J. P. Gordon, "Theory of the soliton self-frequency shift," **Optics Letters**, vol. 11, no. 10, pp. 662–664, 1986.

[13] E. M. Dianov, A. V. Luchnikov, A. N. Pilipetskii, and A. M. Prokhorov, "Long-range interaction of picosecond solitons through excitation of acoustic waves in optical fibers," **Applied Physics B**, vol. 54, pp. 175–180, 1992.

[14] L. F. Mollenauer and J. P. Gordon, "Birefringence-mediated timing jitter in soliton transmission," **Optics Letters**, vol. 19, no. 6, pp. 375–377, 1994.

[15] C. R. Menyuk, "Stability of solitons in birefringent optical fibers: I: Equal propagation amplitudes," **Optics Letters**, vol. 12, no. 8, pp. 614–616, 1987.

[16] S. G. Evangelides, L. F. Mollenauer, J. P. Gordon, and N. S. Bergano, "Polarization multiplexing with solitons," **J. Lightwave Tech.**, vol. 10, no. 1, pp. 28–35, 1992.

[17] A. Hasegawa, "Numerical study of optical soliton transmission amplified periodically by the stimulated Raman process," **Appl. Opt.**, vol. 23, no. 19, pp. 3302–3309, 1984.

[18] L. F. Mollenauer, J. P. Gordon, and M. N. Islam, "Soliton propagation in long fibers with periodically compensated loss," **IEEE J. of Quant. Elec.**, vol. QE-22, no. 1, pp. 157–173, 1986.

[19] L. F. Mollenauer, S. G. Evangelides, and H. A. Haus, "Long-distance soliton propagation using lumped amplifiers and dispersion shifted fiber," **J. Lightwave Tech.**, vol. 9, no. 2, pp. 194–197, 1991.

[20] K. J. Blow and N. J. Doran, "Average soliton dynamics and the operation of soliton systems with lumped amplifiers," **IEEE Photonics Technology Letters**, vol. 3, no. 4, pp. 369–371, 1991.

[21] A. Hasegawa and Y. Kodama, "Guiding-center soliton in optical fibers," **Optics Letters**, vol. 15, no. 24, pp. 1443–1445, 1990.

[22] J. P. Gordon and H. A. Haus, "Random walk of coherently amplified solitons in optical fiber transmission," **Optics Letters**, vol. 11, no. 10, pp. 665–667, 1986.

[23] W. Forysiak, F. M. Knox, and N. J. Doran, "Average soliton propagation in periodically amplified systems with stepwise dispersion-profiled fiber," **Optics Letters**, vol. 19, no. 3, pp. 174–176, 1994.

[24] P.-L. Francois and T. Georges, "Reduction of averaged soliton interaction forces by amplitude modulation," **Optics Letters**, vol. 18, no. 8, pp. 583–585, 1993.

[25] N. J. Smith and W. J. Firth, "Suppression of soliton interactions by periodic phase modulation," **Optics Letters**, vol. 19, no. 1, pp. 16–18, 1994.

[26] Y. Kodama and S. Wabnitz, "Reduction of soliton interaction forces by bandwidth limited amplification," **Electronics Letters**, vol. 27, no. 21, pp. 1931–1933, 1991.

[27] A. Mecozzi, J. D. Moores, H. A. Haus, and Y. Lai, "Soliton transmission control," **Optics Letters**, vol. 16, no. 23, pp. 1841–1843, 1991.

[28] L. F. Mollenauer, J. P. Gordon, and S. G. Evangelides, "The sliding-frequency guiding filter: an improved form of soliton jitter control," **Optics Letters**, vol. 17, no. 22, pp. 1575–1577, 1992.

[29] Y. Kodama and S. Wabnitz, "Analysis of soliton stability and interactions with sliding filters," **Optics Letters**, vol. 19, no. 3, pp. 162–164, 1994.

[30] L. F. Mollenauer, P. V. Mamyshev, and M. J. Neubelt, "Measurement of timing jitter in filter-guided soliton transmission at 10 Gbits/s and achievement of 375 Gbits/s-Mm, error free, at 12.5 and 15 Gbits/s," **Optics Letters**, vol. 19, no. 10, pp. 704–706, 1994.

[31] L. F. Mollenauer, E. Lichtman, M. J. Neubelt, and G. T. Harvey, "Demonstration, using sliding-frequency guiding filters, of error-free soliton transmission over more than 20Mm at 10Gbit/s, single channel, and over more than 13Mm at 20Gbit/s in a two-channel WDM," **Electronics Letters**, vol. 29, no. 10, pp. 910–911, 1993.

[32] A. Mecozzi and H. A. Haus, "Effect of filters on soliton interactions in wavelength-division-multiplexing systems," **Optics Letters**, vol. 17, no. 14, pp. 988–990, 1992.

[33] J. S. Russell, "Report of the committee on waves," in **Report of the 7th Meeting of British Association for the Advancement of Science**, (Liverpool), 1838, pp. 417–496.

[34] D. J. Korteweg and G. de Vries, "On the change of form of long waves advancing in a rectangular channel, and on a new type of long stationary

wave," **Philos. Mag.**, vol. 5, no. 39, pp. 422–443, 1895.

[35] A. Hasegawa and F. Tappert, "Transmission of stationary nonlinear optical pulses in dispersive dielectric fibers. I. anomalous dispersion," **Applied Physics Letters**, vol. 23, pp. 142–144, 1973.

[36] V. E. Zakharov and A. B. Shabat, "Exact theory of two-dimensional self-focusing and one-dimensional self-modulation of waves in nonlinear media," **Soviet Physics JETP**, vol. 34, no. 1, pp. 62–69, 1972.

[37] L. F. Mollenauer, R. H. Stolen, and J. P. Gordon, "Experimental observation of picosecond pulse narrowing and solitons in optical fibers," **Physical Review Letters**, vol. 45, no. 13, pp. 1095–1098, 1980.

[38] K. Iwatsuki, K. Suzuki, S. Nishi, and M. Saruwatari, "80 Gbit/s optical soliton transmission over 80km with time/polarization division multiplexing," **IEEE Photonics Technology Letters**, vol. 5, no. 2, pp. 245–248, 1993.

[39] H. A. Haus, "Optical fiber solitons, their properties and uses," **Proc. IEEE**, vol. 81, no. 7, pp. 970–983, 1993.

[40] M. N. Islam, **Ultrafast Fiber Switching Devices and Systems**. Cambridge University Press, 1992.

[41] M. W. Chbat, B. Hong, M. N. Islam, C. E. Soccolich, and P. R. Prucnal, "Ultrafast soliton-trapping AND gate," **J. Lightwave Tech.**, vol. 10, no. 12, pp. 2011–2016, 1992.

[42] M. N. Islam, C. E. Soccolich, and C.-J. Chen, "All-optical inverter with one picojoule switching energy," **Electronics Letters**, vol. 27, no. 2, pp. 130–132, 1991.

[43] J. R. Sauer, M. N. Islam, and S. P. Dijaili, "A soliton ring network," **J. Lightwave Tech.**, vol. 11, no. 12, pp. 2182–2190, 1993.

[44] K. J. Blow, N. J. Doran, and B. K. Nayar, "Experimental demonstration of optical soliton switching in an all-fiber nonlinear Sagnac interferometer," **Optics Letters**, vol. 14, no. 14, pp. 754–756, 1989.

[45] A. B. Aceves and S. Wabnitz, "Switching dynamics of helical solitons in a periodically twisted birefringent fiber filter," **Optics Letters**, vol. 17, no. 1, pp. 25–27, 1992.

[46] S. Wabnitz, S. Trillo, E. M. Wright, and G. I. Stegeman, "Wavelength-dependent soliton self-routing in birefringent fiber filters," **J. Opt. Soc. Am. B**, vol. 8, no. 3, pp. 602–613, 1991.

[47] D. C. Psaila and C. M. de Sterke, "Soliton propagation in twin-core fiber rocking filters," **Optics Letters**, vol. 18, no. 22, pp. 1905–1907, 1993.

[48] Y. S. Kivshar, "Switching dynamics of solitons in fiber directional couplers," **Optics Letters**, vol. 18, no. 1, pp. 7–9, 1993.

[49] S. Trillo and S. Wabnitz, "Weak-pulse-activated coherent soliton switching in nonlinear couplers," **Optics Letters**, vol. 16, no. 1, pp. 1–3, 1991.

[50] T.-T. Shi and S. Chi, "Nonlinear photonic switching by using the spatial soliton collision," **Optics Letters**, vol. 15, no. 20, pp. 1123–1125, 1990.

[51] J. S. Aitchison, A. M. Weiner, Y. Silberberg, D. E. Leaird, M. K. Oliver, J. L. Jackel, and P. W. E. Smith, "Experimental observation of spatial soliton interactions," **Optics Letters**, vol. 16, no. 1, pp. 15–17, 1991.

[52] J. Bian and A. K. Chan, "The design of an all-optical spatial soliton switch in a lossy nonlinear medium," **Micro. and Opt. Tech. Lett.**, vol. 5, no. 9, pp. 433–439, 1992.

[53] G. E. Torres-Cisneros, J. J. Sanchez-Mondragon, and V. A. Vysloukh, "Asymmetric optical Y junctions and switching of weak beams by using bright spatial-soliton collisions," **Optics Letters**, vol. 18, no. 16, pp. 1299–1301, 1993.

[54] S. Blair, K. Wagner, and R. McLeod, "Asymmetric spatial soliton dragging," **Optics Letters**, vol. 19, no. 23, pp. 1943–1945, 1994.

[55] P. Frycz, E. Infeld, and J. C. Samson, "Spontaneous transition from flat to spherical solitons," **Physical Review Letters**, vol. 69, no. 7, pp. 1057–1060, 1992.

[56] P. Emplit, M. Haelterman, and J.-P. Hamaide, "Picosecond dark soliton over a 1-km fiber at 850 nm," **Optics Letters**, vol. 18, no. 13, pp. 1047–1049, 1993.

[57] J. E. Rothenberg and H. K. Heinrich, "Observation of the formation of dark-soliton trains in optical fibers," **Optics Letters**, vol. 17, no. 4, pp. 261–263, 1992.

[58] G. A. Swartzlander, Jr., "Dark-soliton prototype devices: analysis by using direct-scattering theory," **Optics Letters**, vol. 17, no. 7, pp. 493–495, 1992.

[59] R. Jin, M. Liang, G. Khitrova, H. M. Gibbs, and N. Peyghambarian, "Compression of bright optical pulses by dark solitons," **Optics Letters**, vol. 18, no. 7, pp. 494–496, 1993.

[60] M. Shalaby and A. J. Barthelemy, "Observation of the self-guided propagation of a dark and bright soliton pair in a focusing nonlinear medium," **IEEE J. of Quant. Elec.**, vol. 28, no. 12, pp. 2736–2741, 1992.

[61] S. Trillo, S. Wabnitz, E. M. Wright, and G. I. Stegeman, "Optical solitary waves induced by cross-phase modulation," **Optics Letters**, vol. 13, no. 10, pp. 871–873, 1988.

[62] L. F. Mollenauer, S. G. Evangelides, and J. P. Gordon, "Wavelength division multiplexing with solitons in ultra-long distance transmission using lumped amplifiers," **J. Lightwave Tech.**, vol. 9, no. 3, pp. 362–367, 1991.

[63] P. Andrekson, N. A. Olsson, J. R. Simpson, T. Tanbun-Ek, R. A. Logan, and K. W. Wecht, "Observation of collision induced temporary soliton carrier frequency shifts in ultra-long fiber transmission systems," **J. Lightwave Tech.**, vol. 9, no. 9, pp. 1132–1135, 1991.

[64] S. R. Friberg, "Soliton fusion and steering by the simultaneous launch of two different-color solitons," **Optics Letters**, vol. 16, no. 19, pp. 1484–1486, 1991.

[65] Y. Kodama and A. Hasegawà, "Effects of initial overlap on the propagation of optical solitons at different wavelengths," **Optics Letters**, vol. 16, no. 4, pp. 208–210, 1991.

[66] T. Aakjer, J. H. Povlsen, and K. Rottwitt, "Effects of initial overlap in a wavelength-division-multiplexed soliton transmission system," **Optics Letters**, vol. 18, no. 22, pp. 1908–1910, 1993.

[67] M. Nakazawa, Y. Kimura, K. Suzuki, and H. Kubota, "Wavelength multiple soliton amplification and transmission with an Er^{3+}-doped optical fiber," **J. Appl. Phy.**, vol. 66, no. 7, pp. 2803–2812, 1989.

[68] J. D. Moores, "Ultra-long distance wavelength-division-multiplexed soliton transmission using inhomogeneously broadened fiber amplifiers," **J.**

Lightwave Tech., vol. 10, no. 4, pp. 482–486, 1992.

[69] P. Andrekson, N. A. Olsson, P. C. Becker, J. R. Simpson, T. Tanbun-Ek, R. A. Logan, and K. W. Wecht, "Observation of multiple wavelength soliton collisions in optical systems with fiber amplifiers," **Applied Physics Letters**, vol. 57, no. 17, pp. 1715–1717, 1990.

[70] F. Matera, M. Romagnoli, M. Settembre, S. Wabnitz, and Y. Kodama, "Ultimate capacity of WDM soliton transmissions with sliding filters," in **Nonlinear Guided Waves and Their Applications, 1995 Technical Digest Series**, Vol. 6, (Optical Society of America, Washington, DC), 1995, pp. 133–135.

[71] Y. Sakai, R. J. Hawkins, and S. R. Friberg, "Soliton-collision interferometer for the quantum nondemolition measurement of photon number: numerical results," **Optics Letters**, vol. 15, no. 4, pp. 239–241, 1990.

[72] S. R. Friberg, S. Machida, and Y. Yamamoto, "Quantum-nondemolition measurement of the photon number of an optical soliton," **Physical Review Letters**, vol. 69, no. 22, pp. 3165–3168, 1992.

[73] H. A. Haus and Y. Lai, "Quantum theory of soliton squeezing: a linearized approach," **J. Opt. Soc. Am. B**, vol. 7, no. 3, pp. 386–392, 1990.

[74] Y. Lai, "Quantum theory of soliton propagation: a unified approach based on the linearization approximation," **J. Opt. Soc. Am. B**, vol. 10, no. 3, pp. 475–484, 1993.

[75] A. F. Benner, **Wavelength-multiplexed solitons in optical communications networks**. PhD thesis, University of Colorado, Boulder, Colorado, 1992.

[76] B. M. Nyman, S. G. Evanglides, G. T. Harvey, L. F. Mollenauer, P. V. Mamyshev, M. L. Saylors, S. K. Korotky, U. Koren, V. Mizrahi, T. A. Strasser, J. J. Veselka, J. D. Evankow, A. Lucero, J. Nagel, J. Sulhoff, J. Zyskind, P. C. Corbett, M. A. Mills, and G. A. Ferguson, "Soliton WDM transmission of 8X2.5 Gb/s, error free over 10 Mm," in **Optical Fiber Communication Conference, 1995 Technical Digest Series**, Vol. 8, postdeadline paper PD21, (Optical Society of America, Washington, DC), 1995.

[77] H. A. Haus and M. N. Islam, "Theory of the soliton laser," **IEEE J. of Quant. Elec.**, vol. QE-21, no. 8, pp. 1172–1188, 1985.

[78] E. Desurvire, "Lightwave Communications: The Fifth Generation," **Scientific American, Special Issue, The Computer in the 21st Century**, pp. 54–61, 1995.

[79] A. F. Benner, "Development of the color center laser: Toward a source of optical solitons," **OCS Tech. Report 90-12, University of Colorado at Boulder**, 1990.

[80] S. R. Friberg, W. Jiang, Y. Sakai, and R. J. Hawkins, "Observation of two-color soliton collisions in optical fiber," in **Ultrafast Phenomena VII**, (Springer-Verlag Berlin, Heidelberg), 1990, pp. 184–186.

[81] P. A. Andrekson, N. A. Olsson, M. Haner, J. R. Simpson, T. Tanbun-Ek, R. A. Logan, D. Coblentz, H. M. Presby, and K. W. Wecht, "32 Gb/s optical soliton data transmission over 90 km," **IEEE Photonics Technology Letters**, vol. 4, no. 1, pp. 76–79, 1992.

[82] M. Ding and K. Kikuchi, "Limits of long-distance soliton transmission in optical fibers with laser diodes as pulse sources," **IEEE Photonics Technology Letters**, vol. 4, no. 6, pp. 667–670, 1992.

[83] P. A. Morton, V. Mizrahi, P. A. Andrekson, T. Tanbun-Ek, R. A. Logan, P. Lemaire, D. L. Coblentz, A. M. Sergent, K. W. Wecht, and P. F. Sciortino, Jr., "Mode-locked hybrid soliton pulse source with extremely wide operating frequency range," **IEEE Photonics Technology Letters**, vol. 5, no. 1, pp. 28–31, 1993.

[84] P. V. Mamyshev, "Dual-wavelength source of high repetition rate, transform-limited optical pulses for soliton transmission," **Optics Letters**, vol. 19, no. 24, pp. 2074–2076, 1994.

[85] G. T. Harvey and L. F. Mollenauer, "Harmonically mode-locked fiber ring laser with an internal Fabry-Perot stabilizer for soliton transmission," **Optics Letters**, vol. 18, no. 2, pp. 107–109, 1993.

[86] D. Abraham, R. Nagar, and G. Eisenstein, "Self-starting low-noise fiber soliton laser," **Optics Letters**, vol. 18, no. 18, pp. 1508–1510, 1993.

[87] J. B. Schlager, Y. Yamabayashi, D. L. Franzen, and R. I. Juneau, "Mode-locked, long-cavity, erbium fiber lasers with subsequent soliton-like compression," **IEEE Photonics Technology Letters**, vol. 1, no. 9, pp. 323–325, 1989.

[88] M. J. Guy, D. U. Noske, and J. R. Taylor, "Generation of femtosecond

soliton pulses by passive mode locking of an ytterbium-erbium figure-of-eight fiber laser," **Optics Letters**, vol. 18, no. 17, pp. 1447–1449, 1993.

[89] K. Tamura, C. R. Doerr, H. A. Haus, and E. P. Ippen, "Soliton fiber ring laser stabilization and tuning with a broad intracavity filter," **IEEE Photonics Technology Letters**, vol. 6, no. 6, pp. 697–699, 1994.

[90] C. R. Ó. Cochláin, R. J. Mears, and G. Sherlock, "Low threshold tunable soliton source," **IEEE Photonics Technology Letters**, vol. 5, no. 1, pp. 25–28, 1993.

[91] A. E. Siegman, **Lasers**. University Science Books, 1986.

[92] D. J. Kuizenga and A. E. Siegman, "FM and AM mode locking of the homogenous laser — Part I: Theory," **IEEE J. of Quant. Elec.**, vol. QE-6, no. 11, pp. 694–708, 1970.

[93] X. Shan, D. Cleland, and A. Ellis, "Stabilising Er fibre soliton laser with pulse phase locking," **Electronics Letters**, vol. 28, no. 2, pp. 182–184, 1992.

[94] B. E. A. Saleh and M. C. Teich, **Fundamentals of Photonics**. John Wiley and Sons, 1991.

[95] J. Keating and J. Santos, "Laser diode temperature controller and current driver circuits," **OCS Tech. Report 91-32, University of Colorado at Boulder**, 1991.

[96] W. H. Press, S. A. Teukolsky, W. T. Vetterling, and B. P. Flannery, **Numerical Recipes in C: The Art of Scientific Computing**. Cambridge University Press, 1992.

[97] A. R. Chraplyvy, "Limitations on lightwave communications imposed by optical-fiber nonlinearities," **J. Lightwave Tech.**, vol. 8, no. 10, pp. 1548–1557, 1990.

[98] W. F. Magic, **A Source Book in Physics**. McGraw-Hill, 1935.

[99] H. Goldstein, **Classical Mechanics**. Addison-Wesley, 1950.

[100] R. B. Lindsay and H. Margenau, **The Foundations of Mechanics**. Dover Publications, 1957.

[101] S. Chakravarty, M. J. Ablowitz, J. R. Sauer, and R. B. Jenkins, "Multisoliton interactions and wavelength-division multiplexing," **Optics Letters**, vol. 20, no. 2, pp. 136–138, 1995.

[102] D. Marcuse, A. R. Chraplyvy, and R. W. Tkach, "Effect of fiber nonlinearity on long-distance transmission," **J. Lightwave Tech.**, vol. 9, no. 1, pp. 121–128, 1991.

[103] N. Shibata, K. Nosu, K. Iwashita, and Y. Azuma, "Transmission limitations due to fiber nonlinearities in optical FDM systems," **IEEE J. Sel. Areas in Comm.**, vol. 8, no. 6, pp. 1068–1077, 1990.

[104] R. N. Bracewell, **The Fourier Transform and Its Applications.** McGraw-Hill, 1986.

[105] A. F. Evans and J. V. Wright, "Constraints on the design of single-channel, high-capacity (> 10 Gb/s) soliton systems," **IEEE Photonics Technology Letters**, vol. 7, no. 1, pp. 117–119, 1995.

[106] D. Marcuse, "Single-channel operation in very long nonlinear fibers with optical amplifiers at zero dispersion," **J. Lightwave Tech.**, vol. 9, no. 3, pp. 356–361, 1991.

[107] D. Marcuse, "Bit-error rate of lightwave systems at the zero-dispersion wavelength," **J. Lightwave Tech.**, vol. 9, no. 10, pp. 1330–1334, 1991.

[108] J. B. D. Soole, A. Scherer, H. P. LeBlanc, N. C. Andreadakis, R. Bhat, and M. A. Koza, "Monolithic InP/InGaAsP/InP grating spectrometer for the 1.48-1.56μm wavelength range," **Applied Physics Letters**, vol. 58, no. 18, pp. 1949–1951, 1991.

[109] J. B. D. Soole, Y. Silberberg, A. Scherer, H. P. LeBlanc, N. C. Andreadakis, and C. Caneau, "Fast high-efficiency integrated waveguide photodetectors using novel hybrid verical/butt coupling geometry," **Applied Physics Letters**, vol. 61, no. 1, pp. 13–15, 1992.

[110] M. G. Young, U. Koren, B. I. Miller, M. A. Newkirk, M. Chien, M. Zirngibl, C. Dragone, B. Tell, H. M. Presby, and G. Raybon, "A 16×1 wavelength division multiplexer with integrated distributed Bragg reflector lasers and electroabsorption modulators," **IEEE Photonics Technology Letters**, vol. 5, no. 8, pp. 908–910, 1993.

[111] D. J. Blumenthal, R. J. Feuerstein, and J. R. Sauer, "First demonstration

of multihop all-optical packet switching," **IEEE Photonics Technology Letters**, vol. 6, no. 3, pp. 457–459, 1994.

[112] M. L. Loeb and G. R. Stilwell, Jr., "High-speed data transmission on an optical fiber using a byte-wide WDM system," **J. Lightwave Tech.**, vol. 6, no. 8, pp. 1306–1311, 1988.

[113] H. Stark and J. W. Woods, **Probability, Random Processes, and Estimation Theory for Engineers**. Prentice-Hall, 1986.

[114] W. Feller, **An Introduction to Probability Theory and Its Applications**. John Wiley and Sons, 1971.

[115] J. D. Gibbons, **Nonparametric Statistical Inference**. McGraw-Hill, 1971.

APPENDIX A

MATHEMATICAL DERIVATIONS

A.1 Frequency shifts during collisions between two solitons

The mean frequency of any pulse whose evolution is described by a function u can be written as

$$\langle \omega_u \rangle = \frac{1}{\mathcal{E}} \operatorname{Im} \int \left(\frac{\partial u^*}{\partial t} \right) u \, dt, \tag{A.1}$$

where $\mathcal{E}$ is the pulse energy. If the mean frequency varies during propagation, we can describe its evolution by taking the derivative with respect to z, as in

$$\frac{d\langle \omega_u \rangle}{dz} = \frac{1}{\mathcal{E}} \operatorname{Im} \int \frac{d}{dz} \left[\left(\frac{\partial u^*}{\partial t} \right) u \right] dt. \tag{A.2}$$

The energy does not vary in z if the system is lossless. The integrand in (A.2) can be rewritten as

$$\frac{d}{dz} \left(\frac{\partial u^*}{\partial t} u \right) = \frac{\partial u^*}{\partial t} \frac{\partial u}{\partial z} + u \frac{\partial}{\partial t} \left(\frac{\partial u^*}{\partial z} \right). \tag{A.3}$$

If ω_u varies because of cross-phase modulation with a second pulse v, the coupled NLSE in Eqs. (3.4) and (3.5) can be used to substitute for $\partial u/\partial z$ and $\partial u^*/\partial z$ in (A.3). Upon simplification,

$$\frac{d}{dz} \left(\frac{\partial u^*}{\partial t} u \right) = \frac{i}{2} \frac{\partial u^*}{\partial t} \frac{\partial^2 u}{\partial t^2} - \frac{i}{2} \frac{\partial^3 u^*}{\partial t^3} u - i \left(\frac{\partial |u|^2}{\partial t} + 2 \frac{\partial |v|^2}{\partial t} \right) |u|^2. \tag{A.4}$$

If the pulse envelope $|u|$ is symmetric and is multiplied by some phase factor, integrating the first three terms and taking the imaginary part yields zero (since the integral of an even function times an odd function is zero). Thus,

$$\frac{d\langle \omega_u \rangle}{dz} = -\frac{2}{\mathcal{E}} \int \frac{\partial |v|^2}{\partial t} |u|^2 dt = \frac{2}{\mathcal{E}} \int \frac{\partial |u|^2}{\partial t} |v|^2 dt. \tag{A.5}$$

By replacing u with v, the variation in the frequency of v is given by

$$\frac{d\langle\omega_v\rangle}{dz} = \frac{2}{\mathcal{E}}\int \frac{\partial|v|^2}{\partial t}|u|^2 dt, \tag{A.6}$$

so that

$$\frac{d\langle\omega_v\rangle}{dz} = -\frac{d\langle\omega_u\rangle}{dz}. \tag{A.7}$$

If u and v are solitons, and their evolution is described by Eqs. (3.1) and (3.2), then the shift in the frequency Ω_u is given by Eq. (3.9), and

$$\delta\Omega_u = \frac{1}{\Omega}\int \mathrm{sech}^2(t+\Omega z)\mathrm{sech}^2(t)\, dt. \tag{A.8}$$

Through the use of trigonometric identities and the integral relation,

$$\begin{aligned}\int \frac{2\,dx}{(\cos x + a)^2} &= \frac{2a}{(a^2-1)^{3/2}} \times \tan^{-1}\left[\left(\frac{a-1}{a+1}\right)^{1/2}\tan(x/2)\right] - \\ &\quad \frac{\sin x}{(a^2-1)(\cos x + a)},\end{aligned} \tag{A.9}$$

the analytic solution for the frequency shift is given by

$$\delta\Omega_u = -\delta\Omega_v = \frac{4}{\Omega}\frac{\Omega z\cosh(\Omega z) - \sinh(\Omega z)}{\sinh^3(\Omega z)}. \tag{A.10}$$

The shift in the frequency of v is equal in magnitude but opposite in sign to the shift in the frequency of u, based on Eq. (A.7). Since a shift in frequency corresponds to a shift in velocity, the integral of Eq. (A.10) yields a timing displacement in u. Since $d(\coth x)/dx = -\sinh^{-2}(x)$ and since

$$\int \frac{x\,\cosh(x)}{\sinh^3(x)}dx = \frac{1}{2}\int \frac{dx}{\sinh^2(x)} - \frac{x}{2\,\sinh^2(x)}, \tag{A.11}$$

it is straightforward to show that the timing shift is given by

$$\begin{aligned}|\delta t_u| &= \int_{-\infty}^{\infty} \delta\Omega_u(z)\, dz \\ &= \frac{4}{\Omega}\int_{-\infty}^{\infty} \frac{\Omega z\cosh(\Omega z) - \sinh(\Omega z)}{\sinh^3(\Omega z)}dz = \frac{4}{\Omega^2}.\end{aligned} \tag{A.12}$$

A.2 First order effects during N-soliton collisions

To describe the interaction between N WDM solitons at a collision, the second term of the summation in (3.25) must be determined. This term is given by

$$\begin{aligned}\sum_{j=1}^{N} q_j^{(1)}(z,t) &= -\sum_{j,k=1}^{N} (D^{-1}MD^{-1})_{jk} \\ &= -\sum_{j,k=1}^{N} \mathrm{sech}(S_j)\mathrm{sech}(S_k) \times \\ &\qquad \exp[i(\chi_j+\chi_k)]\, M_{jk} \\ &= -\frac{1}{2}\sum_{j,k=1}^{N} \mathrm{sech}(S_j)\mathrm{sech}(S_k) \times \\ &\qquad \exp[i(\chi_j+\chi_k)]\,(M_{jk}+M_{kj}), \end{aligned} \tag{A.13}$$

where D and M represent the diagonal and off-diagonal components, respectively, of the matrix A used to derive the exact N soliton solution in Eq. (3.16). The parameters S_j and χ_j, defined in Eqs. (3.19) and (3.20), describe the spatial variation and phase of the jth soliton, and $q_j^{(1)}(z,t)$ describes the first order evolution of the jth soliton. If the frequency separation between adjacent channels is $\Omega = \epsilon^{-1}$, $q_j^{(1)}(z,t)$ is $\mathrm{O}(\epsilon)$ since the M_{jk} are $\mathrm{O}(\epsilon)$. If we take the frequency separation between the jth and kth channels to be $\Omega_j - \Omega_k = (j-k)\Omega$ and substitute for M_{jk} and M_{kj} using Eq. (3.18),

$$\begin{aligned}\sum_{j=1}^{N} q_j^{(1)}(z,t) &= -\sum_{\substack{j,k=1 \\ j\neq k}}^{N} ([\mathrm{sech}(S_k)\exp(i\chi_k) + \mathrm{sech}(S_j)\exp(i\chi_j)] - \\ &\qquad i(j-k)\Omega[\mathrm{sech}(S_k)\exp(i\chi_k)\tanh(S_j) - \\ &\qquad \mathrm{sech}(S_j)\exp(i\chi_j)\tanh(S_k)])/ \\ &\qquad [4+(j-k)^2\Omega^2]. \end{aligned} \tag{A.14}$$

We are analyzing interactions only to leading order, so $\mathrm{O}(\epsilon^2)$ effects can be neglected if Ω is large, and the first two terms in (A.14) can be dropped,

yielding

$$\sum_{j=1}^{N} q_j^{(1)}(z,t) \approx \sum_{\substack{j,k=1 \\ j\neq k}}^{N} \frac{\operatorname{sech}(S_k)\exp(i\chi_k)\tanh(S_j) - \operatorname{sech}(S_j)\exp(i\chi_j)\tanh(S_k)}{i(k-j)\Omega}$$

$$\approx -2i\epsilon \sum_{j=1}^{N} \left[\operatorname{sech}(S_j)\exp(i\chi_j) \left(\sum_{\substack{k=1 \\ k\neq j}}^{N} \frac{\tanh(S_k)}{j-k} \right) \right]. \qquad \text{(A.15)}$$

A single term in the summation over j, as in

$$q_j^{(1)}(z,t) = -2i\epsilon \operatorname{sech}(S_j)\exp(i\chi_j) \left(\sum_{\substack{k=1 \\ k\neq j}}^{N} \frac{\tanh(S_k)}{j-k} \right), \qquad \text{(A.16)}$$

represents the first order correction in space (or time) to the soliton whose evolution is described by $q_j^{(0)}(z,t) = \operatorname{sech}(S_j)\exp(i\chi_j)$.

The spectrum of $q_j^{(0)}(z,t)$ is $\tilde{q}_j^{(0)}(z,\omega) = \pi \operatorname{sech}[\pi\alpha_j/2]\exp(i\Phi_j)$, where the Φ_j are defined in Eq. (3.28) and $\alpha_j = \omega - \Omega_j$. To understand the spectral distortion to leading order for an N-soliton collision, the Fourier transform of $q_j^{(1)}(z,t)$ is required. To simplify the analysis, we consider only a single term in the summation over k,

$$q_{jk}^{(1)}(z,t) = -2i\epsilon \operatorname{sech}(S_j)\exp(i\chi_j)\frac{\tanh(S_k)}{j-k}, \qquad \text{(A.17)}$$

and take its transform,

$$\tilde{q}_{jk}^{(1)}(z,\omega) = -\frac{2i\epsilon}{j-k}\int_{-\infty}^{\infty} \operatorname{sech}(S_j)\exp(i\chi_j)\tanh(S_k)\exp(i\omega t)\,dt. \qquad \text{(A.18)}$$

By defining variables $S = S_j$ and $S_{jk} = S_j - S_k = (j-k)\Omega z - (t_{oj} - t_{ok})$,

$$\tilde{q}_{jk}^{(1)}(z,\omega) = -\frac{2i\epsilon\exp(i\Phi_j)}{j-k}\int_{-\infty}^{\infty} \operatorname{sech}(S)\tanh(S - S_{jk})\exp(i\alpha_j S)\,dS$$

$$= -\frac{2i\epsilon\exp(i\Phi_j)}{j-k} I, \qquad \text{(A.19)}$$

where we rename the integral as I.

By letting $y = \exp(S)$ and $y_o = \exp(S_{jk})$, the integral becomes

$$I = \int_0^\infty \frac{2(y^2 - y_o^2)\exp(i\alpha_j \ln y)}{(y^2+1)(y^2+y_o^2)} dy. \tag{A.20}$$

The integrand of I has singularities at $y = i, -i, iy_o, -iy_o$, so I can be rewritten as an integral over a contour in the upper-half of the complex plane, so that

$$I = \frac{2\pi i}{\exp(-\pi\alpha_j)+1}(R_i + R_{iy_o}), \tag{A.21}$$

where the residues at i and iy_o are given by

$$R_i = \frac{2(1+y_o^2)}{2i(1-y_o^2)} \exp(-\pi\alpha_j/2) \tag{A.22}$$

$$R_{iy_o} = \frac{-4\,y_o}{2i(1-y_o^2)} \exp(i\alpha_j S_{jk} - \pi\alpha_j/2). \tag{A.23}$$

The factor of $\exp(-\pi\alpha_j)$ in the denominator of I acts to translate the negative real axis in the contour to the positive real axis, since the limits of integration in Eq. (A.20) are taken only from 0 to ∞. Substituting for R_i, R_{iy_o}, y and y_o, the integral becomes

$$I = \pi\mathrm{sech}(\pi\alpha_j/2)\left[\frac{i\sin(\alpha_j S_{jk})}{\sinh(S_{jk})} + \frac{\cos(\alpha_j S_{jk}) - \cosh(S_{jk})}{\sinh(S_{jk})}\right]. \tag{A.24}$$

Near the center of the collision, $S_{jk} \to 0$, so

$$I = i\pi\mathrm{sech}(\pi\alpha_j/2)\frac{\sin(\alpha_j S_{jk})}{\sinh(S_{jk})} \tag{A.25}$$

and

$$\tilde{q}_{jk}^{(1)}(z,\omega) = 2\pi\epsilon\,\mathrm{sech}(\pi\alpha_j/2)\exp(i\Phi_j)\frac{\sin(\alpha_j S_{jk})}{(j-k)\sinh(S_{jk})}. \tag{A.26}$$

Thus, the correction factor to $\tilde{q}_j^{(0)}(z,\omega)$ is

$$\begin{aligned}\tilde{q}_j^{(1)}(z,\omega) &= 2\pi\epsilon\,\mathrm{sech}(\pi\alpha_j/2)\exp(i\Phi_j)\left(\sum_{\substack{k=1\\k\neq j}}^{N}\frac{\sin(\alpha_j S_{jk})}{(j-k)\sinh(S_{jk})}\right) \\ &= 2\epsilon\,\tilde{q}_j^{(0)}(z,\omega)\left(\sum_{\substack{k=1\\k\neq j}}^{N}\frac{\sin(\alpha_j S_{jk})}{(j-k)\sinh(S_{jk})}\right).\end{aligned} \tag{A.27}$$

A.3 Products of independent random variables

In order to predict the effects of collisions on bit error rates in WDM soliton systems, we must know the mean $\langle \Delta t \rangle$ and the variance $\langle \Delta t^2 \rangle$ of the timing displacement in Eq. (5.13). If the wavelength shifts $\Delta\lambda_j$ were the same at each collision, the statistical distribution of Δt would be identical to that of the Wilcoxon signed-rank test, common in nonparametric statistics[115]. However, since the positions at which soliton collisions occur are random variables, independent of any perturbation, the wavelength shifts $\Delta\lambda_j$ are random, and the relative skew at the end of the fiber is a sum of the products of two random variables, Δb_j and $\Delta\lambda_j$, where Δb_j represents a difference between two bit values in the fiber.

If we recognize that these two variables are independent and for clarity represent the wavelength shift by a random process X, the difference between bit values as Y, and the product as Z, then the probability density function of $Z = XY$ is[113]

$$f_Z(z) = \int \frac{1}{|y|} f_X\left(\frac{z}{y}\right) f_Y(y)\, dy, \tag{A.28}$$

where the density functions of X and Y are $f_X(x)$ and $f_Y(y)$, respectively. All integrals here are taken over $\{-\infty, \infty\}$. If data is random and uniformly distributed, Δb_j equals zero with probability 1/2, or ± 1, each with probability 1/4, such that the density function of Y may be written as a sum of impulse functions, as in

$$f_Y(y) = \frac{1}{2}\,\delta(y) + \frac{1}{4}\,\delta(y-1) + \frac{1}{4}\,\delta(y+1), \tag{A.29}$$

where each impulse function has unit area. Substituting Eq. (A.29) into

Eq. (A.28) yields the density function of Z,

$$f_Z(z) = \frac{1}{2}\,\delta(z) + \frac{1}{4}\,f_X(z) + \frac{1}{4}\,f_X(-z). \tag{A.30}$$

The last two terms in (A.30) are apparent given Eq. (A.28), while the impulse in z is less obvious. A standard definition[104] of an impulse function is

$$\delta(z) = \lim_{y \to 0} \frac{g(z/y)}{|y|}, \tag{A.31}$$

where the function g must have unit area and be bounded in the z direction. (Oftentimes, g is simply a rectangular or Gaussian pulse.) Hence, the impulse in z from Eq. (A.30) results from the fact that

$$\begin{aligned} \delta(z) &= \int \frac{1}{|y|}\, f_X\left(\frac{z}{y}\right)\, \delta(y)\, dy \\ &= \lim_{y \to 0} \frac{f_X(z/y)}{|y|}, \end{aligned} \tag{A.32}$$

where we know the area of the density function f_X has unit area and assume that it is bounded in z.

Since the mean of the random variable X is

$$m_X = \int x\, f_X(x)\, dx, \tag{A.33}$$

it is relatively straightforward to show that the mean value m_Z is zero using

$$\begin{aligned} m_Z &= \int z\, f_Z(z)\, dz \\ &= \int z \left[\frac{1}{2}\,\delta(z) + \frac{1}{4}\,f_X(z) + \frac{1}{4}\,f_X(-z)\right] dz \\ &= \frac{m_X}{4} - \frac{m_X}{4} \\ &= 0. \end{aligned} \tag{A.34}$$

Consequently, the variance is given by

$$\sigma_Z^2 = \int (z - m_z)^2\, f_Z(z)\, dz$$

$$
\begin{aligned}
&= \int z^2 \left[\frac{1}{2}\,\delta(z) + \frac{1}{4}\,f_X(z) + \frac{1}{4}\,f_X(-z)\right] dz \\
&= \frac{m_{2X}}{4} + \frac{m_{2X}}{4} \\
&= \frac{m_{2X}}{2}, \qquad \text{(A.35)}
\end{aligned}
$$

where the quantity m_{2X} is the second moment of the random variable X about the origin. Since the second moment about the origin is defined as

$$m_{2X} = m_X^2 + \sigma_X^2, \qquad \text{(A.36)}$$

the variance in z is

$$\sigma_Z^2 = \frac{m_X^2 + \sigma_X^2}{2}, \qquad \text{(A.37)}$$

such that σ_Z^2 is simply half of the second moment of X about the origin. Substituting for X and Z, the variance of the product $\Delta b_j \Delta\lambda_j$ is given by

$$\langle (\Delta b_j \Delta\lambda_j)^2 \rangle = \frac{\langle \Delta\lambda \rangle^2 + \langle \Delta\lambda^2 \rangle}{2}, \qquad \text{(A.38)}$$

where $\langle \Delta\lambda \rangle$ and $\langle \Delta\lambda^2 \rangle$ are the mean and variance of the wavelength shifts $\Delta\lambda_j$.

APPENDIX B

PROGRAM LISTINGS

Program listings are included in this appendix as follows:

3solidl.c, 3solmath.c — computes the exact three-soliton solution in Eq. (3.16) in space and in frequency. Output data is formatted for use in either IDL or Mathematica .

fpkfnd.ma, spkfnd.ma — computes position and shift of each frequency and spatial peak in Mathematica.

jitter.c, length.c, thrput.c — computes jitter, system length and throughput for various system parameters.

B.1 Numerical three-soliton solution to NLSE

B.1.1 IDL compatible version This version is to be used for plotting with IDL graphics.

```
/*************************************************************
3solidl.c -
C program for computing the exact waveform describing soliton
propagation in fiber - based upon the exact three soliton
solution to the NLS equation - and for computing the spectrum
of the waveform using a standard FFT routine.

VARIABLES, USES, and UNITS:
points - number of complex elements in variation coordinate
xwindow - full length of time axis

FIELD VARIABLES:
(u_t) - coordinate space variable
*************************************************************/
```

```
#include <stdio.h>
#include <math.h>

#ifndef TOOLS_C
#include "tools.c"
#endif

#ifndef DEFS_H
#include "defs.h"
#endif

#ifndef TYPES_H
#include "types.h"
#endif

#ifndef COMPLEX_H
#include "complex.h"
#endif

#ifndef COMPLEX_C
#include "complex.c"
#endif

#ifndef DFOUR1_C
#include "dfour1.c"
#endif

/* important parameters for run */
#define points 1024      /* pts computed at each x step */
#define xwindow (100.0)  /* width of spatial window    */
#define init_t (0.25)    /* initial time                */
#define final_t (0.75)   /* final time                  */
#define solitons 3       /* solution for 3 solitons     */
                         /* this should never change -  */
                         /* unless N-soliton solution   */
                         /* is used at later date       */
#define num_steps 50     /* time steps                  */

/* array variables */
dcomplex    u_t[points]; /* total field */
dcomplex    u_1[points]; /* 1st component of field */
```

```
dcomplex    u_2[points]; /* 2nd component of field */
dcomplex    u_12[points];/* 1st+2nd component of field */
dcomplex    u_3[points]; /* 3rd component of field */
int         myi_p[points];  /* VP's position in array */
double      x_p[points];    /* VP's transverse coord */
double      s_cnst[4];
double      chi_cnst[4];
dcomplex    cden[4][4];
double      s[4];
double      chi[4];
dcomplex    lninvgam[4];
dcomplex    invgam[4];
dcomplex    gamconj[4];
double      rfac[4];
dcomplex    c[4][4];
double      sol_pos[4];
double      sol_omg[4];
double      sol_phase[4];
double      sol_amp[4];

/* serial variables */
int          num_solitons;
double       time;
dcomplex     u_tden;
dcomplex     u_tnum1;
dcomplex     u_tnum2;
dcomplex     u_tnum;
dcomplex     zero;
FILE        *spacfile, *freqfile;
FILE        *spacfile1, *spacfile2, *spacfile3;
FILE        *freqfile1, *freqfile2, *freqfile3;
                /* FE arrays for output */
char        buffer[MAXLINE+1];/* buffer for input strings */
char        filename[MAXLINE+1];/* output file name */

main()
{
    int     n; /* for counting array positions */
    int     j; /* for counting solitons */
    int     i; /* for counting solitons */
    int     k; /* for counting time steps and loading files */
```

```
printf("Scaling processor transverse coordinates\n");
    for (n=0;n<points;n++) {
        myi_p[n] = n;
        x_p[n] = (double) xwindow*(myi_p[n]-points/2)/points;
    }

/* Initialize omegas in ascending order - if only two solitons
   are wanted, set sol_amp[3]=0.0  */
printf("Initializing input waveform.\n");
    sol_pos[1] = 5.0;
     sol_omg[1] = -10.0;
     sol_phase[1] = 2.0*M_PI*(0.0/1000.0);
     sol_amp[1] = 1.0;
    sol_pos[2] = -5.0;
     sol_omg[2] = 0.0;
     sol_phase[2] = 2.0*M_PI*(0.0/1000.0);
     sol_amp[2] = 1.0;
    sol_pos[3] = 10.0;
     sol_omg[3] = 10.0;
     sol_phase[3] = 2.0*M_PI*(0.0/1000.0);
     sol_amp[3] = 1.0;

    if (sol_amp[3] == 0.0) {
       num_solitons = solitons - 1;
    } else {
       num_solitons = solitons;
    }

printf("Input filename for space data storage : ");
    getline(buffer,MAXLINE,stdin);
    (void) strncpy(filename,buffer,strlen(buffer)-1);
    printf("Opening space data storage file\n");
    if ((spacfile = fopen(filename,"w")) == (FILE *)NULL) {
        printf( "Can't write to space data file.\n");
        exit(1);
    }

printf("Input filename for frequency data storage : ");
    getline(buffer,MAXLINE,stdin);
    (void) strncpy(filename,buffer,strlen(buffer)-1);
    printf("Opening frequency data storage file\n");
    if ((freqfile = fopen(filename,"w")) == (FILE *)NULL) {
```

```
        printf( "Can't write to frequency data file.\n");
        exit(1);
    }

/* Begin while loop through different time steps */

    for (k=0;k<=num_steps;k++) {
      time = (double) init_t + (k * (final_t-init_t)/num_steps);

/* Set values of terms which are
   constant at all field positions */

    for (i=1;i<=solitons;i++) {
      s_cnst[i] = 2.0*sol_amp[i]*sol_omg[i]*time
                  + sol_amp[i]*sol_pos[i];
      chi_cnst[i] = (pow(sol_omg[i],2.0)-pow(sol_amp[i],2.0))*
                    time+ sol_omg[i]*sol_pos[i]-sol_phase[i];
      for (j=1;j<=solitons;j++) {
if (j==i) {
  cden[i][j].r = 1.0;
          cden[i][j].i = 0.0;
        }
        else {
  cden[i][j].r = sol_amp[i] + sol_amp[j];
          cden[i][j].i = sol_omg[i] - sol_omg[j];
}
      }
    }

/* Initialize field */

    zero.r=0.0;
    zero.i=0.0;

    for (n=0;n<points;n++) {
        u_t[n].r = 0.0;
        u_t[n].i = 0.0;
    }

/* Start calculation of field at
   each transverse space position */
```

```
    for (n=0;n<points;n++) {

/* Determine space and phase terms for each field component */

      for (j=1;j<=solitons;j++) {
        s[j] = sol_amp[j]*x_p[n] - s_cnst[j];
        chi[j] = sol_omg[j]*x_p[n] - chi_cnst[j];
        lninvgam[j].r = -s[j];
        lninvgam[j].i = -chi[j];
        invgam[j] = Cexp(lninvgam[j]);
        gamconj[j] = Cexp(Rconjg(lninvgam[j]));
/*        if (j==3)
          rfac[j] = cosh(s[j]);
        else
          rfac[j] = cosh(s[j])/sol_amp[j];*/
      }

/* Calculate matrix coefficients */

      for (i=1;i<=solitons;i++) {
        for (j=1;j<=solitons;j++) {
          if (j==i) {
            c[i][j].r = cos(chi[i])*cosh(s[i]);
            c[i][j].i = -sin(chi[i])*cosh(s[i]);
          }
          else
            c[i][j] = Cdiv(Cadd(invgam[i],gamconj[j]),
                           cden[i][j]);
        }
      }

/* Calculate the field at the space position

  Multiplication by sol_amp[3] allows program to be generalized
  for 2 soliton collision by setting sol_amp[3] equal to zero */

      u_tden = Cadd(RCmul(sol_amp[3],
                          Cadd(Cmul(Csub(Cmul(c[1][3],
                                              c[2][2]),
                                         RCmul(sol_amp[2],
                                               Cmul(c[1][2],
                                                    c[2][3]))),
```

```
                                    RCmul(sol_amp[1],
                                          c[3][1])),
                                Cmul(Csub(Cmul(c[1][1],
                                               c[2][3]),
                                          RCmul(sol_amp[1],
                                                Cmul(c[1][3],
                                                     c[2][1]))),
                                     RCmul(sol_amp[2],
                                           c[3][2])))),
                           Cmul(Csub(RCmul(sol_amp[1]*sol_amp[2],
                                           Cmul(c[1][2],
                                                c[2][1])),
                                     Cmul(c[1][1],
                                          c[2][2])),
                                c[3][3]));

u_1[n]=Cdiv(
            Cadd(
                 Cmul(
                      RCmul(
                            sol_amp[1],
                            c[3][3]),
                      Csub(
                           RCmul(
                                 sol_amp[2],
                                 c[1][2]),
                           c[2][2])
                     ),
                 RCmul(
                       sol_amp[3]*sol_amp[1],
                       Cadd(
                            Cmul(
                                 RCmul(
                                       sol_amp[2],
                                       c[2][3]),
                                 Csub(
                                      c[3][2],
                                      c[1][2])
                                ),
                            Cmul(
                                 c[1][3],
                                 Csub(
```

```
                                        c[2][2],
                                        RCmul(
                                              sol_amp[2],
                                              c[3][2]))
                                    )
                                )
                            )
                        ),
                    u_tden
                   );

u_2[n]=Cdiv(
            Cadd(
                 Cmul(
                      RCmul(
                            sol_amp[2],
                            c[3][3]),
                      Csub(
                           RCmul(sol_amp[1],
                                 c[2][1]),
                           c[1][1])
                     ),
                 RCmul(
                       sol_amp[3]*sol_amp[2],
                       Cadd(
                            Cmul(
                                 RCmul(
                                       sol_amp[1],
                                       c[1][3]),
                                 Csub(
                                      c[3][1],
                                      c[2][1])
                                ),
                            Cmul(
                                 c[2][3],
                                 Csub(
                                      c[1][1],
                                      RCmul(
                                            sol_amp[1],
                                            c[3][1]))
                                )
                           )
```

```
                                )
                            ),
                        u_tden
                       );

    u_3[n]=Cdiv(
                RCmul(
                      sol_amp[3],
                      Cadd(
                           Cmul(
                                c[2][2],
                                Csub(
                                     RCmul(
   sol_amp[1],
   c[3][1]),
     c[1][1])
                                ),
                           Cadd(
                                Cmul(
                                     RCmul(
   sol_amp[1]*sol_amp[2],
   c[1][2]),
                                     Csub(
                                          c[2][1],
  c[3][1])
                                ),
                                Cmul(
                                     RCmul(
   sol_amp[2],
   c[3][2]),
                                     Csub(
  c[1][1],
  RCmul(
sol_amp[1],
c[2][1]))
                                )
                           )
                      )
                ),
            u_tden
           );
```

```
     u_12[n] = Cadd(u_1[n],u_2[n]);

     u_t[n] = Cadd(u_12[n],u_3[n]);
/*     u_t[n]=u_12[n];*/

    }

/* Store space and spectral data points */

    store_time_data(time);

/* My fft */
    dfour1(&((double)u_t[0].r)-1,points,-1); /* FFT */

/*dfour1(&((double)u_12[0].r)-1,points,-1); FFT of u_12*/
/*dfour1(&((double)u_3[0].r)-1,points,-1); FFT of u_3*/

/*     for (n=0;n<points;n++) {
       u_t[n] = Cadd(u_12[n],u_3[n]);
     }*/

    store_freq_data(time);



/* End the for loop */

  }

printf("Closing Data Files\n");
    fclose(spacfile);
    fclose(freqfile);

} /* End of main */


/*************************************************************
store_time_data -
    Subroutine for storing the time and field data
    in a IDL-compatible data file.
    Requires these external variables #defined:
```

```
    points -      number of elements in the array
    The data file must be opened and closed externally.
*************************************************************/
store_time_data( location )
    double   location;
{
    int k;
printf("time = %f\n", location);
    for (k=0; k<=(points-1); k++ ) {
/*        fprintf(spacfile,"%16.14f+I*%16.14f,",
            u_t[k].r,u_t[k].i );*/
        fprintf(spacfile,"%.4e ",Cabs(u_t[k]));
        if ( k%4-3 == 0) fprintf(spacfile,"\n " );
    }
}  /* End of subroutine store_time_data */


/*************************************************************
store_freq_data -
    Subroutine for storing the frequency field data
    in a IDL-compatible data file.
    Requires these external variables #defined:
    points -      number of elements in the array
    The data file must be opened and closed externally.
*************************************************************/
store_freq_data( location )
    double location;
{
    int k;
    for (k=0;k<points/2; k++) {
/*        fprintf(freqfile,"%12.10f+I*%12.10f,",
            u_t[points/2+k].r,u_t[points/2+k].i);*/
          fprintf(freqfile,"%.4e ",Cabs(u_t[points/2+k]));
        if ( k%4-3 == 0) fprintf(freqfile,"\n" );
    }
    for (k=points/2;k<=(points-1); k++) {
/*        fprintf(freqfile,"%12.10f+I*%12.10f,",
            u_t[k-points/2].r,u_t[k-points/2].i);*/
          fprintf(freqfile,"%.4e ",Cabs(u_t[k-points/2]));
        if ( k%4-3 == 0) fprintf(freqfile,"\n " );
    }
}  /* End of subroutine store_freq_data */
```

B.1.2 Mathematica compatible version

This version is used with Mathematica to compute positions of frequency and spatial peaks.

```
/*************************************************************
        3sol.c -
C program for computxing the exact waveform describing soliton
propagation in fiber - based upon the exact three soliton
solution to the NLS equation - and for computing the spectrum
of the waveform using a standard FFT routine.

VARIABLES, USES, and UNITS:
points - number of complex elements in variation coordinate
xwindow - full length of time axis

FIELD VARIABLES:
(u_t) - coordinate space variable
*************************************************************/

#include <stdio.h>
#include <math.h>

#ifndef TOOLS_C
#include "tools.c"
#endif

#ifndef DEFS_H
#include "defs.h"
#endif

#ifndef TYPES_H
#include "types.h"
#endif

#ifndef COMPLEX_H
#include "complex.h"
#endif

#ifndef COMPLEX_C
#include "complex.c"
#endif
```

```
#ifndef DFOUR1_C
#include "dfour1.c"
#endif

/* important parameters for run */
#define points 4096
#define xwindow (400.0)
#define init_t (-1.0)
#define final_t (1.0)
#define solitons 3
#define num_steps 100

/* array variables */
dcomplex    u_t[points];
dcomplex    u_1[points];
dcomplex    u_2[points];
dcomplex    u_3[points];
int         myi_p[points];  /* VP's position in array */
double      x_p[points];    /* VP's transverse coord */
double      s_cnst[4];
double      chi_cnst[4];
dcomplex    cden[4][4];
double      s[4];
double      chi[4];
dcomplex    lninvgam[4];
dcomplex    invgam[4];
dcomplex    gamconj[4];
double      rfac[4];
dcomplex    c[4][4];
double      sol_pos[4];
double      sol_omg[4];
double      sol_phase[4];
double      sol_amp[4];

/* serial variables */
int          num_solitons;
double       time;
dcomplex     u_tden;
dcomplex     u_tnum1;
dcomplex     u_tnum2;
dcomplex     u_tnum;
FILE        *spacfile, *freqfile;
```

```
FILE        *spacfile1, *spacfile2, *spacfile3;
FILE        *freqfile1, *freqfile2, *freqfile3;
                /* FE arrays for output */
char        buffer[MAXLINE+1];/* buffer for input strings */
char        filename[MAXLINE+1];/* output file name */

main()
{
    int     n; /* for counting array positions */
    int     j; /* for counting solitons */
    int     i; /* for counting solitons*/
    int     k; /* for counting time steps and loading files */

printf("Scaling processor transverse coordinates\n");
    for (n=0;n<points;n++) {
        myi_p[n] = n;
        x_p[n] = (double) xwindow*(myi_p[n]-points/2)/points;
    }

/* Initialize omegas in ascending order - if only two solitons
   are wanted, set sol_amp[3]=0.0  */
printf("Initializing input waveform.\n");
    sol_pos[1] = 5.0;
     sol_omg[1] = -10.0;
     sol_phase[1] = 2.0*M_PI*(0.0/1000.0);
     sol_amp[1] = 1.0;
    sol_pos[2] = -5.0;
     sol_omg[2] = 0.0;
     sol_phase[2] = 2.0*M_PI*(0.0/1000.0);
     sol_amp[2] = 1.0;
    sol_pos[3] = 10.0;
     sol_omg[3] = 10.0;
     sol_phase[3] = 2.0*M_PI*(0.0/1000.0);
     sol_amp[3] = 1.0;

    if (sol_amp[3] == 0.0) {
       num_solitons = solitons - 1;
    } else {
       num_solitons = solitons;
    }

printf("Input filename for space data storage : ");
```

```
    getline(buffer,MAXLINE,stdin);
    (void) strncpy(filename,buffer,strlen(buffer)-1);
    printf("Opening space data storage file\n");
    if ((spacfile = fopen(filename,"w")) == (FILE *)NULL) {
        printf( "Can't write to space data file.\n");
        exit(1);
    }

printf("Input filename for frequency data storage : ");
    getline(buffer,MAXLINE,stdin);
    (void) strncpy(filename,buffer,strlen(buffer)-1);
    printf("Opening frequency data storage file\n");
    if ((freqfile = fopen(filename,"w")) == (FILE *)NULL) {
        printf( "Can't write to frequency data file.\n");
        exit(1);
    }

printf("Writing run parameters to space data file\n");
    fprintf(spacfile,
            "(* Exact 3-soliton solution - Parameters*)\n");
    fprintf(spacfile,"points = %d;\n",points);
    fprintf(spacfile,"xwindow = %f; \n",xwindow);
    fprintf(spacfile,"numsolitons = %d; \n",num_solitons);
    fprintf(spacfile,"omega1 = %f;\n",sol_omg[1]);
    fprintf(spacfile,"omega2 = %f;\n",sol_omg[2]);
    fprintf(spacfile,"omega3 = %f;\n",sol_omg[3]);
    fprintf(spacfile,"initpos1 = %f;\n",sol_pos[1]);
    fprintf(spacfile,"initpos2 = %f;\n",sol_pos[2]);
    fprintf(spacfile,"initpos3 = %f;\n",sol_pos[3]);
    fprintf(spacfile,"initt = %f;\n",init_t);
    fprintf(spacfile,"finalt = %f;\n",final_t);
    fprintf(spacfile,"timesteps = %d;\n",num_steps);
    fprintf(spacfile,"amplist = {\n");

printf("Writing run parameters to frequency data file\n");
    fprintf(freqfile,
            "(* Exact 3-soliton solution - Parameters*)\n");
    fprintf(freqfile,"points = %d;\n",points);
    fprintf(freqfile,"xwindow = %f; \n", xwindow);
    fprintf(freqfile,"numsolitons = %d; \n",num_solitons);
    fprintf(freqfile,"omega1 = %f;\n",sol_omg[1]);
    fprintf(freqfile,"omega2 = %f;\n",sol_omg[2]);
```

```
    fprintf(freqfile,"omega3 = %f;\n",sol_omg[3]);
    fprintf(freqfile,"initpos1 = %f;\n",sol_pos[1]);
    fprintf(freqfile,"initpos2 = %f;\n",sol_pos[2]);
    fprintf(freqfile,"initpos3 = %f;\n",sol_pos[3]);
    fprintf(freqfile,"initt = %f;\n",init_t);
    fprintf(freqfile,"finalt = %f;\n",final_t);
    fprintf(freqfile,"timesteps = %d;\n",num_steps);
    fprintf(freqfile,"freqlist = {\n");

/* Begin while loop through different time steps */

    for (k=0;k<=num_steps;k++) {
      time = (double) init_t + (k * (final_t-init_t)/num_steps);

/* Set values of terms which are
   constant at all field positions */

    for (i=1;i<=solitons;i++) {
      s_cnst[i] = 2.0*sol_amp[i]*sol_omg[i]*time +
                  sol_amp[i]*sol_pos[i];
      chi_cnst[i] = (pow(sol_omg[i],2.0)-
                     pow(sol_amp[i],2.0))*time
                   + sol_omg[i]*sol_pos[i] - sol_phase[i];
      for (j=1;j<=solitons;j++) {
        if (j==i) {
          cden[i][j].r = 1.0;
          cden[i][j].i = 0.0;
        }
        else {
          cden[i][j].r = sol_amp[i] + sol_amp[j];
          cden[i][j].i = sol_omg[i] - sol_omg[j];
        }
      }
    }

/* Initialize field */

    for (n=0;n<points;n++) {
        u_t[n].r = 0.0;
        u_t[n].i = 0.0;
    }
```

```
/* Start calculation of field at each
   transverse space position */

    for (n=0;n<points;n++) {

/* Determine space and phase terms for each field component */

      for (j=1;j<=solitons;j++) {
        s[j] = sol_amp[j]*x_p[n] - s_cnst[j];
        chi[j] = sol_omg[j]*x_p[n] - chi_cnst[j];
        lninvgam[j].r = -s[j];
        lninvgam[j].i = -chi[j];
        invgam[j] = Cexp(lninvgam[j]);
        gamconj[j] = Cexp(Rconjg(lninvgam[j]));
        if (j==3)
          rfac[j] = cosh(s[j]);
        else
          rfac[j] = cosh(s[j])/sol_amp[j];
      }

/* Calculate matrix coefficients */

      for (i=1;i<=solitons;i++) {
        for (j=1;j<=solitons;j++) {
          if (j==i) {
            c[i][j].r = cos(chi[i])*rfac[i];
            c[i][j].i = -sin(chi[i])*rfac[i];
          }
          else
            c[i][j] = Cdiv(Cadd(invgam[i],
                           gamconj[j]),cden[i][j]);
        }
      }

/* Calculate the field at the space position

  Multiplication by sol_amp[3] allows program to be generalized
  for 2 soliton collision by setting sol_amp[3] equal to zero */

      u_tden = Cadd(RCmul(sol_amp[3],
                        Cadd(Cmul(Csub(Cmul(c[1][3],
                                            c[2][2]),
```

```
                                        Cmul(c[1][2],
                                             c[2][3])),
                                   c[3][1]),
                              Cmul(Csub(Cmul(c[1][1],
                                             c[2][3]),
                                        Cmul(c[1][3],
                                             c[2][1])),
                                   c[3][2]))),
                         Cmul(Csub(Cmul(c[1][2],
                                        c[2][1]),
                                   Cmul(c[1][1],
                                        c[2][2])),
                              c[3][3]));

u_1[n]=Cdiv(
            Cadd(
                 Cmul(
                      c[3][3],
                      Csub(c[1][2],c[2][2])
                     ),
                 RCmul(
                       sol_amp[3],
                       Cadd(
                            Cmul(
                                 c[2][3],
                                 Csub(c[3][2],c[1][2])
                                ),
                            Cmul(
                                 c[1][3],
                                 Csub(c[2][2],c[3][2])
                                )
                           )
                      )
                ),
            u_tden
           );

u_2[n]=Cdiv(
            Cadd(
                 Cmul(
                      c[3][3],
                      Csub(c[2][1],c[1][1])
```

```
                    ),
                RCmul(
                      sol_amp[3],
                      Cadd(
                           Cmul(
                                c[1][3],
                                Csub(c[3][1],c[2][1])
                               ),
                           Cmul(
                                c[2][3],
                                Csub(c[1][1],c[3][1])
                               )
                          )
                     )
               ),
           u_tden
          );

u_3[n]=Cdiv(
           RCmul(
                 sol_amp[3],
                 Cadd(
                      Cmul(
                           c[2][2],
                           Csub(c[3][1],c[1][1])
                          ),
                      Cadd(
                           Cmul(
                                c[1][2],
                                Csub(c[2][1],c[3][1])
                               ),
                           Cmul(
                                c[3][2],
                                Csub(c[1][1],c[2][1])
                               )
                          )
                     )
                ),
           u_tden
          );

u_t[n] = Cadd(Cadd(u_1[n],u_2[n]),u_3[n]);
```

```
/*      u_t[n]=Cdiv(Cadd(u_1[n],u_2[n]),u_tden);*/
    }

/* Store space and spectral data points */

    store_time_data(time);

/* My fft */
    dfour1(&((double)u_t[0].r)-1,points,-1); /* FFT */

     dfour1(&((double)u_1[0].r)-1,points,-1);
     dfour1(&((double)u_2[0].r)-1,points,-1);
     dfour1(&((double)u_3[0].r)-1,points,-1);

    store_freq_data(time);

/* End the for loop */
  }

printf("Closing Data Files\n");
    fprintf(spacfile,"};\n\n");
    fclose(spacfile);
    fprintf(freqfile,"};\n\n");
    fclose(freqfile);

} /* End of main */

/*************************************************************
store_time_data -
    Subroutine for storing the time and field data
    in a Mathematica-compatible data file.
    Requires these external variables #defined:
    points -      number of elements in the array
    The data file must be opened and closed externally.
*************************************************************/
store_time_data( location )
    double   location;
{
    int k;
printf("time = %f\n", location);
    if (location > init_t)
        fprintf(spacfile,",\n");
```

```
    fprintf(spacfile,"(* time=%7.5f *)\n{",location );
    for (k=0; k<=(points-2); k++ ) {
/*        fprintf(spacfile,"%16.14f+I*%16.14f,",
            u_t[k].r,u_t[k].i );*/
        fprintf(spacfile,"%16.14f,",Cabs(u_t[k]));
        if ( k%4-3 == 0) fprintf(spacfile,"\n " );
    }
    fprintf(spacfile,"%16.14f}",Cabs(u_t[(points-1)]));
}  /* End of subroutine store_time_data */

/*************************************************************
store_freq_data -
    Subroutine for storing the frequency field data
    in a Mathematica-compatible data file.
    Requires these external variables #defined:
    points -      number of elements in the array
    The data file must be opened and closed externally.
*************************************************************/
store_freq_data( location )
    double location;
{
    int k;
    if (location > init_t)
        fprintf(freqfile,",\n");
    fprintf(freqfile,"(* time=%7.5f *)\n{",location );
    for (k=0;k<points/2;k++) {
/*        fprintf(freqfile,"%12.10f+I*%12.10f,",
            u_t[points/2 + k].r,u_t[points/2 + k].i);*/
          fprintf(freqfile,"%16.14f,",Cabs(u_t[points/2 + k]));
        if ( k%4-3 == 0) fprintf(freqfile,"\n " );
    }
    for (k=points/2;k<=(points-2);k++) {
/*        fprintf(freqfile,"%12.10f+I*%12.10f,",
            u_t[k-points/2].r,u_t[k-points/2].i);*/
          fprintf(freqfile,"%16.14f,",Cabs(u_t[k-points/2]));
        if ( k%4-3 == 0) fprintf(freqfile,"\n " );
    }
/*    fprintf(freqfile,"%12.10f+I*%12.10f}",
        u_t[points/2 - 1].r,u_t[points/2 - 1].i);*/
      fprintf(freqfile,"%16.14f}",Cabs(u_t[points/2-1]));
}  /* End of subroutine store_freq_data */
```

B.2 Peak finding algorithms

B.2.1 Frequency peaks This program solves for a LaGrange polynomial that interpolates the points at the top of each frequency peak and them computes the shifts that result at a collision (a spline interpolation could be used instead).

```
(*fpkfnd.ma: mathematica file for calculating
frequency domain separations for colliding
wavelength-multiplexed solitons. *)

(*make absolute value lists from the space and frequency
domain value lists. amplist and freqlist must be
two-dimensional arrays of complex field values.
The dimensions are space and time for amplist,
frequency and time for freqlist. *)

(* Test code for computing Fourier transform of spatial
data in Mathematica to compare with results from C *)
(*flist=Array[f,{timesteps+1,points}];
iflist=Array[if,{timesteps+1,points}];
freqlist=Array[fl,{timesteps+1,points}];
Do[
   flist[[i]]=Fourier[amplist[[i]]];
   iflist[[i]]=Abs[flist[[i]]];
   Do[
      freqlist[[i,points/2+1-j]]=iflist[[i,j]];
      freqlist[[i,points+1-j]]=iflist[[i,j+points/2]],
   {j,1,points/2}],
{i,1,timesteps+1}]*)

absamplist = Map[Abs,amplist,{1}];
absfreqlist = Map[Abs,freqlist,{1}];

peaks=Array[maxpt,{numsolitons}]
shift=Array[s,{numsolitons,timesteps+1,2}]
omega=Array[om,{3}]
pos=Array[p,{3}]
omega[[1]]=omega1
omega[[2]]=omega2
```

```
omega[[3]]=omega3
om=omega2-omega1
pos[[1]]=initpos1
pos[[2]]=initpos2
pos[[3]]=initpos3

(* User input: time step at which to find maxima if
done manually *)
(*i = 1;*)

(* Plot out absamplist[i] and absfreqlist[i] to
    make sure they each have the required two peaks at
    the i-th time step *)

(*ListPlot[freqlist[[i]],
   PlotRange -> {0,Max[Max[freqlist]]},
   PlotJoined -> True];*)

Do[

   Do[
      maxval[x_] = x == Max[absfreqlist[[i]]];
      highpoint = Select[absfreqlist[[i]],maxval];
      xlist = Position[absfreqlist[[i]],highpoint[[1]]];
      peaks[[k]]=xlist[[1,1]];
      Do[absfreqlist[[i,xlist[[1,1]]-n]]=0,{n,-20,20,1}],

   {k,1,numsolitons}];

   peaks=Sort[peaks];

   Do[

      For [j = 1,j<=5,j++,
           x[j] = (2*Pi*points/xwindow)
                  *(peaks[[k]]-4+j-Length[freqlist[[i]]]/2)
(*                *(peaks[[k]]-3+j-Length[freqlist[[i]]]/2)*)
                    /Length[freqlist[[i]]];
           y[j] = freqlist[[i,peaks[[k]]-3+j]]];

      P1 = y[1]; P2 = y[2]; P3 = y[3]; P4 = y[4]; P5 = y[5];
      P12 = ((x-x[2])P1 - (x-x[1])P2)/(x[1]-x[2]);
```

```
        P23 = ((x-x[3])P2 - (x-x[2])P3)/(x[2]-x[3]);
        P34 = ((x-x[4])P3 - (x-x[3])P4)/(x[3]-x[4]);
        P45 = ((x-x[5])P4 - (x-x[4])P5)/(x[4]-x[5]);
        P123 = ((x-x[3])P12 - (x-x[1])P23)/(x[1]-x[3]);
        P234 = ((x-x[4])P23 - (x-x[2])P34)/(x[2]-x[4]);
        P345 = ((x-x[5])P34 - (x-x[3])P45)/(x[3]-x[5]);
        P1234 = ((x-x[4])P123 - (x-x[1])P234)/(x[1]-x[4]);
        P2345 = ((x-x[5])P234 - (x-x[2])P345)/(x[2]-x[5]);
        P12345 = ((x-x[5])P1234 - (x-x[1])P2345)/(x[1]-x[5]);
        deriv=D[P12345,x];
        a=FindRoot[deriv==0,{x,omega[[k]]}];
        freq=N[a[[1,2]]];

        omtime=om (initt + (i-1) (finalt-initt)/timesteps);
        shift[[k,i]]={N[omtime],N[om/2 (freq-omega[[k]]),10]},

    {k,2,2}],

{i,1,timesteps+1}]
```

B.2.2 Spatial peaks This program solves for a LaGrange polynomial that interpolates the points at the top of each spatial peak and them computes the displacement that remains after a collision.

```
(*spkfnd.ma: mathematica file for calculating space shifts
     for colliding wavelength-multiplexed solitons. *)

absamplist = Map[Abs,amplist,{1}];
(* User input: time step at which to find maxima *)
(*i = 1;*)
peaks=Array[maxpt,{numsolitons}]
shift=Array[s,{numsolitons,timesteps+1,2}]
test=Array[t,{numsolitons,timesteps+1,2}]
omega=Array[om,{3}]
pos=Array[p,{3}]
omega[[1]]=omega1
omega[[2]]=omega2
omega[[3]]=omega3
om=omega2-omega1
pos[[1]]=initpos1
pos[[2]]=initpos2
pos[[3]]=initpos3
(*
ListPlot[amplist[[i]],
         PlotRange -> {0,Max[Max[amplist]]},
         PlotJoined -> True];
*)
Do[
   Do[
      maxval[x_] = x == Max[absamplist[[i]]];
      highpoint = Select[absamplist[[i]],maxval];
      xlist = Position[absamplist[[i]],highpoint[[1]]];
      peaks[[k]]=xlist[[1,1]];
      Do[absamplist[[i,xlist[[1,1]]-n]]=0,{n,-20,20,1}],
   {k,1,numsolitons}];

   peaks=Sort[peaks];
   omtime=(2 (i-1)/timesteps - 1) omegatmax;
(*   omtime=-10+((-7.5+10)/timesteps) (i-1);*)

   Do[
```

```
        xcexp = pos[[k]] + (2 omega[[k]]/om) omtime;

        For [j = 1,j<=5,j++,
             x[j] = xwindow*(peaks[[k]]-4+j-
                        Length[amplist[[i]]]/2)
                        /Length[amplist[[i]]];
             y[j] = amplist[[i,peaks[[k]]-3+j]]];

        P1 = y[1]; P2 = y[2]; P3 = y[3]; P4 = y[4]; P5 = y[5];
        P12 = ((x-x[2])P1 - (x-x[1])P2)/(x[1]-x[2]);
        P23 = ((x-x[3])P2 - (x-x[2])P3)/(x[2]-x[3]);
        P34 = ((x-x[4])P3 - (x-x[3])P4)/(x[3]-x[4]);
        P45 = ((x-x[5])P4 - (x-x[4])P5)/(x[4]-x[5]);
        P123 = ((x-x[3])P12 - (x-x[1])P23)/(x[1]-x[3]);
        P234 = ((x-x[4])P23 - (x-x[2])P34)/(x[2]-x[4]);
        P345 = ((x-x[5])P34 - (x-x[3])P45)/(x[3]-x[5]);
        P1234 = ((x-x[4])P123 - (x-x[1])P234)/(x[1]-x[4]);
        P2345 = ((x-x[5])P234 - (x-x[2])P345)/(x[2]-x[5]);
        P12345 = ((x-x[5])P1234 - (x-x[1])P2345)/(x[1]-x[5]);

        deriv=D[P12345,x];
        a=FindRoot[deriv==0,{x,xcexp}];
        xc=N[a[[1,2]]];
        test[[k,i]]={N[omtime],N[xc,10]};
        shift[[k,i]]={N[omtime],N[xc - xcexp-.024585522,10]},

    {k,3,numsolitons}],

{i,25,timesteps+1}]
```

B.3 System performance computations

B.3.1 Jitter computations This program computes the variance in the relative pulse arrival times of adjacent soliton pulses in each of N wavelength channels.

```
/*************************************************************
jitter.c -
C program for computing the jitter in both arrival time and
frequency resulting from WDM soliton collisions in a fiber,
and for computing the maximum system length for various
values of the pulse width tau to insure BER<10^-9.
All units are in ps, km, nm unless otherwise specified.

*************************************************************/

#include <stdio.h>
#include <math.h>

#ifndef TOOLS_C
#include "tools.c"
#endif

#ifndef DEFS_H
#include "defs.h"
#endif

/* important parameters for run */

#define chnls 4       /* max number of chnls */
#define tduty (0.2)   /* duty cycle of temporal pulses */
#define wduty (0.2)   /* "duty cycle" of spectral pulses */
#define La (25.0)     /* amplifier spacing */
#define tau (20.0)    /* pulse FWHM */
#define alpha (0.048)/* loss coefficient km^(-1) */
#define wc (1550.0)   /* center wavelength */
#define w0 (1535.0)   /* zero dispersion wavelength */
#define s0 (2./30.)   /* dispersion slope in ps/nm^2-km */
#define L (10000.0)   /* total link length */
#define c (3.0E5)     /* speed of light nm/ps */
#define twopi (2.0*M_PI)
```

```
/* array variables */

double      w[chnls];         /* channel wavelength */
double      wvar_[chnls][chnls];/* intermediate variance */
double      tvar_[chnls];       /* intermediate variance */
double      tvar__[chnls][chnls];/* intermediate variance */
double      wvar[chnls];/* variance in channel wavelength */
double      tvar[chnls];      /* variance in arrival time */
double      d[chnls];         /* variance in arrival time */
double      ber[chnls];       /* ber  */
double      wstd[chnls];    /* std dev in chnl wavelength */
double      tstd[chnls];      /* std dev in arrival time */

/* serial variables */
double      erfarg;
double      T;              /* bit period */
double      Lc;             /* length for collision */
double      Zc;             /* distance between collisions */
double      z0;             /* soliton period */
double      dbar;           /* average dispersion value */
double      n;              /* collisions per link length */
double      ratio;          /* Lc/La */
double      wsep;           /* adjacent wavelength separation */
double      wsep1;          /* adjacent wavelength separation */
double      cijsep;         /* channel wavelength spacing */
double      lossfac;        /* alpha*La */
double      coeff1;         /* coefficients for computing shift */
double      coeff2;
double      x;              /* 2.8*ratio */
double      tvar_n;         /* n^3/6 */
double      sum;            /* sum of harmonic coefficients */
double      dw;             /* wavelength shift */
double      dwvar;          /* var in indiv wavelength shifts */
double      maxL;           /* max sys length given N and tau */
int         maxi;     /* indice for channel with max jitter */
FILE        *constfile,*distfile;
                /* FE arrays for output */
char        buffer[MAXLINE+1];/* buffer for input strings */
char        filename[MAXLINE+1];/* output file name */

main()
```

```
{
    int     i; /* indices for counting */
    int     j;
    int     k;
    int     m;
    int     h;

/* get filename for storing constants */

printf("Input filename for storing constants: ");
    getline(buffer,MAXLINE,stdin);
    (void) strncpy(filename,buffer,strlen(buffer)-1);
    printf("Opening constants storage file\n");
    if ((constfile = fopen(filename,"w")) == (FILE *)NULL) {
        printf( "Can't write to data file.\n");
        exit(1);
    }

/* get filename for storing length data */

printf("Input filename for storing length data: ");
    getline(buffer,MAXLINE,stdin);
    (void) strncpy(filename,buffer,strlen(buffer)-1);
    printf("Opening length storage file\n");
    if ((distfile = fopen(filename,"w")) == (FILE *)NULL) {
        printf( "Can't write to data file.\n");
        exit(1);
    }

/*    for (h=0;h<121;h++) {
      tau = 20.0+((double) h*.25);*/

/* compute and define useful values */

    wsep = (0.3148*wc*wc)/(wduty*tau*c);
    T = tau/tduty;
    lossfac = alpha*La;
    coeff1 = 4.0*1.763*lossfac*La*wc*wc/
             (3.0*M_PI*M_PI*M_PI*tau);

/* compute wavelengths */
```

```
    for (i=0;i<chnls;i++) {
      w[i]=wc - w0 - wsep*((chnls - 1.)/2. - i);
      if (w[i] < 0) printf("Wavelength out of range\n");
    }
/*    wsep1=0.625;
    w[0]=5.0;
    w[1]=w[0]+wsep1;
    w[2]=w[1]+wsep1;
    w[3]=w[2]+wsep1;
    w[4]=w[3]+wsep1;
    w[5]=w[4]+wsep1;
    w[6]=w[5]+wsep1;
    w[7]=w[6]+wsep1;
    w[8]=w[7]+wsep1;
    w[9]=w[8]+wsep1;
    w[10]=w[9]+wsep1;
    w[11]=w[10]+wsep1;
    w[12]=w[11]+wsep1;
    w[13]=w[12]+wsep1;
    w[14]=w[13]+wsep1;
    w[15]=w[14]+wsep1;*/

    for (i=0;i<chnls;i++) {
      d[i]=w[i]*s0;
    }


/* begin channel loop */
   /* defn of dwvar checked in rsrch notebook pg II-71 */

    sum=0.0;
    for (i=0;i<chnls-1;i++) {
      for (j=i+1;j<chnls;j++) {

cijsep = fabs(w[i]-w[j]);
dbar = (w[i]+w[j])*s0/2.;
        z0 = tau/(dbar*wduty*wsep);
Lc = 2.0*tau/(dbar*cijsep);
Zc = T/(dbar*cijsep);
ratio = Lc/La;
x = 2.8*ratio;
coeff2 = coeff1*coeff1*pow(x,8.0)/(z0*z0);
```

```
n = L/Zc;
tvar_n = n*n*n/6.;
dwvar = 0.0;
sum = 0.0;
for (m=1;m<=25;m++) {
  sum += pow(pow((double) m,3.0)/
         (pow(sinh(m*x),2.0)*
         sqrt(lossfac*lossfac + twopi*twopi*m*m)),2.0);
}
dwvar = coeff2*sum*1.0E-10/2.0;
tvar__[i][j] = dbar*dbar*dbar*dwvar*cijsep;
tvar__[j][i] = tvar__[i][j];
wvar_[i][j] = n*dwvar/2.;
wvar_[j][i] = wvar_[i][j];
        fprintf(constfile,"%4.6f\n%4.6f\n%4.6f\n%4.6f\n%.6e\n",
              cijsep,dbar,Lc,z0,dwvar);
/*      fprintf(distfile,"%.6e\n",dw);*/
      }
    }

/* Variance in each channel is sum of its variances between each
   other individual channel */

    for (i=0;i<chnls;i++) {
      tvar_[i] = 0.0;
      wvar[i] = 0.0;
    }

    for (i=0;i<chnls;i++) {
      for (j=0;j<chnls;j++) {
if (i==j);
else {
  wvar[i] += wvar_[i][j];
  tvar_[i] += tvar__[i][j];
}
      }
      tvar[i] = L*L*L*tvar_[i]/(6.*T);
      erfarg=(double) 0.4*T/sqrt(2.*tvar[i]);
      ber[i]=erfc(erfarg);
/*      fprintf(distfile,"%.6e %.6e\n",wvar[i],tvar[i]);*/
      fprintf(distfile,"%4.3f %1.2f %.2e %.1e\n",w[i]+w0,d[i],
      sqrt(tvar[i]),ber[i]);
```

```
    }

/* Find which channel has largest jitter and compute maximum
   system length assuming that the allowable jitter is no
   greater than 2*tau, i.e. r=.4 for tduty=.2 */

    maxi = 0;
    for (i=1;i<chnls;i++) {
      if (tvar_[i]>tvar_[maxi]) maxi = i;
    }

    maxL=1.4774*tau/pow(tvar_[maxi],1./3.);
    fprintf(distfile,"%3.2f %.3e\n",tau,maxL);

/*    }*/


} /* End of main */
```

B.3.2 Maximum system lengths This program computes the maximum system length versus τ with N constant.

```
/*************************************************************
length.c -
C program for computing the jitter in both arrival time and
frequency resulting from WDM soliton collisions in a fiber,
and for computing the maximum system length for various
values of the pulse width tau to insure BER<10^-9, where
the number of channels is constant for all tau.
All units are in ps, km, nm unless otherwise specified.

*************************************************************/

#include <stdio.h>
#include <math.h>

#ifndef TOOLS_C
#include "tools.c"
#endif

#ifndef DEFS_H
#include "defs.h"
#endif

/* important parameters for run */

#define chnls 32      /* number of chnls */
#define tduty (0.2)   /* duty cycle of temporal pulses */
#define wduty (0.2)   /* "duty cycle" of spectral pulses */
#define La (25.0)     /* amplifier spacing */
/*#define tau (50.0)*/  /* pulse FWHM */
#define alpha (0.048  /* loss coefficient km^(-1) */
#define wc (1550.0)   /* center wavelength */
#define w0 (1535.0)   /* zero dispersion wavelength */
#define s0 (2./30.)   /* dispersion slope in ps/nm^2-km */
#define L (10000.0)   /* total link length */
#define c (3.0E5)     /* speed of light nm/ps */
#define twopi (2.0*M_PI)

/* array variables */
```

```
double      w[chnls];    /* channel wavelength */
double      wvar_[chnls][chnls];/* intermediate variance */
double      tvar_[chnls];/* intermediate variance */
double      tvar__[chnls][chnls];/* intermediate variance */
double      wvar[chnls]; /* variance in channel wavelength */
double      tvar[chnls]; /* variance in arrival time */
double      wstd[chnls]; /* std dev in chnl wavelength */
double      tstd[chnls]; /* std dev in arrival time */

/* serial variables */
double      tau;
double      T;          /* bit period */
double      Lc;         /* length for collision */
double      Zc;         /* distance between collisions */
double      z0;         /* soliton period */
double      dbar;       /* average dispersion value */
double      n;          /* collisions per link length */
double      ratio;      /* Lc/La */
double      wsep;       /* adjacent wavelength separation */
double      cijsep;     /* channel wavelength spacing */
double      lossfac;    /* alpha*La */
double      coeff1;     /* coefficients for computing shift */
double      coeff2;
double      x;          /* 2.8*ratio */
double      tvar_n;     /* n^3/6 */
double      sum;        /* sum of harmonic coefficients */
double      dw;         /* wavelength shift */
double      dwvar;      /* var in indiv wavelength shifts */
double      maxL;       /* max sys length given N and tau */
int         maxi;       /* indice for channel with max jitter */
FILE        *constfile,*distfile;
                /* FE arrays for output */
char        buffer[MAXLINE+1];/* buffer for input strings */
char        filename1[MAXLINE+1];/* output file name */
char        filename2[MAXLINE+1];/* output file name */

main()
{
    int     i; /* indices for counting */
    int     j;
    int     k;
```

```
    int     m;
    int     h;

/* get filename for storing constants */

printf("Input filename for storing constants: ");
    getline(buffer,MAXLINE,stdin);
    (void) strncpy(filename1,buffer,strlen(buffer)-1);
    printf("Opening constants storage file\n");
    if ((constfile = fopen(filename1,"w")) == (FILE *)NULL) {
        printf( "Can't write to data file.\n");
        exit(1);
    }

/* get filename for storing length data */

printf("Input filename for storing length data: ");
    getline(buffer,MAXLINE,stdin);
    (void) strncpy(filename2,buffer,strlen(buffer)-1);
    printf("Opening length storage file\n");
    if ((distfile = fopen(filename2,"w")) == (FILE *)NULL) {
        printf( "Can't write to data file.\n");
        exit(1);
    }

    for (h=0;h<31;h++) {
      tau = 20.0+(double) h;

/* compute and define useful values */

    wsep = (0.3148*wc*wc)/(wduty*tau*c);
    T = tau/tduty;
    lossfac = alpha*La;
    coeff1 = 4.0*1.763*lossfac*La*wc*wc/
             (3.0*M_PI*M_PI*M_PI*tau);

/* compute wavelengths */

    for (i=0;i<chnls;i++) {
      w[i]=wc - w0 - wsep*((chnls - 1.)/2. - i);
      if (w[i] < 0) printf("Wavelength out of range\n");
    }
```

```
/* begin channel loop */
   /* defn of dwvar checked in rsrch notebook pg II-71 */

    sum=0.0;
    for (i=0;i<chnls-1;i++) {
      for (j=i+1;j<chnls;j++) {

cijsep = fabs(w[i]-w[j]);
dbar = (w[i]+w[j])*s0/2.;
        z0 = tau/(dbar*wduty*wsep);
Lc = 2.0*tau/(dbar*cijsep);
Zc = T/(dbar*cijsep);
ratio = Lc/La;
x = 2.8*ratio;
coeff2 = coeff1*coeff1*pow(x,8.0)/(z0*z0);
n = L/Zc;
tvar_n = n*n*n/6.;
dwvar = 0.0;
sum = 0.0;
for (m=1;m<=25;m++) {
  sum += pow(pow((double) m,3.0)/
         (pow(sinh(m*x),2.0)*
         sqrt(lossfac*lossfac + twopi*twopi*m*m)),2.0);
}
dwvar = coeff2*sum*1.0E-10/2.0;
tvar__[i][j] = dbar*dbar*dbar*dwvar*cijsep;
tvar__[j][i] = tvar__[i][j];
wvar_[i][j] = n*dwvar/2.;
wvar_[j][i] = wvar_[i][j];
        fprintf(constfile,"%4.6f\n%4.6f\n%4.6f\n%4.6f\n%.6e\n",
              cijsep,dbar,Lc,z0,dwvar);
/*      fprintf(distfile,"%.6e\n",dw);*/
      }
    }

/* Variance in each channel is sum of its variances
   between each other individual channel */

    for (i=0;i<chnls;i++) {
      tvar_[i] = 0.0;
      wvar[i] = 0.0;
```

```
    }

    for (i=0;i<chnls;i++) {
      for (j=0;j<chnls;j++) {
if (i==j);
else {
  wvar[i] += wvar_[i][j];
  tvar_[i] += tvar__[i][j];
}
      }
      tvar[i] = L*L*L*tvar_[i]/(6.*T);
/*      fprintf(distfile,"%.6e %.6e\n",wvar[i],tvar[i]);*/
    }

/* Find which channel has largest jitter and compute maximum
   system length assuming that the allowable jitter is no
   greater than 2*tau, i.e. r=.4 for tduty=.2 */

    maxi = 0;
    for (i=1;i<chnls;i++) {
      if (tvar_[i]>tvar_[maxi]) maxi = i;
    }

    maxL=1.4774*tau/pow(tvar_[maxi],1./3.);
    fprintf(distfile,"%3.0f %.3e\n",tau,maxL);

    }


} /* End of main */
```

B.3.3 System throughput This program computes the data throughput versus τ with L constant.

```
/*************************************************************
thrput.c -
C program for computing the jitter in both arrival time and
frequency resulting from WDM soliton collisions in a fiber,
and for computing the throughput for various
values of the pulse width tau to insure BER<10^-9, where
the system length is constant for all tau.
All units are in ps, km, nm unless otherwise specified.

*************************************************************/

#include <stdio.h>
#include <math.h>

#ifndef TOOLS_C
#include "tools.c"
#endif

#ifndef DEFS_H
#include "defs.h"
#endif

/* important parameters for run */

#define maxchnls 96  /* number of chnls */
#define tduty (0.2)  /* duty cycle of temporal pulses */
#define wduty (0.333)/* "duty cycle" of spectral pulses */
#define La (25.0)    /* amplifier spacing */
/*#define tau (50.0)*/ /* pulse FWHM */
#define alpha (0.048)/* loss coefficient km^(-1) */
#define wc (1550.0)  /* center wavelength */
#define w0 (1535.0)  /* zero dispersion wavelength */
#define s0 (2./30.)  /* dispersion slope in ps/nm^2-km */
#define L (10000.0)  /* total link length */
#define c (3.0E5)    /* speed of light nm/ps */
#define twopi (2.0*M_PI)

/* array variables */
```

```
double      w[maxchnls];    /* channel wavelength */
double      wvar_[maxchnls][maxchnls];/*intermediate variance*/
double      tvar_[maxchnls];/* intermediate variance */
double      tvar__[maxchnls][maxchnls];/*intermediate variance*/
double      wvar[maxchnls]; /* variance in channel wavelength */
double      tvar[maxchnls]; /* variance in arrival time */
double      wstd[maxchnls]; /* std dev in chnl wavelength */
double      tstd[maxchnls]; /* std dev in arrival time */

/* serial variables */
double      tau;     /* pulse intensity FWHM */
int         chnls;   /* number of chnls */
double      T;       /* bit period */
double      Lc;      /* length for collision */
double      Zc;      /* distance between collisions */
double      z0;      /* soliton period */
double      dbar;    /* average dispersion value */
double      n;       /* collisions per link length */
double      ratio;   /* Lc/La */
double      wsep;    /* adjacent wavelength separation */
double      cijsep;  /* channel wavelength spacing */
double      lossfac; /* alpha*La */
double      coeff1;  /* coefficients for computing shift */
double      coeff2;
double      x;       /* 2.8*ratio */
double      tvar_n;  /* n^3/6 */
double      sum;     /* sum of harmonic coefficients */
double      dw;      /* wavelength shift */
double      dwvar;   /* var in indiv wavelength shifts */
double      thrput;  /* maximum throughput per tau */
int         maxi;    /* indice for channel with max jitter */
int         test;    /* test value for chnl loop */
FILE        *constfile,*distfile;
                /* FE arrays for output */
char        buffer[MAXLINE+1];/* buffer for input strings */
char        filename1[MAXLINE+1];/* output file name */
char        filename2[MAXLINE+1];/* output file name */

main()
{
    int     i; /* indices for counting */
```

```
    int     j;
    int     k;
    int     m;
    int     h;

/* get filename for storing constants */

printf("Input filename for storing constants: ");
    getline(buffer,MAXLINE,stdin);
    (void) strncpy(filename1,buffer,strlen(buffer)-1);
    printf("Opening constants storage file\n");
    if ((constfile = fopen(filename1,"w")) == (FILE *)NULL) {
        printf( "Can't write to data file.\n");
        exit(1);
    }

/* get filename for storing throughput data */

printf("Input filename for storing throughput data: ");
    getline(buffer,MAXLINE,stdin);
    (void) strncpy(filename2,buffer,strlen(buffer)-1);
    printf("Opening throughput storage file\n");
    if ((distfile = fopen(filename2,"w")) == (FILE *)NULL) {
        printf( "Can't write to data file.\n");
        exit(1);
    }

    chnls=3;
    for (h=0;h<31;h++) {
      tau = 20.0+(double) h;

    test = 0;
    for (chnls=chnls-1;test<1;chnls++) {

/* compute and define useful values */

    wsep = (0.3148*wc*wc)/(wduty*tau*c);
    T = tau/tduty;
    lossfac = alpha*La;
    coeff1 = 4.0*1.763*lossfac*La*wc*wc/
             (3.0*M_PI*M_PI*M_PI*tau);
```

```
/* compute wavelengths */

    for (i=0;i<chnls;i++) {
      w[i]=wc - w0 - wsep*((chnls - 1.)/2. - i);
      if (w[i] < 0) printf("Wavelength out of range\n");
    }

/* begin channel loop */
   /* defn of dwvar checked in rsrch notebook pg II-71 */

    sum=0.0;
    for (i=0;i<chnls-1;i++) {
      for (j=i+1;j<chnls;j++) {

cijsep = fabs(w[i]-w[j]);
dbar = (w[i]+w[j])*s0/2.;
       z0 = tau/(dbar*wduty*wsep);
Lc = 2.0*tau/(dbar*cijsep);
Zc = T/(dbar*cijsep);
ratio = Lc/La;
x = 2.8*ratio;
coeff2 = coeff1*coeff1*pow(x,8.0)/(z0*z0);
n = L/Zc;
tvar_n = n*n*n/6.;
dwvar = 0.0;
sum = 0.0;
for (m=1;m<=25;m++) {
  sum += pow(pow((double) m,3.0)/
         (pow(sinh(m*x),2.0)*
         sqrt(lossfac*lossfac + twopi*twopi*m*m)),2.0);
}
dwvar = coeff2*sum*1.0E-10/2.0;
tvar__[i][j] = dbar*dbar*dbar*dwvar*cijsep;
tvar__[j][i] = tvar__[i][j];
wvar_[i][j] = n*dwvar/2.;
wvar_[j][i] = wvar_[i][j];
/*      fprintf(distfile,"%.6e\n",dw);*/
      }
    }

/* Variance in each channel is sum of its
   variances between each other individual channel */
```

```
    for (i=0;i<chnls;i++) {
      tvar_[i] = 0.0;
      wvar[i] = 0.0;
    }

    for (i=0;i<chnls;i++) {
      for (j=0;j<chnls;j++) {
if (i==j);
else {
  wvar[i] += wvar_[i][j];
  tvar_[i] += tvar__[i][j];
}
      }
      tvar[i] = L*L*L*tvar_[i]/(6.*T);
/*      fprintf(distfile,"%.6e %.6e\n",wvar[i],tvar[i]);*/
    }

/* Find which channel has largest jitter and compute maximum
   system length assuming that the allowable jitter is no
   greater than 2*tau, i.e. r=.4 for tduty=.2 */

    maxi = 0;
    for (i=1;i<chnls;i++) {
      if (tvar[i]>tvar[maxi]) maxi = i;
    }

    if (chnls == maxchnls) {
      test=1; /* stop        */
      h=31;   /* computation */
      printf("Maximum number of channels reached\n");
    }
    if (tvar[maxi] > pow(0.4*T/6.1,2.0)) {
      test = 1;
      thrput = (double) (chnls - 1.)*1000./T;  /* in Gb/s */
      fprintf(distfile,"%3d %3.1f %.3e\n",chnls-1,tau,thrput);
    }

    }
    }

} /* End of main */
```